LEACHING OF SOME SULPHIDE MINERALS OF NICKEL UNDER ACIDIC OXIDIZING CONDITIONS

by

ANARGYROS S. TZAMTZIS

Min. and Met. Engineer

National Technical University of Athens

A Thesis submitted for the degree of

Doctor of Philosophy

of the

University of London

and for the

Diploma of Imperial College

July, 1976

DEDICATED TO MY FATHER AND MOTHER

ABSTRACT

A monosulphide solid solution of iron and nickel containing 36.5 wt % iron, 25.0 wt % nickel and 38.5 wt % sulphur was synthesized from the elements. Electron probe analysis of the material showed that it was homogeneous while x-ray diffraction analysis showed that it did not contain any other phase.

The sulphide was leached with ferric chloride solutions and the effects of temperature, particle size, ferric concentration, acid concentration, stirring speed and sample weight on the rate of dissolution were studied.

The apparent activation energy calculated indicated a reaction rate controlled by both transport and chemical mechanisms.

Pentlandite, $(Fe,Ni)_9S_8$, containing 32.25 wt % iron, 33.92 wt % nickel, 0.25 wt % platinum and 0.25 wt % palladium was synthesized. X-ray diffraction and electron probe analysis of the synthesized sulphide showed that a second phase, pyrrhotite, was present together with the pentlandite. Platinum in the metallic form, formed discrete crystals, while palladium formed a solid solution with pentlandite.

Pentlandite was leached with ferric chloride under various conditions and the effect of the different vairables on the rate of leaching was studied. The amount of orthorhombic sulphur and sulphate formed varied with the different conditions of the experiments. No new phases were identified. The apparent activation energies calculated at different stages of the dissolution suggest a process controlled by a chemical reaction and a diffusion mechanism. The chemical reaction is more important in determining

the rate of dissolution at the beginning of the experiment, while the diffusion mechanism was predominant at the end of the experiment.

A very small amount of platinum and palladium passed into the solution and started reprecipitating as the redox-potential of the solution decreased due to the reduction of ferric ions.

CONTENTS

INTRODUCTION

Nickel is one of the more abundant elements and one of the common metals in the universe and it makes large contributions to many of mankind's endeavours.

Pentlandite is the commonest of the nickel minerals and accounts for about three-quarters of the nickel mined in the world. Nickeliferrous pyrrhotite is the second main nickel source after pentlandite.

Pyrometallurgy remains still the main process for nickel recovery from both sulphide and oxide minerals, but hydrometallurgy in the last decades has become important for nickel extraction. A large number of hydrometallurgical plants are today in operation in many places in the world.

Ammonia and sulphuric acid are the commonest leaching agents in hydrometallurgy while ferric chloride might be for economical reasons the only alternative.

Very little work has been reported on the acid non autoclave leaching of the iron-nickel sulphides. Therefore, the present work is an attempt to clarify the kinetics of the leaching of monosulphide solid solution of iron and nickel and pentlandite which are the two main sources of nickel recovery. Since the use of synthetic minerals has been found more effective than using specific natural ores for determining the mechanisms which are operative during leaching, the iron-nickel sulphides subjected to leaching in the present work were synthesized from the elements. Ferric chloride solutions were used as the oxidizing agent and the leaching experiments were carried out under atmospheric pressure.

The chemistry of the leaching of the sulphides was complicated because of the big number of the different species present in the solution and the formation of a sulphur layer around the surface of the particles which had an unfavourable effect on the reproducibility of the results.

The mechanisms of dissolution of the monosulphide solid solution and pentlandite as well as the chemical reactions believed occurring are described in the text.

Pentlandite deposits are one of the main sources for the platinum group metals. For this reason, small amounts of platinum and palladium were added in pentlandite and their behaviour during leaching was studied. It was proved that both of these metals were practically kept out of the solution and remained in the residue.

CHAPTER I
LITERATURE SURVEY

1.1 LEACHING

1.1.1 Previous Work on Acid and Salt Leaching of Nickel and Iron Sulphide Concentrates

Although the use of 'wet' methods, has been well known for many years for the extraction of the coinage metals from their ores, it is only during the last three decades that there has been apparent and markedly increased interest in applying these methods for the extraction of other metals.

Until the 1940's pyrometallurgy was essentially the only means utilised for primary extraction of nickel from its ores. This was due in part to the natural tendency of early nickel metallurgy to follow in the path of established sulphide copper ore treatment, the more so in the case of the Canadian ores since there were nickel-copper deposits.

In recent years hydrometallurgy has become an important means of recovering nickel from ores. Several plants now employ hydrometallurgical methods to obtain nickel from oxide-ores and pentlandite-rich sulphide concentrates. Others process nickeliferous pyrrhotite concentrates for recovery of high-grade iron ore and nickel.

Pentlandite is the commonest of the sulphide ore minerals of nickel and accounts for about three quarters of the nickel mined in the world. It is almost invariably associated with larger amounts of pyrrhotite and chalcopyrite, various other sulphides like millerite (NiS), heazlewoodite (Ni_3S_2), polydymite (Ni_3S_4), violarite (Ni_2FeS_4), siegenite ($(Co,Ni)_3S_4$), precious metals and gangue materials. Nickeliferous pyrrhotite is the second main source for nickel recovery after pentlandite, mainly because pyrrhotite is an abundant mineral in nearly all sulphide nickel ores, much more abundant, in fact, than the nickel minerals themselves. Hydrometallurgy of nickel sulphides then, mainly deals with the extraction of nickel from these two minerals.

The acid and salt leaching of nickel mattes and concentrates has been the subject of various studies and patents since early in the century.

In 1908 Gunther and Franke (1) invented a process of treating metallic sulphides or mattes, which consists broadly in bringing the copper-nickel concentrates to reaction with chlorine, either in the form of gas or in the form of HCl. Copper was dissolved preferentially and the nickel from the solid residue was dissolved by the elimination of cupric salts from the solution.

Choppin and Faulkenberry (2) studied the oxidation of aqueous sulphide solution by hypochlorites. They found that sulphur and sulphate are formed as end-products in quantities depending upon the concentration of the reactants, the temperature and hydrogen ion concentration of the reaction medium. High sulphide concentrations increase the formation of sulphur and high hypochlorite concentrations increase the sulphate formation. An increase in temperature increases the sulphate formation, while there is a distinct minimum in the production of sulphate in the region of a pH of 10 with increased sulphate formation at values above and below this point.

A patent by I. G. Farbenindustrie (3) describes a process of treating a nickel-copper or a cobalt-copper matte by aqueous hydrochloric acid, where the sulphur content of the matte is less than one third and more than one fifth of the copper content. With this sulphur content a high amount of nickel or cobalt and too small amount of copper passes into solution and therefore a good separation of nickel or cobalt and copper is obtained.

Another early patent by I. G. Farbenindustrie (4) describes a process for the separation of nickel from copper contained in nickel-copper matte. It is done by treating the said matte with copper chloride solution, forming nickel chloride and cuprous chloride, according to the reactions:

$$Ni + 2CuCl_2 = 2CuCl + NiCl_2 \quad (1.1)$$

$$Cu + 2CuCl_2 = 2CuCl \quad (1.2)$$

One part of the nickel chloride - cuprous chloride solution is employed for the treatment of further amounts of nickel-copper matte where all the copper precipitates by the action of nickel in the matte, according to the reaction:

$$Ni + 2CuCl = NiCl_2 + 2Cu \quad (1.3)$$

From the solution of nickel chloride thus obtained, nickel is electrolytically deposited while the chlorine released is used to convert cuprous chloride in the other part of the solution into cupric chloride necessary for the treatment of further amounts of nickel-copper matte.

In the early 1950's, we meet the first industrial application of hydrometallurgical extraction of nickel from nickel sulphide concentrate. Three big plants were built by Sherrit Gordon, National Lead and Howe Sound (5). National Lead and Howe Sound leach with sulphuric acid, while Sherrit Gordon uses ammonia.

Several workers (6), (7), (8), (9) and (10) have studied the chemistry of the oxidation of iron sulphide in neutral and acid solutions. The principal reactions of interest are approximated by the following equations:

$$FeS + 2O_2 = FeSO_4 \quad (1.4)$$

$$4FeSO_4 + 2H_2SO_4 + O_2 = 2Fe_2(SO_4)_3 + 2H_2O \quad (1.5)$$

$$Fe_2(SO_4)_3 + H_2O = Fe_2O_3 + 3H_2SO_4 \quad (1.6)$$

$$6FeSO_4 + 11/2O_2 = 2Fe_2(SO_4)_3 + Fe_2O_3 \quad (1.7)$$

$$FeS + H_2SO_4 = FeSO_4 + H_2S \quad (1.8)$$

$$2H_2S + O_2 = 2H_2O + 2S^o \quad (1.9)$$

$$H_2S + Fe_2(SO_4)_3 = 2FeSO_4 + H_2SO_4 + S^o \quad (1.10)$$

A kinetic study of the oxidation of pyrite in aqueous suspention by molecular oxygen is described by McKay and Halpern (11). The overall rate of oxidation is proportional to the pyrite surface area and to the oxygen partial pressure, and is independent of the composition of the solution. However, the latter is important in determining the destribution of products. High temperatures and low acidities favour the formation of sulphuric acid, while the opposite conditions are conducive to the production of elemental sulphur.

Some characteristics of the oxidative leaching of nickel mattes were given by Khudyakov and Yaroslavtsev (12). They suggested that the oxidation of the sulphur of the sulphides takes stepwise. The stability of the form of sulphur depends on the pH of the solution, the oxygen partial pressure and the temperature. The sulphate ions have a catalytic effect on the oxidation of the sulphides. Sulphides having a small value of negative electrochemical potential dissolve more easily than the sulphides having positive electrochemical potential. So, sulphides increase in solubility in this order: FeS, MnS, ZnS, CoS, Ni_3S_2, PbS, FeS_2, CuS. A kinetic difficulty, arising from the existence of more than one stage of oxidation of many complex ions of sulphur, leads to the preferential oxidation of the simplest sulphides.

The chemistry of the acid autoclave leaching of the monosulphides of nickel, cobalt and iron was determined by their thermodynamic properties by Dobrokhotov (13). With sulphuric acid, at 115^{o}C, in the absence of air, only iron sulphide dissolved. The admission of oxygen led to a vigorous oxidation of the ferrous sulphate and a dissolving of the nickel and cobalt sulphides. The absence of ferric sulphate ions in the initial periods of oxidative leaching and the peculiar change in the ferric sulphate concentration during processing both indicated that the oxidation of sulphide ions goes mainly with involvement of the iron ions. As a result, he suggested, that the general reaction involved in the oxidative leaching of sulphides were the following:-

$$S^{2-} + 2Fe^{3+} = S^{o} + 2Fe^{2+} \quad (1.11)$$

$$S^{o} + 4H_2O + 6Fe^{3+} = SO_4^{2-} + 8\,H^{+} + 6Fe^{2+} \quad (1.12)$$

$$S^{2-} + 4H_2O + 8Fe^{3+} = SO_4^{2-} + 8H^{+}\ 8Fe^{++} \quad (1.13)$$

$$4Fe^{2+} + 4H^{+} + O_2 = 4Fe^{3+} + 2H_2O \quad (1.14)$$

Since sulphuric acid, for economical reasons, is the most common reagent in the acid leaching of sulphides, a lot of studies and patents have appeared dealing with the sulphuric acid leaching of nickel sulphides.

A patent by McGauley (14) describes a process for treating copper-bearing minerals containing iron, nickel, cobalt sulphides. The process employs two-step leaching, an acidic leaching followed by a neutralizing leach. Oxidation is employed in each. The acidic leach takes place in the presence of ferric sulphate to obtain a solution of the sulphates of the metals. During the neutralizing leaching, ammonia is introduced in the solution in sufficient amount to convert the iron first into insoluble ferric hydroxide. Further addition of ammonium sulphate and ammonia converts nickel and cobalt into insoluble ammonium sulphate double salts, but any copper sulphate remains dissolved.

Several plants, (15), (16), use methods for separating metal values from a nickel sulphide ore concentrate, containing sulphides of nickel, cobalt, copper, iron and precious metals, together with gangue materials. The concentrate is smelted to form a matte which is subjected to the action of aqueous sulphuric acid to obtain an aqueous sulphate solution containing nickel, cobalt, and iron and a residue containing substantially all the copper and precious contents of the matte.

The composition of various Cu-Ni mattes and their hydrometallurgical treatment was studied by Govorov (17). Experiments with two-stage counter

current leaching of mattes with sulphuric acid showed that iron can be extracted as ferrous sulphate in a neutral solution containing non-ferrous and associated metals; nickel, cobalt and residual iron can be extracted from the residue with fresh sulphuric acid solution; copper and other metals remain in the second residue; and 70% of sulphur is evolved as hydrogen sulphide during the first leaching. Good separation was possible only with mattes in which the ratio iron:nickel is greater than 3.5 and the sulphur and magnetite content is lower than 29 and 2% respectively.

Dobrokhotov and Onuchkina (18) leached iron and sulphur-rich nickel concentrates under pressure. The amounts of nickel and cobalt extracted increased with time; but although the ferrous and ferric concentrations in the solution increased initially, they then dropped, due to hydrolysis. Enough acid was produced to maintain a pH of 1-1.5. At 15 atm oxygen partial pressure and at 115^{o}-120^{o}C the dissolution was complete within four hours, leaving a residue of almost pure sulphur.

Further kinetic studies of the autoclave leaching of cobalt concentrated matte were carried out by Dobrokhotov and Maiorova (19). The research was carried out with samples of industrial material containing 22.8% nickel, 5.02% cobalt, 1.0% copper, 44% iron and 27.1% sulphur. They found that an increase in the acidity of the solution increased the rate of nickel and cobalt dissolution and the rate of sulphur oxidation to an elemental state. An increase in acidity was most effective up to a sulphuric acid concentration of 0.02 mole per litre. A further increase of the acid content, slightly increasing the rate of nickel and cobalt dissolution, markedly increased only the yield of elemental sulphur. The latter contributed to the formation of a sulphur alloy which finally led to a drop in nickel and cobalt extraction. With thin layers of this alloy corresponding to the dimensions of the ground material, the rate of dissolution for the matte components was proportional to square root of the oxygen pressure. Increasing the temperature accelerated leaching. Calculating the apparent activation energy, provided the following results:

Dissolution of nickel: E_{Ni} = 4.20 Kcal/mole

Dissolution of cobalt: E_{Co} = 3.00 Kcal/mole

Oxidizing sulphide sulphur to sulphate: E = 5.00 Kcal/mole

Oxidizing sulphide sulphur to elemental: E = 4.48 Kcal/mole

The low E values, underscored the overall diffusion character of the rate determining process. The rate of matte dissolution in moderately acid media, expressed in nickel terms, can be written in the following approximate equation:

$$K_{Ni} = \frac{d(Ni)}{dt} = 0.0967(3.5 + C_{H_2SO_4}).P_{O_2}^{0.5} \cdot e^{-2115/T} \cdot Re^{0.60}$$

where Re = Reynolds number

When there was a reduction of partical dimension and an increase of stirring speed the kinetic indexes of the process improved markedly.

A hydrometallurgical separation of metallized copper-nickel converter matte was described by Maslenitskii and Zverevich (20). In this matte the copper was represented by sulphides like Cu_2S and the nickel by the metallic phase. After thirty hours of leaching in a synthesized analyte containing: 30-35 nickel, 30 sulphuric acid, 100 sodium sulphate and 15 grams per litre boric acid, the leaching residue contained 72.46% copper and 3.14% nickel.

Another method of autoclave treatment of intermediate products from the flotation separations of converter matte, based on the greater solubility of nickel sulphide over that of copper sulphide, was proposed by Maslenitskii and Chugaev (21). Experiments with mattes with a copper:nickel ratio in the region 1.3:1 at temperatures between 130° and 150°C for 1 hour showed that up

to 50% of the nickel can pass into solution without dissolving large amounts of copper. Because a more thorough nickel recovery was accompanied by substantial copper passage into solution, the matte was treated in a two-stage counter current leaching system. The starting intermediate product was treated with a solution, obtained during the second leaching stage and containing copper and nickel sulphates. In the second stage a fresh solution was used to treat the solid deposit from the previous decoppering.

A patent for leaching nickel and associated non-ferrous metal values from a high grade nickel matte was described by Mackiw et al (22). The matte was mixed with sulphuric acid forming a slurry the total amount of sulphur in which was the stoichiometric amount required to combine with the non ferrous metals as sulphates; the slurry was subjected to a first stage leach at 120°C with an oxygen pressure of about 10 psi and a pH between 3.5 and 5.5. The first stage residue was subjected to a second stage leach at a temperature above 120°C and under a partial oxygen pressure above about 10 psi. The solutions from the first and second stage after removing copper and iron were treated for recovery of pure nickel and cobalt. The residue from the second leach stage contained all the precious metals.

Klyueva (23) measured the solubility of oxygen in sulphuric acid at elevated temperatures, and the effect of sulphides on the solubility. High oxygen pressures and low temperatures favoured the solubility. In the presence of sulfides in the solution, the solubility of oxygen decreased. At high temperatures the oxygen solubility decreased as the sulphide solubility increased

The extraction of nickel from a New Caledonian garnierite ore in sulphuric acid of several concentrates, under oxygen partial pressure of 5 and 10 atm was studied by Tankiuchi Kentaro (24). He found that in 5% sulphuric acid solution, oxygen promotes the extraction of nickel and depresses the dissolution of iron. The nickel recoveries at 215°C under atmospheric

air and oxygen partialpressures of 5 and 10 atm were 89.2, 92.5 and 96.3% respectively. In 15 and 20% sulphuric acid solutions the effects of oxygen in the nickel extraction and on the depression of iron dissolution were small.

Solutions containing hydrochloric acid, chlorides or chlorine have been used by many investigators in the leaching of nickel sulphides.

The reaction of acid chlorine solution with soluble sulphide ions has been studied out by several workers (2), (25), (26), (27). Sulphate and elemental sulphur were found as end products, the latter being favoured by the presence of a low concentration of oxidant relative to that of sulphide.

Of direct bearing on the matter discussed are an early American patent (28) and an Australian patent (29). The former advocates stirring powdered ore with an aqueous solution of ferric chloride, chlorine oxides and chlorine. In the latter it is claimed that both metal and sulphur can be obtained by electrolysis, in a diaphragm cell, of a metal ore slurry in brine. It was suggested by Sherman and Strickland (27) that the dissolution of pyrite ores in acid chlorine solution is transport-controlled, while only sulphate is produced as end-product.

Jackson and Strickland (30) determined the rates of reaction and the products of the reaction between acid chlorine water and the more common sulphide minerals. With the exception of galena, the kinetics were transport-controlled. The two iron minerals FeS and FeS_2 gave only sulphate (fig. 1). The presence of iron, as a hydrated and chloride complexed ferric ion was the only factor common to the surface of pyrrhotite, pyrite, and arsenopyrite during the reaction with chlorine.

Sericov and Orlova (31) studied the salt leaching of products of copper-nickel production. Materials investigated were nickel powder, nickel,

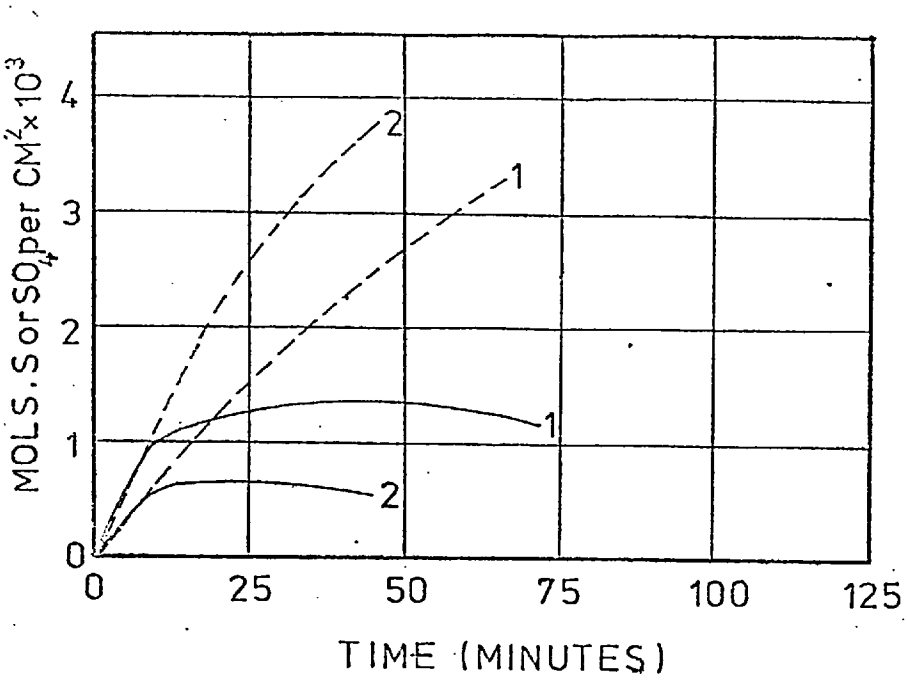

FIG. 1. Rate of Sulphur and Sulphate Production from Pyrrhotite.
Full line sulphur; dotted line, sulphate. Curve 1, 25°C pH 1.0; chlorine concentration 12.9×10^{-3}M
Curve 2, 25°C, pH 0.41; chlorine concentration 17.8×10^{-3}M
(Jackson and Strickland)

copper and iron sulphides and a magnetic fraction of intermediate matte in aqueous solution of copper, nickel and salts. The best solvents for nickel sulphide were cupric chloride which extracted 94% of nickel after two hours at 130°C and ferric chloride which showed similar extraction at 150°C. The copper sulphide dissolved in cupric chloride and ferric chloride solution but solutions had to be made at low temperatures; the iron sulphide dissolved in copper and nickel salts and the best solvent was cupric chloride at about 230°C.

Tseft and Kryukova (32) leached mattes containing 58% iron, 20% sulphur and 20% nickel with ferric chloride and hydrochloric acid solutions;

the nickel was readily extracted in 0.5M ferric chloride at the boiling point of the solution. Ferric chloride was preferred as an oxidizing agent, since it fixed the sulphide as sulphur, with less than 2% as sulphate. They found that increasing the temperature from room temperature to boiling point increased the extraction by a factor of 3; and that 15-25% excess oxidant gave the best extractions. They suggested the following reactions may take place:

$$FeS + 2HCl = FeCl_2 + H_2S \quad (1.15)$$

$$Fe + 2HCl = FeCl_2 + H_2 \quad (1.16)$$

$$Ni_3S + 6HCl = 3NiCl_2 + 2H_2S + H_2 \quad (1.17)$$

$$CoS + 2HCl = CoCl_2 + H_2S \quad (1.18)$$

$$FeS + NiCl_2 = FeCl_2 + NiS \quad (1.19)$$

$$Fe + NiCl_2 = FeCl_2 + Ni \quad (1.20)$$

$$CoS + NiCl_2 = CoCl_2 + NiS \quad (1.21)$$

$$MeS + 2FeCl_3 = MeCl_2 + 2FeCl_2 + S \quad (1.22)$$

A hydrometallurgical method for processing Ni matte with complex extraction of the components nickel, cobalt, iron and sulphur was investigated by Kryukova (33). The process of leaching the matte with ferrous chloride in hydrochloric acid and the effects of temperature, duration of leaching and concentration of the reagents were studied. Nickel and cobalt can be separated from the solution by treating it with matte and hydrogen sulphide and iron by electrolytic precipitation .

Kryukova and Tseft (34) studied the kinetics of dissolving metallic nickel and iron with hydrochloric acid and iron chloride solutions. The dissolution rate of iron in hydrochloric acid solutions was 30 times that of nickel. The apparent activation energies were 16.6 for nickel dissolution

and 13.0 Kcal/mole for iron dissolution. The dissolution rates of nickel and iron in ferric chloride were almost equal and were more than 100 times those in hydrochloric acid. Apparent activation energies were 3.2 Kcal/mole for both iron and nickel dissolution. A comparison of the activation energies and the temperature coefficients for both iron and nickel dissolution showed that dissolution in hydrochloric acid takes place in the chemically controlled region, while dissolution in ferric chloride occurs in the diffusion controlled region.

A method was studied by Klets and Serikov (35) for bulk autoclave and non autoclave leaching of sulphide complex ore in salts with ferric chloride. The temperature effect was studied at temperatures between 20^{o} and $80^{o}C$ and at each temperature the effects of leaching duration and of oxidant concentration were shown. They found that temperature was the main controlling factor of the leaching rate, while oxidant amount did not play an essential role. With an eight hour experiment cycle and an oxidant amount 1.0 and 0.7 times the theoretical required metal recovery was copper 93, nickel 92 and 95, cobalt 90.1 and 91.7 and iron 71.5 and 84.4% respectively, while sulphur and a large part of the platinum group metals remained in the precipate.

The general effect of various physico-chemical factors on dissolution of sulphides contained in minerals, concentrates and mattes was studied by Tseft and Serikov (36). For acid leaching of sulphides they found that the dependence of the dissolution rate of sulphides of certain metals was more complex than purely diffusion or kinetic leaching. From a study of the physico-chemical foundation of salt exchange decomposition it was concluded that by using a copper salt it is possible to extract nickel, cobalt and iron from copper-nickel concentrates by means of autoclave dissolution. The concentration of sulphur ion in the case of salt dissolution can be decreased

by varying the electrochemical potential, as a result of which copper can be extracted with other non-ferrous metals and trace elements from sulphides.

Kryukova and Tseft (37) studied the leaching of nickel and iron powders and finely ground nickel matte in 1.0m ferric chloride solution in the temperature range 22°-78°C. The interaction rate of metallic nickel and iron and fine matte was about the same: 0.85, 0.95 and 1.0 mg/sq.cm./min respectively, while the temperature coefficient in the investigated temperature range was 1.2-1.3. Granulated nickel matte was leached at 22°-109°C, with a solution containing ferric ions 100 and ferrous ions 50 gm/lit; at lower temperatures the leaching rate was too slow, while at 109°C with 16% excess ferric chloride after 1 hour the leached amounts were: nickel 98, cobalt 98.7 and iron 91.5%.

Gerbatenko and Gogolinshaya (38) studied the conditions of autoclave free single-stage periodic and three-stage counter current leaching of nickel matte with hydrochloric acid. It was found that temperature was the main controlling factor; by increasing the temperature from 20° to 90°C the nickel extraction was increased three-fold at 15 minutes and two-fold at 120 minutes. At 70°-100°C during 1-2 hours and with 4-5% hydrochloric acid excess, the following extractions were achieved: nickel 97.2-97.8%, cobalt 99.75-99.5% and iron 99.3-99.5%.

According to another method (39), finely ground nickel-cobalt raw oxides, roasted mattes, or speiss were attacked in two stages by aqueous hydrochloric acid, first with 10 and then with 100 gm/lit., both for two hours at 95°C. The metal concentration and the yields respectively were cobalt 44-80, 97.30-99.10; nickel 13-60, 96.60-98.60; iron 21-50, 87.5-100; arsenic 8-39, 72.60-98.10; and copper 9 gm/lit., 84%. Precious metals and the last 1-10% of the nickel and cobalt may be recovered if they are subjected to an additional roast and subsequent treatment. Hydrochloric acid under oxygen pressure is an attractive method of attack of complex

materials such as speiss and various residues, since it permits the elimination of arsenic, iron, chromium and aluminium as insoluble arsenates. Precipitated precious metals may be recovered from the arsenate precipitation.

Mayor et al (40) developed a process for the recovery of nickel from a material containing nickel and optionally copper by treating it with an aqueous solution of cupric chloride and a chloride selected from the group consisting of alkali metal chlorides and alkaline earth metal chlorides. The cupric chloride can be converted into insoluble copper hydroxychloride by using an oxidant such as air to act upon the solution. Copper hydroxychloride can be dissolved after separation in hydrochloric acid resulting in the reproduction of cupric chloride. Nickel is recovered from the copper free solutions by cementation with iron. Therefore the separation treatment is based on the following reactions:

$$2\,CuCl_2 + Ni = NiCl_2 + 2CuCl \qquad (1.23)$$

$$2CuCl + H_2O + \tfrac{1}{2}O_2 = CuCl_2Cu(OH)_2 \qquad (1.24)$$

$$CuCl_2Cu(OH)_2 + 2HCl = 2CuCl_2 + 2H_2O \qquad (1.25)$$

the sum of which is

$$Ni + \tfrac{1}{2}O_2 + 2HCl = NiCl_2 + H_2O \qquad (1.26)$$

Ingraham et al (41) studied the leaching of pyrrhotite with hydrochloric acid. It was found that when non-stoichiometric pyrrhotite is leached under non-oxidizing conditions, both hydrogen sulphide and elemental sulphur are formed according to the reaction:

$$Fe_7S_8 + 14HCl = 7Fe^{2+} + 14Cl^- + 7H_2S + S \qquad (1.27)$$

The amount of sulphur is proportional to the non-stoichiometry of the pyrrhotite. Pyrrhotite leaching in hydrochloric acid is rapid but, when minimum conditions of acidity and/or temperature are not met, the sulphur

coating becomes protective and the reaction ceases. Fig. 2 delineates a shaded plateau, which represents complete dissolution of the sample and its boundaries show the conditions required for achieving complete dissolution.

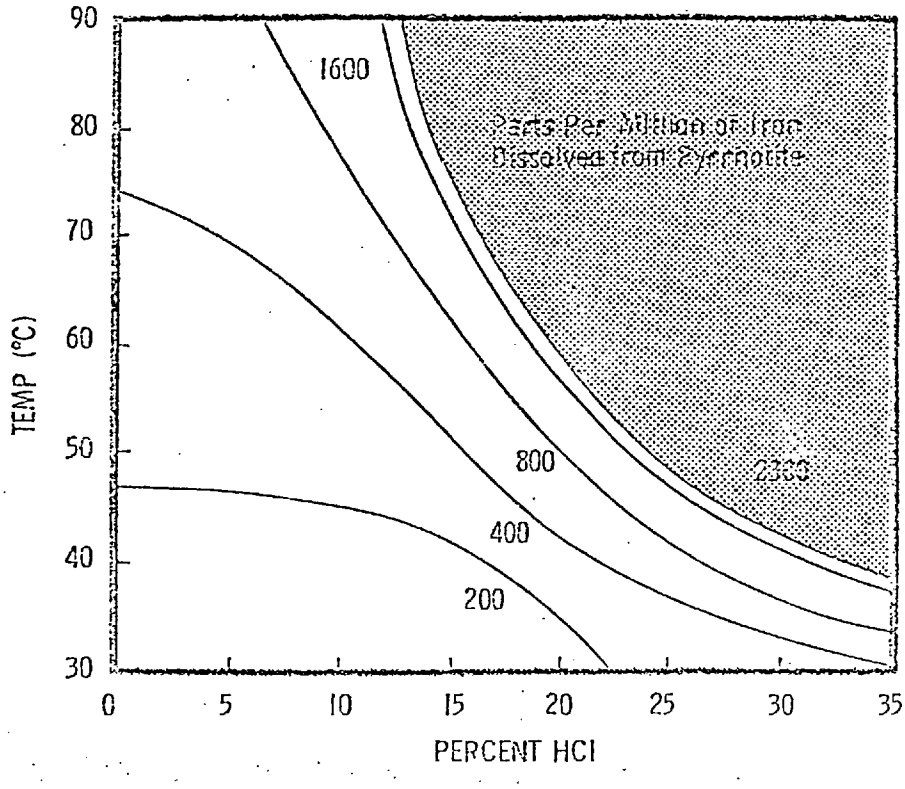

FIG. 2. Effect of Initial Starting Conditions on the Amount of Iron Dissolved before the Reaction is Stopped by an Impermeable Sulphur Coating (Ingraham et al)

Subramanian et al (42) studied the hydrometallurgical processing of pyrrhotite. They found that leaching in ferric sulphate solution and regeneration of the leachant are both too slow to be considered for practical process. Ferric chloride solution is a rapid leachant and its regeneration is simple. However, other impurities dissolve along with iron, the removal of which might be a difficult operation. Leaching in non-oxidizing media

such as hydrochloric acid or sulphuric acid can achieve the selective dissolution of iron under suitable conditions. Oxygen pressure leaching results in an iron oxide product carrying most of the copper and all the lead, together with a considerable amount of sulphur.

They suggested two feasible processes for the recovery of elemental sulphur, iron oxide and non-ferrous metals from pyrite. The first step in both processes is thermal decomposition of pyrite yielding sulphur and pyrrhotite. This material may be subjected to an oxygen pressure leaching to yield sulphur and an iron oxide from which non-ferrous metals could be removed and recovered by chlorination. In the other process pyrrhotite may be activated by treatment with hydrogen, iron powder or a mixture of iron oxide and carbon, and in the activated state reacted with dilute sulphuric acid. The non-ferrous metals remain as a residue with low iron concentration, while sulphur is recovered from the evolved hydrogen sulphides.

The Falconbridge matte leach process (43) is based on the following principles. When finely divided copper-nickel converted matte is treated with strong hydrochloric acid, the nickel is selectively dissolved, leaving copper and platinum metals as an insoluble sulphide residue. Thus, a good separation between copper and nickel is obtained. Because the solubility of nickel chloride in pregnant solution decreases with increasing hydrochloric acid concentrations, the nickel chloride can be precipitated from the solution by increasing, rather than by neutralizing the acidity of the solution. Conversion of the nickel sulphide to metal can be then effected either by electrowinning from dissolved crystals, or by hydrogen reduction of oxide obtained by high temperature hydrolysis of the chloride.

Van Weert et al (44) studied the hydrochloric acid leaching of nickeliferous pyrrhotites from the Sudbury District. It was found that substantially complete leaching of iron from these pyrrhotites can be achieved using only 10-50% excess hydrochloric acid, while pentlandite remained insoluble. Hydrogen sulphide and elemental sulphur as products account for

up to 83% and 15% of the contained sulphur respectively. The rates of iron and nickel dissolution increase with the rate of acid addition. Magnetite contained in the concentrate dissolves preferentially to the pyrrhotite at low acid concentrations, resulting in the formation of ferric ions in batch leaching solutions, according to the reaction:

$$Fe_3O_4 + 8HCl = FeCl_2 + 2FeCl_3 + 4H_2O \quad (1.27)$$

The appearance of ferric ions in the solution gives rise to an instantaneous increase of the redox potential of the solutions which cause a temporary inhibition of hydrogen sulphide evolution.

The subsequent reduction of the ferric ion is brought about slowly either by pyrrhotite, according to reaction 1.28 or indirectly by hydrogen sulphide (1.30), which is generated by acid leaching of the pyrrhotite according to the intermediate reaction (1.29).

$$Fe_7S_8 + 14FeCl_3 = 21FeCl_2 + 8S \quad (1.28)$$

$$Fe_7S_8 + 16\ HCl = 5FeCl_2 + 2FeCl_3 + 8H_2S \quad (1.29)$$

$$H_2S + 2FeCl_3 = 2FeCl_2 + 2HCl + S \quad (1.30)$$

As the rate of decrease in redox potential is dependent on the hydrochloric acid concentration, reaction (1.29) appears to be dominant, from which it follows that the reduction of the ferric ion is brought about indirectly by the hydrogen sulphide in this system.

Because nitric acid is costly and the reactions with sulphides are difficult to control, especially in so far as NO_2 production is concerned, industrial application for recovery of metals has been substantially zero, although a few processes have been described.

Joseph (45) extracted nickel and copper with a dilute solution of nitric acid. Pazdnikov and Pavlyuk (46) described a method for processing cobalt-nickel mattes by oxidizing and dissolving them in a mixture of nitric and sulphuric acids. The process was represented by the following basic reactions:

$$2MeS + 2H_2SO_4 + 2HNO_3 = 2MeSO_4 + N_2O_3 + 3H_2O + 2S \quad (1.31)$$

$$4FeS + 6H_2SO_4 + 6HNO_3 = 2Fe_2(SO_4)_3 + 3N_2O_3 + 9H_2O + 4S \quad (1.32)$$

$$2S + 6HNO_3 = 2H_2SO_4 + 3N_2O_3 + H_2O \quad (1.33)$$

The extraction for cobalt and nickel was about 96-98%.

The mechanism of wet oxidation of natural pyrrhotite and decomposed pyrite catalysed by nitric acid was studied by Bjorling and Kolta (47). They found that the iron sulphide reacts rapidly at temperatures above 80°C and the temperature should be kept below the melting point of sulphur. It was suggested that the oxidation of sulphides is not dependent on high oxygen pressure or on high temperature as mentioned by some other authors (8), (11). Higher rates of reaction can be achieved by having the pH as low as 0.3, while high pH (up to 1.9) favours more complete hydrolysis of ferric nitrate and less formation of sulphate. The leaching of natural pyrrhotite did not differ much from that of the pyrrhotite prepared from the thermal decomposition of pyrite.

A French patent (48) describes the recovery of nickel and other secondary metals from nickel mattes. The nickel sulphide concentrate, after being dispersed or put in suspension is leached under oxidizing conditions with nitric acid, preferably in the presence of an oxygen containing gas. The nitrous gas generated being constantly reconverted to nitric acid and recycled, while the resulting salt solution is denitrified in a sulphatation phase, so that

the final solution contains sulphates of nickel as well as secondary metals, e. g. iron, copper, cobalt. The latter were separated so that the final pure nickel sulphate can be recovered by fractional crystalization.

A similar method was studied by Kmetova (49). Sulphide concentrates of non-ferrous metals were leached and oxidized for sometime in nitric acid solutions. Under properly selected conditions, soluble salts of non-ferrous metals were formed and separated from elemental sulphur and iron hydroxide which were concentrated in the insoluble residue. The oxides of nitrogen which form were oxidized to nitric acid by the oxygen of the air. The optimum temperature for the dissolution reaction process was $90^{o}C$.

The dissolution of nickel in nitric acid was also studied by Petrachkov et al (50). They suggested that nickel dissolves in nitric acid according to the reaction:

$$4Ni + 10HNO_3 = 4Ni(NO_3)_2 + NH_4NO_3 + 3H_2O \qquad (1.34)$$

If the ammonium nitrate concentration is more than 70 gr./lit., there is a limiting effect of it in the reaction. They suggested a continuous process for solution of nickel in a circulating mixture of nitric acid, nickel nitrate ($Ni(NO_3)_2$) and ammonium nitrate (NH_4NO_3) without the concentration of ammonium nitrate building up continuously to reach a limiting value.

A millerite (NiS) concentrate containing amounts of cobalt, copper, iron and zinc was dissolved by Gardon and Bozec (51), to give a solution containing nickel sulphate and nickel nitrate. It was then diluted, potassium sulphate added and extracted with Bu_3PO_4 to remove NO_3^-. The solution was then neutralized with $Ca(OH)_2$ and treated with $NiCO_3$ to precipitate copper and iron.

A major constituent of the copper-nickel mattes is heazlewoodite (Ni_3S_2). From this point of view its behaviour during the acid leaching has been examined by several authors.

Chugaev (52) studied the oxidative dissolution of Ni_3S_2 at elevated temperatures and oxygen pressures. The dissolution of Ni_3S_2 in sulphuric acid at temperatures between 100 and 150°C and at oxygen pressures between zero and 45 atm produces an intermediate product, the monosulphide NiS. The dissolution can be described by the following reactions:

$$Ni_3S_2 + H_2SO_4 + \tfrac{1}{2}O_2 = 2NiS + NiSO_4 + H_2O \qquad (1.35)$$

$$NiS + 2O_2 = NiSO_4 \qquad (1.36)$$

Results of the kinetic experiments on the study of the effect of acidity on the rate of dissolution of the sulphide showed that the maximum rate of dissolution is at low acid concentrations. Raising the acidity of the solution above 3-6 gm/lit significantly lowers the rate.

Oxygen pressures above 8 atm retard reaction 1.35 which forms monosulphide and higher pressures equalize the rates of reactions 1.35 and 1.36. Under these conditions the dissolution can be described by the following reaction:

$$Ni_3S_2 + H_2SO_4 + 4.5O_2 = 3NiSO_4 + H_2O \qquad (1.37)$$

Using the rotating disc method Khydyakov and Smirnov (53) compared the dissolution rate of Ni_3S_2 with that of the binary sulphide, $(FeS)_2Ni_3S_2$, during the acid oxidation autoclave leaching at temperatures between 100° and 200°C. It was found that the rate of dissolution of nickel from the Ni_3S_2 was faster than the rate for the binary sulphide. This was due to the

oxidation of the bivalent iron to trivalent and hydrolysis of the latter on the disc surface, creating diffusion resistance. Increases of the acid content in the solution had a favourable effect on the nickel passed to solution and an unfavourable effect on iron hydrolysis; a temperature increase favourably influenced both of these processes. In selecting optimum leaching conditions for cobalt-nickel mattes their composition has to be taken into consideration. They suggested that it is desirable to have metallized mattes with low sulphur contents (12-15%) and less iron. Then the process of autoclave leaching can be conducted at high temperatures and good separation of the deposit from the solution obtained.

Chugaev (54), (55) investigated the interaction of copper-nickel mattes with copper sulphate solution at various temperatures and oxygen pressures. During this interaction, hydrolytic precipitation of copper and step-wise oxidation of sulphur takes place. Examining the oxidation of Cu_2S in aqueous solution of copper sulphate, it is evident that the process of oxidation takes place by step-wise rising of the valency of copper in the lattice of the sulphide with subsequent oxidation of sulphur to sulphate. Intermediate phases Cu_9S_5 and CuS are formed. The peculiarity of copper-nickel matte oxidation is the progressive oxidation of Ni_3S_2 and Cu_2S.

The interaction of Ni_3S_2 with copper sulphate in the absence of oxygen leads to the formation of Cu_2S, CuS, NiS films which prevent the process. Presence of oxygen pressure accelerates the reaction and favours the hydrolysis of copper in the form of basic salts. The acid liberated during the hydrolysis reacts with Ni_3S_2. Chugaev suggested that the dissolution occurred via these two reactions:

$$Ni_3S_2 + 2CuSO_4 = Cu_2S + 2NiSO_4 + NiS \qquad (1.38)$$

$$NiS + CuSO_4 = CuS + NiSO_4 \qquad (1.39)$$

Gerlach et al (56) studied the acid pressure leaching of both Ni_3S_2 and NiS and the dependence of the rate of the reaction on the sulphuric acid initial concentration, oxygen partial pressure, temperature and the solid material surface. The leaching rate goes through a maximum which is at a sulphuric acid initial concentration of about 60 gr./lit. The effect of oxygen partial pressure on the rates of dissolution of nickel and the formation of sulphate is shown in fig. 3. A proportionality was also

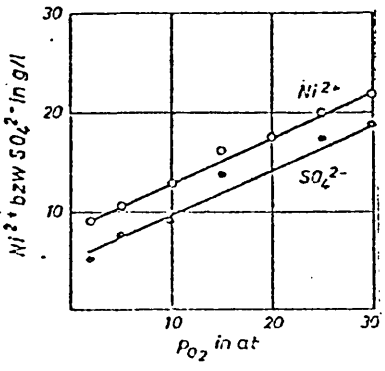

FIG. 3 Quantity of Nickel Extracted of Sulphate formed from Ni_3S_2. Temperature 90°C leaching time 60 mins. (Gerlach et al)

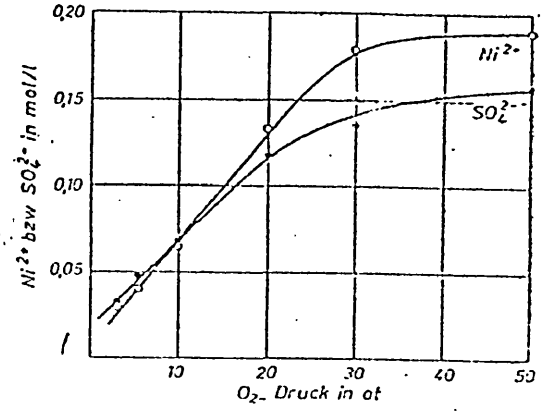

FIG. 4 Pressure Dependence of Nickel Extraction or Sulphate Formation from NiS. Temperature 90°C oxygen pressure 10 atm leaching time 90 mins. (Gerlach et al)

obtained for the dependence of the leaching rate on the solid material surface. The following equations were obtained for the dependence of the leaching on the temperature, at the same time taking into consideration the oxygen partial pressure and the surface:

$$\frac{d(Ni)}{dt} = 1.68.10^{-3}.p^{0.7}.F.\exp(-9350/RT) \quad \text{mol/lit/min}$$

$$\frac{d(SO_4^{2-})}{dt} = 1.58.10^{-2}.p^{0.74}.F.\exp(-11400/RT) \quad \text{mol/lit/min}$$

F = surface area of Ni_3S_2

In the leaching experiments with NiS, this solid could be identified in the form of millerite (β-NiS) and the high temperature modification (α-NiS). It was found that the rate of reaction was independent of the sulphuric acid initial concentration and of the addition of ferrous ions in the solution. The dependence of nickel and sulphate ion formation on the oxygen partial pressure shows a shape similar to an adsorption isotherm (Fig. 4). At pressures greater than 30 atm the reaction rate was independent of the oxygen partial pressure. A proportionality between the leaching rate and the specific surface can be assumed. Studying the effect of temperature in the range between 60° and 120°C, the following rate laws of nickel extraction from NiS were proposed:

$$\frac{d(Ni)}{dt} = 9.51.10^{-6}.p^{1.45}.F.\exp(-7080/RT) \quad \text{mol/lit/min.}$$

$$\frac{d(SO_4^{2-})}{dt} = 4.66.10^{-5}.p^{0.76}.F.\exp(-7080/RT) \quad \text{mol/lit/min}$$

F = surface area of NiS.

From their results it was suggested that the formation of nickel ions from Ni_3S_2, which is proportional to the rate of solution, takes place approximately four times as fast as those from NiS. The formation also of sulphate ions occurs in Ni_3S_2 leaching considerably more quickly than in the case of the solution of NiS. There was no evidence that a homogeneous covering layer of NiS on Ni_3S_2 formed, but Ni_3S_2 and NiS occur alongside

each other throughout the whole duration of pressure leaching. It was suggested that NiS forms a continuous partial covering of the Ni_3S_2 in the form of islands, which cover about 50% of the Ni_3S_2 surface.

They suggested that the sulphuric acid pressure leaching of Ni_3S_2 can be summarized in the following equations:-

$$Ni_3S_2 = Ni^{2+} + 2NiS \quad (1.40)$$

$$Ni_3S_2 + 4O_2 = 3Ni^{2+} + 2SO_4^{2-} \quad (1.41)$$

$$Ni_3S_2 + O_2 + 4H^+ = 3Ni^{2+} + 2S + H_2O \quad (1.42)$$

$$NiS + 2O_2 = Ni^{2+} + SO_4^{2-} \quad (1.43)$$

$$NiS + \tfrac{1}{2}O_2 + 2H^+ = Ni^{2+} + S + H_2O \quad (1.44)$$

During the leaching a constant ratio occurred between the oxidation products sulphur and sulphate. In the case of NiS at 90°C and 10 atm oxygen partial pressure approximately 100% of its sulphur is transformed into sulphate, while in the case of Ni_3S_2 under the same conditions 96% sulphate and 4% sulphur were formed.

Totlani and Balachandra (57) studied the effect of different parameters in the acid pressure leaching of copper and nickel sulphide concentrates and proposed the optimum conditions. They found that the nickel recovery increases with increase in oxygen partial pressure, showing a tendency to level off beyond 300 p.s.i.. 500 p.s.i. is likely to be the optimum oxygen pressure for continuous operations. On increasing leaching temperature to 113°C the nickel and copper recoveries both increase. Further increase in temperature lowers the metal recovery. So 110°-113°C is the optimum temperature for the leaching. The influence of sulphuric acid concentration was studied in the range of a mole ratio of H_2SO_4/Cu 0.74 to 1.01. Since nickel recovery decreased with increasing mole ratio of H_2SO_4/Cu, it was indicated that a mole ratio around 0.74 is the optimum one.

Llanos et al (58) studied the leaching behaviour of nickel-copper mattes having a wide range of copper and sulphur contents, in acidic copper sulphate solutions. They found that the time needed to leach these mattes is inversely proportional to the sulphur content in the matte, but almost insensitive to the matte nickel:copper ratio.

Contact of the matte with lixiviant causes a rapid dissolution of nickel due to cementation reaction:-

$$Ni^{o} + Cu^{2+} = Ni^{2+} + Cu^{o} \qquad (1.45)$$

Mattes high in copper and low in sulphur show an increase in the copper concentration during the early leaching stages, due to oxidation and dissolution of the metallic copper from the nickel alloy:

$$2Cu + \tfrac{1}{2}O_2 = Cu_2O \qquad (1.46)$$

$$Cu_2O + 4H^{+} + \tfrac{1}{2}O_2 = 2Cu^{++} + 2H_2O \qquad (1.47)$$

Reaction 1.46 and 1.47 are faster than reaction 1.45 during the first minutes of leaching, but reaction 1.47 decreases sharply as the solution pH reaches about 2.

In high sulphur mattes, most of the nickel is present as Ni_3S_2 and the dissolution has the form given in the reaction 1.35.

Aqueous copper also reacts with Ni_3S_2 in the absence of oxygen according to reaction 1.38 and in the presence of oxygen according to reaction:

$$Ni_3S_2 + 2Cu^{2+} + \tfrac{1}{2}O_2 = 2NiS + Ni^{2+} + Cu_2O \qquad (1.48)$$

The rate of nickel dissolution is controlled by the rate of cementation of copper on nickel during the first few minutes of the leaching. Then, until

a pH of 3.9 is attained, oxygen transfer between the gas and liquid phase controls the role of dissolution. At higher pH, hydrolysis of aqueous copper and subsequent precipitation of basic copper sulphate dictates the time required to attain a final pH of 5.3. The degree and the rate of this hydrolysis reaction are dependent on temperature.

$$3Cu^{2+} + 3SO_4^{2-} + 4H_2O = CuSO_4 2Cu(OH)_2 + 2HSO_4^- + 2H^+ \quad (1.49)$$

This hydrolysis becomes rate controlling above pH 3.9, particularly during leaching of low sulphur mattes.

Kelt (59) studied the ferric chloride leaching of Ni_3S_2 under various conditions. Her results are in agreement with the prior investigators. The Ni_3S_2 dissolves in three stages; initially only nickel is dissolved from the solid, this leads to the formation of NiS. During the second stage the Ni_3S_2 continues to be oxidized to NiS and the NiS dissolves with the formation of orthorhombic sulphur and a small amount of sulphate. The apparent activation energies calculated from these stages are similar and indicate a reaction rate controlled by a mixed regime. The rate of nickel dissolution during the final part of the reaction is slow and this stage is characterised by the proportion of sulphide oxidised to sulphate.

1.1.2 Acid Leaching of Pentlandite

A large part of the literature survey on pentlandite has been covered in the prior chapter in which the previous work on acid and salt leaching of nickel and iron sulphide concentrates was examined. In this chapter the work of some investigators who have studied the leaching behaviour of pentlandite is dealt with in more detail.

The oxidation leaching of natural sulphides has been studied since very early in the century (60). Sundefur (61) studied the geology and paragenesis of a nickel deposit near Goward in Ontario. Two types of

pentlandite were present - (1) smooth, nearly white, flame lite streamers extending through pyrrhotite; (2) pinkish yellow, rough fractured massive mineral. What is interesting is that along these fractures the latter pentlandite is altered readily to the secondary nickel sulphide violarite ($FeNi_2S_4$). Violarite only rarely replaces the thin stringers of light-coloured pentlandite within the pyrrhotite. Along contacts between pyrrhotite and pentlandite, the violarite may replace both minerals.

The supergene alteration of pentlandite to violarite was also confirmed later by Dennen (62).

The oxidation of primary nickel sulphides was also studied by Michener and Yates (63), and the conclusions they reached are in agreement with those of prior investigators. They found that the first sign of alteration is the development of violarite along cleavage cracks of the pentlandite. Towards the completion of this stage the pyrrhotite begins to develop cracks in which limonite is deposited. At this point the pentlandite is all replaced by violarite, which then starts to leach out. By the time pyrrhotite is half oxidized the violarite (and pentlandite) is practically all removed by dissolution. Up to this point chalcopyrite has remained unaltered and is the last of the three sulphides to be attacked. The final product is limonite and millerite. Limonite is practically free of nickel and with very little copper.

It was found by Lopez and Schulze (64) that the replacement of pentlandite by siegenite $(Ni, Co)_2$ $(Fe, Ni, Co)S_4$ was consistent with a constant sulphur content, a loss of 15.1% in metal and a reduction of 16% in volume. They proposed the following reaction for the alteration of pentlandite to siegenite:

$$(Fe_{2.25}Ni_{2.5}Co_{3.5})S_8 = 2(Fe_{0.5}Ni_{1.25}Co_{1.25})S_4 + 1.25\ Fe + Co \qquad (1.50)$$

The alteration of pentlandite to siegenite is not a replacement 'volume by volume', which is frequently related to metasomatism, but it is fundamentally a chemical replacement and the reduction of volume is a natural effect on this.

Nickel et al (65) studied the supergene alteration of a pyrrhotite-pentlandite deposit at Kambalda, Western Australia. In the transition zone, pentlandite is replaced by violarite, accompanied by a release of iron and nickel. The latter reacts with pyrrhotite to give another type of violarite. The two reactions represented by the following equations:

$$Fe_{1.4}Ni_{4.9}S_{8.0} = Fe_{2.6}Ni_{3.8}S_{8.0} + 1.1Ni^{2+} + 1.5Fe^{2+} + 5.2e^{-} \quad (1.51)$$

(pentlandite) (violarite)

$$0.33Fe_{7}S_{8} + 11Ni^{2+} = 0.33Fe_{3.0}Ni_{3.3}S_{8.0} + 1.32Fe^{2+} + 0.44e^{-} \quad (1.52)$$

(pyrrhotite) (violarite)

After pentlandite has been totally replaced, pyrrhotite is dissolved and together with some nickel and sulphur species deriving from the oxide zone, redeposits as nickel-rich pyrite. At the base of the oxide zone, which coincides approximately with the water table, violarite appears to be unstable and is replaced by nickel carbonates and iron oxides.

The diagramatic representation of the principal reactions that are believed to occur during supergene alteration are given in Fig. 5.

It is believed that the supergene process can be explained in terms of an electrochemical model in which the driving force is the gradient in oxidation potential resulting from access of atmospheric oxygen to the suboutcrop of massive sulphides.

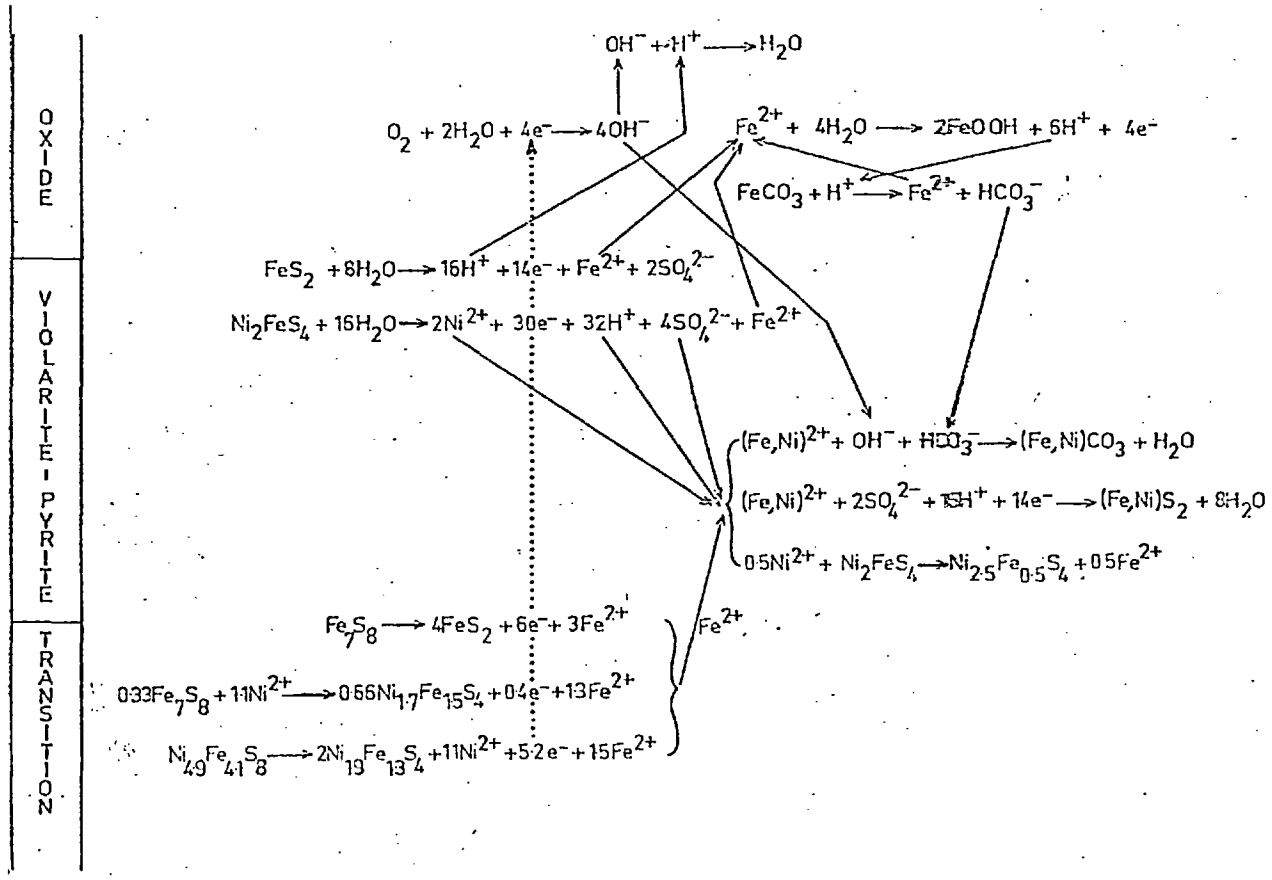

FIG. 5 (Nickel et al)

The mechanism of oxidative leaching of pentlandite in various acid media studied in laboratories proved to be different from the mechanism of leaching of pentlandite in nature. No violarite at all has been noticed in the phases found in the leach residues and in most cases pentlandite dissolved without the formation of any other intermediate phase.

Eliseev and Smirnova (66) studied the dissolution of pentlandite in hydrochloric acid. They suggested that at comparatively low temperatures (around 60°C), pentlandite is partially dissolved in hydrochloric acid, whilst at higher temperatures it dissolves quantitatively. Selective leaching of pentlandite can be achieved by leaching with 3% hydrochloric acid solutions.

Other metals contained in the mineral such as cobalt pass into the solution.

The behaviour of pentlandite during the leaching of pyrrhotite-pentlandite concentrate in ferric chloride solutions was studied by Klets et al (67), at different temperatures and different leaching times. In addition to separation of elemental sulphur in the surface layers, formation of new phases (millerite, beyrichite and troilite) was possible. Initially both nickel and iron dissolved rapidly, but afterwards the nickel concentration decreased, while that of iron became constant. This decrease of nickel concentration was a result of a precipitation of nickel by iron sulphide, due to the higher solubility of iron sulphide than that of nickel sulphide.

At low solution acidities, different solid phases, in particular jarosite, were precipitated as a result of iron hydrolysis. If chalcopyrite was present in the mixture of pyrrhotite and pentlandite, FeS did not precipitate as an independent phase, but was co-precipitated with Cu_2S as cubanite ($Cu_2SFe_3S_5$).

Shneerson et al (68) found that the pyrrhotite had an essential role in the oxidative leaching of sulphides. Several ores containing the three principal sulphide minerals pentlandite, chalcopyrite and pyrrhotite were leached in autoclave under oxygen pressure. It was shown that the rate of leaching out of metals from sulphide nickel ore materials containing no less than 30% sulphides, depends on the pyrrhotite content of ore: the higher the pyrrhotite content, the lower is the leaching rate. This can be seen in Fig. 6.

The inhibition action of pyrrhotite manifests itself in the precipitation of secondary sulphides of non-ferrous metals from solutions according to the general equation:

$$Me^{2+} + FeS = MeS + Fe^{2+} \qquad (1.53)$$

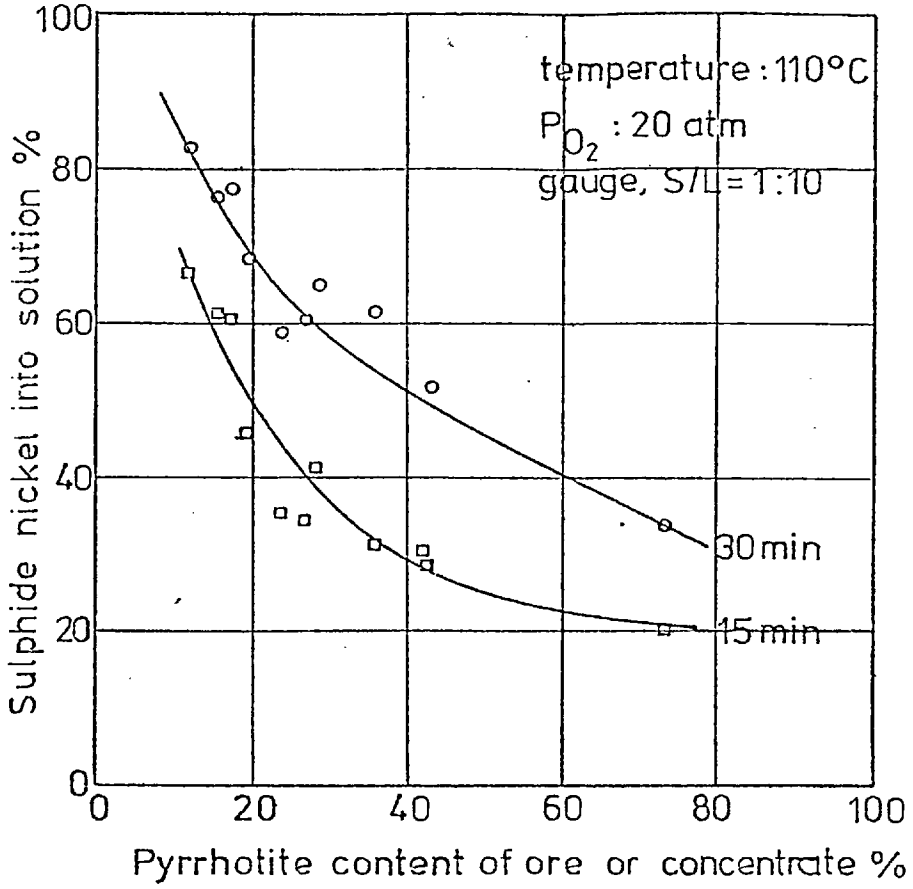

FIG. 6 Influence of Pyrrhotite Content of Starting Material on Extraction of Nickel into Solution (Shneerson et al, (68))

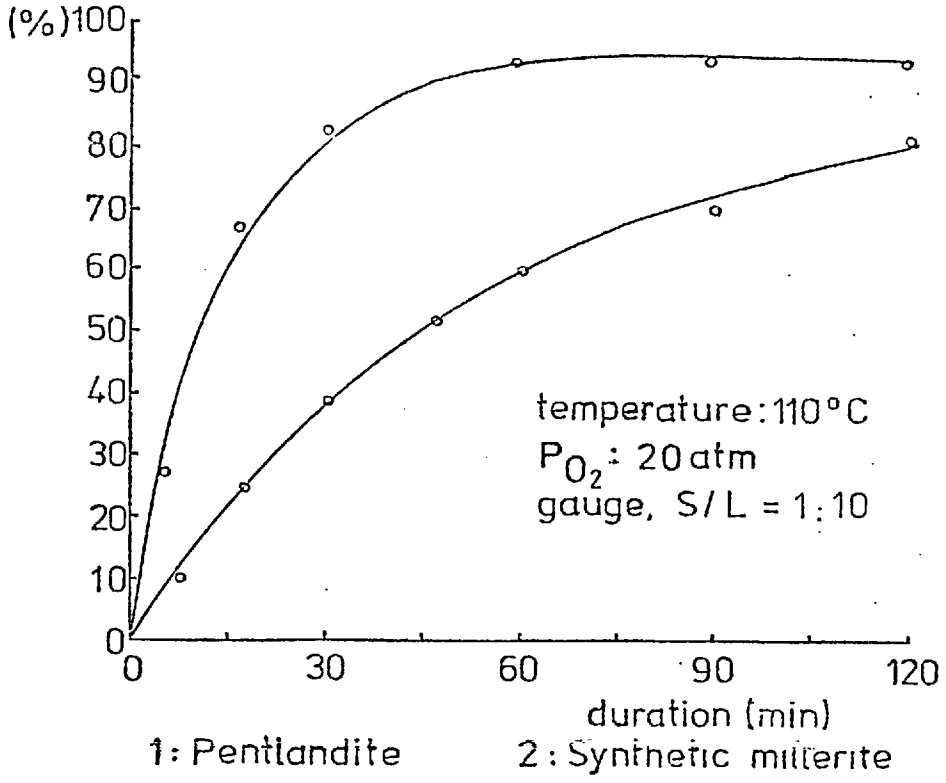

FIG. 7 Leaching-out Rates of Millerite and Pentlandite (Shneerson et al, (68))

The presence in the leaching residues of millerite and covellite which were absent in the starting materials has confirmed the above proposed mechanism for the action of pyrrhotite.

X-ray structural analysis after 1 hour experiment disclosed approximately equal intensities of millerite and pentlandite, while after 4 hours experiment, only millerite was found, no pentlandite being discovered. Thus, millerite oxidizes much more slowly than pentlandite. This fact is also confirmed by Fig. 7, in which the kinetics of transition of nickel into solution during the leaching of synthetic millerite is compared with the oxidation kinetics of pentlandite.

The process of dissolving the pentlandite was independent of oxygen transport into solution. This fact, as well as the high apparent energy of activation (14-20 Kcal/mole) and the reaction order of half with respect to oxygen are evidence that the reaction is chemically controlled.

Saarinen (69) described the Outokumpu Oy's practice for treating nickel sulphide mattes in Finland. The concentration process was planned in such a way that pentlandite and the magnetic pyrites were concentrated together. In this way, a low nickel content was obtained in the concentrate but the nickel yield was high. The nickel matte is dissolved in a two-stage counter current system where the solution of the second stage leaching containing copper is used with the matte coming to the first stage leaching. The reactions which occur during leaching were studied. In the absence of oxygen, the following reaction takes place:-

$$Ni + H_2SO_4 = NiSO_4 + H_2 \qquad (1.54)$$

This reaction is very slow. In the presence of air, the following reaction takes place, which is also slow, because of the low concentration of oxygen in the air:

$$Ni + H_2SO_4 + \tfrac{1}{2}O_2 = NiSO_4 + H_2O \qquad (1.55)$$

The existence of copper in the solution promotes the dissolution of nickel according to the reaction:

$$Ni + Cu^{2+} = Ni^{2+} + Cu \qquad (1.56)$$

The copper which is precipitated is oxidized:

$$Cu + \tfrac{1}{2}O_2 = CuO \qquad (1.57)$$

and dissolved:

$$CuO + H_2SO_4 = CuSO_4 + H_2O \qquad (1.58)$$

Thus the dissolution of nickel goes on until all the nickel in the matte is consumed.

The factors which affect the nickel solubility from the nickel sulphide were discussed. The finer the particle size, the faster the rate of the reaction was. The mixing was essential only for the good dispersion of air in the solution. That is why only in the first stage leaching reactor there is an agitating system. The quantity of the air provided influences the time of the completion of the reaction. Finally, on increasing the temperature the rate of the reaction increases.

The nickel solubility from the nickel sulphide matte using the Outokumpu Oy's practice attained 88-90% and the air consumption was $6m^3$/Kg dissolved nickel.

Vezina (70) studied the acid pressure leaching of a pentlandite-chalcopyrite-pyrrhotite concentrate. The concentrate was treated by pressure oxidation for the recovery of nickel, copper and cobalt. The concentrate was ground to 100% - 325 mesh and pulped with water or acidified water to contain 30% solids; the pulp was then subjected to a 400 psig pressure with oxygen at $110^{o}C$ for 14 hours at a pH about 1.4. Under these

conditions more than 98% of the nickel and cobalt and more than 90% of the copper were extracted. After the removal of copper from the solution, it could be treated for the removal of iron by increasing the pH to about 2 with the addition of $CaCO_3$. After the removal of the solids, the resulting solution was subjected to a liquid-liquid extraction method for the recovery of nickel and cobalt.

Another area of pressure leaching of pentlandite-chalcopyrite-pyrrhotite concentrate has been investigated by the same author (71). It was shown that pressure leaching this concentrate for the recovery of copper, nickel and cobalt selectively for the iron and sulphur can be efficient and selective under conditions which are less severe than those previously imposed (70). Thus, using an oxygen pressure of only 80 psig and an eight-hour retention in the autoclave, more than 98% of the nickel and cobalt and 90.6% of the copper can be extracted. The other leaching conditions were as before, except that the concentrate was ground to about 93% - 20 microns instead of 100% - 325 mesh.

The bacterial leaching of pentlandite in the presence of dissolved ferric ions has been investigated by several workers (72), (73), (74), (75). Razzell and Trussell (72) and Duncan and Trussell (73) showed that various sulphide minerals and ores can be leached rapidly and in good yield by Thiobacillus ferrooxidants. The amount of metal dissolved was dependent on the surface area of the ore but not on the amount. The addition of ferrous or ferric sulphate was not necessary for biological leaching, but its addition was beneficial for the maintenance of pH in the case of ores of minerals low in iron. A surface active agent, Tween 20, increased the rate of leaching of museum-grade chalcopyrite, impure millerite and two chalcopyritic copper ores. Bacterial leaching of millerite, bornite and chalcopyrite was greatest at pH 2.5. They were able to dissolve up to 87% of the nickel from a finely ground pentlandite ore in five days of leaching.

A method of bacteriological extraction of metals from sulphide ores has been described in a US patent by Duncan et al (74). According to their method, finely ground ore was mixed with an aqueous acidic leaching medium and sulphide-oxidizing bacteria i.e. Thiobacillus ferrooxidants. The leaching medium was subjected to agitation at a temperature between 20 and 45^{o}C and a pH at from about 1.5 to about 3 during the reaction. Using this process about 95% of nickel was extracted after 10 days.

Torma (75) investigated the bacterial leaching of nickel and cobalt sulphides and the application of bacterial leaching to low-grade pentlandite ores and concentrates. The concentrates were leached with acidified ferric sulphate solutions at pH 2 and temperature 35^{o}C. Under these conditions and in the absence of bacteria, the leaching proceeds very slowly with the formation of elemental sulphur and small amount of sulphate. Introducing bacteria into the solution, the leaching is accelerated due to the catalytic effect of bacteria on the direct oxidation of the sulphides, the regeneration of the ferric iron and the oxidation of the elemental sulphur to sulphate.

The following reaction for the dissolution of pentlandite was proposed:

$$(Ni, Fe)_9S_8 + 17.625O_2 + 3.5H_2SO_4 = 2.25Fe_2(SO_4)_3 + 3.5H_2O + 4.5NiSO_4 \quad (1.59)$$

The ferric concentration had a small effect on the rate of leaching up to 0.026M Fe^{3+} because of the reaction:-

$$MeS + Fe_2(SO_4)_3 = MeSO_4 + 2FeSO_4 + S \quad (1.60)$$

The optimum pulp density was about 15 to 25% solid; however the effect of the pulp density on the leaching rate was controlled by the metal concentration in the ore or concentrate.

Dutrizac and MacDonald (76) investigated the feasibility of nickel recovery by percolation leaching of pentlandite ore by acidified sulphate solutions in the presence and absence of Thiobacillus ferrooxidants. It was found that in the absence of bacteria, after 12 weeks of leaching, over 80% of the nickel was extracted. Until more than 60% of the nickel had been extracted, the rate of the dissolution remained constant but thereafter it decreased. This was due either to the increasing unavailability of the nickel ore minerals, or because of the formation of impermeable sulphur or jarosite coatings on the minerals.

The concentrations of ferric ion and acid decreased as the solution passed through the ore column, while in contrast the total iron concentration increased, because of the dissolution of iron minerals. The pH of the effluent solution rose very rapidly from the initial value of 1.0 to about 2 to 3 and thereafter, the acid concentration in the effluent increased until it reached the original pH value of 1.0.

An apparent activation energy of 9 Kcal/mole was obtained for the percolation leaching of pentlandite ore in the absence of bacteria.

Similar nickel extractions were obtained by leaching with acidified ferric sulphate solutions containing bacteria. Elemental sulphur was observed in the experiments done in both the presence and absence of bacteria. Only 30% of the theoretical oxidized sulphur was reported in the sulphate form in the presence of bacteria, which indicates that oxygen was inaccessible to the ore in the column.

The probable dissolution reaction occurring in the columns was:

$$18Fe^{3+} + (Ni, Fe)_9S_8 = 22.5Fe^{2+} + 4.5Ni^{2+} + 8S \qquad (1.61).$$

In the absence of bacteria, the rate of nickel extraction increased with increasing ferric ion concentrations or with decreasing acid strength. Also, the leaching rate was found to be relatively independent of the apparent flow rate once a minimum flow had been established.

The phenomenon of formation of a sulphur protective surface coating on the nickel-containing minerals has been noticed by several workers (41), (44). This coating reduces the rate of the nickel extraction and the total amount of nickel extracted. To overcome this difficulty on 'activation' pre-treatment of the sulphides was proposed by Dyson and Scott (77). The main object of the activation treatment was to remove excess sulphur from pyrrhotite and pyrite and to form a more reactive FeS instead. Thus, the nickel concentrates were heated for 1 hour at 750-800^{o}C in a reduction atmosphere. During this procedure other unreactive nickeliferous sulphides such as violarite, millerite and monosulphide solid solution were also converted to acid-soluble compounds. Applying this activation pre-treatment, extraction of about 99% of nickel was achieved on leaching with a small excess of 5M HCl or H_2SO_4, after boiling for 1 hour (HCl) or 2 hours (H_2SO_4).

1.1.3 Ammoniacal Leaching of Nickel Sulphides

Although ammoniacal leaching had been suggested as a means of reacting sulphide nickel ores soon after the turn of the century (78), its first commercial application for extracting nickel was to oxide ore at Nicaro, Cuba.

Sherritt Gordon was the first commercial operation to employ hydrometallurgy for extracting nickel from sulphide ores. In its process pentlandite concentrate is leached in strong aqueous ammonia solution at moderately elevated temperature and pressure. Good extractions are

obtained within the temperature range of 160^{o}-190^{o}F and at 100-150 psig, using air for oxygen supply.

Two conditions must be met if ammonia is to serve as a leaching agent for metal sulphides:

i) the metal must be capable of forming a soluble ammine with ammonia and

ii) the sulphide must be oxidized by suitable means during leaching (79), (80), (81), (82), (83), (84), (85).

Forward and Mackiw (82) postulate a series of reactions for the oxidation of pentlandite with oxygen in ammoniacal solutions as follows:

$$NiS.FeS + 7O_2 + 10NH_3 + 4H_2O = Ni(NH_3)_6SO_4 + 2Fe_2O_3H_2O + 2(NH_4)_2S_2O_3 \quad (1.62)$$

$$2(NH_4)_2S_2O_3 + 2O_2 = (NH_4)_2S_3O_6 + (NH_4)_2SO_4 \quad (1.63)$$

$$(NH_4)_2S_3O_6 + 2O_2 + 4NH_3 + H_2O = NH_4SO_3NH_2 + 2(NH_4)_2SO_4 \quad (1.64)$$

$$NH_4SO_3NH_2 + H_2O \xrightarrow{200^{o}C} (NH_4)_2SO_4 \quad (1.65)$$

Thus, during the ammoniacal leaching of pentlandite, ferric oxide forms a porous covering around the unreacted core of pentlandite, through which the nickel and sulphur ions diffuse outwards, while the oxygen diffuses inwards. The rate of leaching is controlled by temperature, ammonia concentration in the leach liquor, oxygen pressure and the amount of agitation. Of these, temperature and ammonia concentration are the most important, although oxygen and agitation must be provided.

The ammoniacal leaching of nickel sulphides has been studied by several Russian workers.

Naboichenco and Smirnov (86) studied the autoclave leaching of a nickel-cobalt concentrate containing 47.75% nickel, 5.6% cobalt, and 36.8% sulphur with ammonia and sulphuric acid. The optimum conditions for both ammonia and sulphuric acid leaching were determined. Under the optimum conditions 99.8% nickel extracted with ammonia leaching after 40-60 mins. and a liquid:solid ratio 5-7:1, while with sulphuric and leaching 99.4% nickel extracted after 1-2 hours and a liquid:solid ratio 3-9:1. Thus ammonia leaching was recommended.

The effect of temperature, oxygen partial pressure and ammonia and ammonium sulphate concentrations on autoclave leaching of nickel mattes was studied by the same authors in another paper (87). They found that the rate of oxidation of Ni_3S_2 depends to a certain degree on the initial concentration of ammonia in the solution. Temperature at 15^{o}-120^{o}C has little effect on the rate of oxidation. The apparent activation energy calculated was 5970 cal/mole, which places the process in the diffusion region. The partial pressure of oxygen has a large effect on the process rate. The presence of ammonium sulphate affects the concentration equilibrium of free ammonia in the solution. An increase in its concentration in the system increases the rate of oxidation of Ni_3S_2, but when the NH_4/NH_3 ratio is greater than 0.17-0.19, the rate of oxidation decreases again. In the absence of ammonium sulphate, nickel ammoniates are hydrolysed and the oxidation rate is very low. The optimum temperature of the leaching is 80^{o}-90^{o}C. At lower temperatures the leaching rate decreases and 7-8 hours is needed to extract 94-96% of nickel.

1.2 PHASE RELATIONS AND CRYSTAL STRUCTURES IN THE IRON-NICKEL-SULPHUR SYSTEM

1.2.1 Iron-Nickel-Sulphur System Phase Diagrams

The system involving nickel, iron and sulphur is the most important ternary sulphide system in nature, after the copper, iron and sulphur ore. Minerals containing iron, nickel and sulphur as major components are found almost exclusively in or associated with mafic or ultramafic rocks.

During the last decade much new information has been obtained over wide temperature and pressure ranges on the phase relations in systems pertinent to Fe-Ni sulphide ores. A large number of the phases are found as minerals, which in some cases constitute important sources of nickel, iron and related metals.

Early workers on the Fe-Ni-S system include Bornemann (88), Newhouse (89), Vogel and Tonn (90), Zurbrigg (91), Urasor and Filin (92), Colgrove (93), but their results are not reliable, because their experiments made no provisions to prevent the escape of S during annealing.

G.A. Harcourt (94) identified the pentlandite in the ternary system Fe-Ni-S, while Colgrove (95), using pressure bombs and sealed glass tubes, reported a fairly extensive solid solution field for pentlandite.

D. Lundqvist (96), (97) studied the binary system Ni-S and the ternary system Fe-Ni-S by the method of x-ray powder photographs. He confirmed the presence of Ni_3S_2, Ni_6S_5, Ni_7S_6 and NiS in the region between nickel and NiS of binary Ni-S system, and the presence of $(Ni, Fe)_9S_8$ (phase π cubic) in the ternary Fe-Ni-S system. He also measured the

lattice parameters of these compounds and, from these results he presented the isothermal equilibrium sections of the system Ni-Fe-S at 200° and 680°C.

Itaya, Shimada and Ando (98) studied the composition of nickel matte with x-rays and confirmed the presence of $(Ni, Fe)_9S_8$.

Much of the work in the Fe-Ni-S system has been carried out by systematic studies undertaken in the Geophysical Laboratory of the Carnegie Institution, Washington, during the last two decades, mostly through rigid silica tube, quench-type annealing experiments. Kullerud (99), (100), (101), (102), Kullerud et al, (103), Clark and Kullerud (104), Naldrett and Kullerud (105), Naldrett et al (106), Craig (107), (108), Craig and Naldrett (109), Craig et al (110), have developed much of our present understanding of the systems which stems from these studies.

The phase relations at 1,100°C are shown in figure (8). At this temperature the liquid immiscibility field extends from 98 to 46.5 wt % S along the Fe-S join and from 98 to 54.5 wt % S along the Ni-S join. The pyrrhotite solid solution, which first appears on the Fe-S join at 1,192°C (Jensen (111)), at 1,100°C extends from 36.5 to 43.3 wt.% S along the Fe-S join. It protrudes into the ternary system, and the maximum solid solution content of nickel is about 14 wt.% at 1,100°C. This solid solution which at lower temperatures forms a complete series between $Fe_{1-x}S$ and $Ni_{1-x}S$ is referred to as the monosulphide solid solution (Mss) of the Fe-Ni-S system. The stability field of Mss is discussed in detail in section 1.2.2. On cooling, pyrrhotite and liquid sulphur become stable together at 1,083°C and the divariant field containing Mss, liquid and vapor widens gradually with decreasing temperature. At the same time the Mss field extends increasingly further into the ternary system. At 1007°C the NiS_2 phase becomes stable.

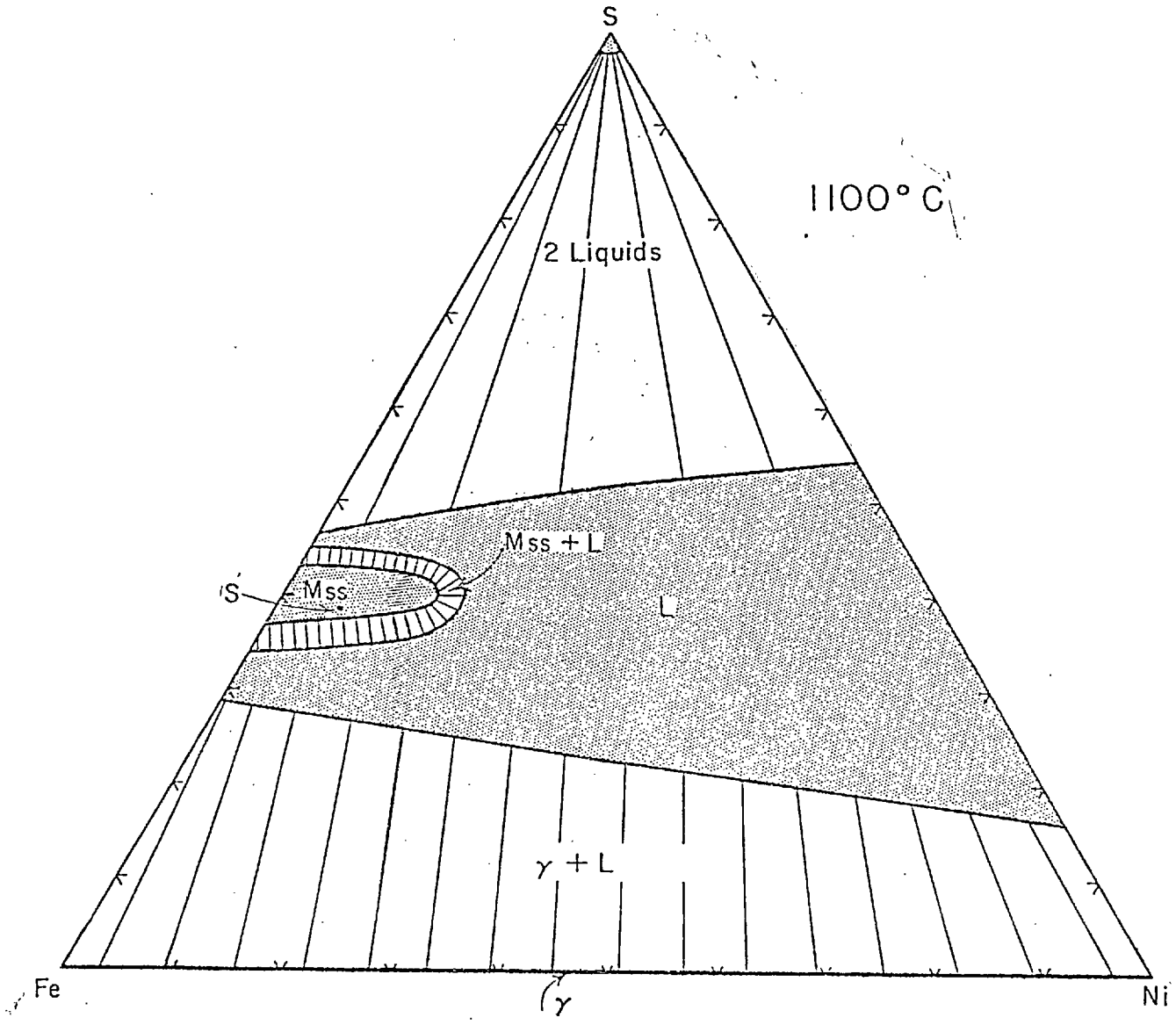

FIG. 8 Phase Relations in the Fe-Ni-S System at 1.100°C (Kullerud et al, (103))

The phase relations at 1,000°C are shown in figure (9). At this temperature the region of liquid immiscibility is narrow, and the maximum Fe content of the NiS_2 phase is about 1 wt.%, as determined by L.A Clark and G. Kullerud (112). On cooling below 1,000°C, the Mss becomes complete between $Fe_{1-x}S$ and $Ni_{1-x}S$ at 992°C. The liquid immiscibility field disappears at 991°C (Kullerud and Yund (113)), and below this temperature NiS_2 becomes stable with liquid sulphur. A eutectic between $Ni_{1-x}S$ and NiS_2 appears at 985°C (Kullerud and Yund (113)), and below this temperature nickel mono- and dissulphide coexist. A eutectic along the Fe-S boundary between Fe and FeS appears at 988°C which is the lowest temperature at which the central liquid field spans the ternary system. The central liquid field, below this temperature gradually shrinks away from the Fe-S boundary, resulting in the development of a univarient field comprised of FeNi solid solution, containing about 31 wt.% Ni, stoichiometric FeS, containing less than 0.5 Wt.% Ni and ternary liquid. Pure Fe inverts at about 910°C from the high-temperature γ to the low temperature α form.

The phase relations at 900°C are shown in figure (10). The solubility of Fe in NiS_2 at this temperature is about 5.5 wt.%, as determined by Clark and Kullerud (112). Cooling below 900°C results in a gradual narrowing of the Mss + sulphur liquid divariant field, a widening of the Mss + (Ni. Fe)S_2 + liquid sulphur univariant field, and an increase in the stability of Fe in NiS_2. A ternary phase, having a metal-to-sulphur ratio of nearly 3:2 and containing a considerable amount of Fe, appears at 862°C in the Mss + central liquid divariant region. On further cooling the solubility of Fe in this $(Ni, Fe)_{3-x}S_2$ phase decreases. It becomes stable on the Ni-S boundary at 806°C. In the sulphur-rich portion of the system, FeS_2 becomes stable at 743°C, and at 729°C the tie lines are established between FeS_2 and NiS_2 (Clark and Kullerud (112)). At about 700°C the tie lines between Mss and central liquid are broken and replaced by the tie lines between $(Ni, Fe)_{3-x}S_2$ and γFeNi.

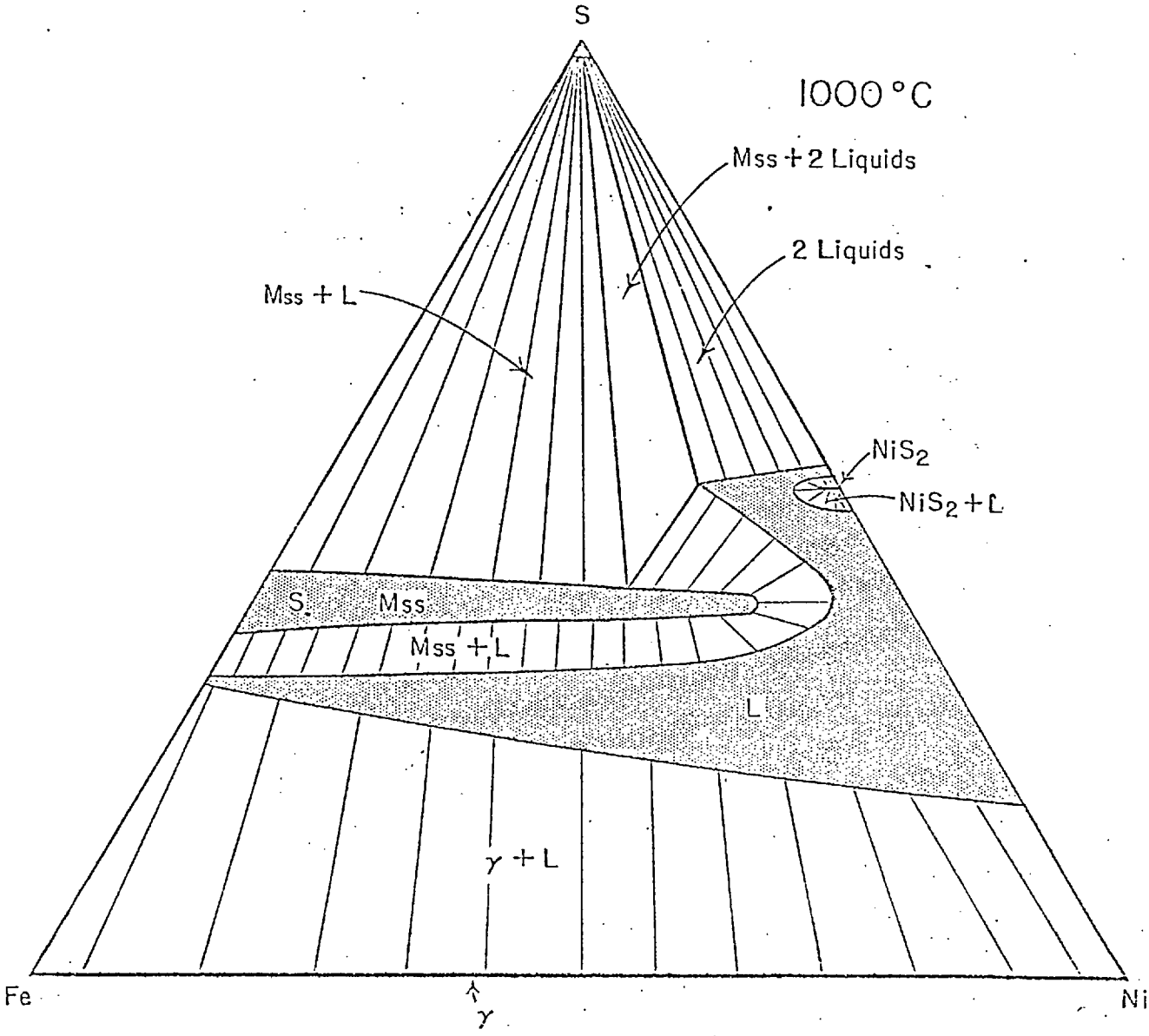

FIG. 9 Phase Relations in the Fe-Ni-S System at 1000°C (Kullerud et al, (103))

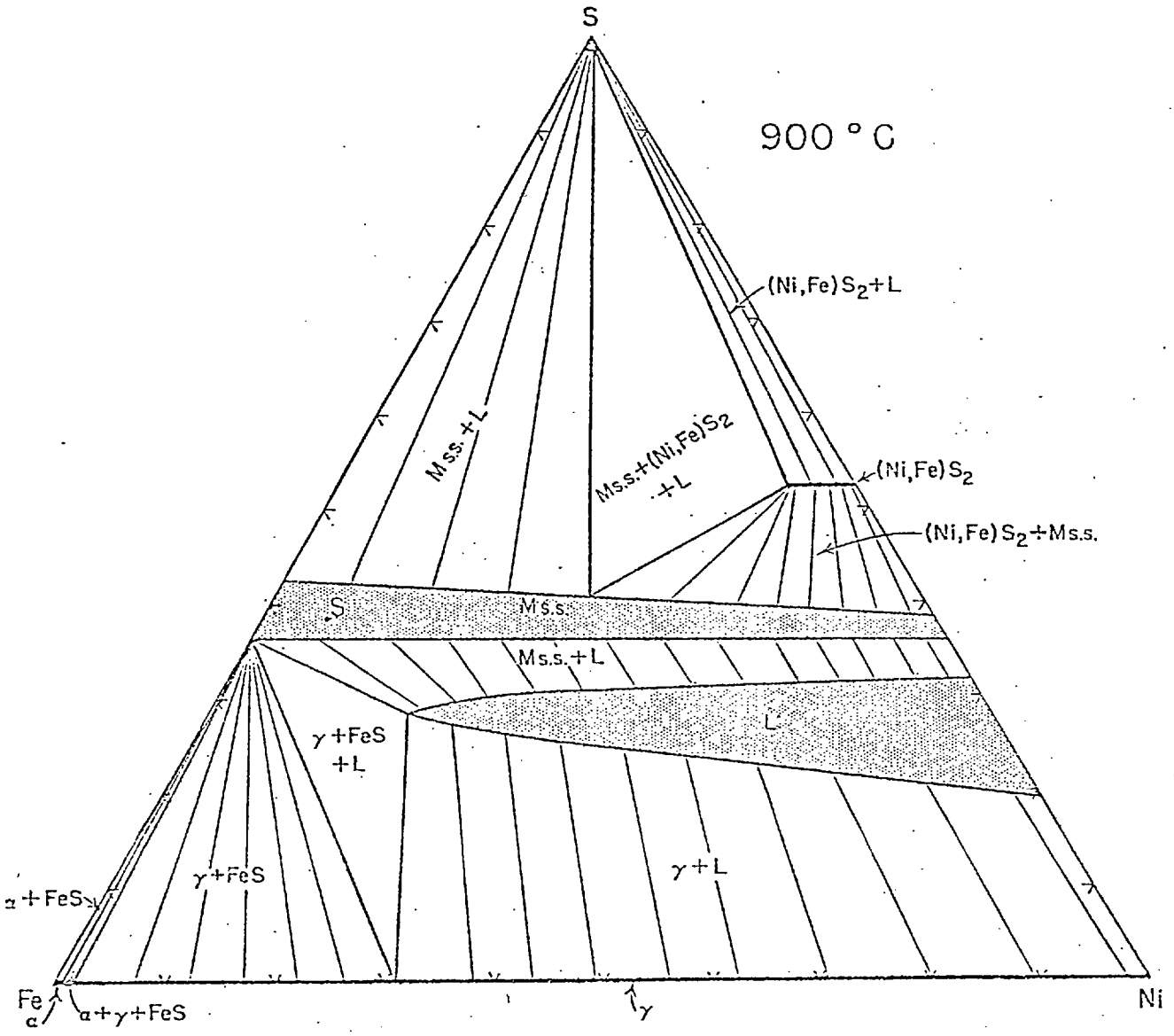

FIG. 10 Phase Relations in the Fe-Ni-S System at 900°C(Kullerud et al, (103))

The phase relations at 650°C are shown in figure (11). As can be seen, the Mss remains complete between $Fe_{1-x}S$ and $Ni_{1-x}S$ while the central liquid field is very small. Further lowering of the temperature leads to the disappearance of the central liquid field at 635°C and to the very important development in the Mss + $(Ni, Fe)_{3\pm x}S_2$ divariant field. At 610°C pentlandite $(Fe.Ni)_9S_8$ the most important source of nickel appears. The stability range of pentlandite is dealt with in detail in section 1.2.3. On further cooling the $(Fe.Ni)_9S_8$ phase forms solid solution on both sides of the 1:1 ratio of the metals. The solid solution on the Fe side intersects the FeS + $(Ni, Fe)_{3\pm x}S_2$ divariant region, and a tie-line change occurs at about 575°C.

At lower temperatures the Ni_7S_6 phase appears at 573°C, and at 446°C the stoichiometric Ni_3S_2 inverts from the high temperature, non quenchable form to the low-temperature, hexagonal heazlewoodite crystal structure (Kullerud and Yund (113)).

The phase relations at 550°C are shown in figure (12). At this temperature heazlewoodite of Ni_3S_2 composition coexists with $(Ni, Fe)_{3\pm x}S_2$ of the high temperature form, while Mss is complete between $Fe_{1-x}S$ and $Ni_{1-x}S$. Complete solid solution between the $Fe_{1-x}S$ and $Ni_{1-x}S$ end members exists even at 300°C.

The phase relations at about 130°C in the central portion of the Fe-Ni-S system are shown in figure (13). No solubilities of Ni in the pyrrhotite type phase are indicated in figure (13) although they may be significant even at 130°C.

Bravoite and violarite are also shown in figure (13). Bravoite is stable only below 137°C (Clark and Kullerud (104)). Because of its

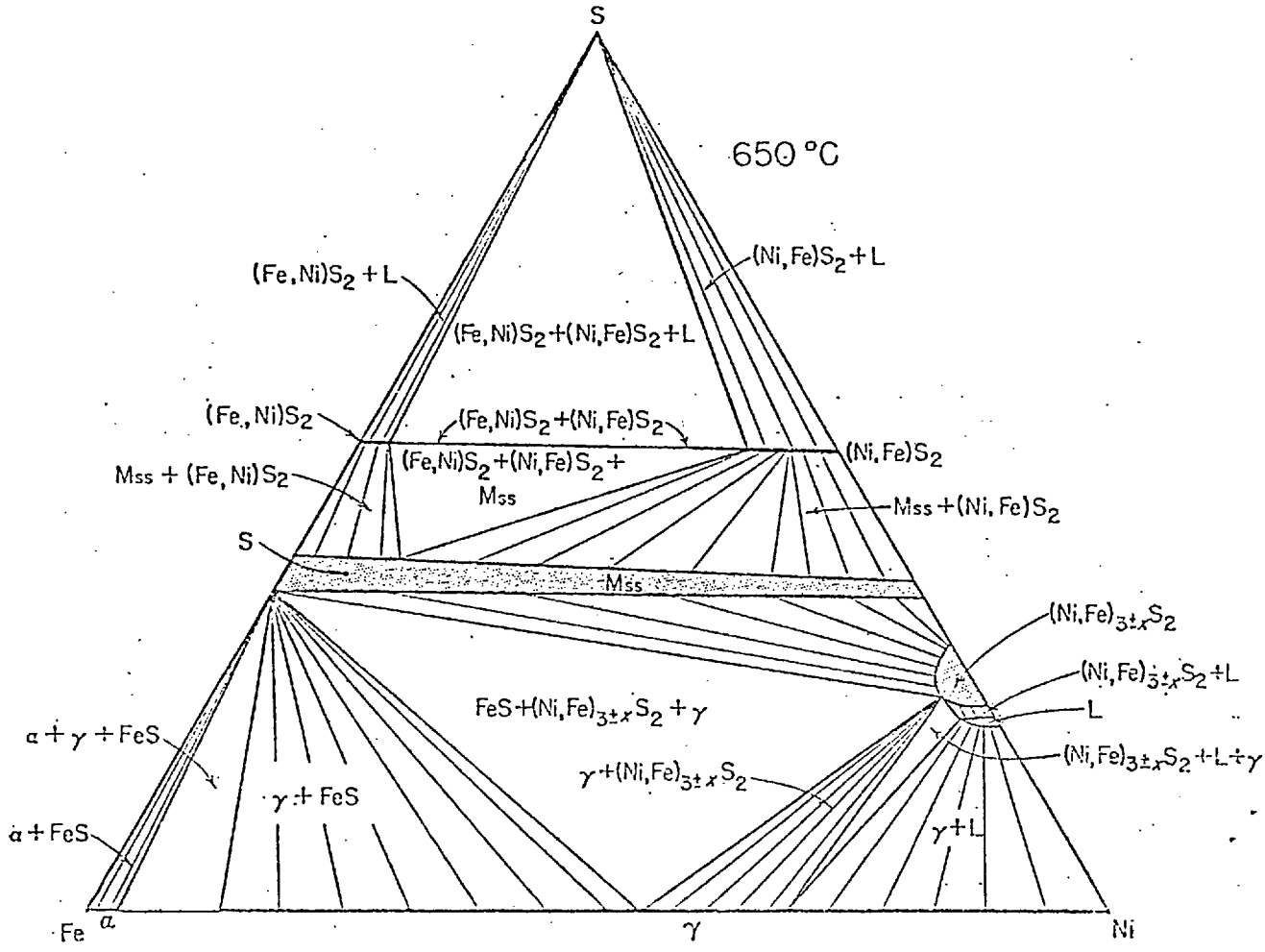

FIG. 11 Phase Relations in the Fe-Ni-S System at 650°C (Kullerud et al, (103))

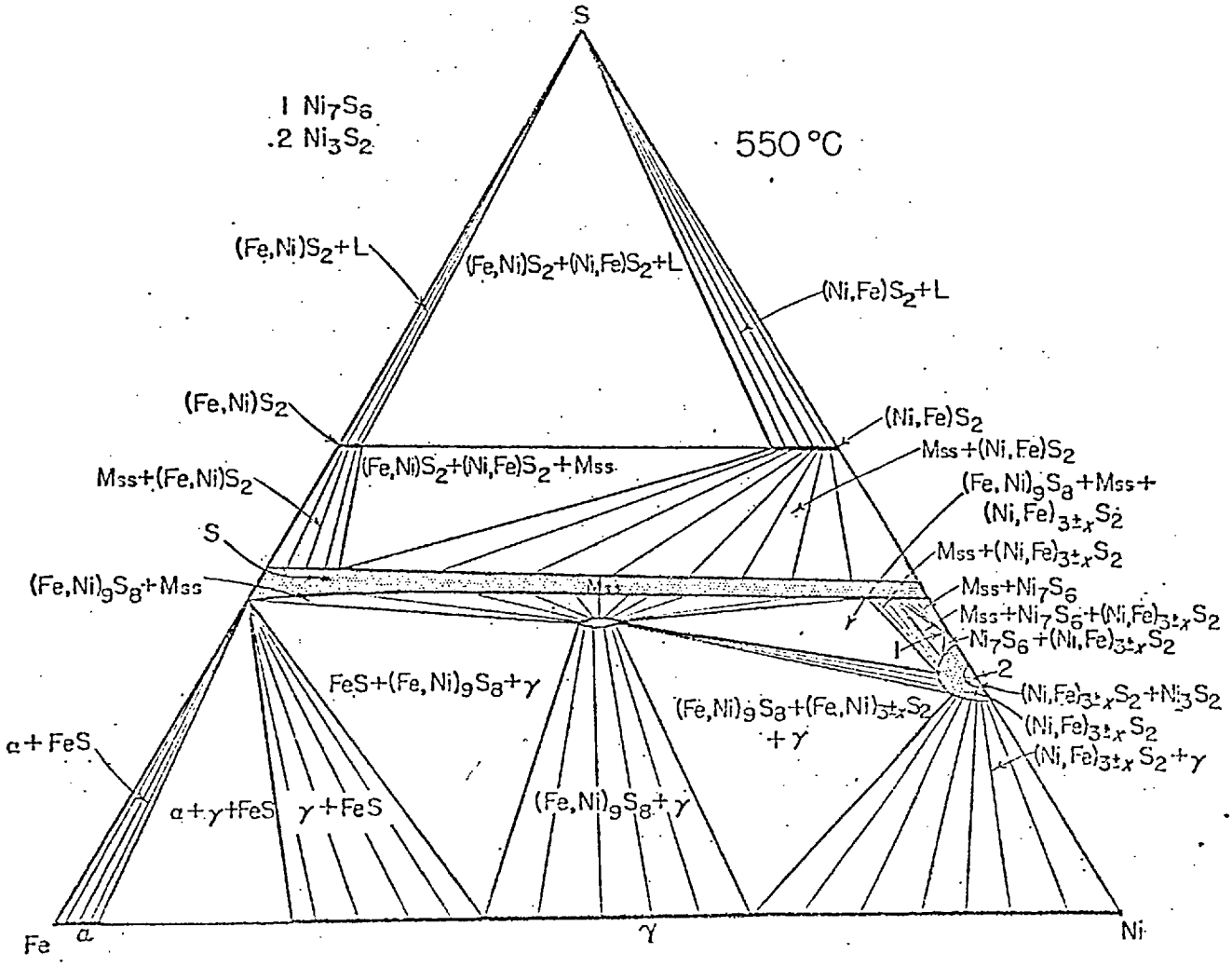

FIG. 12 Phase Relations in the Fe-Ni-S System at 550°C (Kullerud et al, (103))

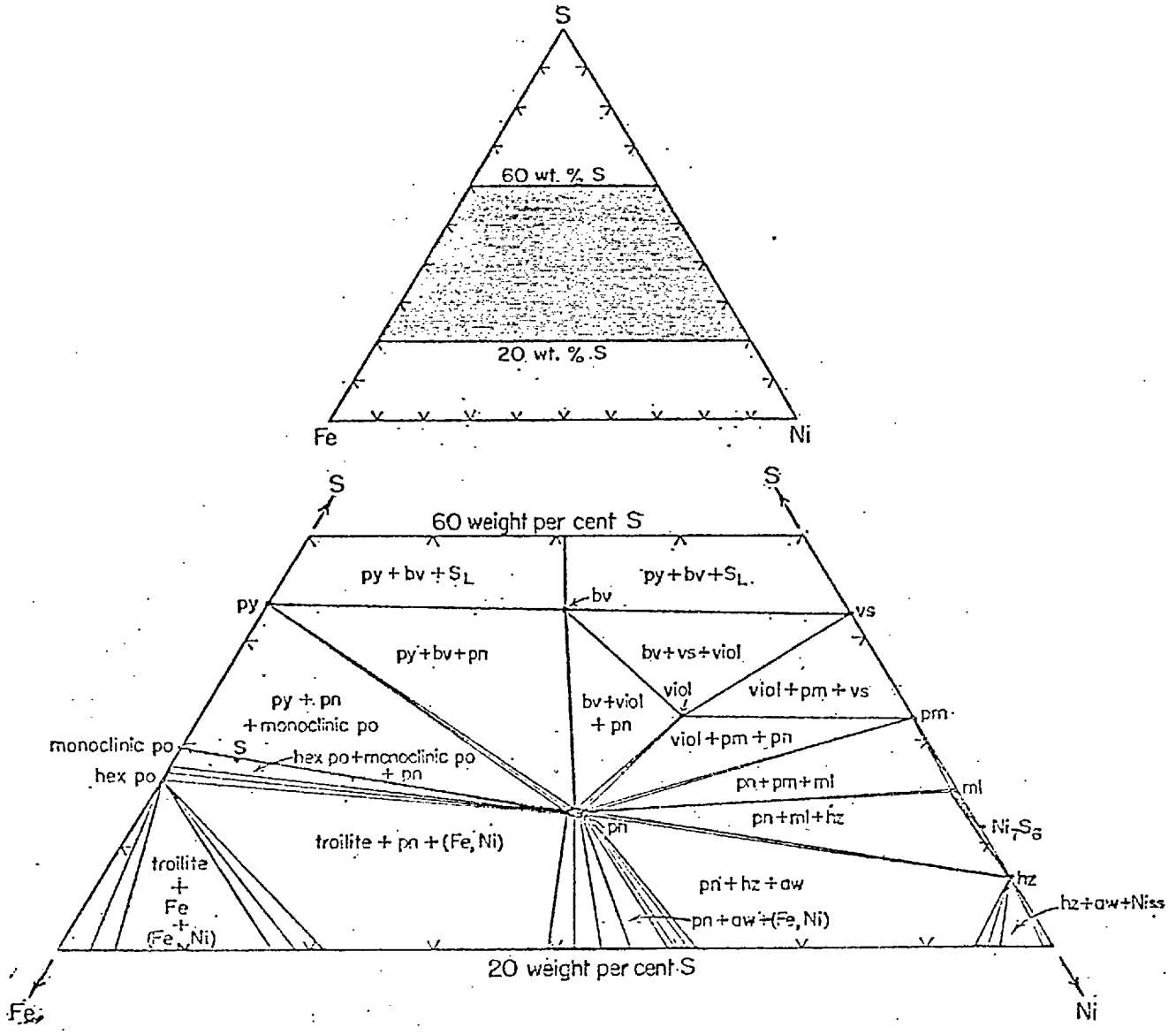

FIG. 13 Tentative Phase Diagram of the Central Portion of the Fe-Ni-S System at about 130°C (Kullerud et al, (103))

similarity to polydymite (stable $356^{o}C$), violarite is assumed to be stable on the isotherm of figure (13). Tie lines are shown connecting pentlandite with millerite, and pentlandite with heazlewoodite.

1.2.2 Monosulphide Solid Solution Stability Field

The monosulphide solid solution (Mss) extends across the entire Fe-Ni-S system through the temperature range from $992^{o}C$ to below $400^{o}C$. The existence of a complete $Fe_{1-x}S$ - $Ni_{1-x}S$ solid solution was first suggested by Hawley, Colgrove and Zurbrigg (114) and was demonstrated by Lundqvist (96).

Naldrett et al (106) gave the sulphur-rich and sulphur-poor limits for most of the solid solution series throughout the temperature range 600^{o} + $300^{o}C$. (Figs. 14, 15 and 16). They suggested that at $300^{o}C$ there is still complete miscibility but the field has narrowed to about one third the width at $600^{o}C$.

Shewman and Clark (115) plotted d_{102} values vs composition and noticed a complete discontinuity in the curve at about 33 at % Ni (Fig. 17). They suggested then that Mss breaks down into two Mss phases, one rich in iron and the other rich in nickel, having different crystal structures.

Misra and Fleet (116) found that the S-poor boundary of the Mss field recedes progressively towards S-rich compositions with the falling temperature. The S limits of the boundary at a section with atomic Fe:Ni ratio 1:1 are estimated as 50.7, 51.0, 51.3 and 51.8 at % S at 600^{o}, 500^{o}, 400^{o} and 300^{o} respectively. Their suggestion that the Mss field, which is continuous between $Fe_{1-x}S$ and $Ni_{1-x}S$ at higher temperatures,

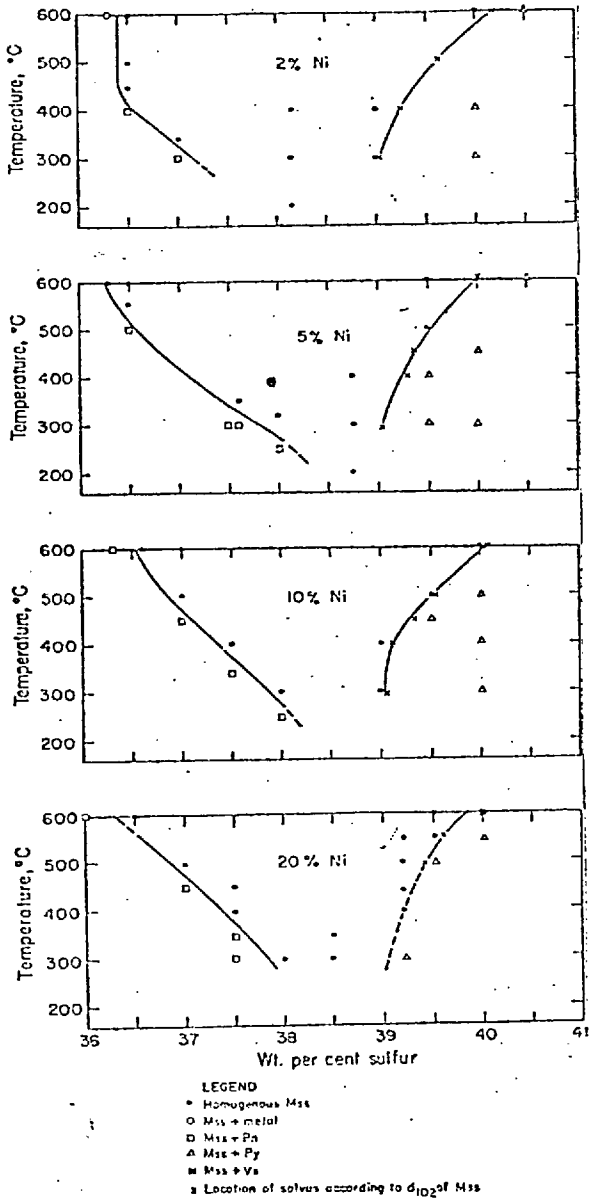

FIG. 14 T-X Sections through the Mss at 2, 5, 10 and 20 wt % Nickel Showing Limits of Homogeneity of the Solid Solution (Naldrett et al, (106))

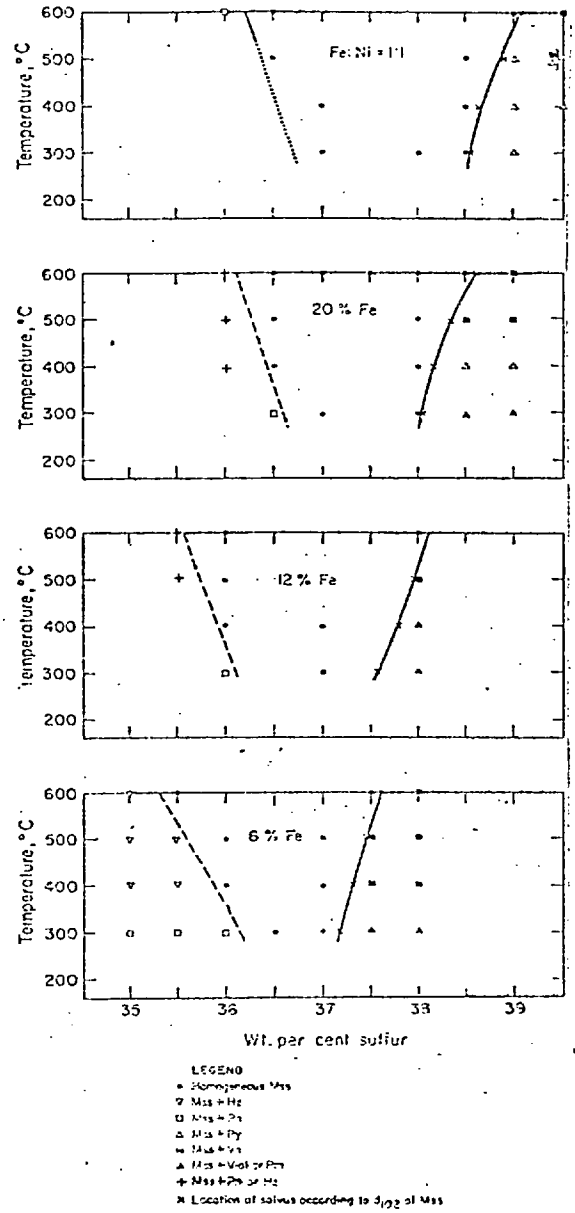

FIG. 15 T-X Sections through the Ms at Fe:Ni Ratio of 1:1 by weight and at 20, 12, and 6 wt % Iron Showing Limits of Homogeneity of the Solid Solution (Naldrett et al, (106))

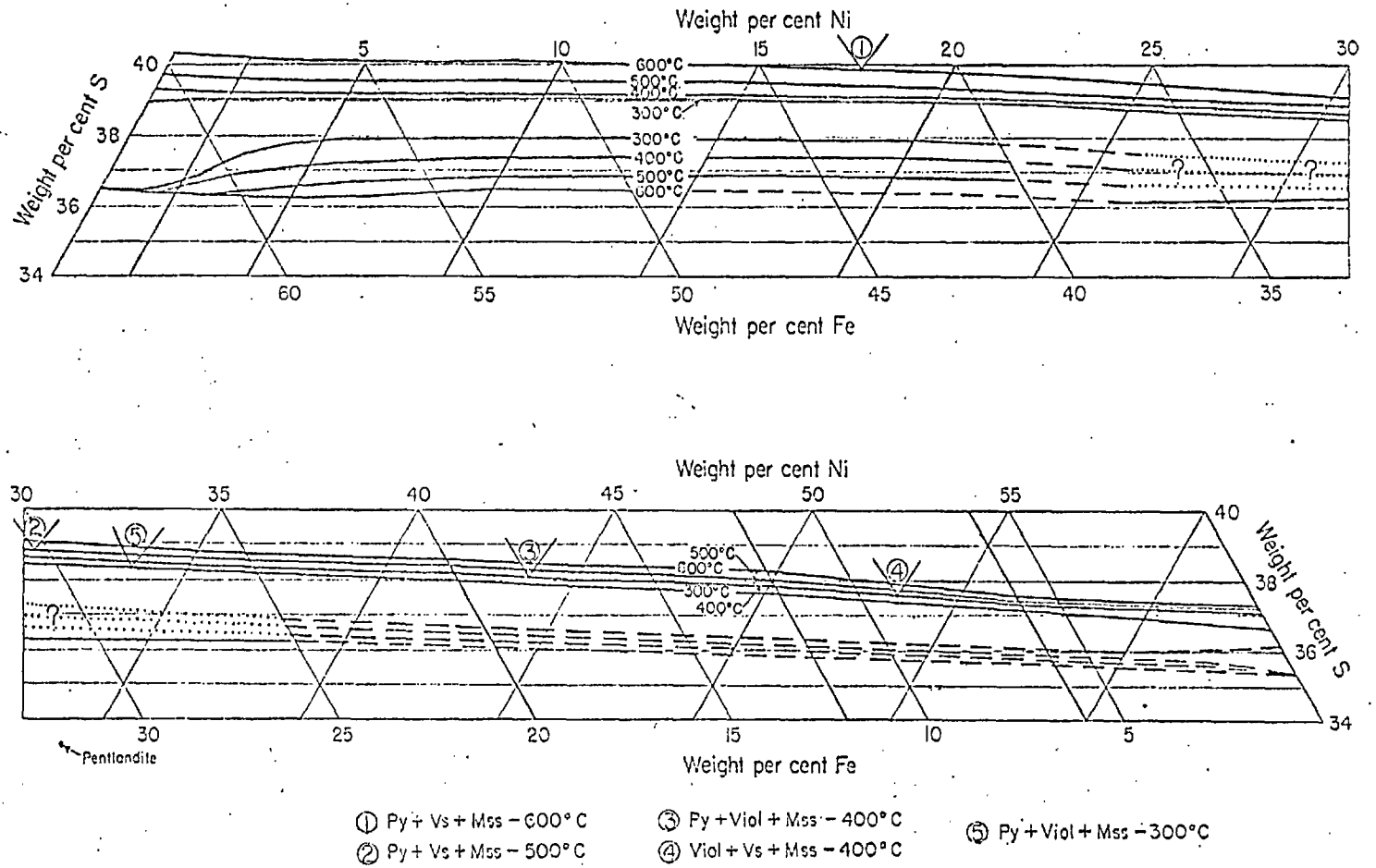

FIG. 16 Band Across the Center of the Fe-Ni-S System Showing Limits of the Mss at 600°, 500°, 400° and 300°C. Dottes curves indicate Inferred Position of Sulvus and Dashed Curves Indicate the Sulvus where it has been Determined Through Textural Interpretation. (Naldrett et al, (106))

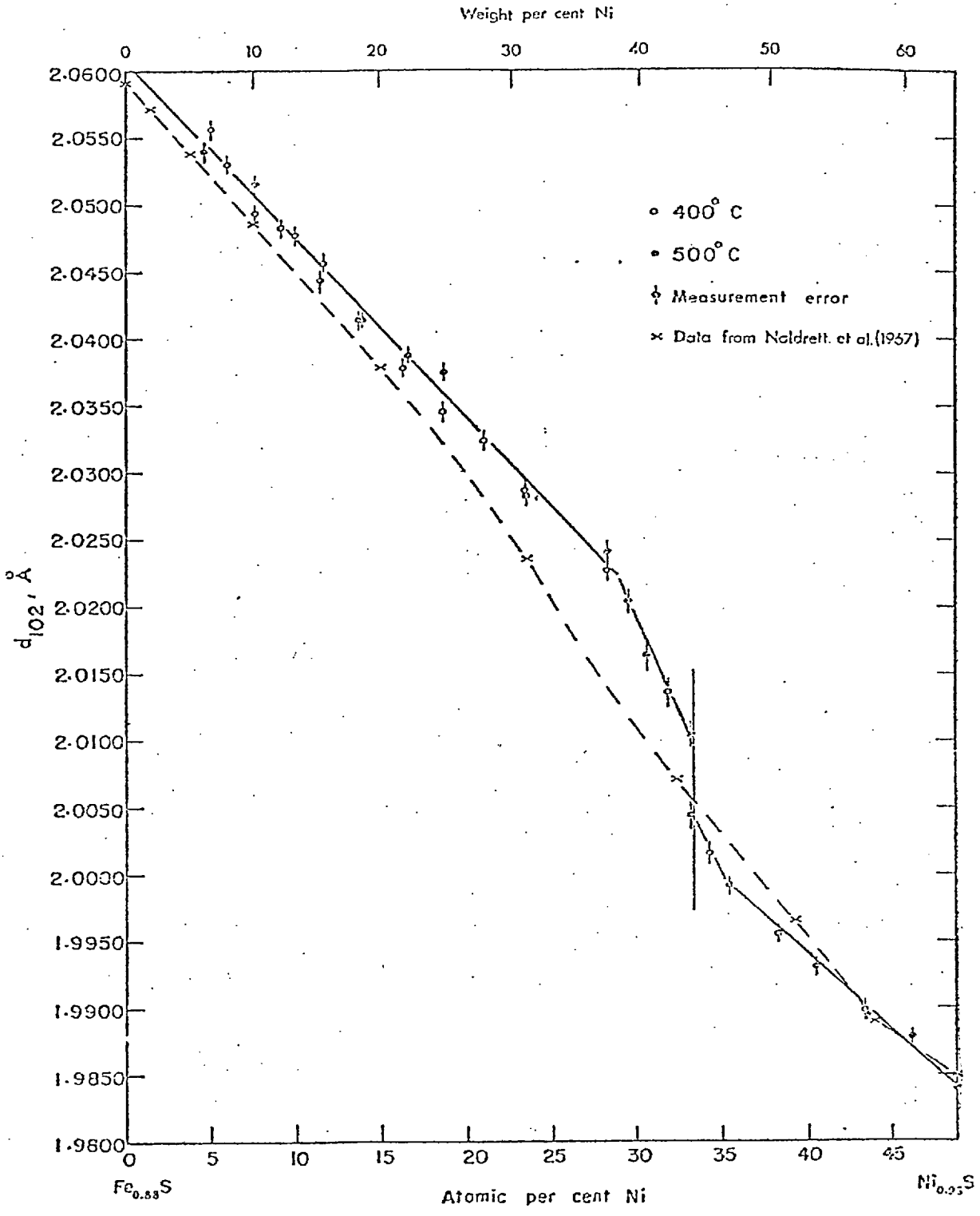

FIG. 17 Variation in d_{102} of the Mss Series as a Function of Nickel Content at 500 and 400°C. The Dashed Curve Represents Data Interpreted from Fig. 4 of Naldrett et al, (106) (Shewman and Clark, (115))

separates at a composition of about 33 at % Ni into two immiscible phases, Mss (1) and Mss (2), is in very good agreement with what was proposed by Shewman and Clark (115). But they suggested that this breakdown occurs at a temperature between 400° and 300°C which is higher than that reported by previous workers (275 ± 10°C, Shewman and Clark (115)); 275 ± 25°C Craig and Naldrett (109)). The Mss (1) phase withdraws progressively towards the Fe-S join with falling temperature, while the composition of the Mss (2) phase is stabilized around 33 at % Ni.

At temperatures below 400°C both the $Fe_{1-x}S$ and $Ni_{1-x}S$ end members of the Mss undergo structural transitions. The $Fe_{1-x}S$ and member undergoes a transformation, designated as β transition, which is characterized by a change in magnetic susceptibility at 315°-320°C as reported by Haraldsen (117), (118). The temperature at which the high-temperature modification of $Fe_{1-x}S$, simple hexagonal NiAs-type, inverts to a variety of lower temperature forms with different superstructures has been given by Haraldsen (119) as 140° ± 40C and by Corlett (120) as about 230°C.

Desborough and Carpenter (121) found three structural types of pyrrhotite, all possessing a superlattice, whose stability fields have been partially determined as follows:

Structural Type	Composition atomic % iron (±0.1)	Thermal Stability ±10°C
a = 2A, 5C, hexagonal	47.3 - 50.0	below 315
a = 2B, b = 2A, 4C monoclinic	46.67 (Fe_7S_8)	below 315
a = 2A, 7C, hexagonal	45.5 - 50.0	above 315

In figure (18) the phase diagram of pyrrhotite is given as it was drawn by Desborough and Carpenter(121). As it is suggested the pyrrhotite-

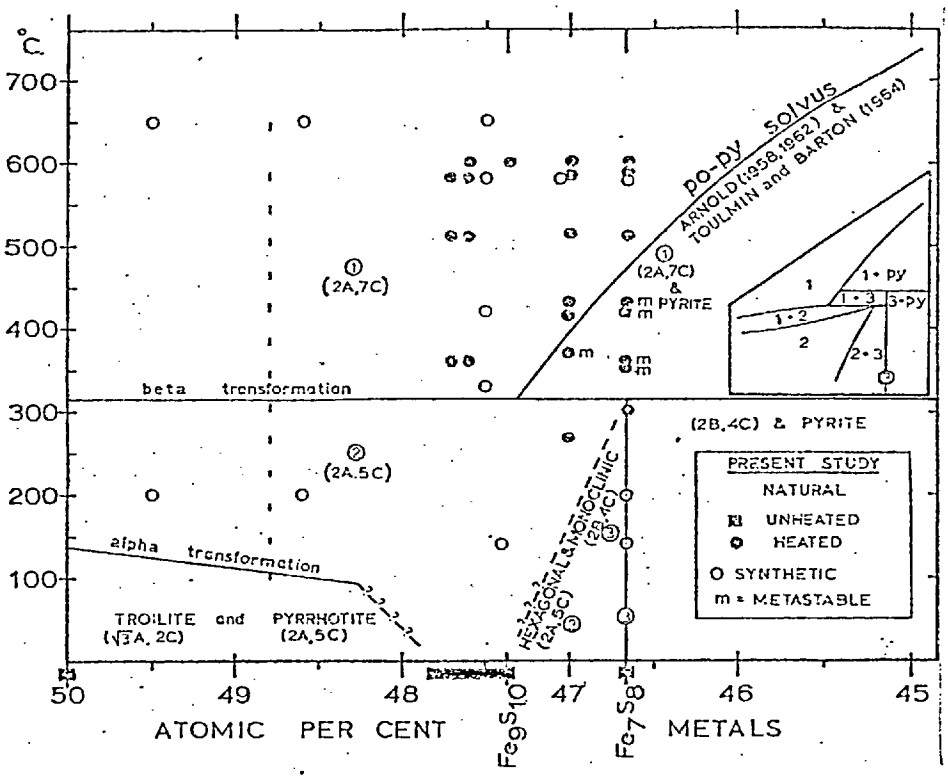

FIG. 18 Tentative Phase Diagram for a Portion of the FeS-FeS_2 System (Desborough and Carpenter (121))

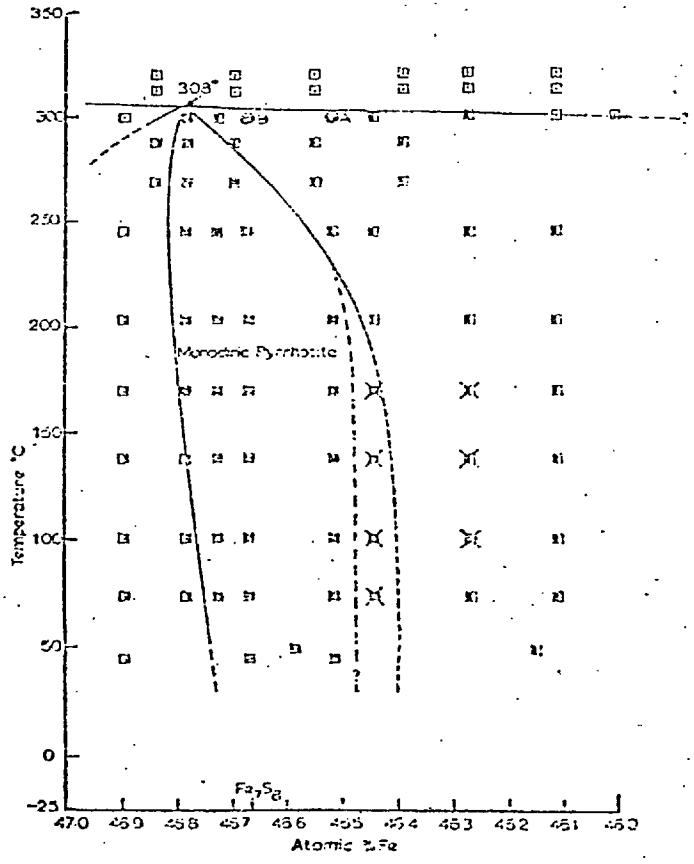

FIG. 19 Stability Field of Monoclinic Pyrrhotite at <1 atm Pressure (Clark, (123))

pyrite solvus terminates at a boundary at 315 $\pm$ 10°C, corresponding to a composition of 47.35 $\pm$ 0.1 atomic percent iron or approximately Fe_9S_{10}. Below 139°C stoichiometric FeS, troilite, has a hexagonal supercell $\sqrt{3}$A, 2C.

Byström (122) described a monoclinic pyrrhotite of composition Fe_7S_8 which Desborough and Carpenter have found possesses a supercell 2B, 2A, 2C.

A.H. Clark (123) drew the stability field of this monoclinic pyrrhotite (Fig. 19) and reported stable formation of it as high as 308°C, but Hall and Yund (124) believe it to be metastable.

The $Ni_{1-x}S$ end member of the Mss exists in only two known forms. The high-temperature form is hexagonal, isostructural with high temperature pyrrhotite and extends from 35.33 (NiS) to 37.8 weight percent sulphur at 600°C and from 35.33 to 37.0 weight percent sulphur at 370°C. At this latter temperature stoichiometric NiS inverts to the low temperature (rhombohedral) millerite structures. The high-temperature form persists with a more sulphur-rich composition (37.0 weight percent sulphur) than NiS down to 282°C, where it breaks down eutectoidally to NiS and Ni_3S_4 as reported by Kullerud and Yund (113).

1.2.3 Composition and Stability Range of Pentlandite

The formula of pentlandite was first settled by crystallographic argument in 1936 by Lindqvist, Lundqvist and Westegren (125). From analogy with the isostructural compound πCo_9S_8 they suggested that pentlandite has a similar metal-to-sulphur ratio, $(Fe.Ni)_9S_8$ and that it is cubic. Lundqvist (97) later found a variation in the Ni:Fe atomic ratio from 0.725 to 1.38 in synthetic pentlandite; the presence of faint pyrrhotite lines in the two synthetic pentlandites of Lindqvist, Lundqvist and Westgren, $Fe_{4.5}Ni_{4.5}S_8$ and $Fe_6Ni_3S_8$ is not consistent with the constancy of the sulphur content reported by Lundqvist for his samples.

Natural pentlandite cannot be regarded as falling wholly within the Fe-Ni-S system. The significant cobalt contents and the large variations reported for the Ni:Fe ratio prompted Eliseev (126) to re-examine the evidence relevant to the composition and formula of pentlandite. He proposed a formula $Fe_4^{iv}\ Ni_4^{iv}\ (Co.Ni.Fe)_{0-1}^{vi}S8$, where the superscript iv refers to tetrahedral and vi to octahedral co-ordination. This formula provides for a variable M:S ratio 1 to 1.125 as well as for a variable Ni:Fe ratio 0.80 to 1.25. Cobalt can be accommodated to a maximum extent of 1/9 of the total metal content, or 7.62 weight per cent Co.

Ibrahim (127), Knop and Ibrahim (128) re-examined the range of compositions of pentlandite and they found that the traditional concept of pentlandite as an iron-nickel sulphide containing small admixtures of cobalt could not be maintained. Instead, pentlandite must be considered a natural face-centered cubic phase π(Fe. Ni.Co. S) within wide composition limits in or close to the M_9S_8 section of the quaternary system Fe-Co-Ni-S (Fig. 20). The M:S ratio of the binary phase π(Co. S) is 9:8 with a very narrow homogeneity range on both sides of Co_9S_8 but in π(Fe, Co, Ni, S) the ratio is somewhat higher and appears to increase with decreasing cobalt content. They proposed that it is quite likely that the sulphur sub-lattice is nearly fully occupied and that departures from stoichiometry are caused by the varying degree of occupancy of the metal sub-lattice.

Soon afterwards pentlandites containing up to 49 weight percent cobalt were reported from the Outokumpu mine, Finland, by Kùovo, Huhma and Vuorelainen (129).

Knop et al (130) showed that the crystal structure of pentlandite does not require a fixed ideal value of the Ni:Fe ratio. Although there was some fluctuation in the results, the Fe:Ni ratio averaged about 1.05:1 for

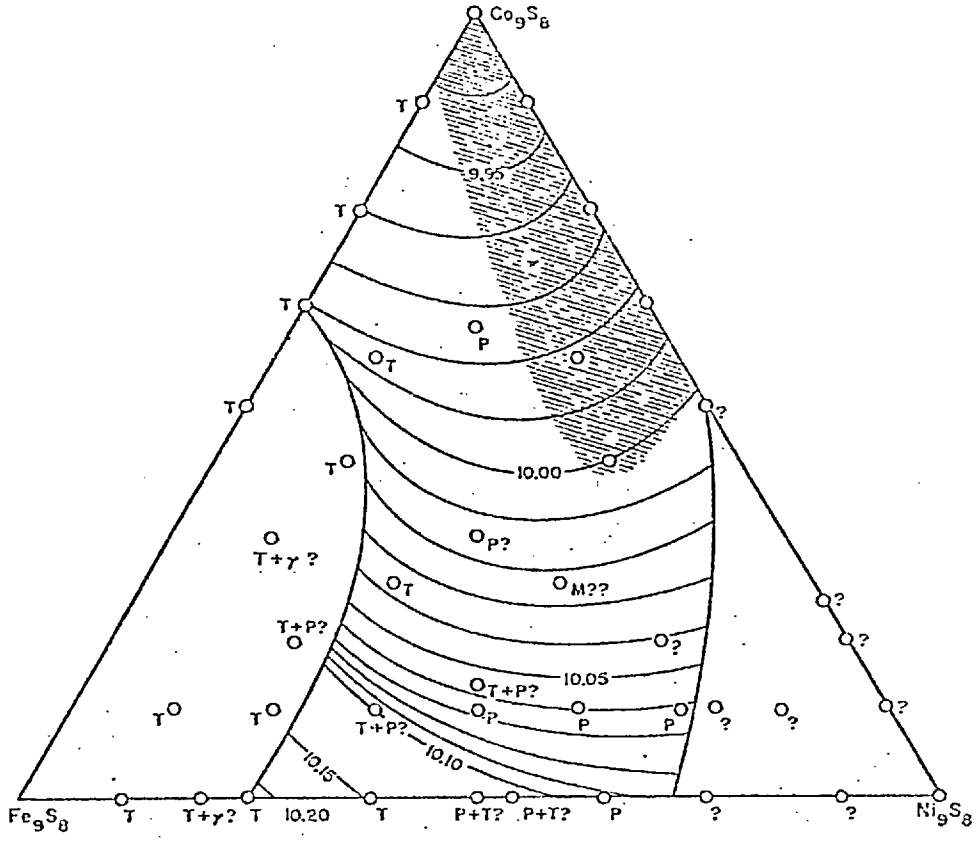

FIG. 20 Limits of Existence of π in the M_9S_8 Section. Shaded area: pure π Area within Curved Boundaries: quasihomogeneous π field.

T: troilite

P: pyrrhotite

M: millerite

(Knop and Ibrahim, (128))

all the pentlandite they examined. They showed that the average metal: sulphur atomic ratio is 1.133 which is slightly higher than the ratio of 1.124 obtained from the M_9S_8 formula. They suggested that the formula range was:

$$Fe_xCo_yNi_z \text{ where } 4.1 < x < 4.7, \quad 0 \leq y < 0.4, \quad 4.0 < z < 4.8$$

Shewman and Clark (115), and Craig and Naldrett (109) examined the monosulphide solid solution (Mss) - pentlandite equilibria and outlined the limits of solid solution of pentlandite at various temperatures (figs. 21, 22). These studies showed clearly, that the composition of pentlandite is closely related to the sulphide mineral assemblage in which it occurs.

Electron microprobe analyses of pentlandite from different districts made by Graterol and Naldrett (131) indicate that the Fe:(Ni + Fe) ratio of pentlandite varies directly with the minerals with which it is associated, ranging from 0.518 for that in association with troilite and intermediate hexagonal pyrrhotite to 0.341 in association with heazlewoodite. The phase diagram suggested by Graterol and Naldrett at low temperature is shown in Figure 23 where the existence of a stable tie-line between pentlandite and pyrite in the Fe-Ni-S system is indicated.

These results are in agreement with those of Harris and Nickel (132). They suggested that the composition of natural pentlandites is intimately related to the sulphide assemblage in which it occurs. Thus, pentlandite in the commonly-found pentlandite-heazlewoodite assemblage contains higher than average nickel contents of about 44 wt.% Ni whereas pentlandite in the pentlandite-awaruite assemblage contains approximately 28 wt.% Ni.

Misra and Fleet (116) determined the Fe and Ni solubility limits of the pentlandite field at temperatures between 200° and 600°C (Figs. 24

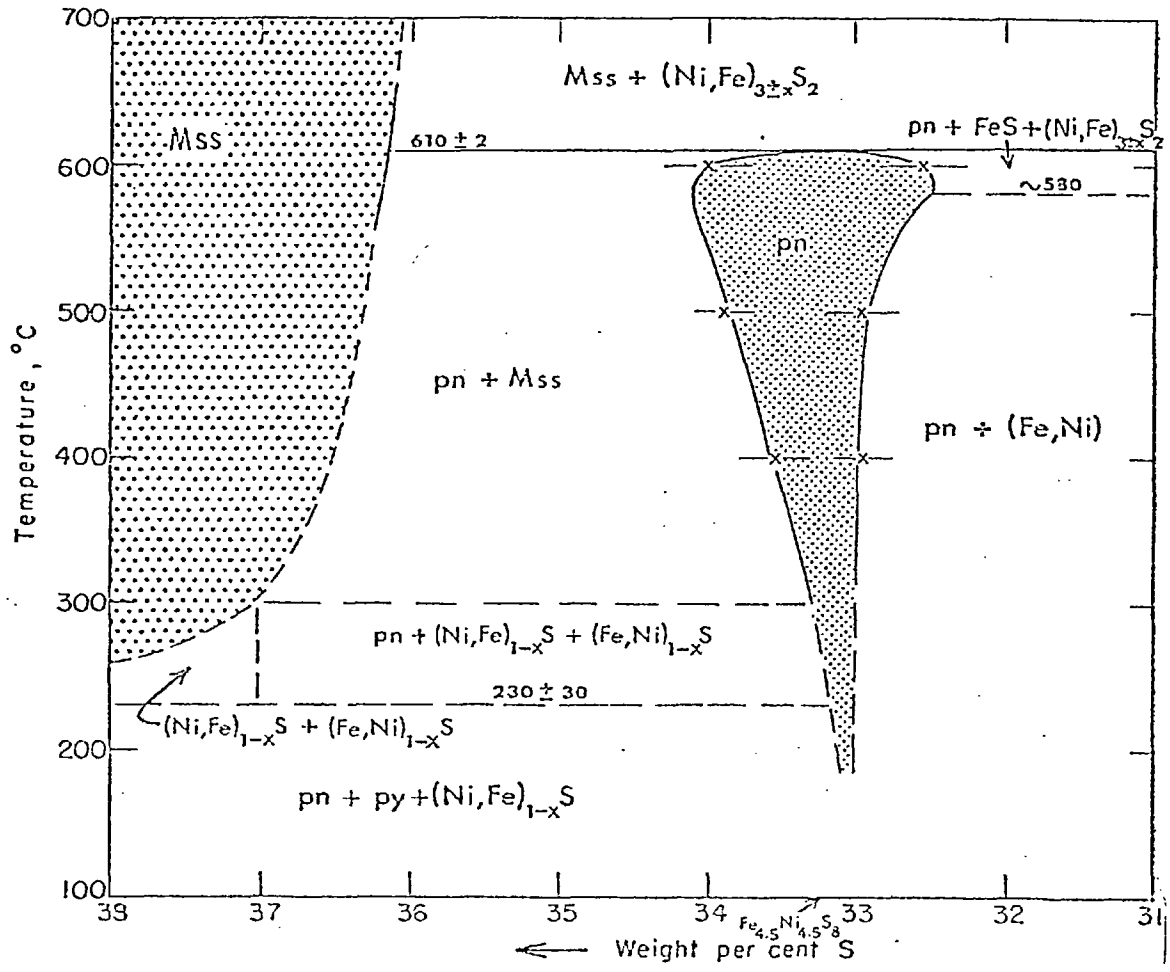

FIG. 21 Phase Relations in the Central Position of the Fe-Ni-S System Along a Section with Atomic Ratio Fe:Ni = 1.1 (Shewman and Clark, (115))

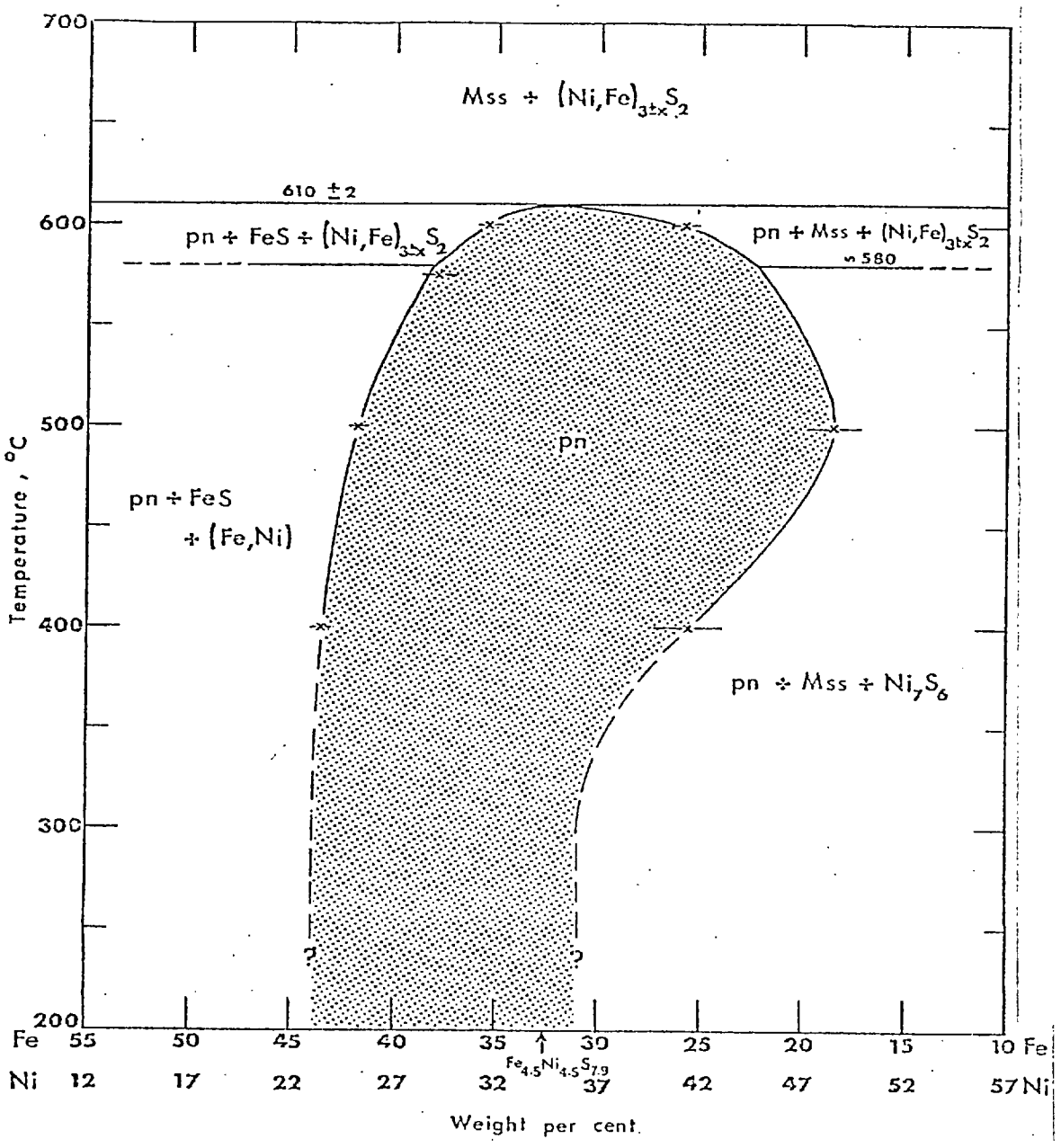

FIG. 22 Vertical Section Through the Pentlandite Solid Solution Field at 33.0 wt % Sulphur (Shewman and Clark, (115))

and 25). The variations in the solid solution limits of pentlandite with temperature, are assymetrical, and somewhat unsystematic. The Fe solubility limit progressively increases with decrease in temperature, from 33 at % Fe at 600°C to a maximum of 40 at % Fe at 285°C and then decreases with falling temperature to 30 at % at 230°C. The Ni solubility limit of the pentlandite solid solution field reaches a maximum of about 41 at % Ni at 600°C and a minimum of 34 at % Ni at 300°C. Most compositions in the pentlandite solid solution field are deficient in S relative to the stoichiometric composition.

Several investigations were made in order to determine the conditions under which pentlandite assemblages may have formed. Kullerud (101) has demonstrated that in the Fe-Ni-S system, pentlandite is unstable above $610^{\circ} \pm 2^{\circ}C$ and forms at this temperature as a result of reaction between the $(Ni,Fe)_{3\pm x}S_2$ and $(Fe,Ni)_{1-x}S$ solid solutions.

Popova, Yershov and Kuznetsov (133) suggest that the decomposition reaction of pentlandite can be expressed in general form by the equation:

$$Fe_{9.4}Ni_{8.6}S_{16} = nFe_{1-x}S + mFe_{9.4-y}Ni_{8.6+z}S_{16} + pS_2\uparrow$$

Naldrett and Kullerud (105) suggested that pentlandite may also form at lower temperature as a result of exsolution from $(Fe,Ni)_{1-x}S$ solid solution.

Several other workers (115), (116), (131), (132) confirmed this by proving that on cooling, the Mss began to break down between 300° and 400°C at a composition of about 33 at. % nickel into two solid solutions and pentlandite.

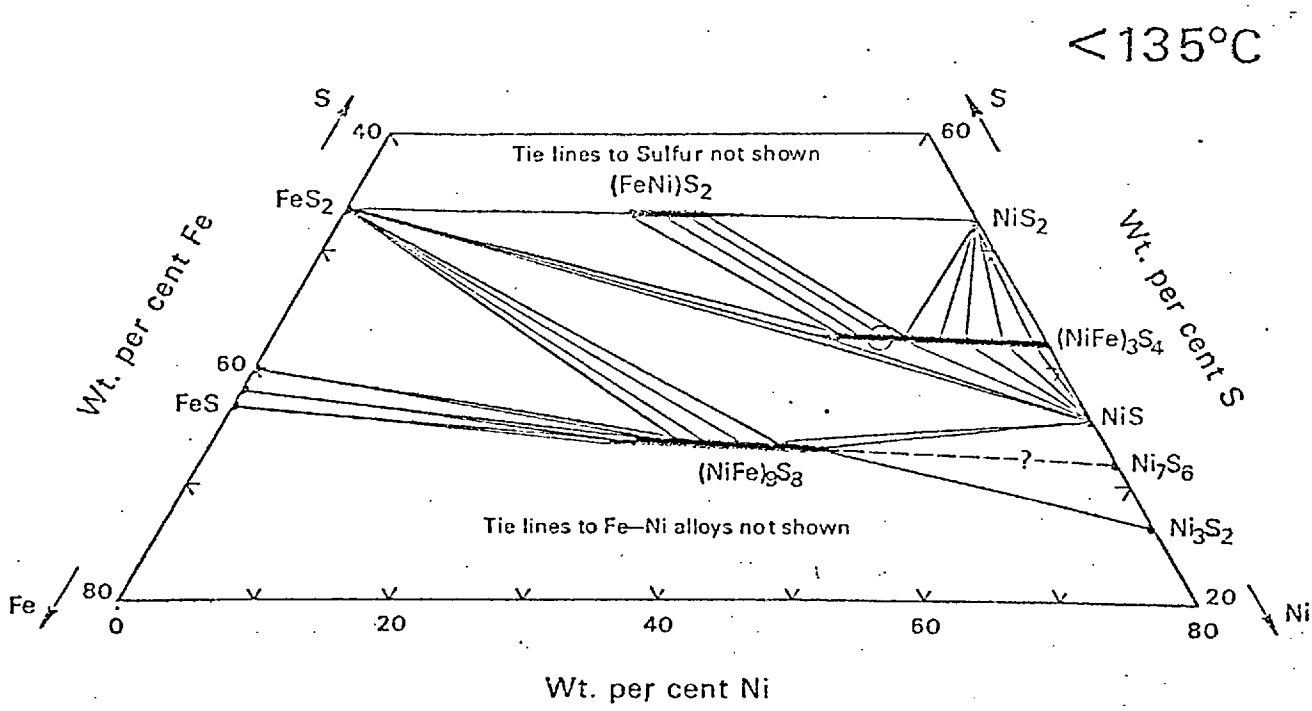

FIG. 23 A Tentative Diagram Showing Phase Relations in the Fe-Ni-S System at Low Temperatures (Graterol and Naldrett, (131))

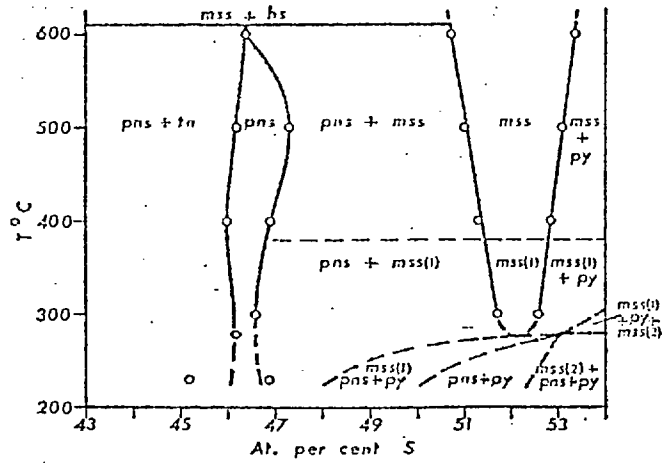

FIG. 24 Section Across Pentlandite Field at Fe:Ni = 1:1 (Misra and Fleet (116))

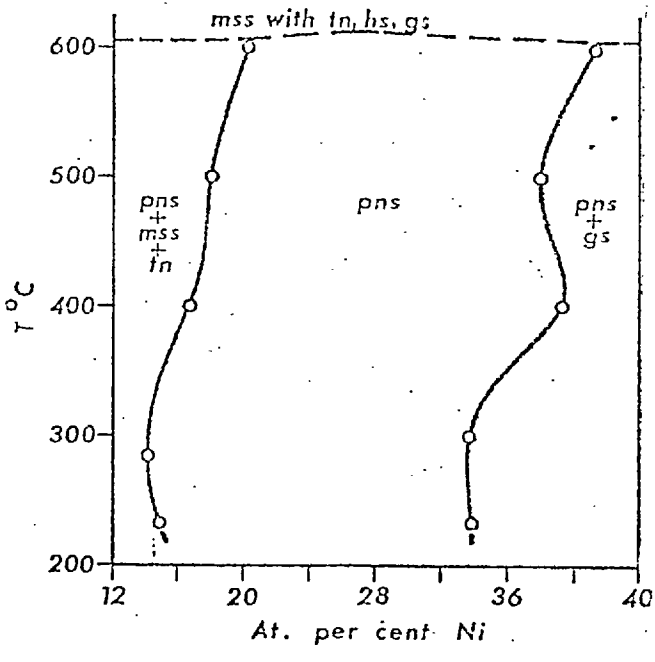

FIG. 25 Section Across Pentlandite Field at 46.4 at % S. (Misra and Fleet, (116))

1.2.4 Crystal Structure of Pyrrhotite and Monosulphide Solid Solution (Mss)

Alsén (134) was the first person to study the crystal structure of pyrrhotite, from data derived from rotating-crystal, laue and powder photographs of crystals from different areas and he assigned pyrrhotite to the NiAs - structure (Fig. 26) with the following cell dimensions:

$a = 3.43$ Å, $\qquad c = 5.68$ Å

Hägg and Sucksdorff (135) investigated artificial preparations of varied iron:sulphur ratio and demonstrated that the variation of composition is the result of omission of metal atoms in the structure. They also discovered that, preparations ranging in composition from 50.0 to 48.3 atomic per cent iron gave powder photographs with superstructure lines. The dimensions of this cell are:

$a = 6.946$ Å $(= \sqrt{3} \times A = B)$
$c = 11.720$ Å $(= 2C)$

Buerger (136) found that material from Morro Velho, Brazil and Schneeberg, Germany exhibited a much larger hexagonal superstructure with $a_1 = a_2 = 6.87$Å $(a = 2A)$ and $c = 22.7$ $(c = 4C)$. Although the composition of the crystals was not known, they were assumed to be iron deficient by virtue of their ferromagnetism. He stated that this cell is probably hexagonal, but the presence of non-space group extinctions suggested that the crystals are twinned and that the true symmetry of pyrrhotite might be monoclinic or orthorhombic.

Bertaut (137) examined a single crystal of pyrrhotite which appeared to have a similar superstructure, with the exception that the symmetry was

monoclinic, the superstructure being monoclinic, 2A, $2A\sqrt{3}$, 4C, $\beta = 89.55^{\circ}$, space group C2/c.

Grønvold and Haraldsen (138) reported that the simple NiAs - cell predominates at room temperature for synthetic compounds from 48.2 to 46.73 atomic per cent iron, whereas more iron-deficient synthetic compounds ranging from 46.73 to 45.44 atomic per cent iron are monoclinic.

The Morro Velho pyrrhotite was re-examined by Wuensch (139). Precession photographs suggested a superstructure with cell dimensions which appeared to be two and four times the A and C dimensions of a NiAs - type substructure. Small displacements of superstructure reflections in the patterns indicated the presence of twinning. It was shown that the true lattice of this pyrrhotite was at least dimensionally monoclinic and it was twinned by a 2-fold rotation about (110). The a and b translations of the cell were twice the orthohexagonal B and A dimensions of the substructure respectively, and was 91.79°. Patterson projections suggested that the superstructure intensities were primarily due to distortion of a NiAs-type arrangement about iron vacancies.

Carpenter and Desborough (140) described a new hexagonal supercell in which a and c are two and five times A and C respectively, of the NiAs-type substructure. This type of supercell was observed in pyrrhotites ranging in composition from about 48.0 ± 0.2 to 47.0 ± 0.2 atomic per cent metals.

Desborough and Carpenter (121) reported that, for quenched pyrrhotites, a pyrrhotite phase with a hexagonal 2A, 5C cell coexisted with the $A\sqrt{3}$, 2C phase below the α-transformation: above the α-transformation and below the β-transformation only the 2A, 5C phase is present in iron-rich compositions; and above the β-transformation all pyrrhotites show a superstructure with a hexagonal 2A, 7C cell (Fig. 18).

Corlett (120) confirmed the existence of two naturally-occurring low-iron pyrrhotite superstructures based on the NiAs-structure. High-temperature photographs show that the transformation from the 4C structure to the NiAs-structure occurs at $225 \pm 10^{\circ}C$ and is unrelated to the magnetic transition above $300^{\circ}C$. Attempts to quench the NiAs-structure produced an orthogonal, apparently hexagonal, type with some sort of 3C repeat distance. In constant, slow cooling always reproduced the 4C structure.

Powder photographs of pyrrhotites in the compositional range 50.0 to 47.7 atomic per cent, taken by Fleet (141) indicated the existence of a superstructure with the hexagonal $A\sqrt{3}$, 2C cell in pyrrhotites having more iron than 48.8 atomic per cent. Pyrrhotites more sulphur-rich than this have a superstructure with a hexagonal 2A, 4C cell. Plots of the lattice parameters of the pyrrhotites studied against composition reveal a marked discontinuity at 48.8 atomic per cent iron. The superstructure phase boundary and the discontinuity are correlated to a structural re-arrangement at this composition.

Fleet (142) confirmed the existence of the hexagonal superstructure of pyrrhotite with a = 2A and c = 3C reported from a quenched, synthetic iron sulphide preparation containing pyrrhotite in equilibrium with pyrite. The x-ray record for it is similar to those for previously reported analogous superstructures, but exhibits reflections in positions equivalent to positions of extinction in the latter.

Morimoto and Nakazawa (143) reported the presence of two new superstructures based on the hexagonal subcell of the NiAs-type: one, in the range $1-x = 0.89$ to 0.93, has a = 90A and c = 3C; the other in the range $1-x = 0.935$ to 0.975, has a = 2A but c irrationally related to C, varying with composition (Fig. 27).

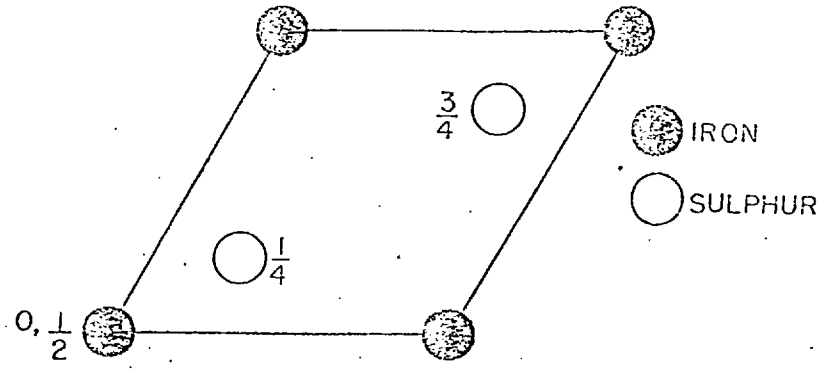

FIG. 26 Diagram of the Simple NiAs Cell Projected on (0001) (Carpenter and Desborough, (140))

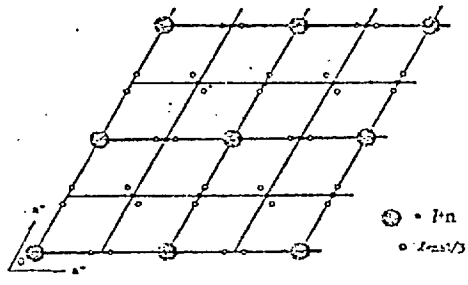

FIG. 27 Reciprocal Lattice Projected on (001) of the 3C Type of Pyrrhotite (Morimoto and Nakazawa, (143))

Fleet and Macrae (144) investigated the crystal structure of hexagonal pyrrhotites, co-existing with troilite. Microscopic and x-ray diffraction studies showed the two unmixed phases had a common crystallographic orientation. The superstructures of the intermediate pyrrhotite in two samples were different from one another and have not been reported previously from natural material, being hexagonal 2A, 6C and hexagonal 2A, 4C.

Evans (145) studied the crystallography of lunar troilite. Euhedral crystals from lunar sample showed a hexagonal habit consistent with the high temperature NiAs-type structure. The superstructure x-ray unit cell as determined by goniostat with a single crystal has a = 5.962 $\pm$ 0.002 and C = 11.750 $\pm$ 0.003Å. Complete three-dimensional counter intensity data have been measured and used to confirm and refine Bertaut's (137) proposed low-temperature crystal structure. The six Fe-S bond lengths in the distorted FeS_6 octahedron were found to be: 2.359, 2.379, 2.415, 2.504, 2.565 and 2.722 Å, all $\pm$ 0.003 Å.

The monosulphide solid solution (Mss) or iron and nickel shows the superstructure of high temperature pyrrhotite (2A, 7C, Desborough and Carpenter (121)). X-ray diffraction studies on Mss of different composition show appreciable variation in the d_{102} values. Shewman and Clark (115) plotted d_{102} values from charges synthesized at 500° and 400°C vs composition (Fig. 17). There is a complete discontinuity in the curve at about 33 atomic per cent Ni. In addition there are sharp changes in slope at 29 and 35 atomic per cent Ni.

From Guinier powder photographs it was shown that the pyrrhotite supercell which develops in some compositions, cooled rapidly from above

315°C are present in Mss from $Fe_{0.83}S$ to about 23 at % Ni. From 23 at % Ni to $Ni_{0.95}S$ the Guinier powder photographs display the niccolite-type patern similar to $Ni_{1-x}S$.

1.2.5 Crystal Structure of Pentlandite

The crystal structure of pentlandite was solved by Lindqvist, Lundqvist and Westgren (125) from powder data. They showed that pentlandite was isostructural with synthetic π(Co,S), Co_9S_8 and consequently wrote its formula as $(Fe.Ni)_9S_8$. The space group of the sulphide was shown to be O_h^5 - Fm3M, and from its experimental density it was inferred that there were four M_9S_8 formula units per unit cell. The 36 metal atoms were distributed over two sets of equivalent lattice sites, one containing 32(f) and the other 4(b) atoms. The 32 sulphur atoms were distributed over 8(c) and 24 (e) equipoints in four-and five-fold co-ordination by metal atoms respectively. The four molecules in its units have atomic parameters as follows:

M (1)	:	(4b)	$\frac{1}{2}$	$\frac{1}{2}$	$\frac{1}{2}$	;	F.C.	
M(2)	:	(32f)	$\pm$(uuu;	$\bar{u}\bar{u}u$;	$\bar{u}uu$;	$u\bar{u}\bar{u}$);	F.C.	
S (1)	:	(8c)	$\frac{1}{4}$	$\frac{1}{4}$	$\frac{1}{4}$;	$\frac{3}{4}$	$\frac{3}{4}$	$\frac{3}{4}$; F.C.
S (2)	:	(24e)	$\pm$(uOO;	OuO;	OOu)	F.C.		

where $u_m = 1/8$ and $u_s = \frac{1}{4}$

Eliseev (126) suggested that the crystal structure of natural pentlandite differed from the structure proposed by Lindqvist, Lundqvist and Westgren in the positions of the octahedrally co-ordinated metal atoms.

He proposed that the four metal atoms are placed in 4 (α) : OOO etc. Eliseev's structure differ from the previous arrangement by concentrating all the metal atoms in the antifluorite-type cell, leaving the alternate cubes empty (Fig. 28).

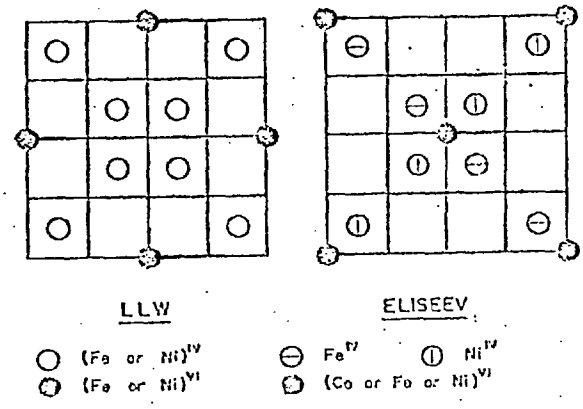

FIG. 2 8. Schematic representation of the differences between the Two Crystal Structures Proposed for Pentlandite by Lindqvist, Lundqvist and Westgren (LLV) and by Eliseev (Knop and Ibrahim (128))

The iron and nickel atoms occupying 32(f) in Eliseev's structure were assumed to be present in the ratio 1:1 and completely ordered. The order arrangement of the metal atoms would be expected to lower the observa summetry of the unit cell.

The space group and the structure proposed by Lindqvist, Lundqvist and Westgren were later confirmed by Pearson and Buerger (146) and by

Knop and Ibrahim (128). The latter calculated the cell dimension for $Fe_{4.5}Ni_{4.5}S_8$ as a = 10.115 $\pm$ 2 Å which is in a very good agreement with that calculated by Lindqvist et al., a = 10.11 Å

Geller (147) studied the crystal structure of Co_9S_8 which is isostructural to pentlandite. He found that the octahedral sites are nearly regular with Co-S distance, 2.39 $\pm$ 0.03 Å, tetrahedral sites are distorted to give the site symmetry 3m, with one Co-S distance being 2.13 $\pm$ 0.02 Å and the other three being 2.21 $\pm$ 0.02 Å. Each of the cobalt atoms with tetrahedral sulphur co-ordination is also linked to three similarly co-ordinated cobalt atoms of a distance of 2.50 $\pm$ 0.02 Å which is essentially the metallic cobalt distance in elementary cobalts, indicating considerable metallic bonding. An S atom in c is at the center of a regular tetrahedron of Co(f) atoms. An S atom in e is co-ordinated to 1Co(b) atom at 2.39Å and 4Co(f) atoms at 2.21Å, the Co atoms being at the corners of a pyramid with square base. Thus on S(c) atom is at the corner of one octahedron and four tetrahedra. In a sulphur tetrahedron each of the three edges involving only S(e) atoms is shared by another tetrahedron. The sulphur octahedra share only corners with tetrahedra.

Work by Knop et al (148) and Vaughan and Ridout (149) suggested a greater preference of iron for the octahedral sites in natural material and a reversal of this situation on annealing. Vaughan and Ridout also suggested that the absence of any paramagnetic moment on the tetrahedral iron atoms indicates delocalisation of the metal d electrons, probably associated with the formation of cubic clusters of tetrahedral metal atoms with very close metal-metal distances, which occur in pentlandite.

Studies on the crystal chemistry of pentlandite by Vaughan and Burns (150) indicate that tetrahedral cations from hybrid $sp^3 + sd^3$ orbitals with the sulphurs, leading to splitting of the metal 3d orbitals into

e and t_2 groups. Metal-metal bonding in pentlandite leads to filled e and t_2 bands and the short distances within the cube-clusters of the tetrahedrally co-ordinated metals. The octahedrally co-ordinated Fe(II) and Co(III) ions believed to have low-spin configuration.

Rajamani and Prewitt (151) studied the crystal structure of pentlandite from Frood Mine, Ontario and cobalt pentlandite from Outokumbu, Finland. The structures of these pentlandites were found to be very similar to that of synthetic Co_9S_8. The interatomic distances in these pentlandites including synthetic Co_9S_8 suggest that the octahedral Co in pentlandite could be divalent, low-spin. The octahedral Fe^{2+} probably is in the high-spin state. The tetrahedral Co-S distance in synthetic Co_9S_8 is identical to the Co-S in Co_3S_4 which is a normal thiospinel and suggests that tetrahedral Co could be divalent. Similarly the tetrahedral M-S distances in natural pentlandites are consistent with divalent cations in tetrahedral co-ordination, although valency for tetrahedral cation is an ambiguous concept because of the delocalization of d electrons. Because of the metal-metal bonding and cluster formation, the total number of d electrons in the unit cell remains uniform, as in an electron compound, in spite of large variations in compositions. Since Co_9S_8 and $Fe_{4.5}Ni_{4.5}S_8$ are the most stable phases with complete solid solution, it can be assumed that the structure is stabilized by seven d electrons per cation. Increasing the Ni content in pentlandite over 4.5 atoms in the formula unit would cause cation vacancies in the tetrahedral sites if the number of d electrons in the cube cluster were kept constant. Therefore the formula for pentlandite can be written:

$$^{vi}(Fe_uNi_v)\ ^{iv}(Fe_xNi_y\ \square_z)_8S_8$$

where x= mole fraction of Fe in the tetrahedral sites

y = mole fraction of Ni in the tetrahedral sites

z = tetrahedral vacancy for Ni-rich compositions or excess cations for Fe-rich compositions.

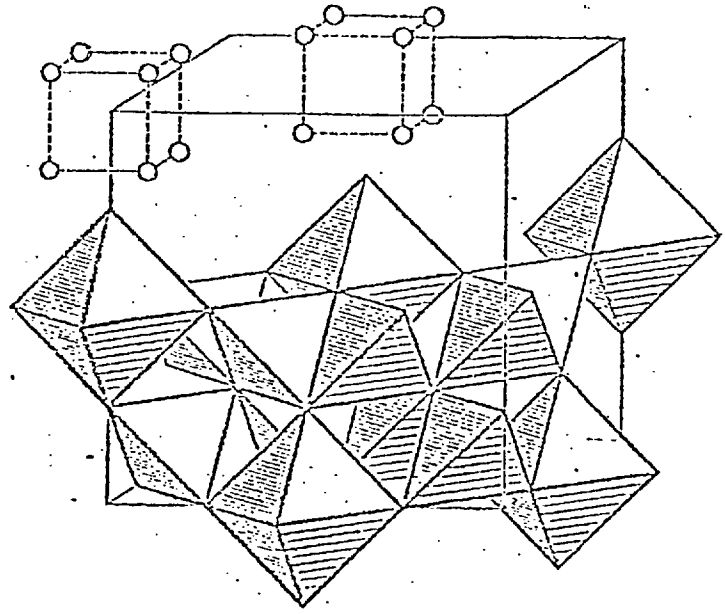

FIG. 29 Cubic Structure of Pentlandite Showing Co-ordination Polyedra around the Cations (Hulliger (152))

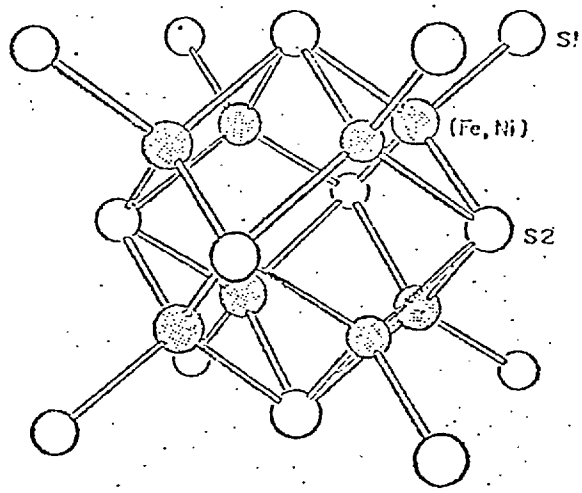

. Part of the Pentlandite structure showing the "cube cluster" of tetrahedral cations which are coordinated to one S1 and three S2 atoms.

FIG. 30 Co-ordination in the Pentlandite Structure (Ramjamani and Prewitt (151))

$$z = ((x \times 6) + (y \times 8) - 7) \div 7$$

and the metal: sulphur ratio in pentlandite will be given by:

$$M/S = (9 - 8z) \div 8 = 1.125 - z$$

CHAPTER 2

EXPERIMENTAL PROCEDURE

2.1 SYNTHESIS OF THE SULPHIDES

2.1.1 Synthesis of Monosulphide Solid Solution (Mss)

Monosulphide solid solution (Mss) was synthesized by heating to 1200°C mixtures of nickel and iron sponge and sulphur to give the required stoichiometry. The analysis of the materials used for the synthesis is given in section 2.5.1.

The nickel and iron sponge were previously reduced in a stream of hydrogen at 500°C. The sulphur powder was dried in an oven at 70°C.

The technique employed for the synthesis, involved the use of a two-compartment silica vessel, similar to those used by King (153). The sulphur powder was placed in the bottom compartment, while the metal powder was introduced into the larger top compartment. The idea of using the two-compartment vessel was to avoid contact of the melted sulphur with the metals which would result in an uncontrolably fast and possibly explosive reaction at some stage as the temperature increased (West (154), Baker (155)).

The silica vessel was evacuated by connecting the open end to an oil-diffusion pump and was sealed with an oxygen torch.

The reaction tube was then placed within the constant temperature zone of a horizontal electric tube furnace, designed to reach 1100°C. The heating was controlled by a transitol electronic controller and the temperature

of the silica vessel checked with a 13% Pt - Pt/Rh thermocouple connected to a compensating. Control to within $\pm 2^{\circ}C$ was then possible.

The temperature was slowly increased to $600^{\circ}C$ and kept at this value for about three days to allow all the sulphur to react with the metal in the vessel. After the end of this period which was indicated by the silica vessel becoming clear of sulphur vapour, it was possible to increase the temperature without any danger, because the vapour pressure over the sulphide is much lower than the vapour pressure over the sulphur.

The temperature was then slowly increased during a period of two days to $1200^{\circ}C$ and kept there for about two hours. At this temperature the content of the vessel was melted as was expected from the study of the phase diagrams of the system Fe-Ni-S (1.2.1). The use of such a high temperature reduced considerably the length of time required for the synthesis of the Mss.

The reactor furnace was then switched off, the silica vessel was allowed to cool slowly to about $600^{\circ}C$ and then it was quenched. The reason for quenching was because as can be seen from the phase diagrams, Mss is not a stable phase at room temperature. Slow cooling to room temperature of the Mss would cause a breakdown of the Mss phase at some temperature between 300° and $200^{\circ}C$ to form two other phases, one rich in iron and the other rich in nickel as is described in details in section (1.22).

One part of the final product was annealed at $550^{\circ}C$ for a period of five days in a silica vessel, previously evacuated and sealed. After the fifth day, the vessel was quenched. No difference at all was observed between the annealed and non-annealed mineral.

The final product obtained was a compact crystalline mass having an opaque colour, lustre strongly metallic. On opening the vessel in air, the crystals immediately changed to tambac colour, normally associated with natural pyrrhotite surfaces.

Several analyses were made to check the homogeneity and the composition of the material.

The microscopic examination on polished sections showed no heterogeneity only one phase being revealed.

The x-ray diffraction patterns of a number of samples from different areas of the solid mass gave only the lines of the Mss (Shewman and Clark (115)).

Electron probe microanalysis confirmed the homogeneity of the material. The picture of the electron probe scans across the polished survace of some grains of the material is given in Figure 31. Three particles of the material were measured (two points on each, six in all) for Fe, Ni and S, the standards being the pure metals and CdS. The results were as follows:

TABLE 1

	S		Fe		Ni	
	wt %	at %	wt %	at %	wt %	at %
particle 1 :	42.60	56.85	35.34	27.08	22.06	16.08
particles 2 + 3 :	42.73	57.01	33.90	25.95	23.36	17.02
average all three	42.69	56.96	34.38	26.34	22.93	16.71
Initial :	38.50	55.00	36.50	26.30	25.00	18.70

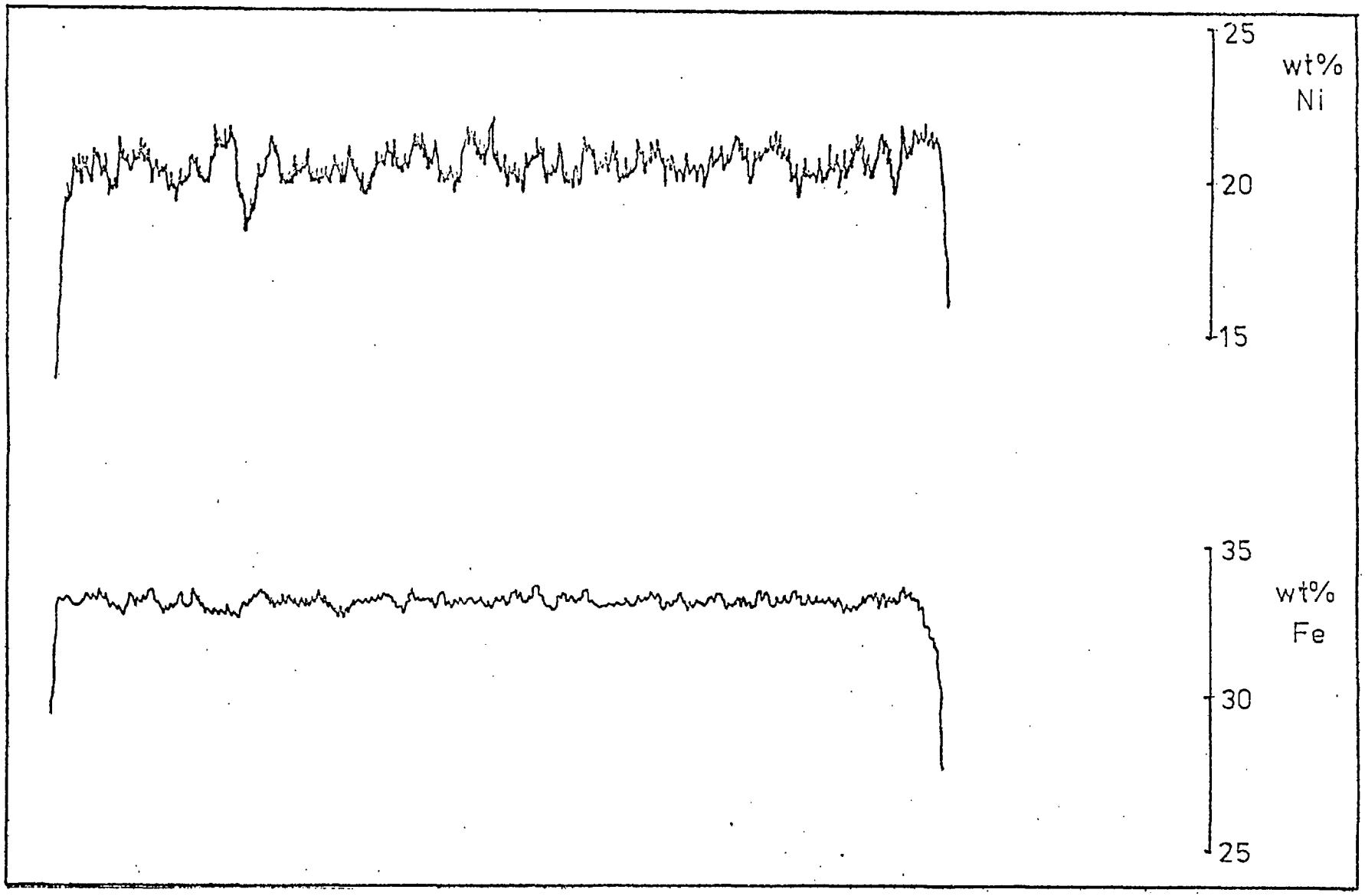

FIG. 31 Electron Microprove Trace Showing the Variation in Nickel and Iron in the Original Mss

Atomic absorption analysis of the material, dissolved in nitric acid using the technique described in section (2.4.1) gave results in good agreement with the initial concentration of the elements used.

	Fe		Ni	
	wt %	at %	wt %	at %
average analysis	37.30	29.58	25.80	19.44
initial concentration	36.50	28.64	25.00	18.68

Finally the composition of the material prepared was checked by means of volumetric analysis for the iron and of gravimetric analysis for the nickel.

The ferric iron was reduced by stannous chloride and titrated with standard 0.1M potassium dichromate. The method used is described in detail in Vogel((156), page 309). The analysis gave 36.74 wt.% Fe which is in very good agreement with the initial amount of iron which was 36.50%.

Nickel was determined by precipitating it as dimethylglyoximate by the addition of an alcoholic solution of dimethylglyoxime to the solution of the material. This method, which is also described in detail in Vogel ((156), page 526) gave results in very good agreement with the initial amount of nickel in the Mss. (24.90 wt % Ni instead of 25.0% of the initial amount.)

2.1.2 Synthesis of Pentlandite

Pentlandite was synthesised using similar heating procedure to that described above for producing monosulphide solid solution. The object was to synthesize pentlandite containing 0.25 wt % platinum and 0.25 wt % palladium, in order to study the behaviour of these metals during the acid

leaching of pentlandite, since the latter is one of the main sources for the recovery of the platinum group metals.

The required amounts of the elements to give the stoichiometry of pentlandite were heated to 1200°C using the two-compartment silica reaction vessel also used for the production of Mss.

The platinum and palladium were added in the reaction vessel in the form of sulphides because it was thought that this form was more likely to provide solid solutions of these metals with pentlandite.

Since only palladium chloride and platinum metal in the form of thin wire were available, in order to produce the sulphides, the palladium chloride was dissolved in hydrochloric acid and platinum wire in hot aqua regia. From these solutions the metals were precipitated as sulphides by hydrogen sulphide produced in a Kipp's apparatus ((156), page 156).

The final pentlandite product was a crystalline mass, very brittle and porous. On opening the vessel in air, the surface was covered by a dull blue layer, probably of oxide. The new surfaces showed a light cream brown colour, with bright metallic lustre.

Microscopic examinations were carried out on a number of samples from different areas of the solid mass, mounted in araldite. In reflected light all the samples showed that the main phase was pentlandite having a cream colour and rather high reflectivity under the microscope. In some samples, using high magnifications a second phase, having a very high reflectivity compared to that of pentlandite, with a pure white colour and tint varying from bluish to yellowish appeared. This phase which was present in a very small amount was determined by electron probe analysis to be platinum.

Under policized light, complete darkness was not attained for pentlandite and a third anisotropic phase in small amounts was also revealed (Fig. C-3.2). This third phase was proved to be pyrrhotite.

X-ray analysis of a number of samples gave lines of both pentlandite and pyrrhotite (Fig. C-1.1, Table B-3.2). No lines corresponding to platinum or palladium content of pentlandite were obtained and this was due to the very low concentration of these metals.

One sample was analysed for nickel, iron, platinum and palladium in the electron probe microanalyser. From this analysis, it was shown that the pentlandite areas were homogeneous considering the iron and nickel content, and a typical picture of the electron probe scans across the surface of pentlandite is given in Figure 32.

Spectrum checks were made for palladium and platinum in the pentlandite areas. Using an area scan (to improve probability of finding these if present only as small spots), palladium was just detectable (2-3 divisions on a background of 18-20), whereas platinum was not.

Palladium and platinum were traced along the same line, as far as possible, as the nickel and iron. Palladium showed a slight presence with a few broad peaks, while again platinum was not detected.

The sample was then traced on the 'white' high reflectivity areas observed under the microscope. The electron probe scans across these areas showed the picture given in figure 33. This peak corresponding to the very sharp increase of platinum concentration as the electron scans entered the 'white' area showed that this metal was concentrated in the 'white areas'; but thus for the nature of the platinum phase in these areas was not identified.

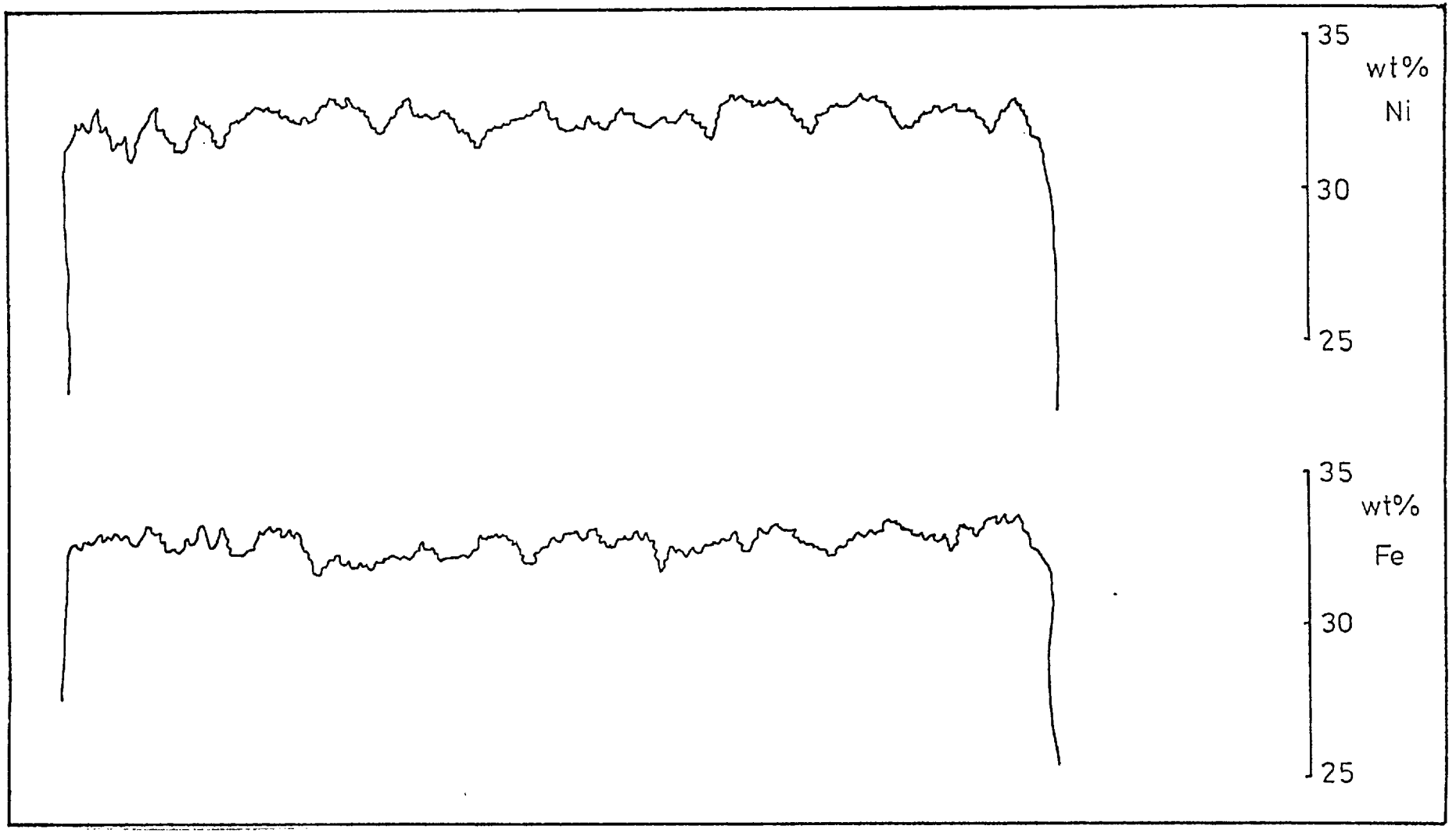

FIG. 32 Electron Microprobe Trace Showing the Variation in Nickel and Iron Composition of the Original Pentlandite

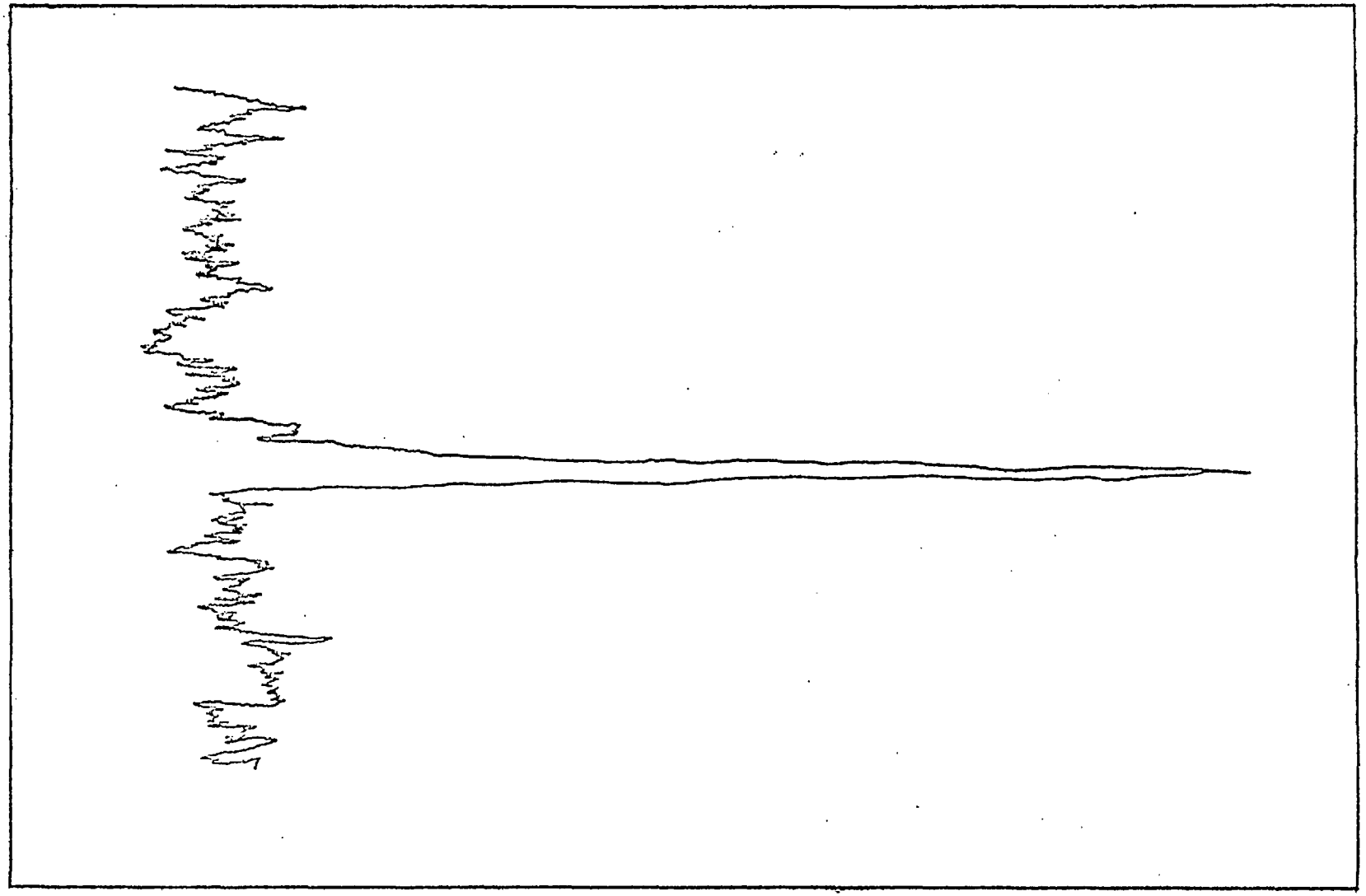

FIG. 33 Electron Microprobe Trace Showing the Existence of a Discrete Platinum Phase in the Original Pentlandite

To determine this, back scattered electron image (B. E. I.) pictures were taken from different areas of the sample containing the 'white' phase. Two series of these pictures are shown in figures 34 and 35. As can be seen from these pictures, areas A (Fig. 34) corresponding to pentlandite show homogeneity for iron, nickel and sulphur. Area B, corresponds to pyrrhotite, indicated by the lighter colour in the picture for iron and by the darker colour in the picture for nickel. Areas C correspond to metallic platinum, since these areas remain dark in the picture for iron, nickel and sulphur.

From these results obtained by the electron probe analysis it was concluded that the synthesized mineral consists mainly of pentlandite, containing small amount of pyrrhotite. Palladium forms a solid solution with pentlandite, while platinum in the metallic form, forms discrete inclusions.

Atomic absorption analysis of the material for nickel and iron gave results very close to the amounts of metals initially used for the synthesis of pentlandite.

	Fe		Ni	
	wt %	at %	wt %	at %
Average analysis:	31.95	26.58	33.54	26.53
Initial concentration:	32.253	26.44	33.921	26.44

The concentration of platinum and palladium in pentlandite was checked using the analytical method described in Section 2. 3. 3. The results obtained were platinum: 0. 23 wt % and palladium: 0. 25 wt %.

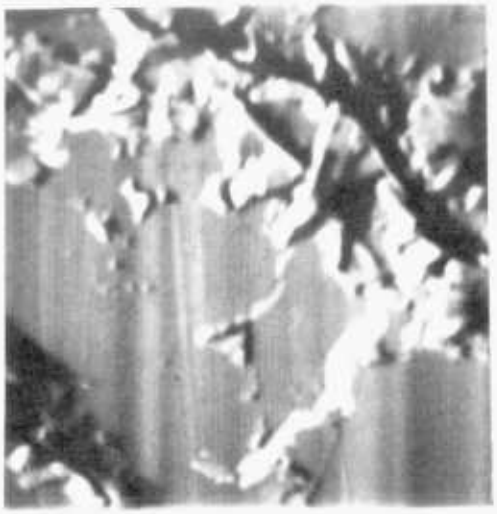

Photomicrograph (x320)

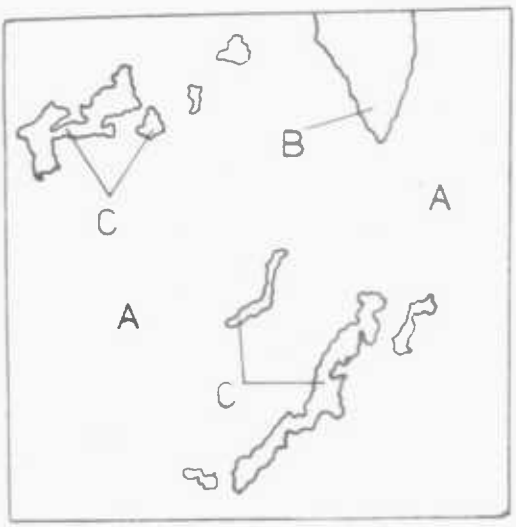

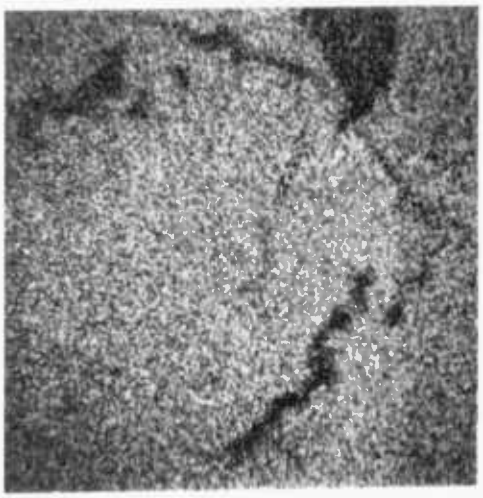

B. E. I. Picture of Nickel

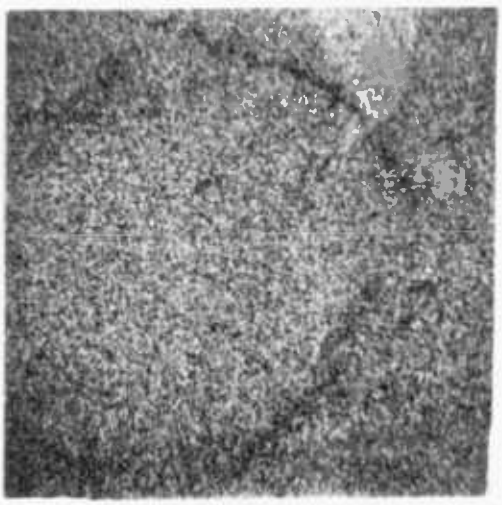

B. E. I. Picture of Iron

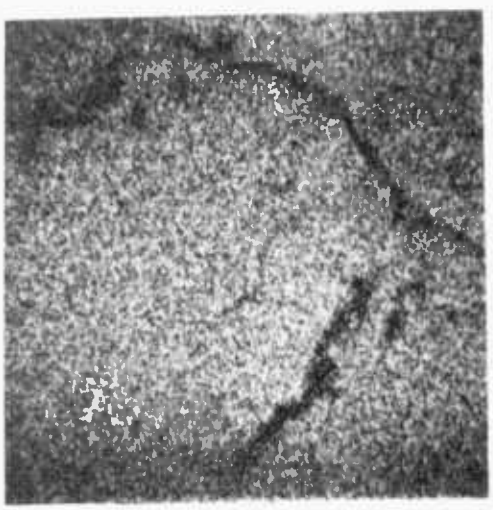

B. E. I. Picture of Sulphur

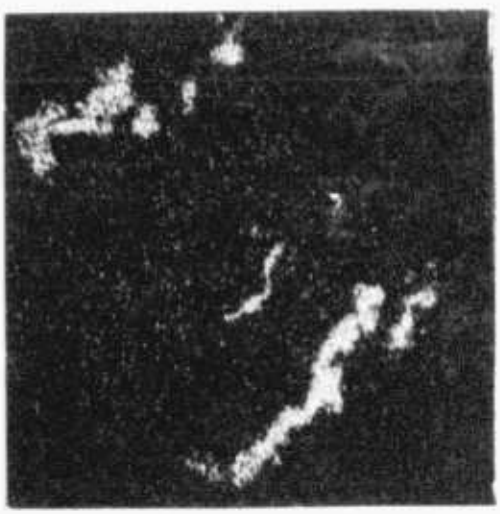

B. E. I. Picture of Platinum

FIG. 34 Back Scattered Electron Image (B. E. I.) Pictures showing the Existence of Pyrrhotite and Metallic Platinum in Pentlandite

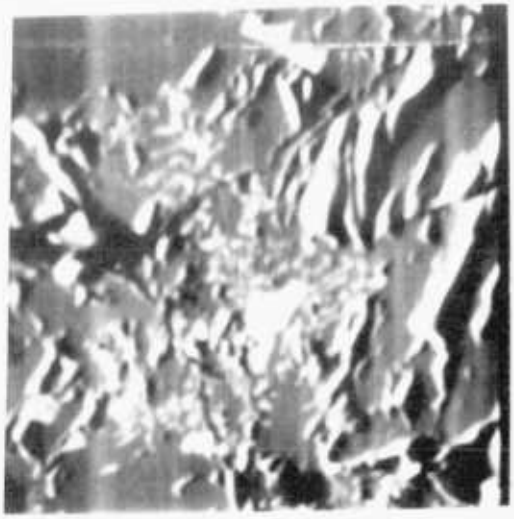

Photomicrograph (x216)

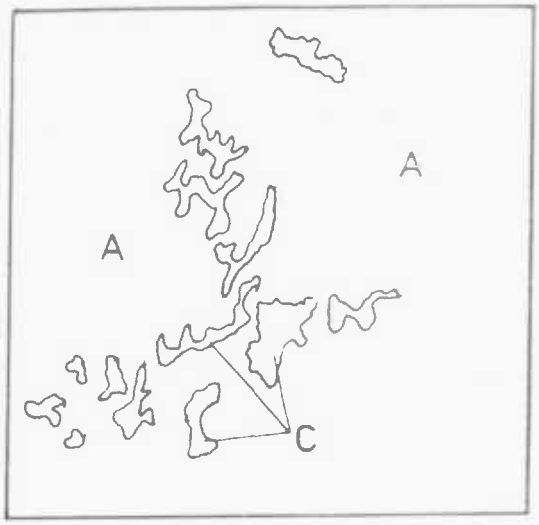

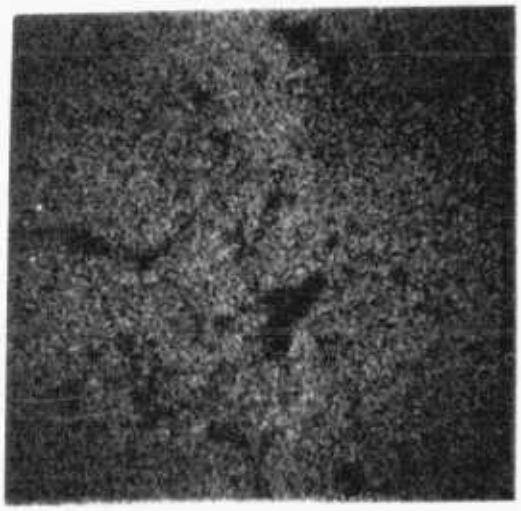

B. E. I. Picture of Nickel

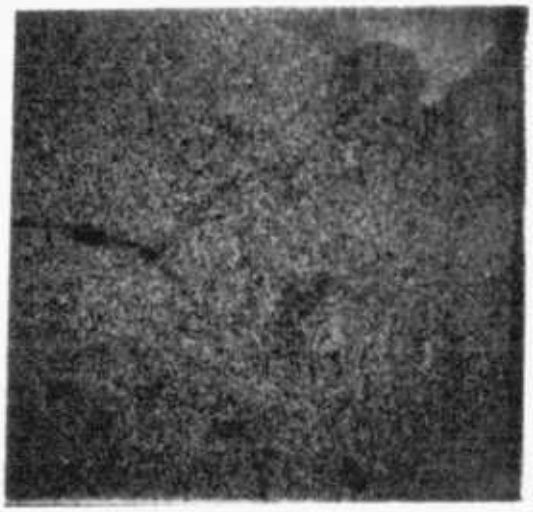

B. E. I. Picture of Iron

B. E. I. Picture of Sulphur

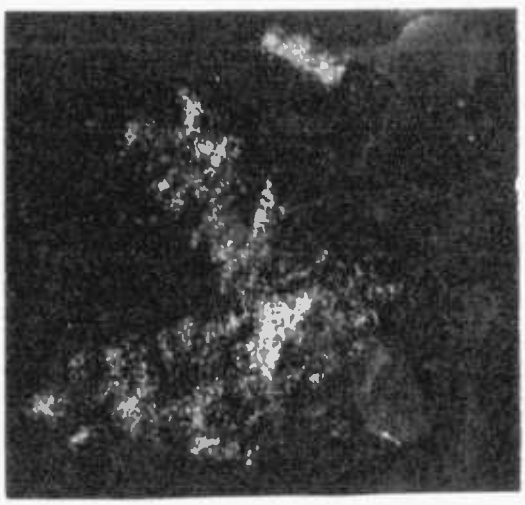

B. E. I. Picture of Platinum

FIG. 35 Back Scattered Electron Image (B. E. I.) Pictures showing the Existence of Metallic Platinum in Pentlandite

2.2 LEACHING APPARATUS AND EXPERIMENTAL PROCEDURE

The apparatus used in all the leach experiments consisted of a 250 cc Quickfit wide reaction vessel connected to a five neck lid by a metallic clip (fig. 36).

The agitation of the leaching system was provided by a simple two-bladed glass propeller held by the central neck of the lid. The rotary movement of the propeller was provided by a RZR laboratory stirrer and the vibrations were damped by passing the propeller through a silicon oil seal. The speed of the stirrer could be varied from 170 to 1800 rpm.

In the other four necks of the lid were a thermometer to check the temperature of the solution, a baffle, in the position opposite to that of the thermometer, to provide sufficient turbulent regime in the solution and keep the particles in suspension, a condenser to avoid evaporation and, in the fourth neck, on the opposite side of the condenser, a tube for direct pipetting of the solution.

Heating of the system was achieved either by using a 300 watts electric heating mantle and a Cressall rotary thermostat to control the temperature, or by immersing the reaction vessel in an oil bath to the level of the vessel lid joint.

The bath capacity was 20 litres with internal measurements of 527 x 247 x 202 mm. The temperature of the oil was controlled by a Griffin Accurostat, a combination of a heater, pump and temperature sensor. The unit controlled temperatures in the range ambient to 95^{o}C with a fluctuation under optimum conditions of 0.02 deg. C. The 1 KW tubular heater is protected by a liquid level cut-out device, and a safety overheat

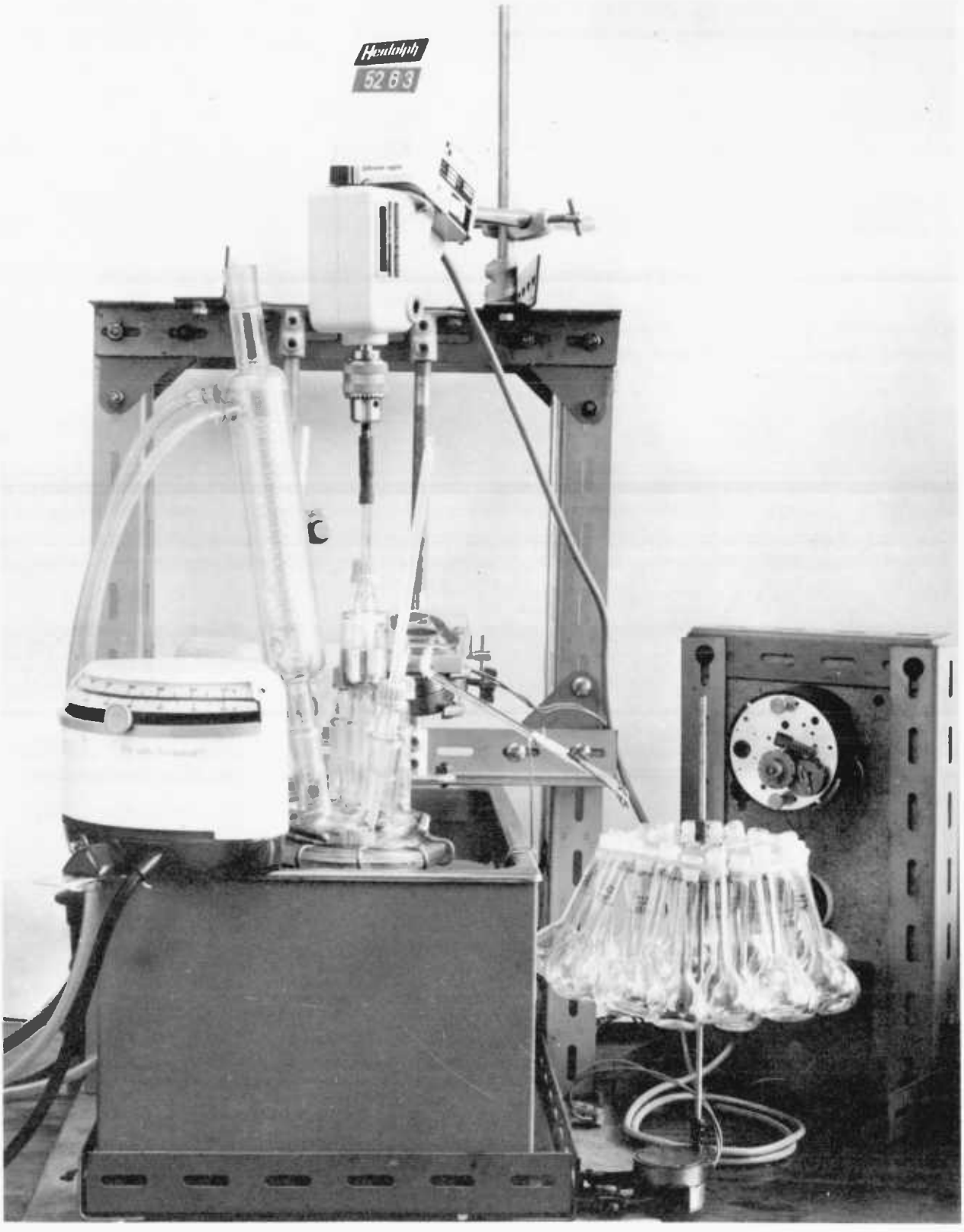

FIG. 36. Leaching apparatus

cut-out operates should the bath temperature rise 2-3^{o}C above the set point. Circulation of the bath liquid is given by a centrifugal pump with an output of 8 litres/minute.

The leaching procedure was carried out as follows:

As soon as the apparatus was set up, 200 mls of leaching solution of the required concentration was poured into the reaction vessel. The whole system was allowed to reach thermal equilibrium and then the solid synthetic material was injected through one of the necks of the lid, using a thin funnel which was immediately afterwards rinsing with solution previously extracted from the reaction vessel, to remove any adhering particles.

The synthetic sulphide material was crushed just before starting the leaching procedure to avoid oxidation of the particles, and was sieved using 100 mm diameter stainless steel sieves to provide the required particle size range.

Aliquots of the leach solution were extracted periodically using a 2 mls pipette. Usually two samples a day were enough, except on the first day of the run, when the sampling was more frequent. Whenever a sample was taken the same volume of fresh leaching solution, kept at the temperature of the run, was injected into the reaction vessel to maintain a constant volume of solution. Calculations involving the determination of final concentrations took into account the dilution factor of the products.

During some of the leaching experiments a small amount of the solid residue was removed from the reaction vessel and was used for x-ray diffraction, electron probe microanalysis and microscopic examination.

At the end of the leaching run the reaction vessel was taken from the heating mantle or the oil bath and left to cool down. Then its content was filtered to separate the leach liquor from the solid residue. The latter was washed with distilled water and acetone and dried. Then it was subjected to x-ray diffraction analysis, microscopic examination, electron probe microanalysis and to atomic absorption analysis, after it was dissolved using the technique described in section (2.4.1). The atomic absorption analysis required the removal of the elementar sulphur from the residue prior to dissolving it. The elementar sulphur was dissolved in CS_2 using a Soxhlet extractor apparatus with single thickness 10 x 50 mm cellulose extraction thimbles for holding the residues.

In order to study the effect of the leaching agent on one surface of the material, a few experiments were carried out using samples of the mineral mounted in araldite regin, so that only one surface was subjected to leaching.

The same apparatus described above was used. Solid slices of the sulphide material were placed in araldite mounts and were suspended through a polythene strip connected to the mount, passing them through one of the necks of the lid of the reaction vessel. At various intervals these mounts were taken out of the solution, remounted and polished and were then subjected to microscopic and electron microprobe examination. Photographs of some of these mounts were also taken (Appendix C).

It was necessary for some leaching experiments to be carried out in the absence of oxygen. In this case the experiments were run under a nitrogen atmosphere, the nitrogen being provided through the condenser. In order to remove all the oxygen from the reaction vessel and the solution

before the reaction started, the supply of nitrogen was started two hours before the addition of the solid to the solution; the flow of the gas was adjusted so as to make the nitrogen pressure in the reaction vessel slightly higher than the atmospheric pressure. Thus any entry of air in the vessel was avoided.

2.3 ANALYSIS OF LEACH SOLUTIONS

2.3.1 Atomic Absorption Spectrophotometry

Since gravimetric analysis for nickel and volumetric analysis for iron were found to be very lengthy, atomic absorption spectrophotometry was applied to analyse nickel and iron concentrations in the leach samples and the final leach solutions. The apparatus used was a single beam Perkin Elmer 290B Spectrophotometer with a graphical read-out on a Perkin Elmer Model 56 pen recorder.

The analyses were made using a multi-element hollow cathode lamp either for the elements Ag-Cu-Fe-Ni-Cr or for the elements Fe-Cu-Ni. The wavelengths used were 2320Å for nickel and 2483Å for iron. Generally the technique described in the Perkin Elmer Analytical Methods Manual (158) for the determination of nickel and iron was followed.

Calibration curves of deflection versus concentration were drawn, using standards prepared from 1000 ppm stock solutions. Hydrochloric acid solution of 0.1m was used as a diluent for both these solutions and the aliquots of the leach liquor. Good linearity for the calibration curves was obtained in the range 0-5 micrograms/ml and the optimum conditions for the equipment used occurred in the working range 0-10 micrograms/ml for both the elements.

The aliquots of the leach solution and the final solutions were diluted, using a 'Hook and Tucker' Variable diluter, so that the nickel and iron concentrations were within the working range. The operation was always checked several times to ensure no errors occurred in the dilution.

2.3.2 Analysis of the sulphate Concentration in the Leach Solutions

Since the existence of sulphate in the leach solutions was confirmed by the formation of a white precipitation of barium sulphate after the addition of a concentrated solution of barium chloride to the leach solutions, determination of the rate of formation of sulphate during the experiments, which should give the rate of oxidation of sulphur to sulphate, seemed to be very useful for the study of the chemical reaction occurring.

These analyses proved to be a difficult problem, the major reason being the very low concentration of sulphate which required a very sensitive method of analysis.

The analyses were made using the method described by Kelt (59). The principle of this method is based on the very low solubility of barium sulphate in water and not very acidic solutions. So if to the leach solutions, a known amount of a standard solution of barium chloride was added, sufficient to react with all the amount of the sulphate present in the leach solution, it was possible to measure the amount of barium remaining in solution by using atomic absorption spectrophotometry and so to determine indirectly the sulphate concentration.

For the calibration for the sulphate analysis, an identical barium chloride solution was added to a number of standard sulphate solutions of different concentrations and the readings of the atomic absorption spectrophotometer were plotted directly against the initial sulphate concentration. In this way it was possible to measure directly the concentration of sulphate in the leach solutions. In Fig. (37) a liquid calibration curve for the sulphate analysis is given.

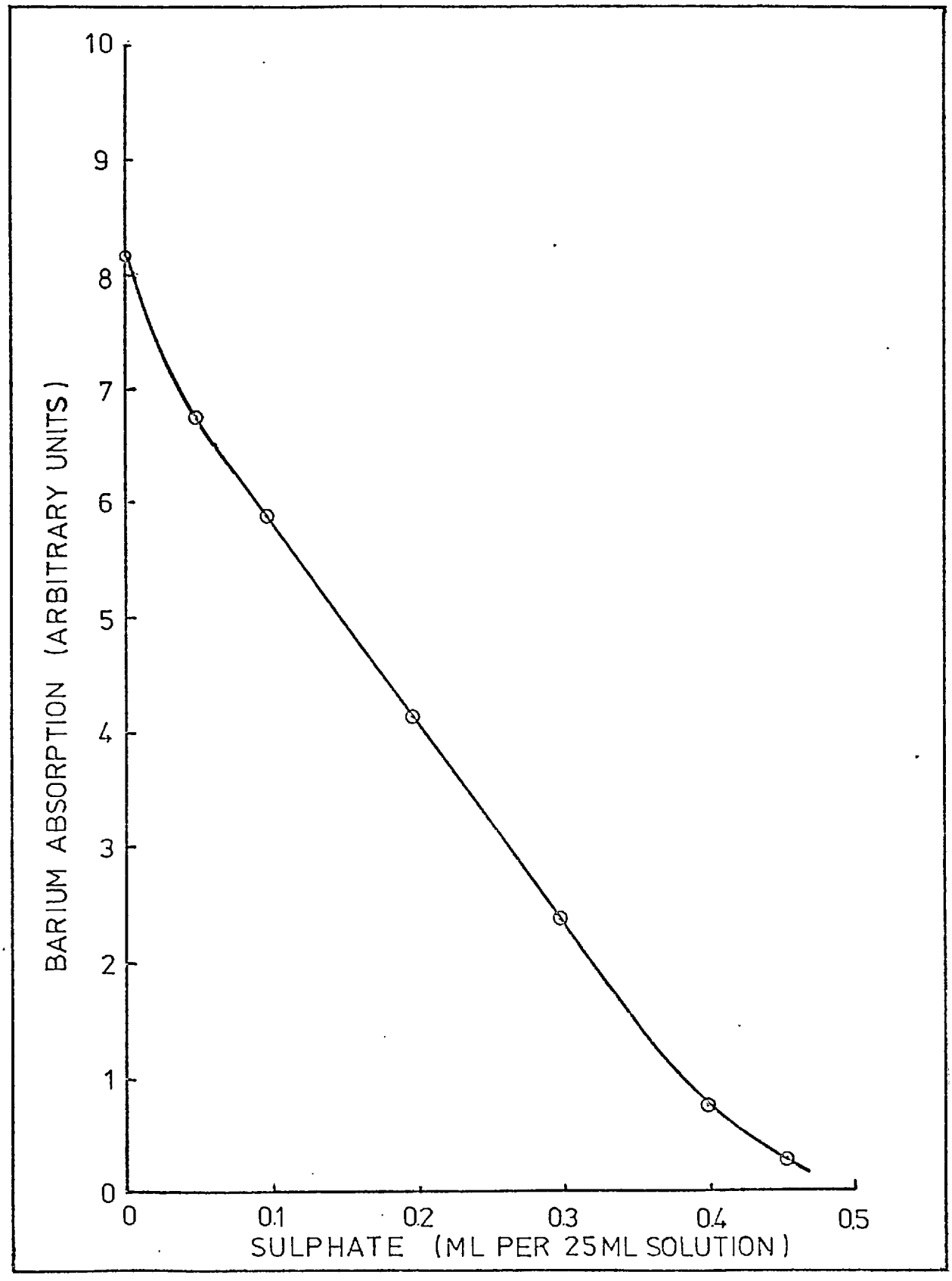

FIG. 37 Calibration Curve for the Determination of Sulphate by Atomic Absorption Spectrophotometry

Since the air/acetylene flame is not sufficiently hot to decompose barium compounds completely, a nitrous oxide/acetylene flame was used in the spectrophotometer. The problem with such a hot flame was that it caused partial ionisation of the barium. To overcome this, a large amount of potassium chloride was added to the solutions, the potassium being preferentially ionised.

The sulphate analysis procedure was carried out as follows:

For making up the standard solutions for the calibration curve, 0.05, 0.1, 0.2, 0.3, 0.4 and 0.45 ml of standard potassium sulphate solution, containing 1 mg/ml SO_4^{--} were pipetted into different 25 ml flasks;to each of these was added 0.5 ml of standard barium chloride solution, containing 1 mg/ml Ba^{2+} and 20 gm/lit potassium chloride, and the solutions were made up to the 25 ml mark. The other solutions for the sulphate analyses were made by pitetting 0.5 ml of each leach solution and 0.5 ml of the standard barium chloride solution into 25 ml flasks and diluting to the 25 ml mark with distilled water.

All the solutions were shaken well and allowed to stand for 24 hours, to obtain a crystalline precipitate of barium sulphate. Because the precipitate affected the analysis in the atomic absorption spectrophotometer, all the solution were centrifused at 3000 rpm for about 10 minutes in a MSE centrifuser and allowed to settle and then the liquid was decanted. carefully.

The clear solutions were analysed for barium, using a Perkin Elmer 290B spectrophotometer, the same one used for the analyses of Ni and Fe.

2.3.3 Analysis of Platinum and Palladium

The determination of platinum and palladium in leach solutions proved to be a very difficult problem for three reasons. The small volume of the leach samples (1-2 ml), the very low concentration of platinum and palladium and the high concentration of iron in the solutions. Since the first two reasons could be overcome by electrothermal atomisation A.A.S., the existence of iron in high concentrations which depressed the sensitivity for platinum and palladium was the reason which caused most of the trouble. For the isolation of iron interference in the analysis of platinum and palladium a new method was developed according to which Pt and Pd were separated from iron by solvent extraction. This method was performed as follows:

Whenever possible 1 ml of sample was taken. To the sample, pipetted into a small separating funnel, was added sufficient concentrated HCl to make the solution 1-2M with respect to HCl.

Two drops of 25% $SnCl_2$ solution in 25% HCl was then added, this was to ensure reduction of Fe, Pt and Pd to their divalent state.

After not less than 2 minutes, 2 ml of a 0.01% dithizone solution in carbon tetrachloride was added. The flask was then shaken for not less than 2 minutes and then allowed to settle for not less than 10 minutes.

The carbon tetrachloride layer was then drawn off into a 10 ml beaker. The extraction was then repeated with a further 2 ml of dithizone reagent.

The combined extracts were then evaporated to dryness. One ml of 60% $HClO_4$ was added and then evaporated to dryness to destroy all organic matter.

Six drops of conc. HCl were added and evaporated to dryness.

Three drops of con. HCl were added followed by exactly 1 ml H_2O and the solution mixed. This solution was then used for measurement of Pt and Pd content by electrothermal atomisation A.A.S.

The instrument used was an I.L. 455 graphite furnace and 151 Spectrometer using background correction (D_2 continuum lamp). The Pt line used was 265.9 nm and the Pd line 247.6nm.

2.4 ANALYSIS OF SOLIDS

2.4.1 Atomic Absorption Analysis

For the analysis of nickel and iron in the leach residues and the original synthetic materials, the equipment and conditions described in section (2.3.1) were used.

The dissolution of the solids was based on a technique described by Pantony (159).

A sample of the solid was attacked with hot nitric acid until sufficient dissolution of the solid had occurred. Usually about 30 ml of the acid was enough for a 0.5 gm sample. The dissolution was carried out in a Kjeldhal flask and the resultant solution was allowed to cool and only then was added to it a small volume of carbon tetrachloride and bromine, for the complete oxidation of the sulphur, the tetrachloride acting as a solvent. About 6 ml of a mixture of two volumes of pure liquid bromine and three volumes of pure carbon tetrachloride was enough for the oxidation of sulphur.

While agitating the flask, the solution was heated gently until complete removal of bromine and carbon tetrachloride. It was then diluted with 0.1 M HCl to within the range desired for direct determination by atomic absorption.

The use of nitric acid was not effective in the case of pentlandite since some sulphur remained after the removal of bromine and carbon tetrachloride. A mixture of two volumes of concentrated nitric acid and one volume of concentrated hydrochloric acid was used instead.

From this solution platinum and palladium were determined following the analytical method described in section (2.3.3).

2.4.2 Microscopic Analysis

Samples of the unleached starting materials and the leach residues to be sent for microscopic observation were mounted in Araldite epoxy resin MY 753 in combination with Araldite hardner HY 951. The samples were ground on a Struers Lunn Minor grinding machine using a series of silicon carbide papers of standardised grits 220, 320, 400 and 600; they were then polished on a Struers DP4 automatic polishing machine, using six micron and one micron DP cloths in turn. Marcon diamond abrasive compound sprays with DP lubricant-red was used for the six micron cloth and DP lubricant-blue for the one micron cloth.

The polished samples were observed with a Reichert Universal camera microscope MeF using reflected light under normal and polarizing conditions. This instrument is suitable for working from macro to oil immersion objectives. Photomicrographs were taken on standard 5 x 4" plates and then developed and printed. Some of the pictures taken are shown in Appendix C.

2.4.3 Electron Probe Microanalysis

Electron probe microanalysis of leach residues and unleached synthetic materials was performed on a JEOL model J x A - 3A made in 1967, fitted with scanning facilities. Some of the more important specifications of the apparatus used are given below:

Probe diameter: 1 micron
Scanning area: Square varying from 40 x 40 to 120 x 120 microns
Magnifications: 300x to 2400 x
Resolution (electron image): 1 micron
Resolution (x-ray image): between 4 and 5 microns
Range of elements: From sodium to uranium (atomic numbers 11 to 92)

Accuracy for quantitative analysis: Usually $\pm$1% for amounts of elements greater than 10 weight per cent.

A built-in low power optical microscope is used to assist in accurately locating the field of interest on the specimen.

Specimens for the microprobe were prepared in exactly the same form as for a normal microscopic examination (Section 2.4.2). The surfaces of the samples must be electrically conducting, so they were vacuum-sputtered with carbon.

The standards used were pure elements in the case of nickel, iron, platinum and palladium and in the case of sulphur, pyrite was used. After adjustment for the background radiation, the 'raw count' data was processed by a computer program (Mason, Frost and Reed, (160)) which calculated the atomic and weight per cents, after correcting for the following effects:

1) Absorbtion effect: due to the fact that the standard and the specimen absorb the emitted radiation by different amounts.

2) Atomic numbers effect: because of the differences in the percentage of electrons back scattered by the standard and the specimen and the difference in electron retandation and x-ray production efficiency due to the difference in atomic number.

3) Characteristic fluorescence factor: to allow for the production of radiation of another wavelength.

The instrument was used for quantitative measurements of the elements at a number of fixed spots on the surface of the specimens. It was

also used for point counting at positions across the grains to find any inhomogeinity in the unleached solids and any change of distribution of the elements in the leach residues. X-ray and back scattered electron data were monitored on an oscilloscope.

2.4.4 X-Ray Diffraction Analysis

For the identification of the phases present both in the unleached starting materials and in the leach residues the method of x-ray powder diffraction was used.

These analyses were performed on a Multiple Guinier de Wolff camera of the focussing type with a focussing monochromator (161). The monochromator is a quartz slab cut at 4.5^{o} to the (101) planes and bent asymmetrically to approximate to a logarithmic spiral; this may be adjusted for various source wavelengths, but does not provide perfect focussing (162). A converging x-ray beam produced by reflecting the incident beam from the crystal monochromator, is transmitted through a specimen and the Guinier camera records the front reflection region of the spectrum. Since the monochromator provides a line focus with a broad x-ray source, four samples can be stacked on one another, if a crystal with a large vertical dimension is used.

This type of camera has the advantage that the monochromator eliminates sufficiently the white radiation in the beam, so that the x-ray patterns have a low background intensity; this allows even very weak lines, such as superstructure lines to be observed. Another advantage of the Guinier camera over the Debye-Sherrer camera is that four samples can be photographed at the same time and that the effective diameter of this camera is twice that of Debye-Sherrer camera with the same diameter and

permits a better separation of lines which lie very close together. One disadvantage of this camera is that it records reflections contained in the range 0^{o}-40^{o} of Bragg angle; reflections whose angles are greater than 40^{o} could not be observed.

The samples for the camera were prepared by grounding a small amount of the material to a sieve size less than 45 microns and were placed in a divided flat holder with four sections and secured by sellotape. Sellotape itself gives several broad diffraction bands, but their positions were noted from photographs taken without samples so they could be eliminated from the patterns obtained with samples.

Because the depth of the particles layer through which the beam passes is very thin in order to avoid any spotiness in the reflection caused by preferentially oriented crystals the sample holder makes a slow retrogressive movement in its own plane. The reference line for the x-ray beam was obtained by removing the lead shutter from the beam path for 4 to 5 seconds while during this exposure the generator power was at the minimum. The exposure time for most of the samples was three hours, at x-ray generator settings of 30 kv and 20 mA. Both copper and cobalt radiations were used; the wavelength of the copper radiation was 1.5418Å and that of cobalt 1.7902Å. Cobalt radiation had the advantage over copper radiation that it does not produce a heavy background in the photographs due to intense fluorescent radiation with iron-containing solids.

Calibration of the films was done by including sodium chloride or silica among the samples for every film taken. By measuring the distance of the sodium chloride or silica lines from the reference line and using the known Bragg angles for these reflections, by plotting d against Δd (Δd is the difference between the calculated and the actual spacing), a relationship between distance and θ was obtained. This relationship was

used in the measurement of the patterns of the other samples on that particular film. The error was greatest at low angles. This calibration was necessary because the actual radius of the camera was calculated to be slightly larger than the specified radius given (5.7 cm). It was also covering mistakes which could come for other reasons such as bad alignments, film shrinkage etc.

The distances on the films were measured using a Hilger and Watts film measuring rule with a vernier attachment. From the θ values obtained, the interplanar spacings (d) were calculated, using the Bragg equation:

$$n\lambda = 2d\sin\theta$$

The intensities of the x-ray patterns were either estimated visually or recorded from the films by a Joyce-Loebl automatic recording microdensitometer model MK III B.

2.5 MATERIALS

2.5.1 Elements for Synthesis of Sulphides

For the synthesis of the sulphides, spectrographically pure elements were used. The analysis of these elements gave the following estimation of the quantity of impurities present.

a) Nickel Sponge - Spectrographically Pure
(Johnson Matthey)

Spectrographic examination:
Iron, 10 ppm; Aluminium, 1 ppm; Calcium, 1 ppm; Sodium, 1 ppm; Copper and Magnesium each less than 1 ppm.

b) Iron Sponge - Spectrographically Pure
(Johnson Matthey)

Spectrographic examination:
Silicon, 3ppm; Magnesium, 2 ppm; Manganese, 2 ppm; Nickel, 2 ppm; Copper and Silver, each less than 1 ppm.

c) Sulphur powder - Spectrographically Pure
(Johnson Matthey)

Spectrographic examination:
Aluminium, 0.5 ppm; Sodium, 0.2 ppm; zinc, 0.2 ppm; Barium, 0.1 ppm; Nickel, 0.1 ppm; Copper 0.05 ppm; Titanium, 0.05 ppm; Magnesium, 0.03 ppm; Manganese, 0.03 ppm; Silver, 0.03 ppm; Boron, 0.01 ppm; Calcium, Iron and Silicon, each less than 1 ppm.

d) Palladium Chloride: Spectrographically Pure
(Johnson Matthey)

e) Platinum Wire: Spectrographically Pure
(Johnson Matthey)

2.5.2 Leaching Agents

All the leaching experiments have been carried out using acidified solutions of ferric chloride or hydrogen peroxide.

The specifications of these leaching agents are given below:-

a) Ferric Chloride ($FeCl_3.6H_2O$)

Analytical Reagent - Hopkin and Williams.
$FeCl_3.6H_2O$ not less than 98.0%
Maximum limits of impurities, in weight per cents:

Insoluble matter	0.003
Free acid (HCl)	0.5
Free chlorine (Cl)	0.001
Nitrogen compounds (NO_3)	0.002
Phosphate (PO_4)	0.001
Sulphate (SO_4)	0.005
Arsenic (As)	0.0001
Calcium group + Mg	0.05
Copper (Cu)	0.0025
Ferrous Iron (Fe)	0.015
Lead (Pb)	0.005
Manganese (Mn)	0.08
Potassium (K)	0.01
Sodium (Na)	0.03
Zinc (Zn)	0.01

b) Hydrogen Peroxide - H_2O_2 (20 volumes)

General purpose reagent (Hopkin and Williams)

Weight per ml about 1.02 gm
Chloride 0.0015% max.
Non-volative matter 0.2% max
6% w/v H_2O_2 minimum

2.5.3 Acids

The leaching solutions were prepared by dissolving the necessary amount of oxidizing agent to give the concentration required in hydrochloric acid.

The presence of acid was required in order to avoid precipitation of iron by hydrolysis.

Nitric acid was used for dissolving the unleached and leached solids before analysis in the atomic absorption spectrophotometer.

The specifications of the acids used are listed below:

a) Hydrochloric acid - Analytical reagent

BDH Chemicals Ltd., Poole England
Hydrochloric acid (HCl) sp. gr. 1.18

Maximum limits of impurities:

Non-volatile matter	0.0005%
Free chlorine (Cl)	0.0002%
Sulphate (SO_4)	0.0002%

Sulphite (SO_3)	0.0001%
Ammonium (NH_4)	0.0003%
Arsenic (As)	0.000002%
Iron (Fe)	0.00004%
Heavy metals (Pb)	0.00008%

b) Nitric acid - Analytical Reagent

BDH Chemicals Ltd., Poole, England

Nitric acid (HNO_3) sp. gr. 1.49

Assay 69.0 to 71% HNO_3

Maximum limits of Impurities

Non-volatile matter	0.001%
Chloride (Cl)	0.00005%
Phosphate (PO_4)	0.0001%
Silicate (SiO_2)	0.00005%
Sulphate (SO_4)	0.0002%
Arsenic (As)	0.000001%
Iron (Fe)	0.00002%
Heavy metals (Pb)	0.00002%
Manganese (Mn)	0.00004%

2.5.4 Reagents for Atomic Absorption Spectrophotometer

The calibration curves for the atomic absorption spectrophotometer were obtained by using solutions of different concentrations prepared from nickel, and iron standard solutions (Hopkin and Williams), containing 1000 ppm w/v of the respective metals in 0.1 N $HClO_4$. Metal contents are within 0.5% of the nominal value.

Solutions for the calibration curve for the sulphate analysis were prepared from barium standard solution (Hopkin and Williams) having the same specifications as the above mentioned solutions.

CHAPTER 3

LEACHING OF MONOSULPHIDE SOLID SOLUTION (Mss): RESULTS AND DISCUSSION

3.1 FERRIC CHLORIDE LEACHING: KINETIC RATE-CURVES EFFECT OF LEACH VARIABLES ON THE RATE OF REACTION

Kinetic data for the leaching of monosulphide solid solution of iron and nickel, consisting of values for metal-ion and sulphate-ion concentrations at various times were obtained and plotted using the apparatus described in section (2.2).

The investigation was based on the determination of the effect of the following reaction variables on the rate of dissolution of nickel by the reactions:

1) Temperature of reaction
2) Average particle size of Mss charge
3) Average stirring speed
4) Ferric concentrations of solutions
5) Acid concentrations of solutions
6) Sample weight.

The most common conditions of the experiments were:

Temperature	:	$95^{o}C$
Particle Size	:	-125 + 90 microns
Stirring Speed	:	1000 rpm
Fe^{3+} conc.	:	0.1M
HCl conc.	:	0.1M
Sample weight	:	1.00 gr.

3.1.1 Effect of Temperature

The effect of temperature on the rate of leaching of Mss was studied at four different temperatures and the results are given in the tables (B - 1.1), (B - 1.2), (B - 1.3), (B - 1.4) and in the figure (38).

From the rate plots it is possible to see, that in the experiments which were run at 80°C and above, the leaching reaction is characterized by a single stage process indicating a uniform mechanism during the dissolution of the Mss. It is also observed that the higher the temperature the further the reaction proceeded.

In the experiment at 60°C, the shape of the curve produced is not the same as that obtained at higher temperatures. This curve seems to be characterized by a three-stage process, a slow one at the beginning and at the end of the reaction and an intermediate fast one. Although the behaviour of the system at this temperature is quite unusual because of the existence of a faster dissolution rate at 60° than at 80° and 95°C, it is well interpreted by the mechanism of the dissolution proposed below.

The curves at all temperatures showed that the dissolution of Mss was sensitive to temperature. Some attempts were made to obtain a rate equation to fit the experimental curves, but they were unsuccessful. Unsuccessful also were attempts made to calculate the critical increment of energy at the beginning of the reaction and this seems to be due to the fast initial removal of nickel.

A not very accurate Arrhenius plot referred to an intermediate stage of the reactions above 80°C, is shown in figure (39). The mean energy of activation calculated from this plot was 15 kcal/mole^{-1}. This is too high for an entirely transport controlled reaction (4 kcal. mole^{-1},

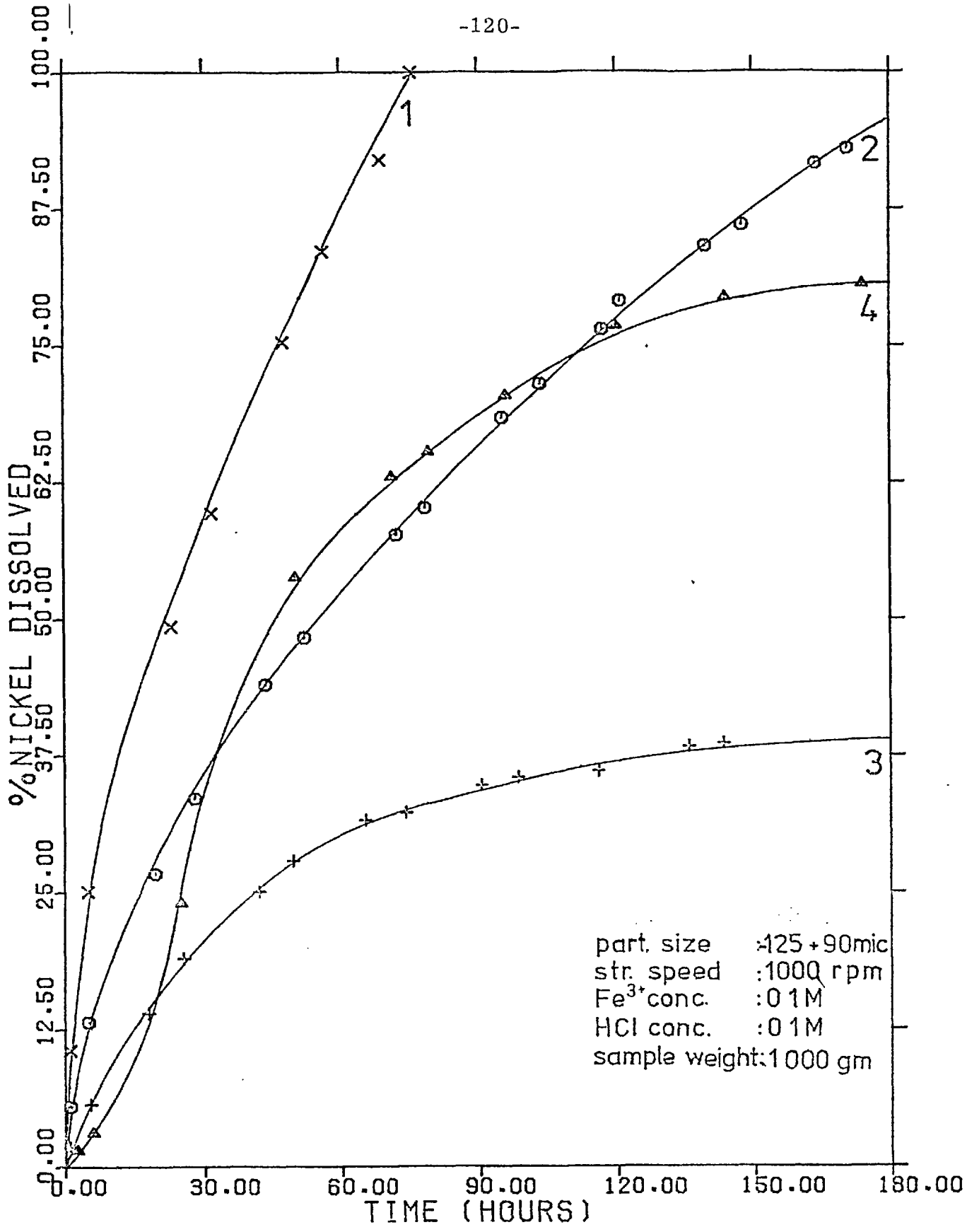

FIG. 38 Effect of Temperature on the Rate of Leaching of Mss

1: 100.5°C 2: 95°C, 3: 80°C, 4: 60°C

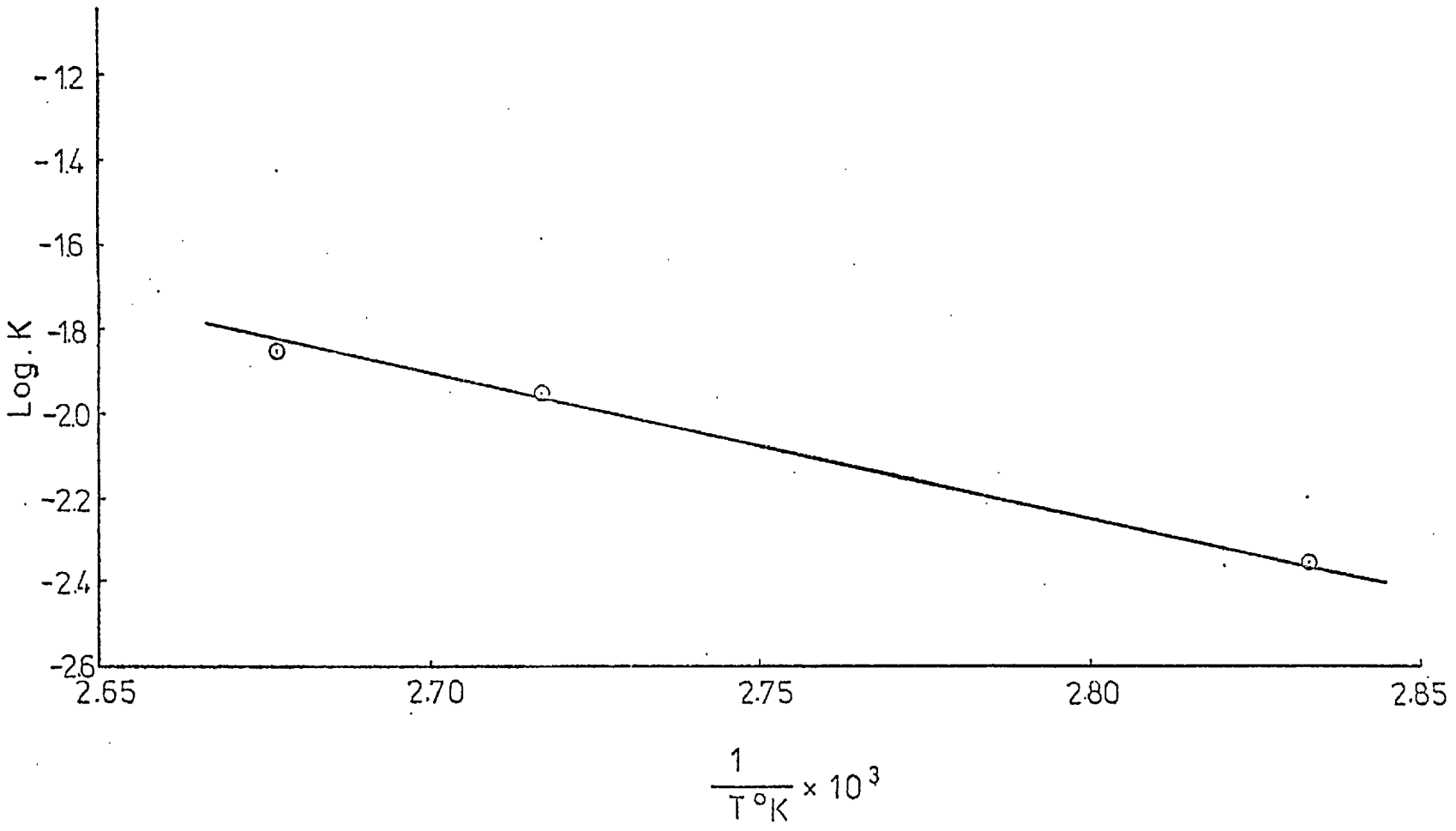

FIG. 39 Arrhenius Plot for the Dissolution of Mss

Burkin (163)) and it is below the value considered, when the reaction is chemically controlled. Thus the reaction seems to be an intermediate process, where the rate is mainly controlled by a chemical reaction but by a transport mechanism as well.

During all stages of the reaction, at low or high temperatures, x-ray powder photographs of the residues showed the existence of elemental sulphur. Elemental sulphur was also found to be stuck on the necks and the wall of the lid covering the reaction vessel.

Microscopic observations of the leach residues showed also the existence of elemental sulphur around the unreacted part of the grains and in pores and cracks.

X-ray results from the residues from experiments run at temperatures above $80^{o}C$ showed the existence of a precipitate of hematite (Fe_2O_3). Such a precipitate did not appear at temperatures below $80^{o}C$. This is due to the fact that at pH values around one, and temperatures 80^{o} and above, hematite is the stable phase as can be seen from the E-pH diagrams for the system $Fe\text{-}H_2O$ (164) and (165). At lower temperatures Fe^{3+} is the stable phase and when the temperature increases Fe^{3+} hydrolyses to hematite.

The results obtained from the x-ray photographs of the leach residues (section 3.4) did not show appreciable variation in Mss parameters, which indicates that the structure of Mss was maintained.

Electron-probe microanalysis (section 3.6) of the leach residues, obtained by point counting across the particles showed the existence of a coating mainly consisting of elemental sulphur and containing some iron

as well, but no nickel, while the unreacted part in the center of the particles showed no appreciable variation of composition within the core and from the original composition.

In such a complex system it is not possible to predict the effect of temperature and of the other factors, because there is not a simple mechanism occurring. The effect of temperature is complicated by the fact that higher temperatures tend to promote hydrolysis of the ferric ions, while the critical increment of energy derived from the Arrhenius plot showed an intermediate situation, in which the reaction rate was controlled in part by the rate of transport of the reactant to the interface of the unreacted part of the grain and in part by chemical factors.

A possible explanation of the mechanism of the reaction occurring which may be derived from the foregoing results is that the whole process is mainly controlled by the oxidation of S^{2-} and electron transfer within the solid structure, simultaneously with the diffusion of ferric ions to the interface. It was proved from the electron probe microanalysis that nickel reacts faster than iron, so at any given time during the progress of the reaction each particle consists of a sulphide core containing Fe and Ni surrounded by a porous envelope, consisting of elemental sulphur and some pyrrhotite, through which the ferric ions diffuse inwards,break down the structure of Mss and oxidize S^{2-}, while the soluble salts of the metals diffuse outwards.

3.1.2 Effect of Particle Size

The effect of particle size on the rate of leaching was studied by using four size fractions, -180 + 125, -125 + 90, -90 + 63 and -63 + 53 microns. The results are given in figure (40) and tables (B-1.3), (B-1.5) (B-1.6), (B-1.7).

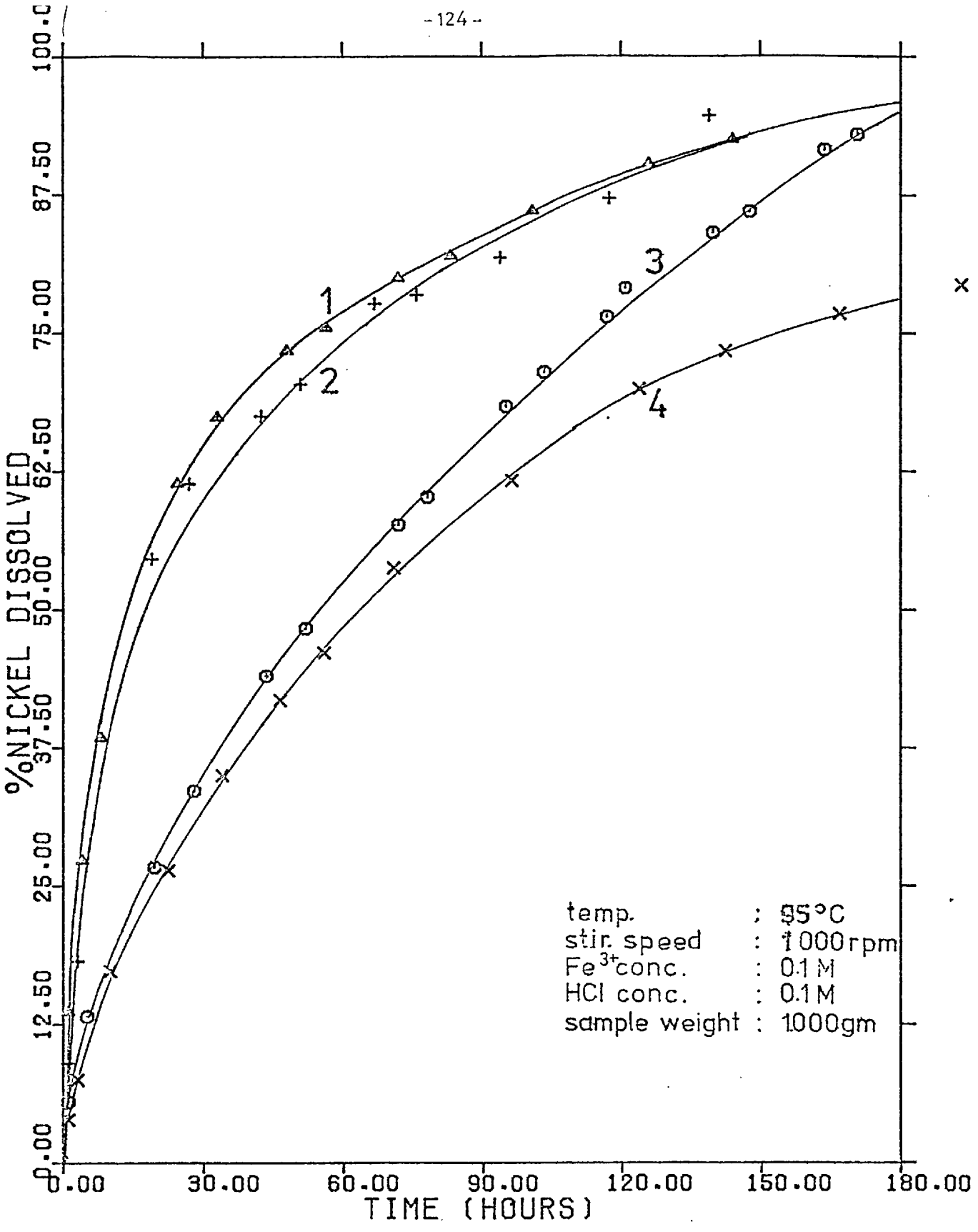

FIG. 40 Effect of Particle Size on the Rate of Leaching of Mss

1: -63 + 53 microns
2: -90 + 63 microns
3: -125 + 90 microns
4: -180 + 125 microns

As can be seen from figure (40), the particle size reduction increased greatly the rate of the reaction. This behaviour was expected from the mechanism proposed during the study of the effect of temperature, i. e. that the dissolution is mainly controlled by a chemical reaction and secondly by a diffusion process through a porous film.

The particle size reduction favours both of the factors controlling the dissolution. The chemical reaction is favoured because of the increase of the surface area per unit mass due to the decrease of the grain size. The diffusion controlled process of the dissolutions is also accelerated. As is known, where the rate-determining step is diffusion through a film, thickness of which increases in proportion to the extent of leaching, the process is parabolic. This is the case in the leaching of Mss, where the Fe^{3+} ions must diffuse through an increasing film of sulphur and FeS. An important practical effect of a parabolic process is the effect of fine grinding. Size reduction reducing the diffusion distances, is much more effective in reducing the time to complete a reaction, if the process is parabolic than if it is linear. Hence the diffusion controlled mechanism of the dissolution is much more affected by the particle size changes than the chemically controlled one.

3.1.3 Effect of Ferric Ion Concentration

Since ferric ion is the oxidizing agent in the solution during the leaching of Mss, it was considered of interest to examine their possible effect on the reaction.

The results of three experiments at different original concentrations of ferric ions are depicted in figure (41) and tables (B-1.3), (B-1.8), (B-1.9).

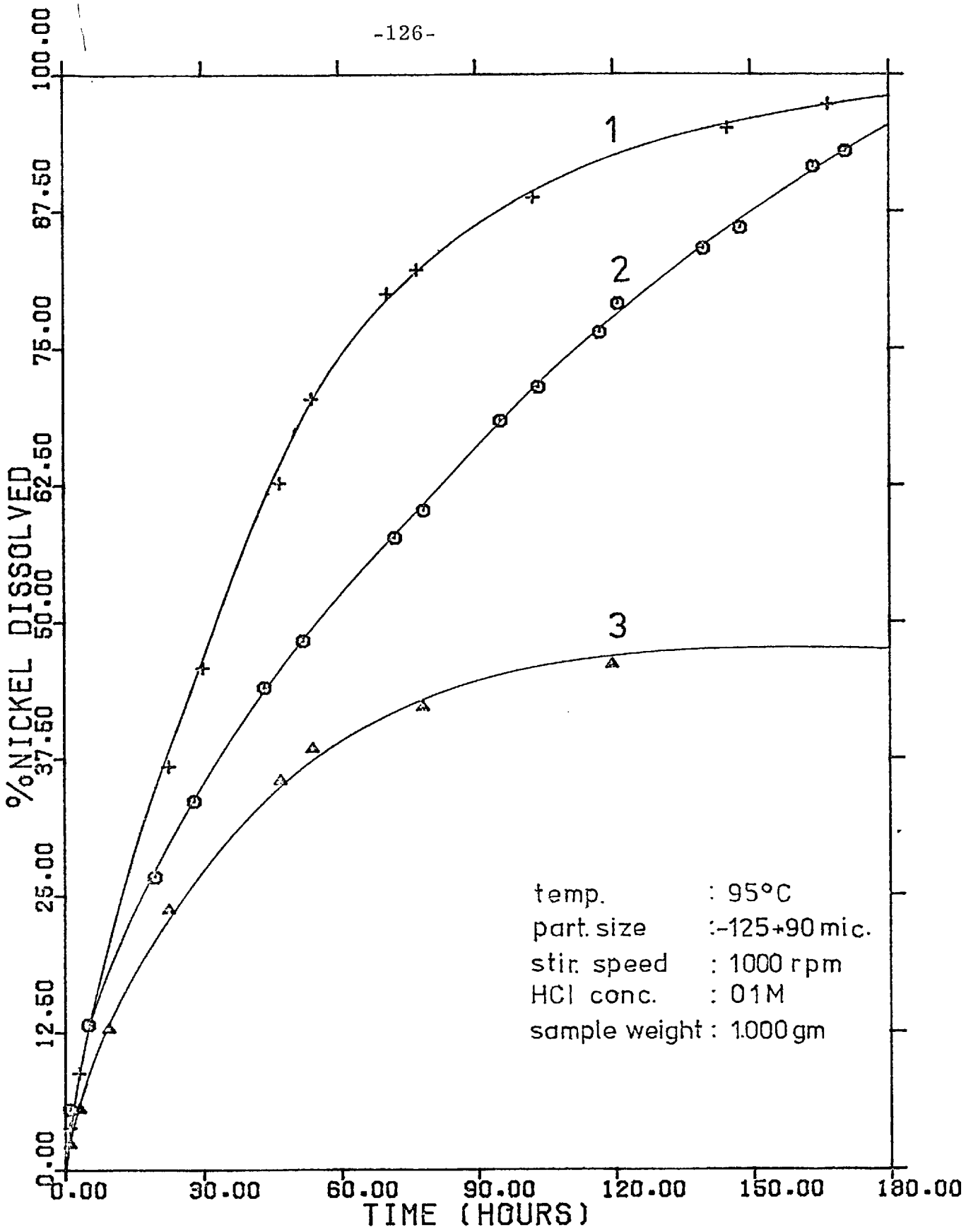

FIG. 41 Effect of Ferric Concentration on the Rate of Leaching of Mss

1: 0.15M Fe^{3+}, 2: 0.10M Fe^{3+}, 3: 0.05M Fe^{3+}

It can be seen that the variation of ferric ion concentration had an appreciable effect on the rate of leaching. This is due to the fact that an increase in the initial concentration of ferric ions favours both the chemical and diffusion mechanisms which control the rate of the reaction.

The shape of the curve obtained in the lowest initial concentration is explained if we consider that all the ferric ions in the solution were consumed. The small increase in the rate of dissolution after the reaction stopped was caused by the re-oxidation of Fe^{2+} to Fe^{3+} by the oxygen of the air.

For the other two curves, it is difficult to make a direct comparison, since extensive and unmeasurable hydrolysis occurred. All these experiments were run at a pH value near one and the appearence of hematite as a hydrolysis product in all the experiments above $80^{o}C$ was expected as can be seen from the E-pH diagrams of the system $Fe-H_2O$ (164).

This iron hydrolysis also is responsible for the slight lowering of pH during the dissolution of the mineral.

3.1.4 Effect of Stirring Speed

Figure (42) and tables (B-1.3), (B-1.10), (B-1.11), show the effect of stirring speed on the rate of dissolution of Mss.

Varying the stirring velocity between 700 and 1800 rpm had a smaller effect on the rate of the reaction than the temperature, the particle size or the Fe^{3+} concentration.

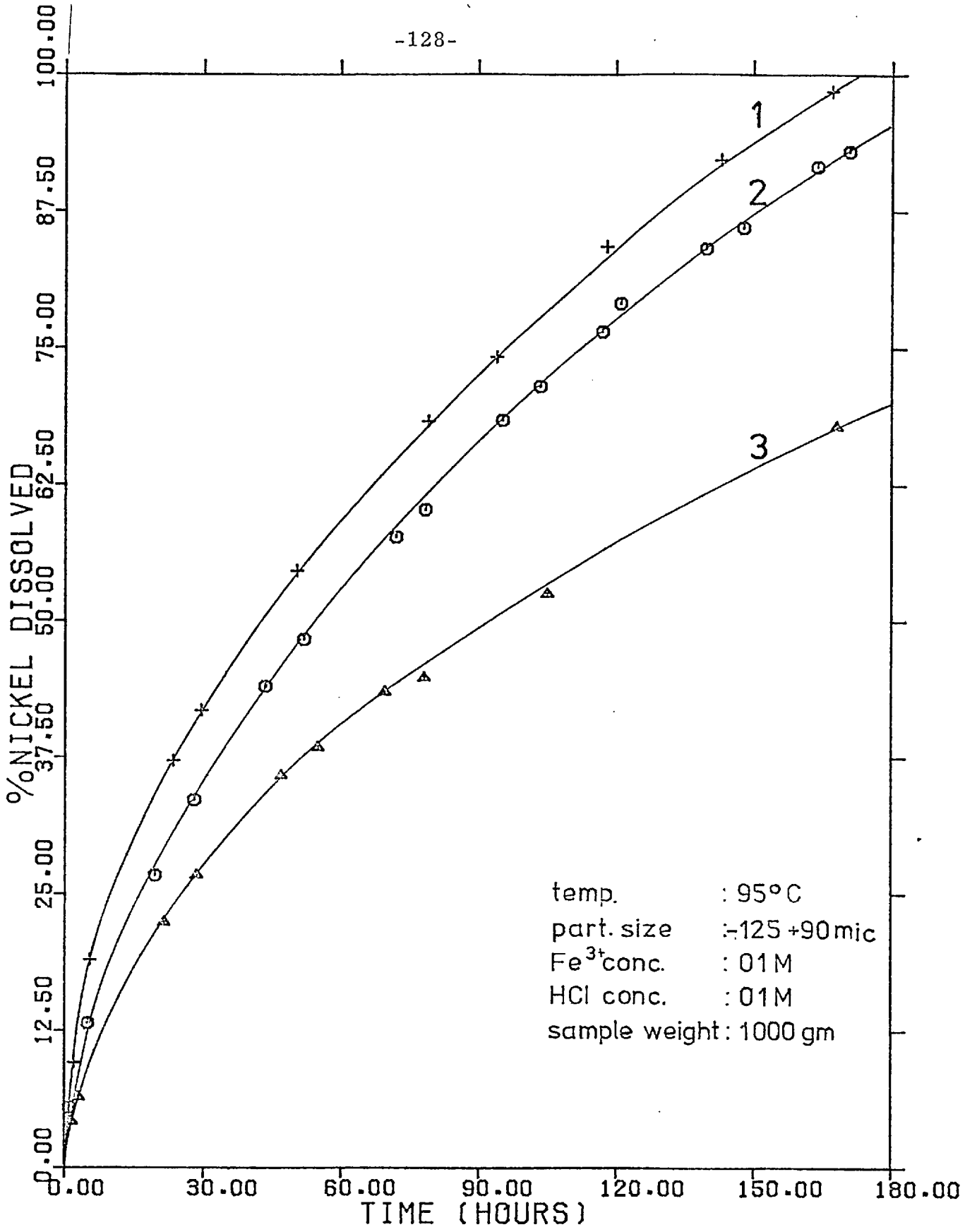

FIG. 42 Effect of Stirring Speed on the Rate of Leaching of Mss

1: 1800 rpm, 2: 1000 rpm, 3: 700 rpm

This is in very good agreement with the mechanism of the dissolution proposed in section (3.1.1). The stirring speed variation affects only the part of the reaction which is physically controlled while the previously examined factors influence both the physically and chemically controlled mechanisms of the dissolution.

This behaviour of the system, together with the results from the point analysis of the leach residues in the electron probe microanalyser confirm that the physically controlled part of the reaction is the diffusion of Fe^{3+} ions through the layer of sulphur and iron sulphide to the reacting interface and not a solid-state diffusion of nickel ions to the outside of the particles.

3.1.5 Effect of Acid Concentration

The hydrochloric acid concentration was expected to have a large effect on the process of leaching. This is because its presence is necessary to maintain the ferric ions in solution, preventing their precipitation although under the most common conditions used in the experiments hydrolysis was not prevented completely.

It was expected therefore, that an increase in the initial hydrochloric acid concentration would increase the amount of nickel extracted and the rate of its dissolution, because it would prevent the precipitation of ferric ions.

It was surprising to find that in two experiments, where the hydrochloric acid concentration was increased to 0.3 and 0.5M the rate of the reaction decreased considerably.

An explanation was obtained by considering the nature of the species which $FeCl_3$ produced in the leach solution and the mechanism of the oxidation of S^{2-} to S^{o}.

There are four kinds of species involving ferric ions in the solution: Fe^{3+}, $FeCl^{2+}$, $FeCl_2^+$ and $FeCl_3$. The proportion of each present in the solution can be determined from a knowledge of the equilibrium constants for the formation of the various chlorides and the initial concentrations of $FeCl_3$ and HCl present in the solution.

Studies have also shown that only the dissociated species are the oxidizing agents in the solution. An increase in the acidity of the solution by addition of hydrochloric acid increases the concentration of chloride ions (Cl^-) as well, which causes an increase in the proportion of the undissociated ferric chloride ($FeCl_3$) in the solution. This results in a decrease in the active ferric concentration in the solution and, as a result, in the decrease of the rate of leaching.

To confirm the correctness of the explanation given above, another experiment was carried out in which the increase in H^+ from 0.1M to 0.3M was obtained by addition of sulphuric acid instead of hydrochloric acid.

The results obtained are given in figure (43) table (B-1.12). It can be seen that the rate of dissolution remained stable and high during the whole course of the experiment. But no quantitative comparison of the effect of the pH on the rate of leaching can be made because the introduction of SO_4^{2-} into the solution changes the chemistry of the system.

3.1.6 Effect of Sample Weight

The effect of sample weight on the rate of leaching was studied using three different quantities and the results are given in figure (44) and tables (B-1.3), (B-1.13) and (B-1.14).

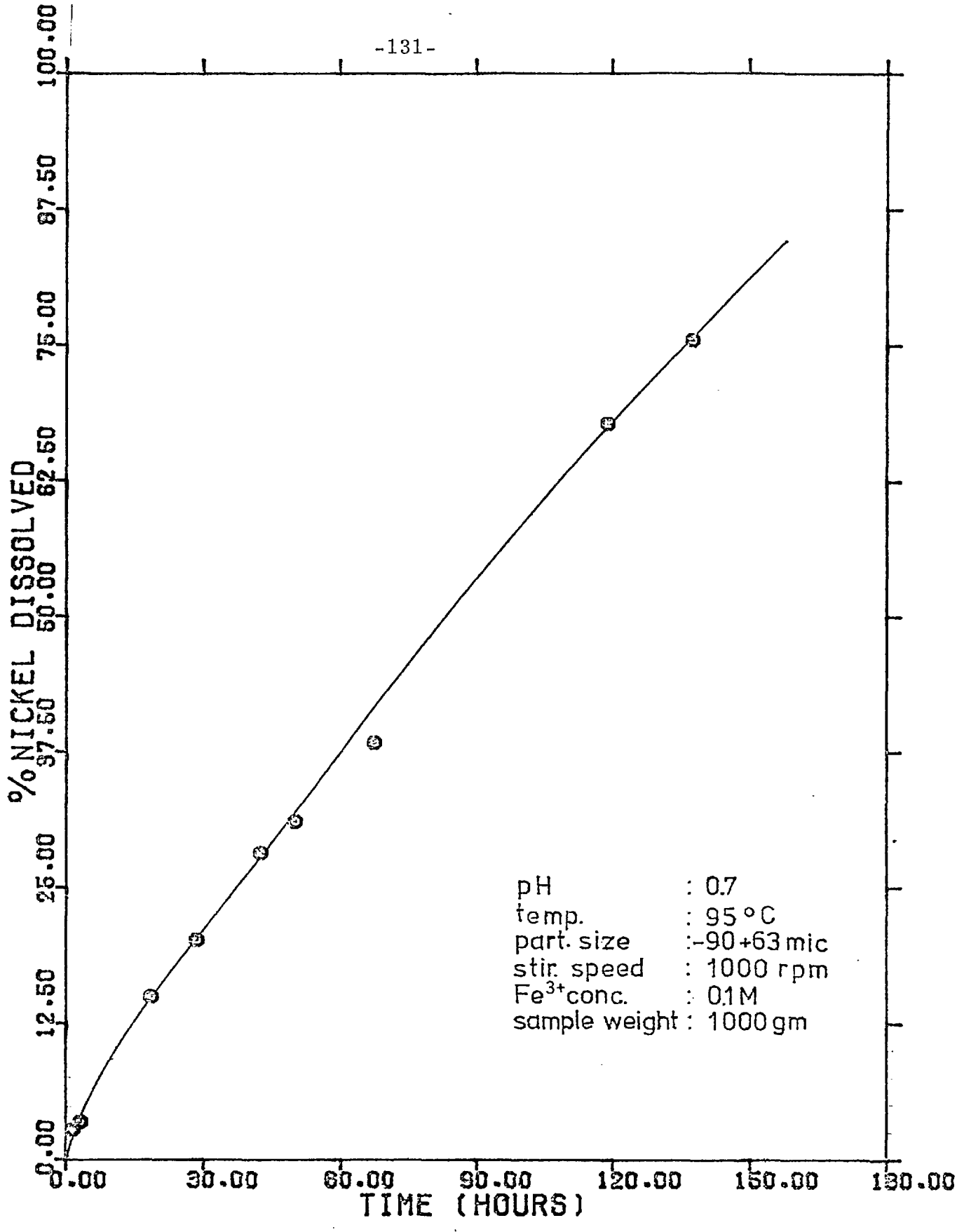

FIG. 43 Effect of H_2SO_4 Addition on the Rate of Leaching of Mss

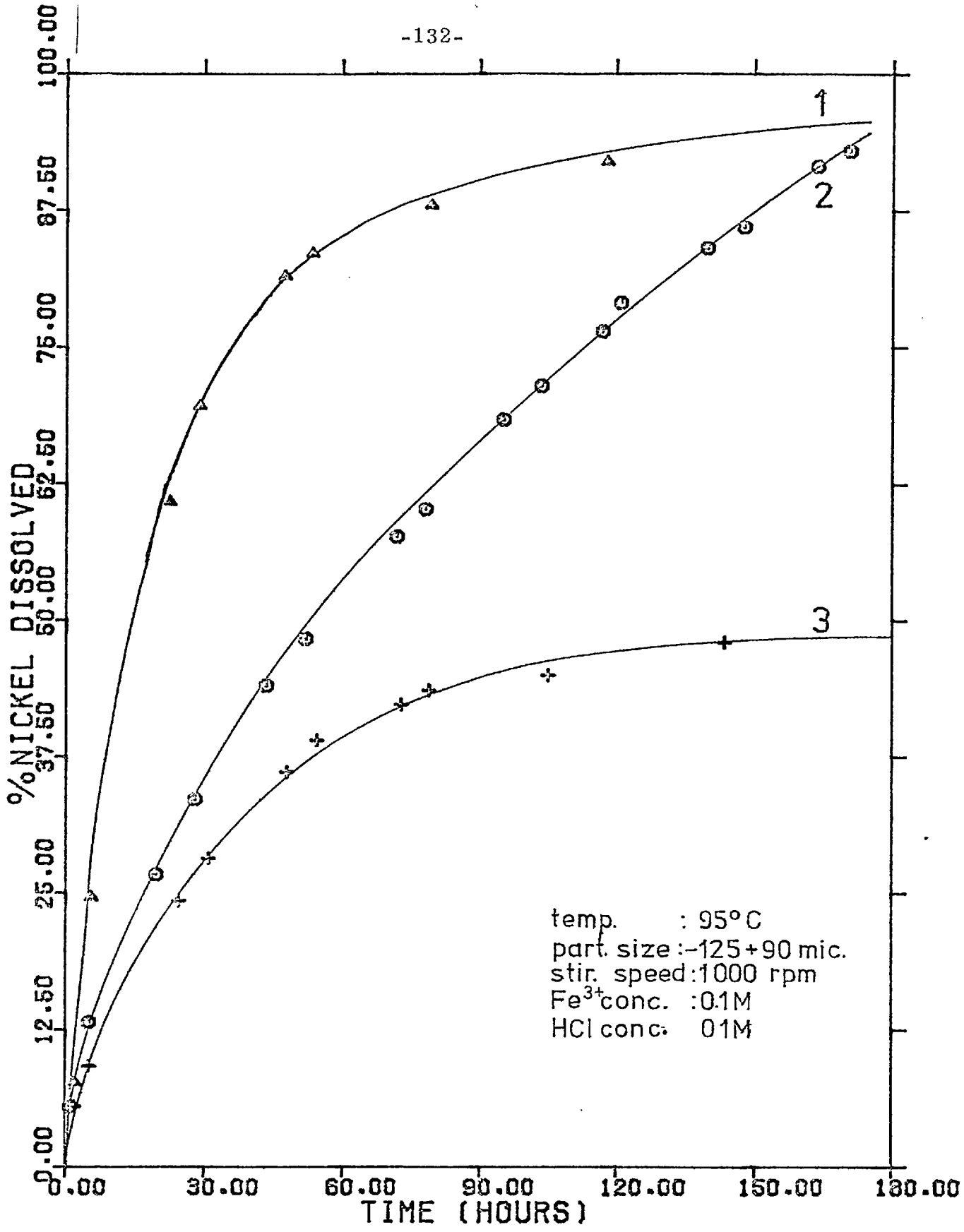

FIG. 44 Effect of Sample Weight on the Rate of Leaching of Mss

1: 0.25 gm, 2: 1 gm, 3: 2 gm

The experiments were carried out under the same conditions, that is at 95°C, with a ferric ion concentration of 0.1M, at a pH about one, a stirring speed of 1000 rpm and a particle size -125 + 90 microns.

As can be seen the sample weight had a significant effect on the nickel dissolution. The greater the sample weight the slower the rate of the reaction. This is due to the faster drop of the original concentration of ferric ions as the sample weight increases, because larger amount of nickel and iron dissolves in unit time.

The shape of the last part of the curve in the experiment where 2.0 grams were added, shows that all ferric ions were consumed and the very slow rate of dissolution subsequently is due to the re-oxidation of Fe^{2+} to Fe^{3+} by the oxygen of the air.

3.2 LEACHING WITH HYDROGEN PEROXIDE

In the progress of the experiments described above it was impossible to study the rate of dissolution of iron compared with the rate of dissolution of nickel. This would give a measurable indication of the variation of composition of the solid residue as iron and nickel were removed at different speeds. Such an analysis for iron was impossible in ferric chloride solutions because of the extensive hydrolysis of ferric ions and the small change of the concentration of iron in the solution due to the dissolution of Mss compared with the high initial concentration of iron.

Hence it was decided to carry out some oxidizing leaches of Mss with a medium not containing iron. The oxidant chosen was hydrogen peroxide. Two experiments were run using hydrogen peroxide. In the first one 50 mls of 20m volume hydrogen peroxide were mixed with 150 mls of 0.3M hydrochloric acid solution and in the second one 50 mls of hydrogen peroxide with 150 mls of 0.5M hydrochloric acid solution. A one gram sample of -90 + 63 microns Mss was leached in both cases at $95^{o}C$. The initial pH for the first experiment was 0.7 and at the end of the experiment it was 0.86 while in the second experiment the pH increased from 0.5 to 0.62.

The results obtained from the analyses of iron and nickel in solution from both experiments by atomic absorption spectrophotometry are presented in figure (45) and tables (B-1.15) and (B-1.16).

In figure (45) the per cent of iron dissolved was plotted vs the per cent of nickel dissolved. A straight line in an angle of 45^{o} was obtained, which indicates that both metals dissolve at the same rate. This is in

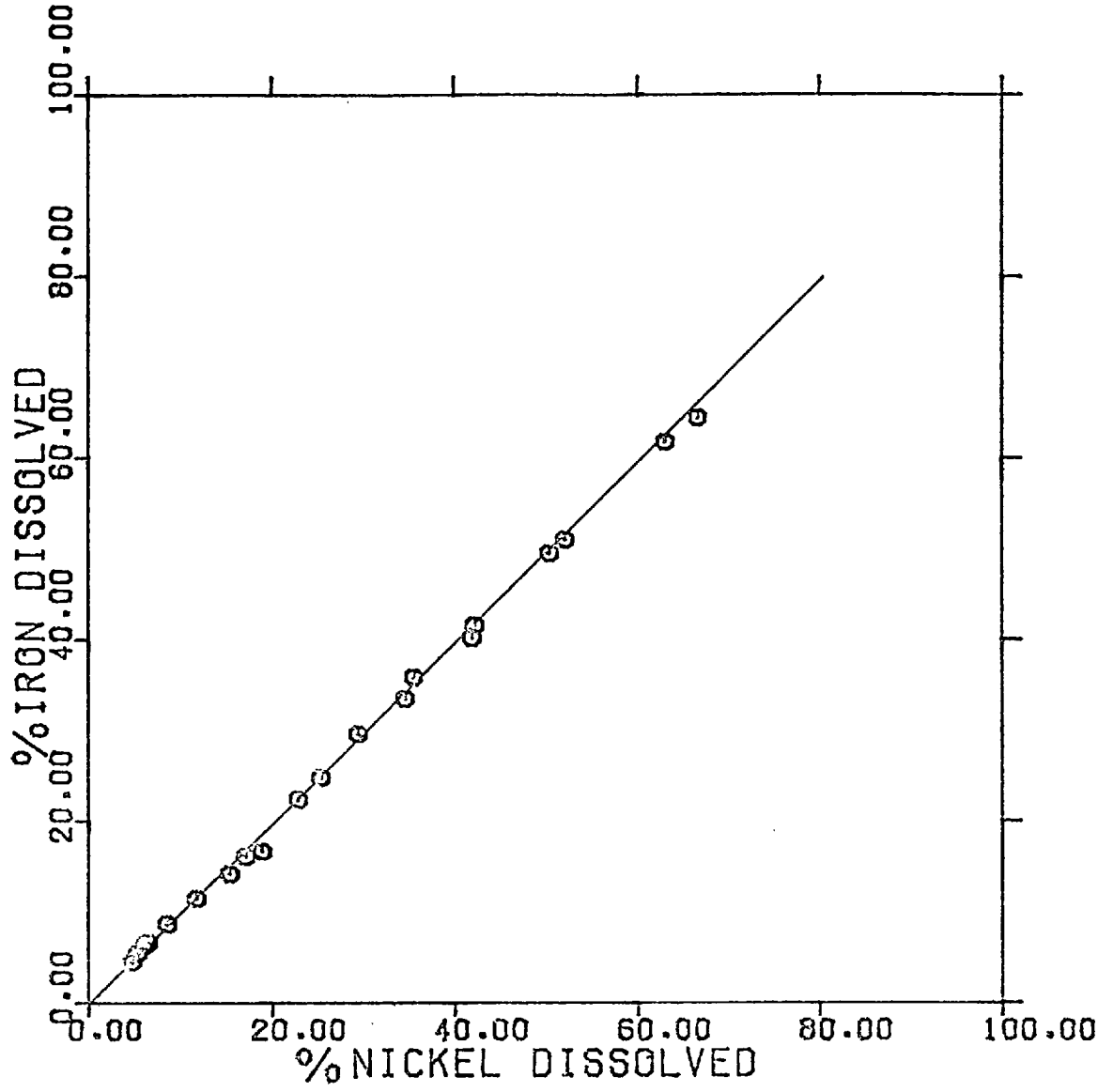

FIG. 45 Curve Relating the Percentage of Iron to that of Nickel Removed during Leaching of Mss with Hydrogen Peroxide

opposition to what was happening in the leaching with ferric chloride, where nickel dissolved faster than iron, and implies a different mechanism occurring from that proposed for the leaching with ferric chloride.

3.3 SULPHATE ANALYSIS OF THE LEACH SOLUTIONS

The experimental study of the leaching of Mss was completed with the analysis of the sulphate in the leach solutions, following the method described in section (2.32).

The results of the sulphate analyses for ferric chloride and hydrogen peroxide leaching of the Mss are given in tables (B-1.17) and (B-1.18) and in figs (46)and (47), where the sulphate concentration has been plotted against the nickel concentration of the leach solutions.

As can be seen from these diagrams, the hydrogen peroxide leaching influences the formation of sulphate,especially at the beginning of the reaction, when almost all the amount of sulphur liberated from the crystal structure of Mss is present as sulphate. Since the only oxidizing agent in the case of hydrogen peroxide leaching is the oxygen, it is likely that at the beginning of the reaction, the sulphide is oxidised directly to sulphate in one stage, while sulphur appears in the later stages of the reaction, when the increase of the sulphate concentration in the solution is negligible.

In the case of ferric chloride leaching both elemental sulphur and sulphate were present at all stages of the experiment. Since ferric chloride will generally only oxidise the sulphide to sulphur, a second oxidising agent, such as oxygen must have been reacting. As can be seen from figure (47) the rate of the oxidation of sulphur to sulphate is low and almost proportional to the nickel dissolution.

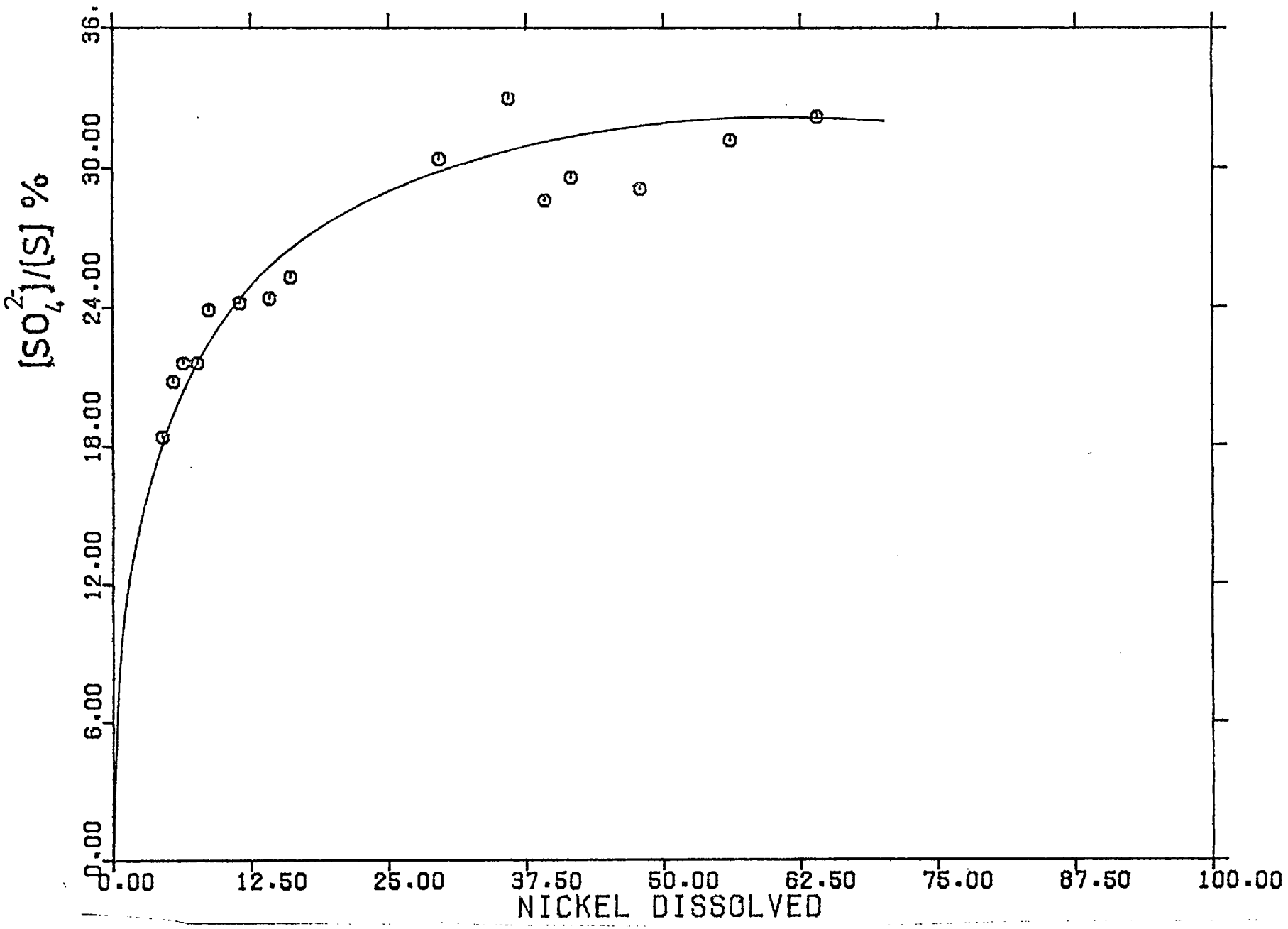

FIG. 46 Sulphate analysis of the Solutions of the Hydrogen Peroxide Leaching of Mss

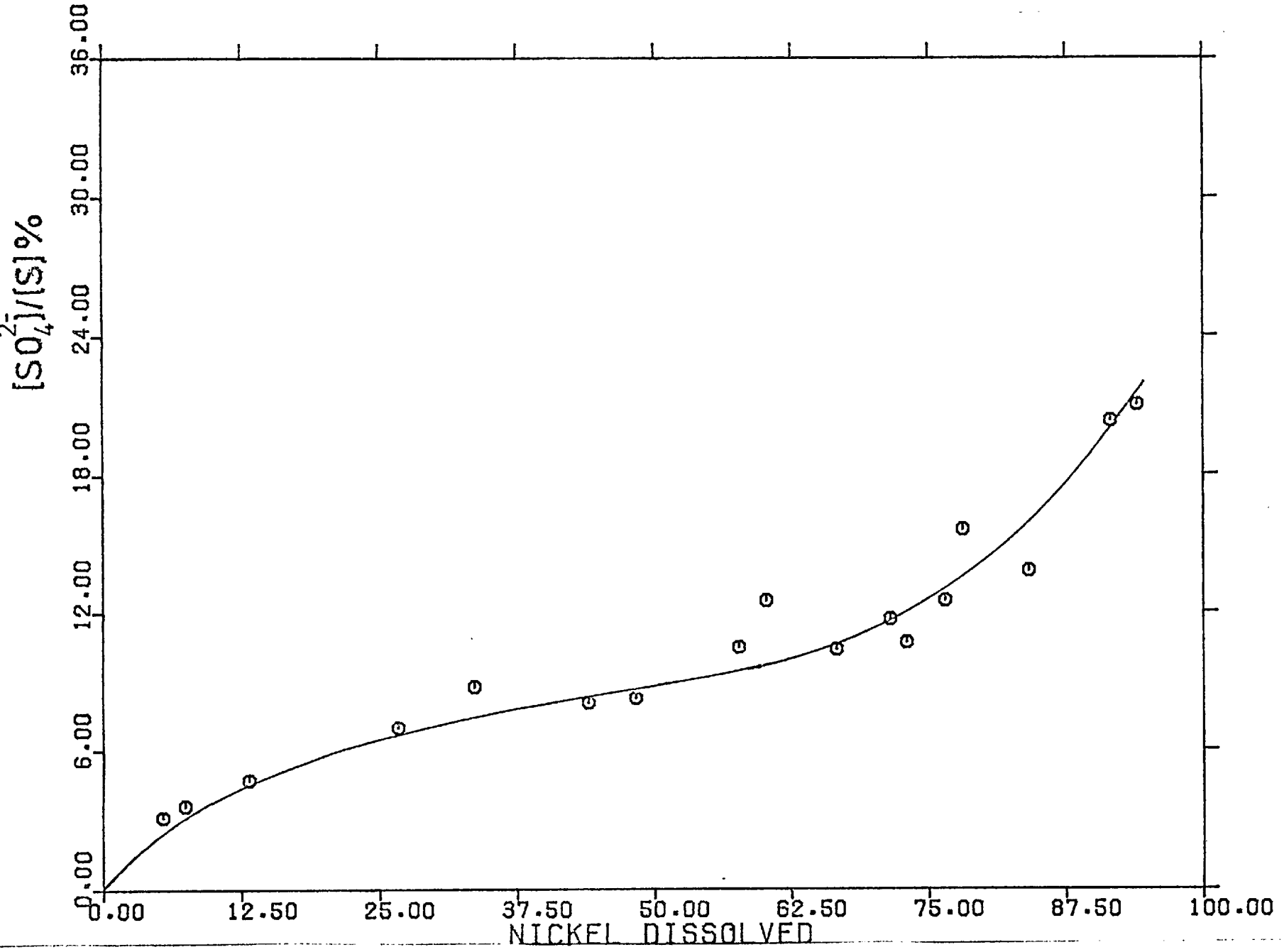

FIG. 47 Sulphate analysis of the Solutions of the Ferric Chloride Leaching of Mss

3.4 MICROSCOPIC INVESTIGATION OF THE LEACH RESIDUES

In order to observe by microscopic means the effect of leaching on the leach residues, solid samples having different amounts of nickel dissolved were taken from the reaction vessel and mounted in araldite. After polishing them using the method described in section (2.4.2) they were observed and photographed in a Reichert Universal Camera Microscope MeF. The corresponding photomicrographs are presented in Appendix C.

Figure C-2.1 shows particles of the Mss after about 10% of the nickel had been dissolved. As can be seen the particles retain the well-defined edges and a very few pores can be noticed on the surface of the particles; but a number of small cracks have already formed mainly at the edges in addition to the long cracks which were already present before the leaching started.

Figure C-2.2 shows particles of a sample from which 40% of the nickel had been removed. The attack which has started on the edges of the particles, which show an uneven surface and irregular edges is clear. As can be seen, attack is apparent also along cracks and around holes. Small amounts of sulphur were found on the edges of the particles and in the cracks and holes, but no other phase was observed to be in the residues.

Residues in a more advanced stage of leaching showed a further attack on the edges of the particles and an increase in the size of cracks and holes. New pores also seem to have formed on the surface of the particles (fig. C-2.3, about 60% Ni dissolved). The original particles also seem to break into many much smaller particles.

Figure C-2.4 shows a picture of particles taken after about 80% of nickel had been leached out. The surface is greatly attacked with the formation of a large number of pores which widen progressively, causing a reduction to the sound regions of the particles. The outline of the initial particles can be recognized from the shape of the dark zones, which consisted of elemental sulphur removed during polishing.

It should be noted, that in no residue microscopically examined was a second phase observed apart from sulphur.

3.5 ELECTRON PROBE MICROANALYSIS

Electron probe microanalysis was used to investigate the homogeneity of the synthetic material prepared and the distribution of the elements in the residues.

The analyses were performed on polished samples in the apparatus described in section (2.4.3).

The results from measurements obtained by point counting across the grains are shown in figure (31) and table (1).

As can be seen, the original mineral shows a reasonable homogeneity where tomography does not interfere (fig. 31).

The microprobe analysis of the leach residues gave a different picture. The electron probe scan for iron, nickel and sulphur gave a rough line, due to the anomalous topography of the surface, because of the formation of cracks and pores. This phenomenon increases with the per cent of metals dissolved.

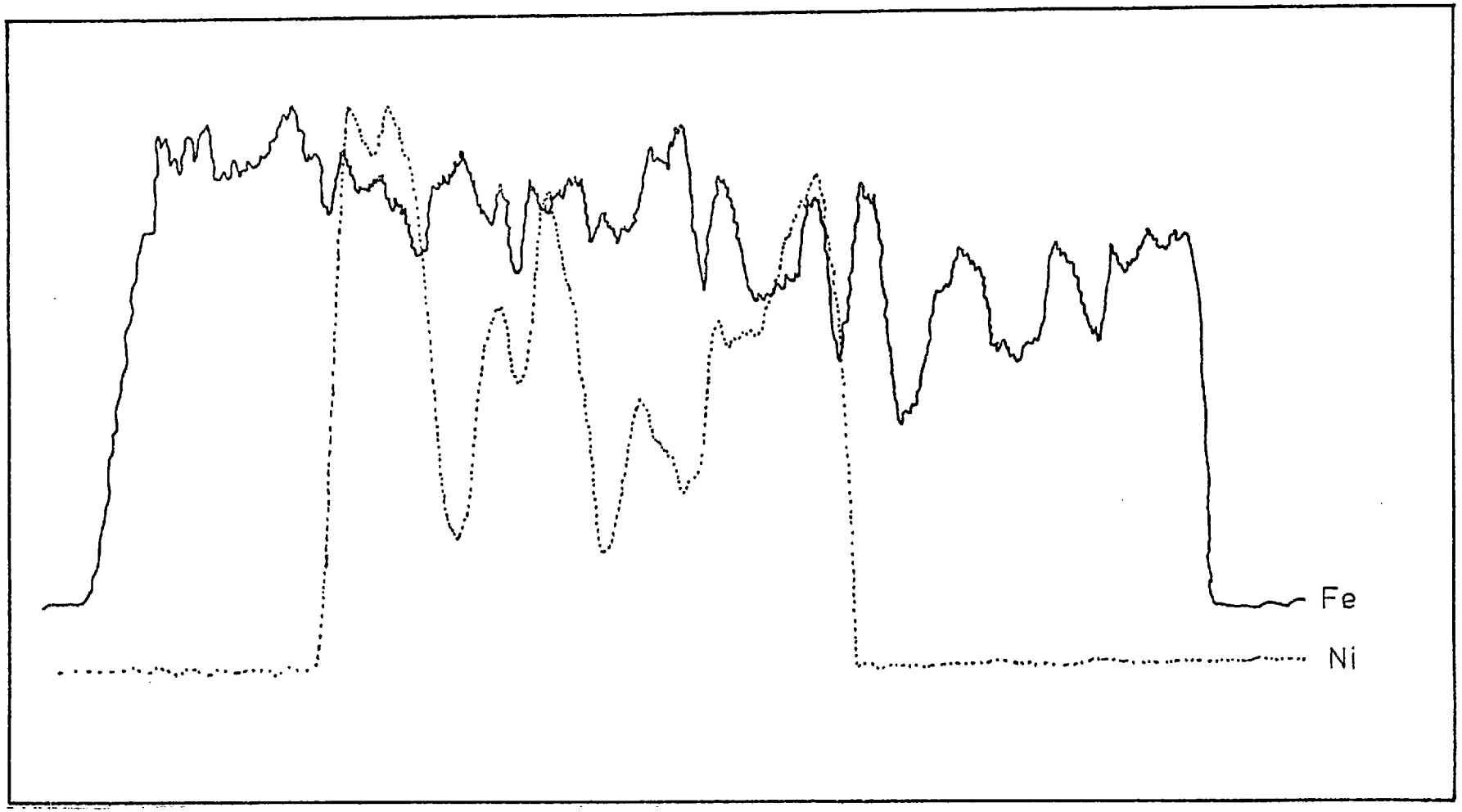

FIG. 48 Electron Microprobe Trace Along a Mss Leach Residue. It shows that Iron Dissolves Slower than Nickel, Participating in the Formation of a Layer around the Particles

The microprobe analysis of the leached residues across the grains showed the existence of a layer which was growing in size as more nickel was dissolved.

It can be seen from figure (46) that in this layer which mainly consisted of sulphur no nickel content is indicated while some iron is present as well.

In the unreacted part in the centre of the grains no accurate measurements could be done because of the formation of cracks and pores. It is obvious that in these cracks and pores the nickel content decreases, while the sulphur content increases. That means that the dissolution of nickel starts from the edges and the cracks and pores of the grains, leaving the sulphur behind to form the coating and fill the holes on the surface of the grains.

The existence of iron in the layer surrounding the unreacted part of the grains indicates that iron dissolves much slower than nickel, participating in the formation of this layer.

The fact that the nickel concentration dropped sharply to zero as the electron beam passed from the unreacted part in the centre of the grains to the surrounding coating (fig. 46) indicates that the diffusion mechanism which partly controls the dissolution is not the diffusion of nickel outwards through the coating, but the diffusion of ferric ions inwards to reach the unreacted part of the grains.

3.6 X-RAY DIFFRACTION RESULTS

X-ray diffraction patterns were taken for the initial solid and most of the leach residues. Table (B-3.1) compares the measured

d-spacings of the original Mss and the leach residues with A. S. T. M. values and the Mss x-ray data given by Shewman and Clark (115). Figure C-1.1 shows the powder photographs of the original Mss and the leach residues from which the data presented in Table (B-3.1) were measured.

As can be seen powder photographs for the residues obtained under different conditions of leaching and at different amounts of nickel dissolved showed slightly different values of the d-spacings and relative intensities for the lines corresponding to Mss.

As nickel and iron were progressively extracted from the solid, new lines which were identified as belonging to orthorhombic sulphur began to appear. On further leaching the intensity the lines of the orthorhombic sulphur increased as a result of the increasing amount of sulphur as the leaching proceeds,while the intensity of the lines belonging to Mss decreased. The assertion that the amount of elemental sulphur increases as the amount of nickel dissolved increases is valid for experiments run under identical conditions, while for experiments under different conditions the amount of sulphur present was controlled by the external variables, such as temperature, particle size, etc. Thus the trend observed was that as the temperature increases and the particle size decreases the proportion of elemental sulphur in the residue decreases. The x-ray photograph of the leach residue from experiment involving hydrogen peroxide leaching also showed that the proportion of elemental sulphur in the residue decreased compared to ferric chloride leaching.

3.7 DISCUSSION

During the experimental study of the factors which affect the leaching of Mss, it was seen that all the results fit well with the proposed mechanism of reaction, according to which the dissolution of Mss is controlled both by a chemical reaction and by diffusion, the influence of the chemical reaction on the rate of dissolution being greater than that of the diffusion.

The effect of the diffusion mechanism on the rate of dissolution increases with the reaction time, as the thickness of the porous layer surrounding the grains increases.

The appearance of both sulphur and sulphate in the leach solutions suggests that two oxidants are competing in the oxidation of Mss:

$$NiS + 2Fe^{3+} = Ni^{2+} + 2Fe^{2+} + S \quad (3.1)$$

$$FeS + 2Fe^{3+} = 3Fe^{2+} + S \quad (3.2)$$

$$NiS + 2O_2 = Ni^{2+} + SO_4^{2-} \quad (3.3)$$

$$FeS + 2O_2 = Fe^{2+} + SO_4^{2-} \quad (3.4)$$

$$S^{o} + 2O_2 + 2Fe^{2+} = SO_4^{2-} + 2Fe^{3+} \quad (3.5)$$

It is suggested the oxygen giving the reactions (3.3), (3.4) and (3.5) comes from the air which dissolves in the solution and it is not oxygen coming from the dissociation of water; otherwise one of the following reactions would occur:

$$NiS + 8Fe^{3+} + 4OH^{-} = Ni^{2+} + SO_4^{2-} + 8Fe^{2+} + 4H^{+} \quad (3.6)$$

$$FeS + 8Fe^{3+} + 4OH^{-} = 9Fe^{2+} + SO_4^{2-} + 4H^{+} \quad (3.7)$$

$$S^{o} + 6Fe^{3+} + 4OH^{-} = 6Fe^{2+} + SO_4^{2-} + 4H^{+} \quad (3.8)$$

However, if one of the last equations occurred, a very rapid change in the ferric:ferrous ratio would be expected. However this does not appear to occur. The exclusion of reactions (3.6) and (3.7) also means that it is not possible for the ferric ion to oxidise the sulphide to sulphate. This has been also confirmed from the fact that when the ferric ion had been exhausted, the dissolution of nickel and iron continued with the formation of large amounts of sulphate.

In most of the experiments, 1 mg of Mss was dissolved in 200 ml of 0.1M ferric chloride; if we assumed that all the sulphur was extracted from the sulphide with an electron transfer of 2, and since reduction of 200 ml of 0.1M $FeCl_3$ to $FeCl_2$ provides 0.02 electrons, while oxidation of gr NiS to S^{o} requires 0.022 electron, there is not sufficient amount of ferric iron to oxidise all the sulphide. This gives an explanation to the very low rate of reaction at the final leaching stage, which is controlled by the appearance of ferric iron at low concentrations.

However the slowing down of the reaction which occurred in the last stages, even when there was sufficient ferric iron to oxidise the total sulphide, was due to the formation of the sulphur layer coating the grains which inhibits contact between the sulphide surface and the solution.

In the experiments where the ferric iron was exhausted, but a large amount of sulphide had not been oxidised, the dissolution continued slowly, independent of the ferric concentration, and with the formation of

a large amount of sulphate. This is due to the fact that the amount of oxygen in the solution remains constant, so reactions (3.3), (3.4) and (3.5) continue independently of the concentration of ferric iron. Some of the oxidation of the sulphide to sulphate, after the ferric iron was exhausted may be due to some re-oxidation of the ferrous to ferric iron.

There was also an indication that as the initial ferric concentration increased so the amount of sulphate produced was decreased. This may partly be due to the decreased solubility of oxygen in concentrated salt solutions.

CHAPTER 4

LEACHING OF PENTLANDITE: RESULTS AND DISCUSSION

4.1 FERRIC CHLORIDE LEACHING: KINETIC RATE CURVES. EFFECT OF LEACH VARIABLES ON THE RATE OF REACTION

The dissolution of pentlandite (Fe, Ni)$_9$S$_8$ was investigated using the same procedure and apparatus as in the leaching experiments of the Monosulphide Solid Solution of iron and nickel (Section 2.2).

Pentlandite was leached with acidified ferric chloride solutions, while in a few experiments hydrogen peroxide was used as the leaching medium.

The effect of the following variables on the leaching rate was investigated: temperature, particle size, stirring speed, ferric ion concentration, acid concentration and sample weight.

The variations in the leaching conditions and the most common conditions selected for the experiments are listed in the following Table 2.

TABLE 2

Variation of Leaching Conditions for Pentlandite		
Variable	Range of Variation	Most common conditions
Temperature	40° - 90°C	80°C
Particle Size	-180 +53 microns	-125 + 93 microns
Stirring speed	700 - 1800 rpm	1000 rpm
Fe^{3+} concentration	0.05 - 0.15M	0.1M
HCl concentration	0.1 - 0.5 M	0.1M
Sample weight	0.500 - 1.000 gm	1.000 gm

4.1.1 Effect of Temperature

The effect of temperature on the leaching rate of pentlandite was studied in the temperature range 40^{o} - 90^{o}C. It was found that of all the variables studied, temperature had the greatest effect on the leaching rate (fig. 49, tables B-2.1, B-2.2, B-2.3 and B-2.4).

From the kinetic rate curves at temperatures above 60^{o}C it can be seen that nickel dissolved in two distinct stages, a fast one followed by a slower second stage. This is very similar to the dissolution of nickel from the monosulphide solid solution of iron and nickel.

The kinetic-rate curve for the experiment run at 40^{o}C is represented by a straight line, indicating a constant-rate reaction. Similar curves for the leaching of pentlandite were obtained by Kelt (59) at 30^{o} and 50^{o}C, while her experiments at temperatures above 60^{o}C gave curves characterized by a two-stage process. Thus, it is suggested that two different mechanisms of dissolution occur, one above 60^{o}C and the other at lower temperatures.

The apparent activation energy for the dissolution process was calculated by using the Arrhenius equation:

$$\ln k = -\frac{Ea}{RT} + C \qquad (4.1)$$

or

$$\log K = -\frac{Ea}{2.303\ RT} + C'$$

where k = rate constant. The rate constant was calculated by dividing the percent of nickel dissolved by the time (in minutes) in which it dissolved.

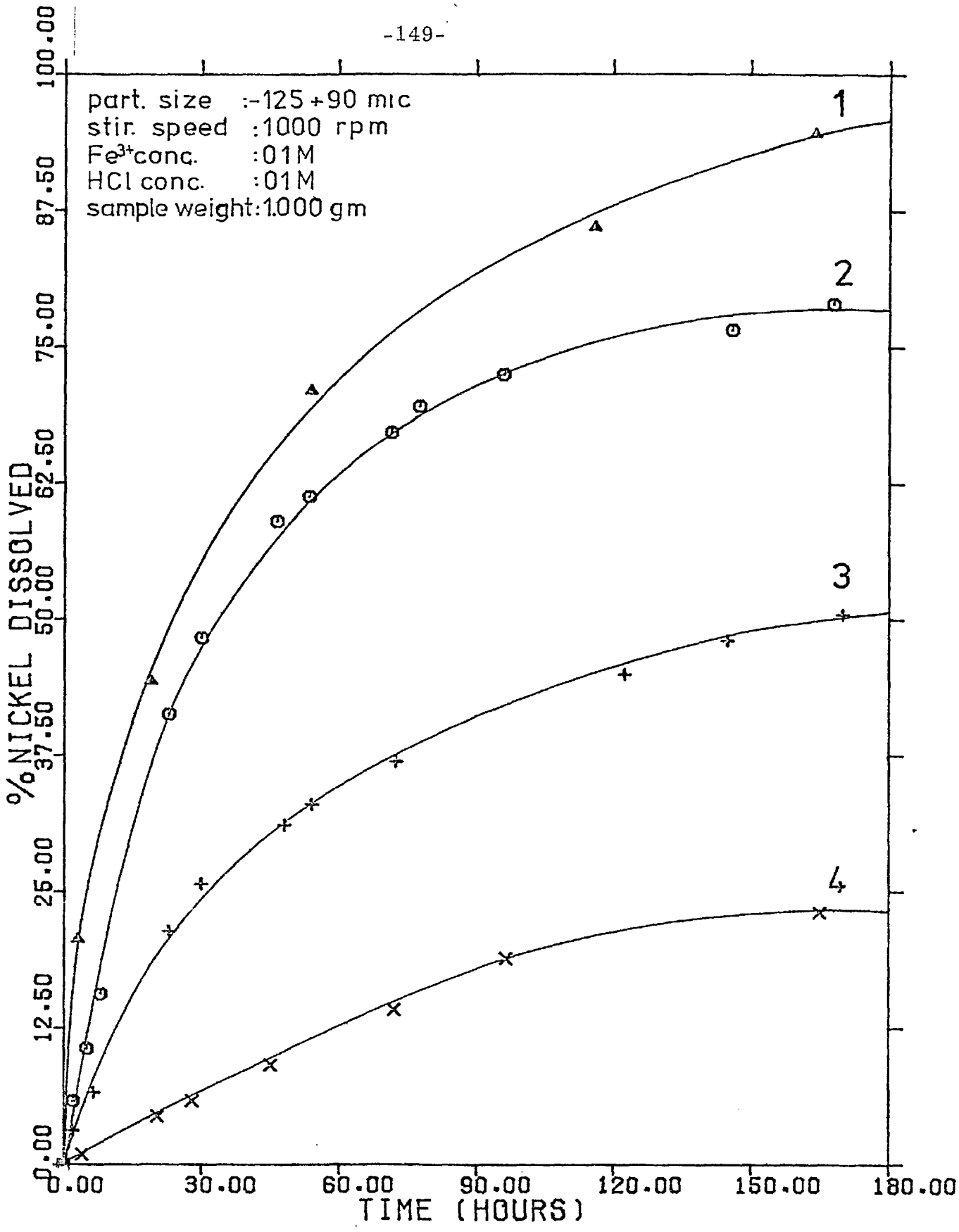

FIG. 49 Effect of Temperature on the Rate of Leaching of Pentlandite

1: 90°C, 2: 80°C, 3: 60°C 4: 40°C

The apparent activation energy for the first stage of dissolution (up to about 20% of nickel dissolved) was calculated to be about 11 kcal/mole (Fig. 50). This critical increment of energy is low for an entirely chemically controlled reaction and high for a transport control reaction. It therefore seems to indicate what the reaction rate is controlled by a mixed regime.

With nickel extractions greater than 20%, the leaching rate was greatly decreased compared with the initial rate. The apparent activation energy calculated for a later stage of the dissolution (after 30 hours of leaching) was found to be 7 kcal/mole, (Fig. 51). This value is slightly above the values normally considered when a reaction is entirely transport controlled (4 kcal/mole).

Considering the shape of the curves and the two values of the apparent activation energies, it is obvious that a chemical reaction and a transport mechanism are the rate determining factors. The chemical reaction has a greater rate at the beginning of the dissolution, while as the dissolution proceeds the transport mechanism becomes more important.

The large effect of temperature on the rate of leaching is due to the fact that it has a favourable influence on both the chemical and transport control mechanisms of dissolution.

An attempt was made to study the effect of temperature on the rate of leaching of iron from pentlandite and compare it with the rate of leaching of nickel. Although the curves for the increase of iron concentration with time had a similar shape to the nickel dissolution curves, it was difficult to compare results for two reacons:

i) because some hydrolysis of ferric ions occurred especially at high temperatures and

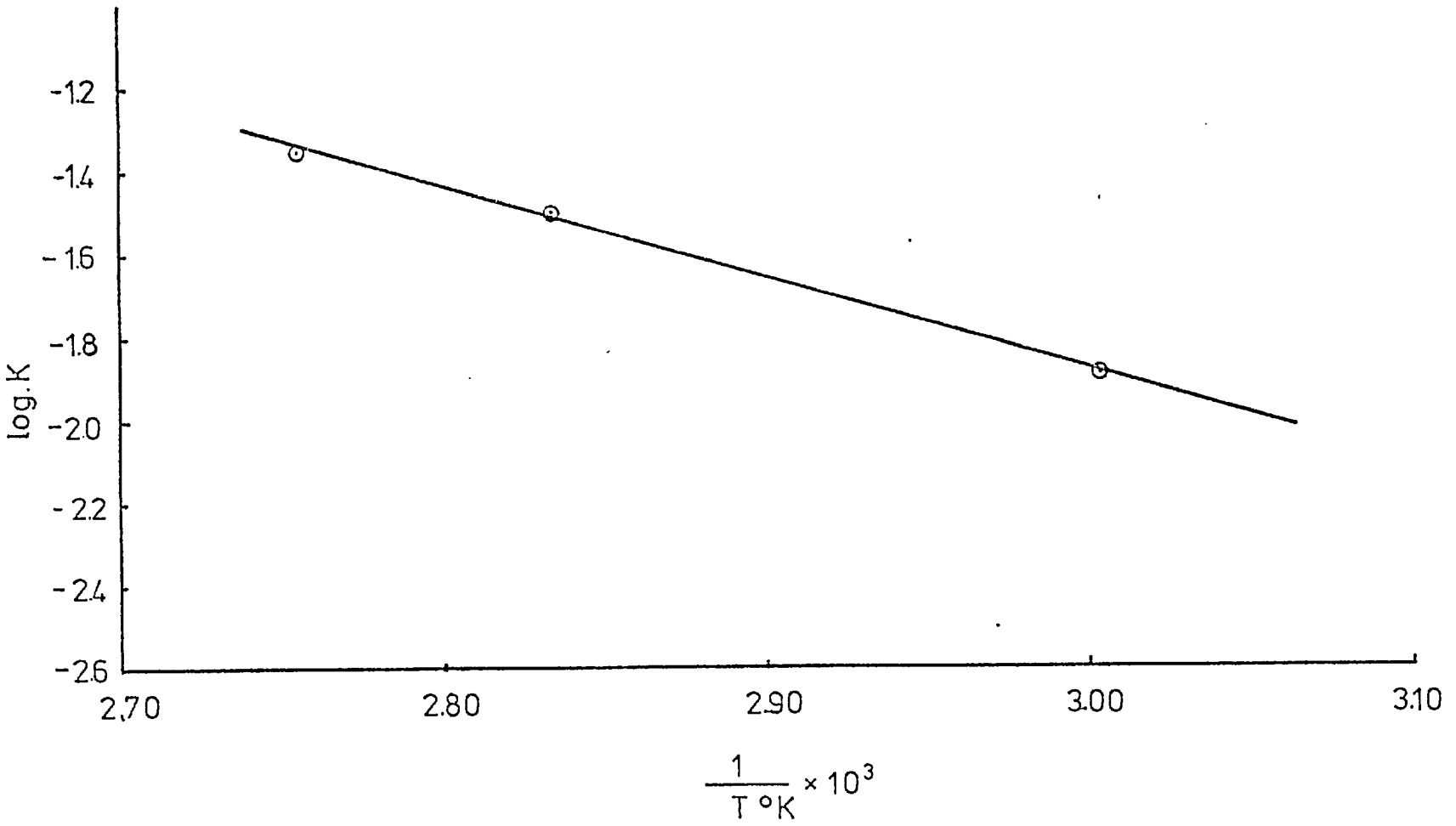

FIG. 50 Arrhenius Plot for First Stage of the Dissolution of Pentlandite

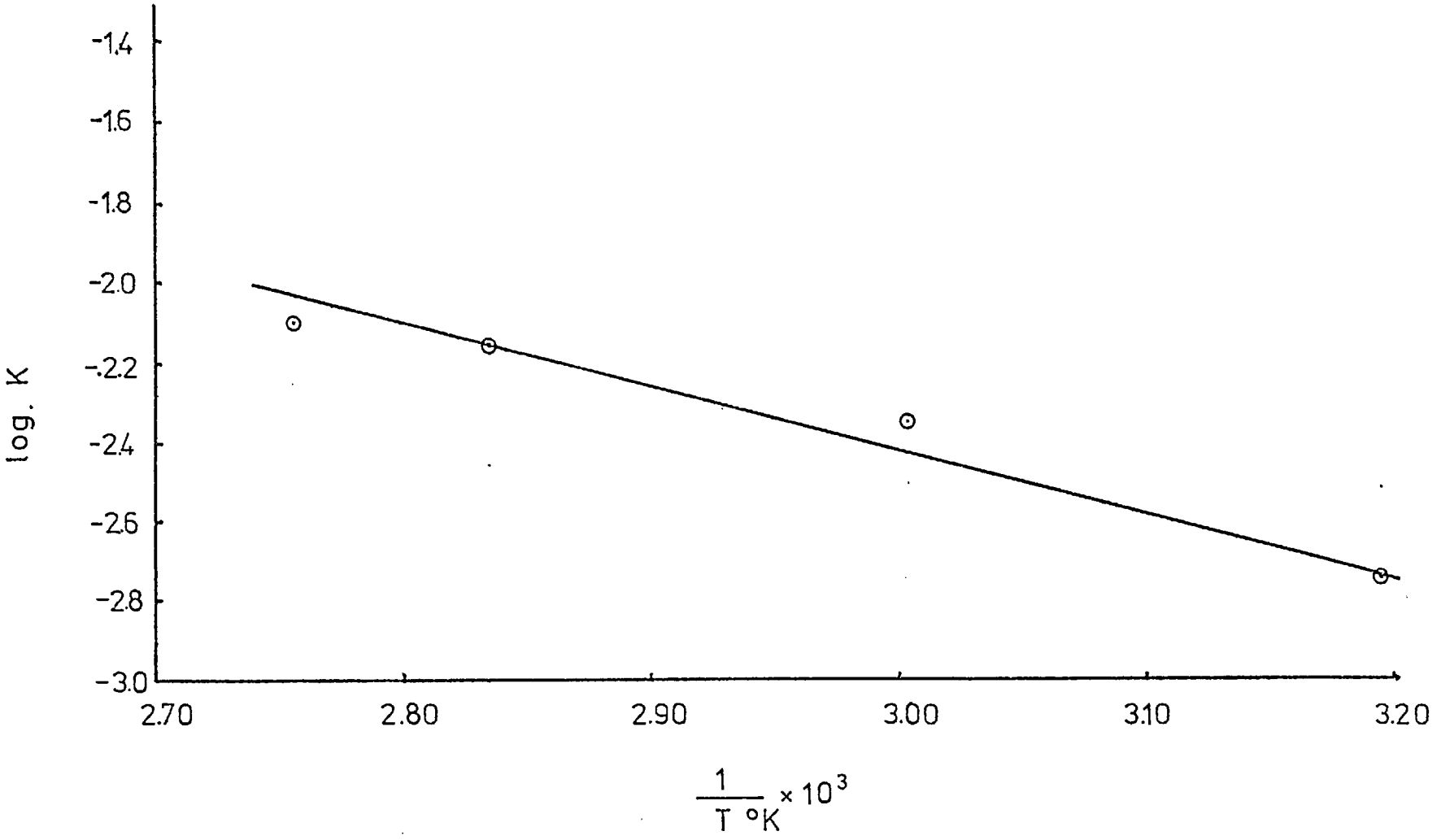

FIG. 51 Arrhenius Plot for Second Stage of the Dissolution of Pentlandite

ii) because of the high initial iron concentration compared to the amount of iron dissolving from pentlandite.

Thus these results only indicate the trend of the dissolution of iron.

Some attempts were made to obtain a rate equation to fit the experimental curves, but all were unsuccessful. This was due to the complexity of the system because of the contribution of two different mechanisms to the reaction and to the fact that higher temperatures tend to promote hydrolysis of ferric ions.

4.1.2 Effect of Particle Size

To investigate the effect of particle size on the rate of leaching, four experiments were carried out using the following average size fractions: -180 + 125, -125 + 90, -90 + 63, -63 + 53 microns.

As can be seen from figure (52) and tables (B-2.1), (B-2.5), (B-2.6), (B-2.7), the variation in the particle size had some effect on the rate of leaching. The smaller the particle size the higher the rate of the extraction and the amount of nickel dissolved.

The results of the experiment with normal particle size (-125 + 93 microns) gave a typical leaching curve with the rate decreasing after 20% of nickel had been extracted. The leaching rates for the different particle sizes although slower or faster gave curves of similar shape.

An increase in the leaching rate with a reduction of particle size indicates a mechanism controlled by a surface reaction as well as a mechanism controlled by a diffusion of one of the reactants through a porous film. A decrease in the particle size favours the surface reaction

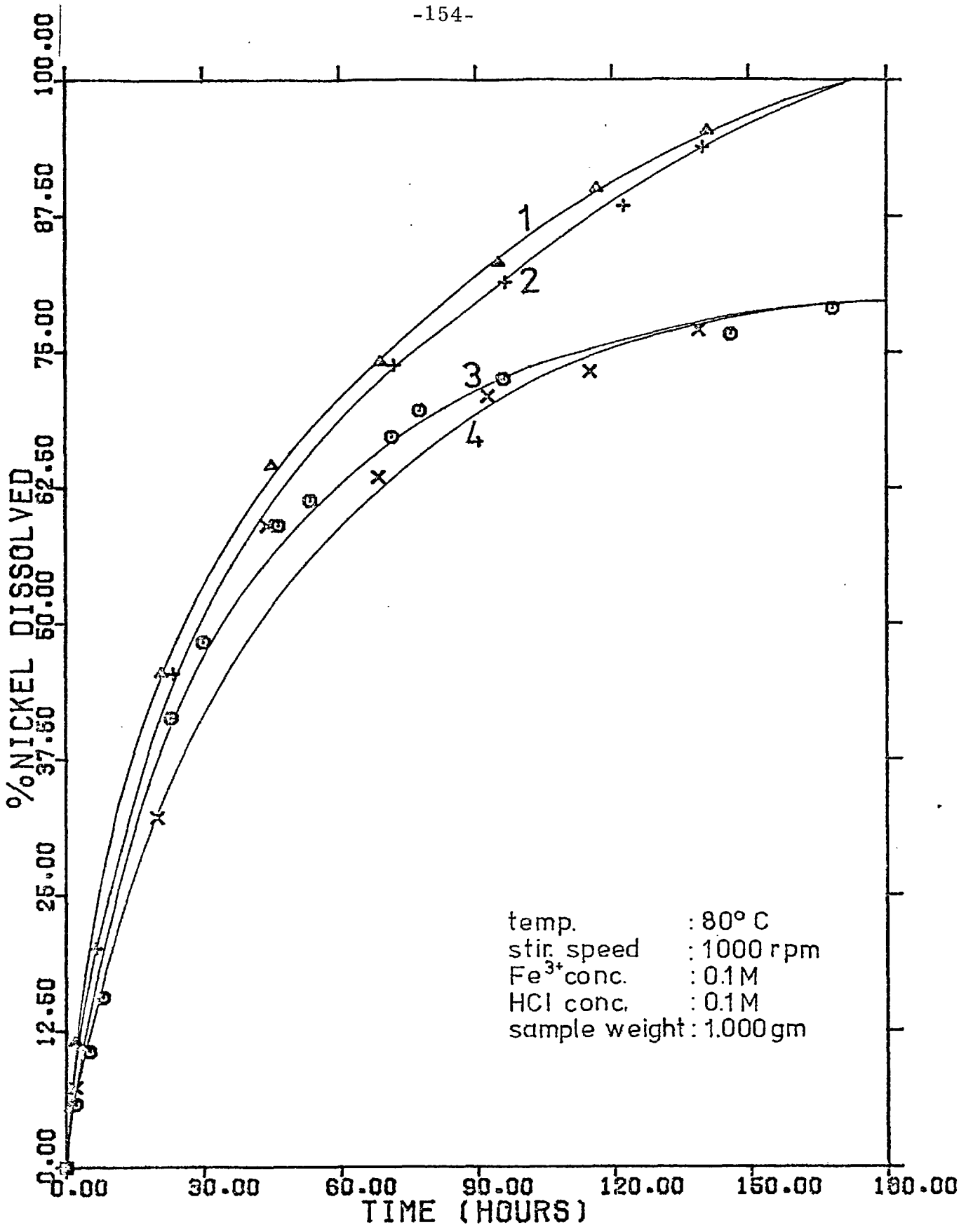

FIG. 52 Effect of Particle Size on the Rate of Leaching of Pentlandite

1: -63 + 53 microns, 2: -90 + 63 microns,

3: -125 + 93, 4: -180 + 125 microns.

since it increases the total active surface area per unit mass and the diffusion mechanism because it reduces the diffusion distances.

Two limiting factors in the particle dimensions are that the size must neither be so small as to permit flotation of the particles nor so great as to prevent suspension.

4.1.3 Effect of Ferric Ions Concentration

Figure (53) shows the effect of ferric ions concentration on the dissolution rate of nickel from pentlandite, while these results are tabled in Tables (B-2.1), (B-2.8), (B-2.9) and (B-2.10).

Ferric ion concentrations of 0.00, 0.05, 0.10 and 0.15 molar were considered. The experiments were carried out at 80^{o}C with 1 gm samples of particle size -125 + 93 microns. The solutions of ferric chloride in hydrochloric acid (pH = 1) were stirred at a speed of 1000 rpm. In the case of the experiment with zero ferric ion concentration an amount of sodium chloride was added so that the chloride concentration in the solution was the same as in the experiment under the most common conditions.

The variation of the initial ferric concentration from 0.05M to 0.15M had no effect on the leaching rate, for the extraction of up to about 20% of the nickel. As the leaching continued, the higher the ferric concentration in the solution the higher was the rate of leaching.

The final slow leaching stage was controlled by the fact that at that stage the ferric iron concentration was low. If we assume that all of the sulphur was extracted from the sulphide with an electron transfer of 2, it will be seen that there was not sufficient ferric ion to oxidize all the sulphide:

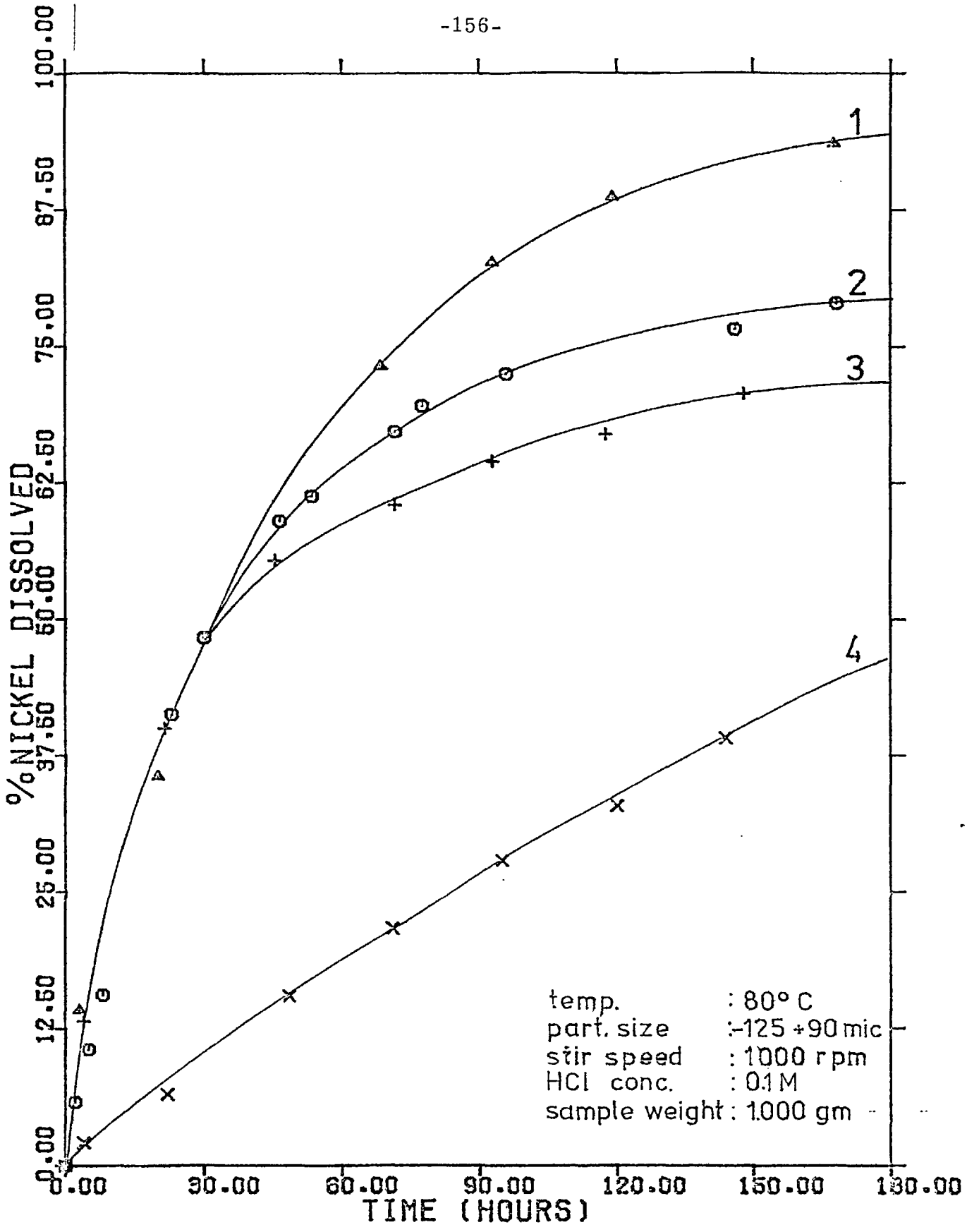

FIG. 53 Effect of Ferric Concentration on the Rate of Leaching of Pentlandite

1: 0.15M Fe^{3+} 2: 0.01M Fe^{3+}

3: 0.05M Fe^{3+} 4: 0.0M Fe^{3+}

Reduction of 200 ml of 0.1M Fe^{3+} to Fe^{2+} provides 0.02 electron equivalents

Oxidation of 1gm $(Fe,Ni)_9S_8$ in 200 ml to S^o requires 0.0207 electron equivalents.

The leaching curve for zero ferric concentration implies an entirely different mechanism. Since there was not ferric ion in the solution the only oxidizing agent of the sulphide was the oxygen from the air which was dissolving in the solution. Thus it seems that under atmospheric pressure the oxidation of the sulphide by ferric ions proceeds much faster than the oxidation by oxygen dissolved in solution.

4.1.4 Effect of Stirring Speed

As it is known that an increase in the leaching rate on increasing the stirring speed is consistent with a reaction rate controlled by a transport mechanism, the effect of stirring speed on the rate of leaching was studied varying the stirring speed from 700 to 1800 rpm.

The results of this study are summarized in figure 54 and tables (B-2.1), (B-2.11), (B-2.12) and (B-2.13).

As can be seen, increasing the velocity from 700 to 1000 rpm had no effect on the rate of leaching. Higher stirring speeds had a very little effect on the rate of the reaction at the beginning of the experiment, but as dissolution proceeded the rate of the reaction began to become more dependent on the stirring speed.

These results are in good agreement and confirm what was suggested in section (4.1.1), that a transport-controlled mechanism predominates over a chemically controlled mechanism as the process of dissolution of the mineral goes on.

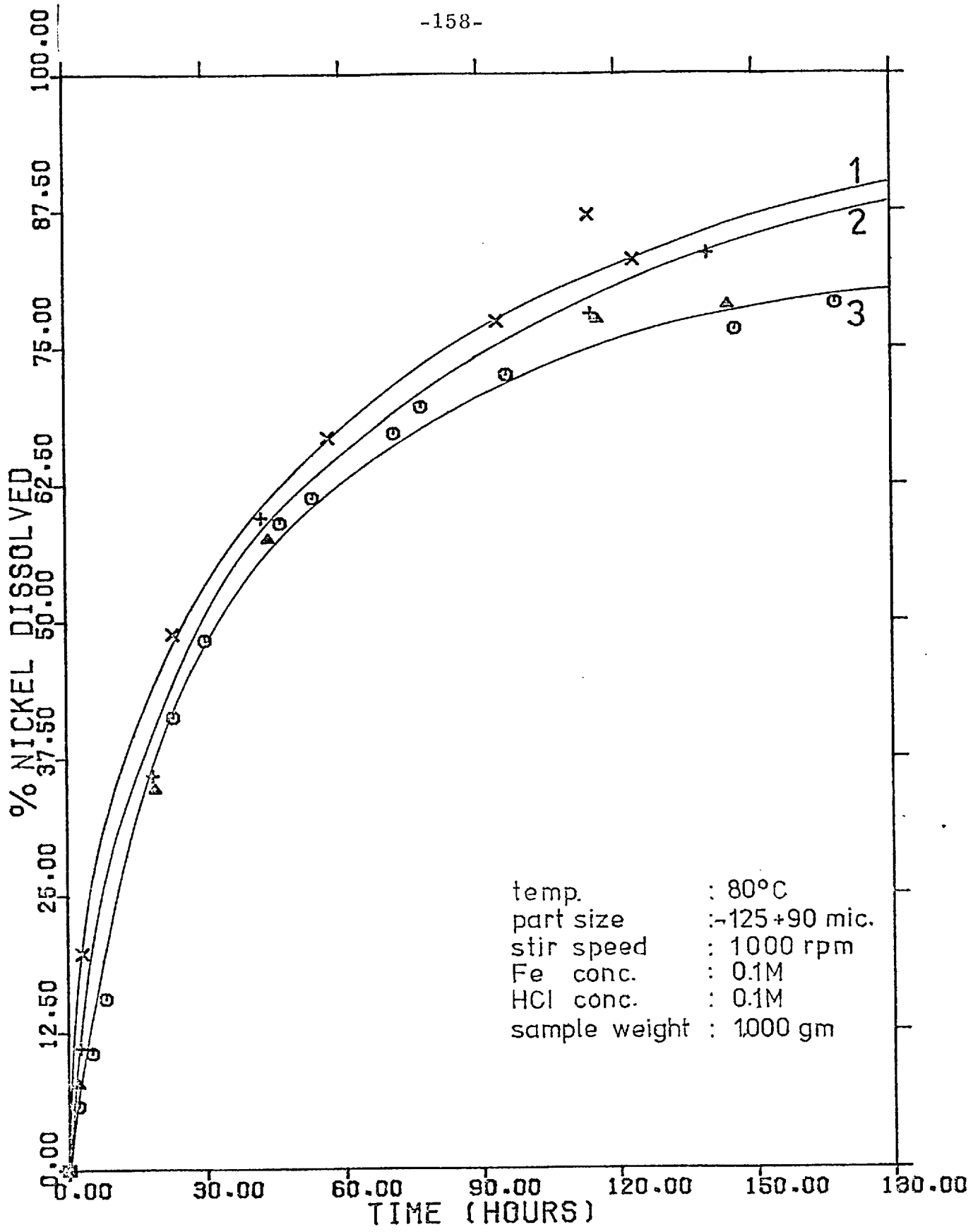

FIG. 54 Effect of Stirring Speed on the Rate of Leaching of Pentlandite

1: 1800 rpm 2: 1400 rpm

3: 1000 rpm, 700 rpm

A problem faced in the study of the effect of stirring speed was that at high stirring speeds the splashing of the liquid on the lid of the leaching vessel became worse and so the amount of solid deposited on it increased. This was more significant when a large amount of nickel had been leached and the particles became porous.

A stirring speed of 1000 rpm was selected for most of the experiments because it was found to be efficient enough to keep the particles in suspension and to avoid much splashing of the liquid.

4.1.5 Effect of Hydrochloric Acid Concentration

The reason hydrochloric acid was added in the solution was to maintain the pH of the solution below a certain value and so prevent hydrolysis of the ferric ions. The value of pH above which ferric ions hydrolyse and precipitate depends on the temperature of the solution.

In most of the leaching runs the ferric chloride was acidified with 0.1M hydrochloric acid in order to maintain the pH below one, this value of pH has been found sufficient to keep ferric ions in solution, in the range of temperatures used in this work.

Measurements of the pH of the solutions before and after leaching showed very little change of the pH during the experiment.

Since there was evidence from previous work (43), (56) that an increase in the initial acidity has an unfavourable effect on the leaching of nickel sulphides, the leaching of pentlandite was studied under three different initial hydrochloric acid concentrations.

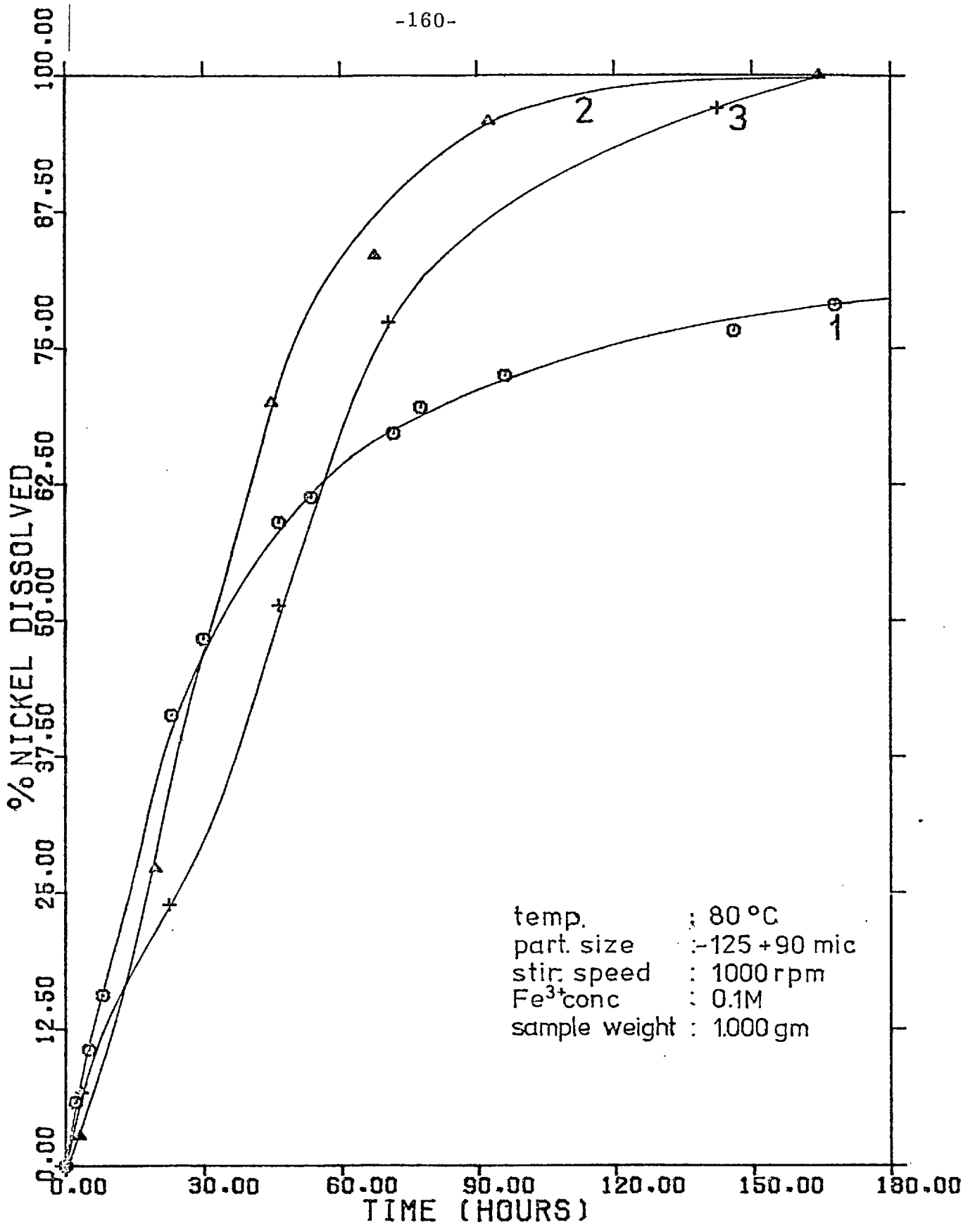

FIG. 55 Effect of Hydrochloric Acid Concentration on the Rate of Leaching of Pentlandite

1: 0.1M HCL, 2: 0.3M HCl, 3: 0.5M HCl

Figure (55) shows the effect of hydrochloric acid concentration, while the results of this study are summarized in Tables (B-2.1), (B-2.14) and (B-2.15).

As can be seen an increase of the acidity caused a decrease of the rate of pentlandite's dissolution in the beginning of the experiment, while as nickel dissolution proceeded, the leaching rate at high acid concentrations increased and the total amount of nickel dissolved increased from 80% in 0.1M HCl to 100% in 0.3 and 0.5M HCl.

A probable explanation of the lower leaching rate at higher acidities in the beginning of the experiment could be the same one with that given in section 3.1.5 for the effect of acid concentration on the rate of monosulphide solid solution of iron and nickel. Higher hydrochloric acid concentrations reduce the amount of undissociated ferric ions in the solution, which are the species providing the oxidizing reaction.

4.1.6 Effect of Sample Weight

The effect of the sample weight on the rate of leaching was studied by varying the loads of pentlandite from 0.5 to 2.0 gm. The experiments were carried out in 200 mls of 0.1M HCl at 80^{o}C with a particle size of -125 + 93 microns and a stirring speed of 1000 rpm, and the results are given in figure (56) and Tables (B-2.1), (B-2.16) and (B-2.17).

As can be seen, sample weight had a significant effect on the rate of leaching. Increasing the sample weight lowered the rate of the reaction and the total amount of nickel dissolved decreased.

The low leaching rates and amount of nickel extracted at high sample weights was due to the rapid reduction of the concentration of ferric

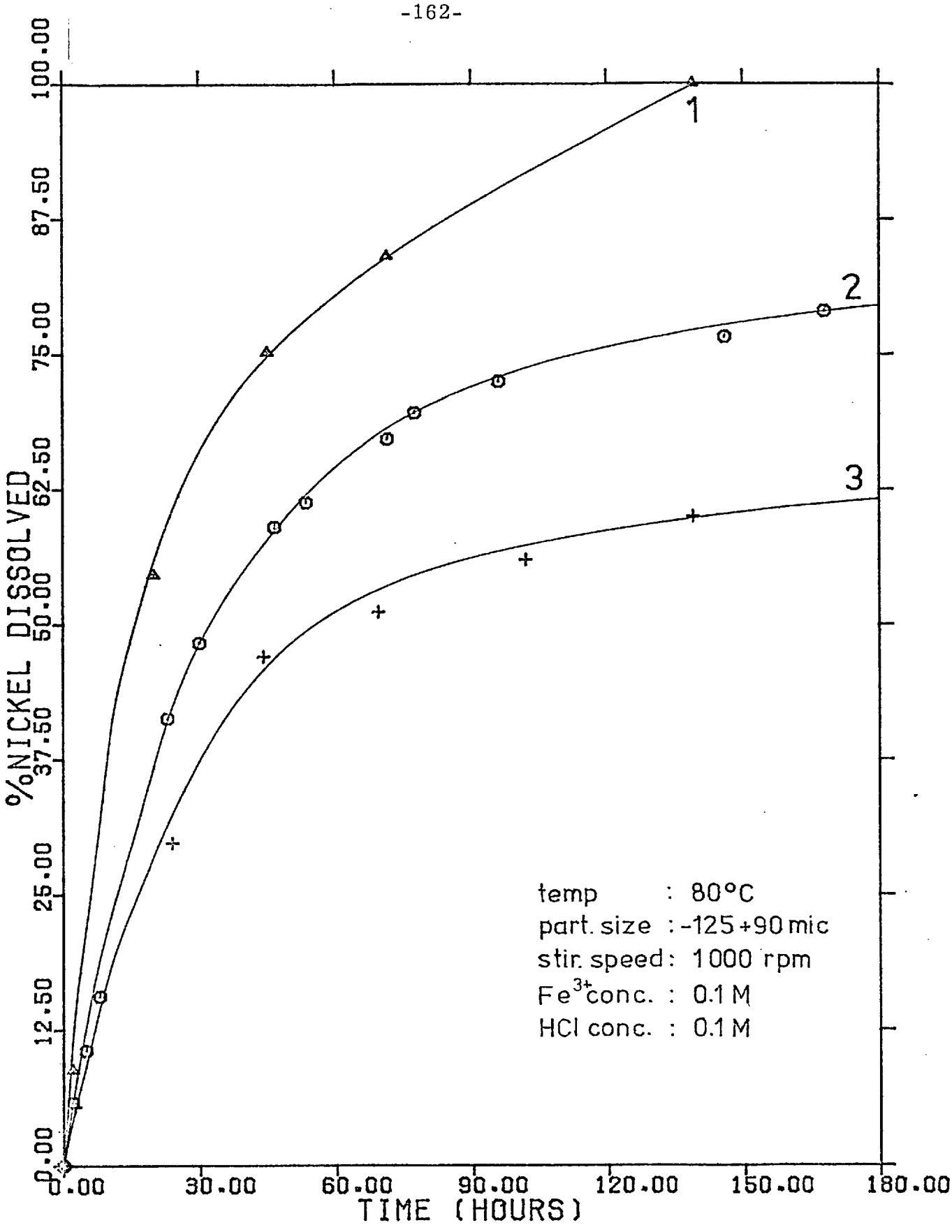

FIG. 56 Effect of Sample Weight on the Rate of Leaching of Pentlandite

1: 0.5 gm, 2: 1.0 gm 3: 2.0 gm

ions and the unavailability of these species at the end of the reaction. Thus only 60% of the Ni dissolved after six days of leaching for the 2.0 gm sample, while the nickel extraction from the 0.5 gm sample at the same time was complete.

Although the number of electrons provided by the reduction of 200 ml of 0.1 Fe^{3+} to Fe^{2+} were sufficient to oxidize only the 50% of the 2.0 gm sample, the dissolution of nickel continued after all the ferric ions were exhausted. This could be due to one of the following factors:-

1. Oxidation of pentlandite by oxygen from air dissolved in the solution.
2. Re-oxidation of Fe^{2+} to Fe^{3+} by air
3. Direct dissolution of pentlandite with HCl by evolution of hydrogen sulphide.

Another factor affecting unfavourably the rate of leaching when a large amount of solid was leached, was that not all the particles of the solid were in intimate contact with the solution, and this seems to be the cause of the lower rate of reaction at higher sample weight at the beginning of the experiment when there is still sufficient concentration of ferris ions.

4.2 LEACHING WITH HYDROGEN PEROXIDE

Because the attempt to compare the dissolution of iron with that of nickel in the ferric chloride leaching of pentlandite was not successful for reasons mentioned in section 4.1.1, it seemed useful to carry out some oxidizing leach experiments without introducing ferric ions.

The oxidant chosen was a solution containing 50 ml of 20-volume hydrogen peroxide and 150 ml of hydrochloric acid solutions adjusted to different pH values. A one gram sample of -180 + 125 microns pentlandite was leached out at 80°C with a stirring speed of 1000 rpm.

Two experiments were carried out: in the first one the hydrogen peroxide solution was mixed with 0.3M HCl and in the second with 0.5M HCl. The results obtained are presented in figures (57) and (58) and in tables (B-2.18) and (B-2.19).

As can be seen, in both experiments about 7% of the nickel was extracted within a few minutes after the introduction of the solid sample into the solution, while subsequently the rate of dissolution of nickel was proportional to the time of leaching.

The rate of leaching was higher in the case of the solution with the lower acidity, which is in agreement with the behaviour of nickel in the ferric chloride leaching of pentlandite in the early stages of dissolution.

Comparing the rate of leaching of pentlandite in ferric chloride with the rate in hydrogen peroxide, it is found that the rate in ferric chloride is much higher than that in hydrogen peroxide at the beginning of the reaction. However given that the rate of dissolution in ferric chloride decreases with

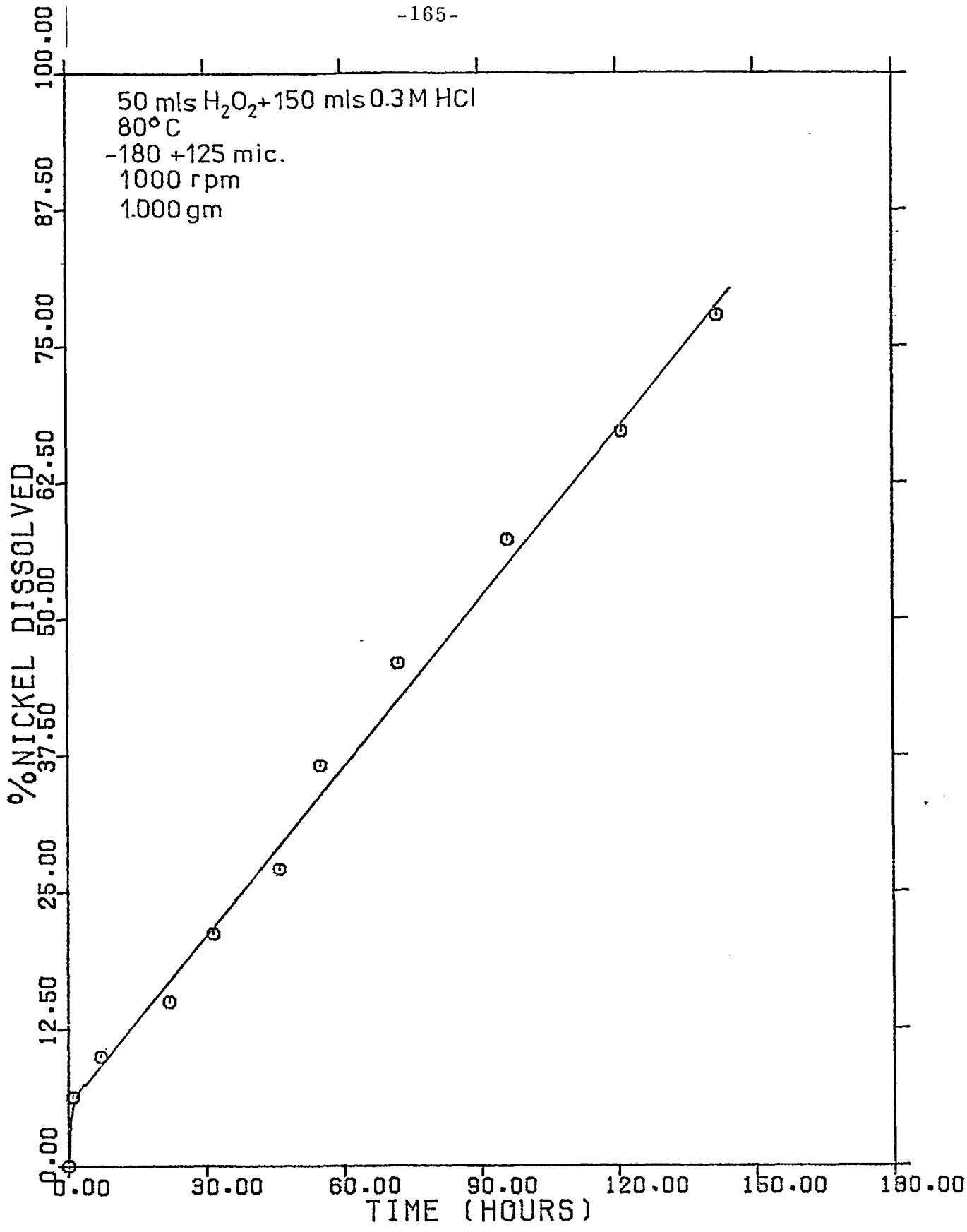

FIG. 57 Hydrogen Peroxide Leaching of Pentlandite

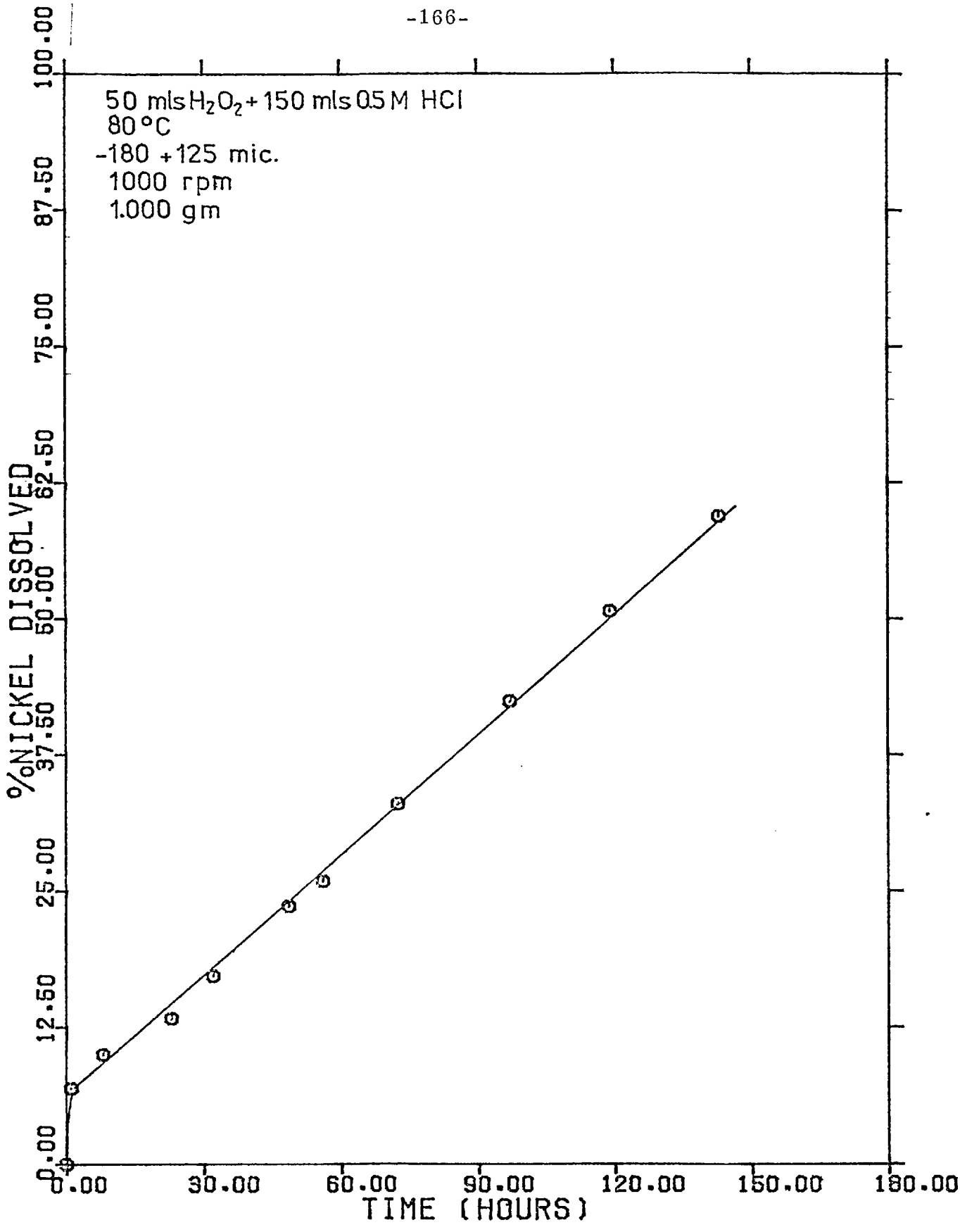

FIG. 58 Hydrogen Peroxide Leaching of Pentlandite

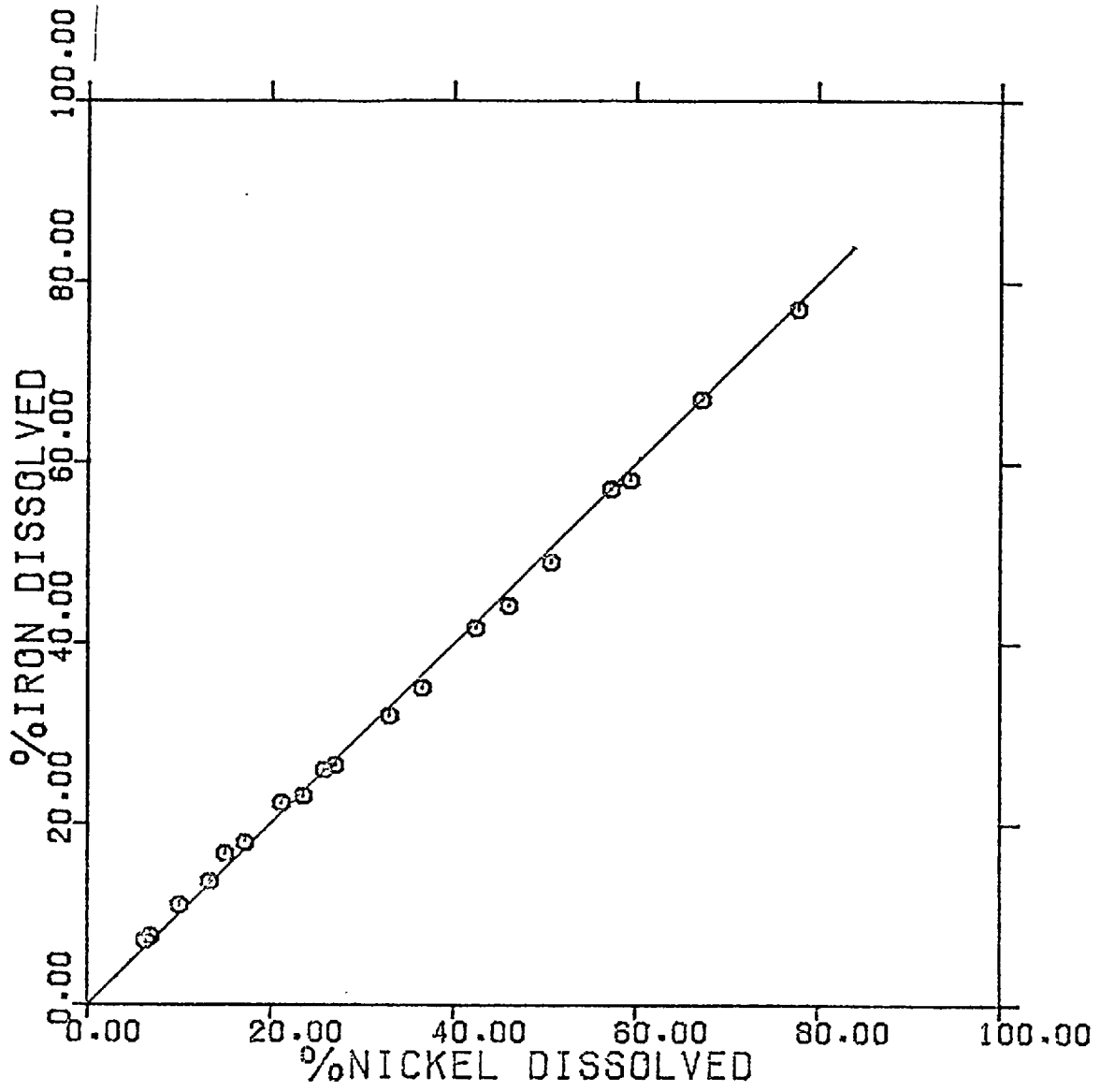

FIG. 59 Curve Relating the Percentage of Iron to that of Nickel Removed during Leaching of Pentlandite in Hydrogen Peroxide

time while the rate in hydrogen peroxide remains constant, there is a moment when the rate in hydrogen peroxide becomes faster than in ferric chloride. Finally 80% of the nickel contained in pentlandite was extracted by hydrogen peroxide leaching after 150 hours, while the same amount of nickel was extracted after 170 hours by ferric chloride leaching.

Iron and nickel analyses from samples taken during the hydrogen peroxide leaching of pentlandite showed that both the metals are extracted with the same speed at all the stages of the dissolution (Fig. 59).

The different shape of the leaching curves in hydrogen peroxide compared to those obtained in ferric chloride indicates that a different mechanism of dissolution occurs in the two oxidants.

4.3 SULPHATE ANALYSIS OF THE LEACH RESIDUES

In all of the leaching experiments both elemental sulphur and sulphate were observed. The sulphate formation was studied in experiments carried out under different conditions by analysing the samples according to the method described in section (2.3.2).

Some of the results obtained are presented in figure (60). As can be seen the sulphate produced generally accounted less than 9% of the available sulphur in the sulphide for the ferric chloride leaching and less than 15% for the hydrogen peroxide leaching. The appearance of sulphate is almost proportional to the nickel concentration.

The amount of sulphate and the ratio of its formation is controlled by different variables. Thus high temperatures and high stirring speeds favoured the formation of sulphate while high ferric concentration, high sulphide concentrations and high acidities favoured the formation of sulphur. Particle size had very little effect on the proportion of sulphur and sulphate

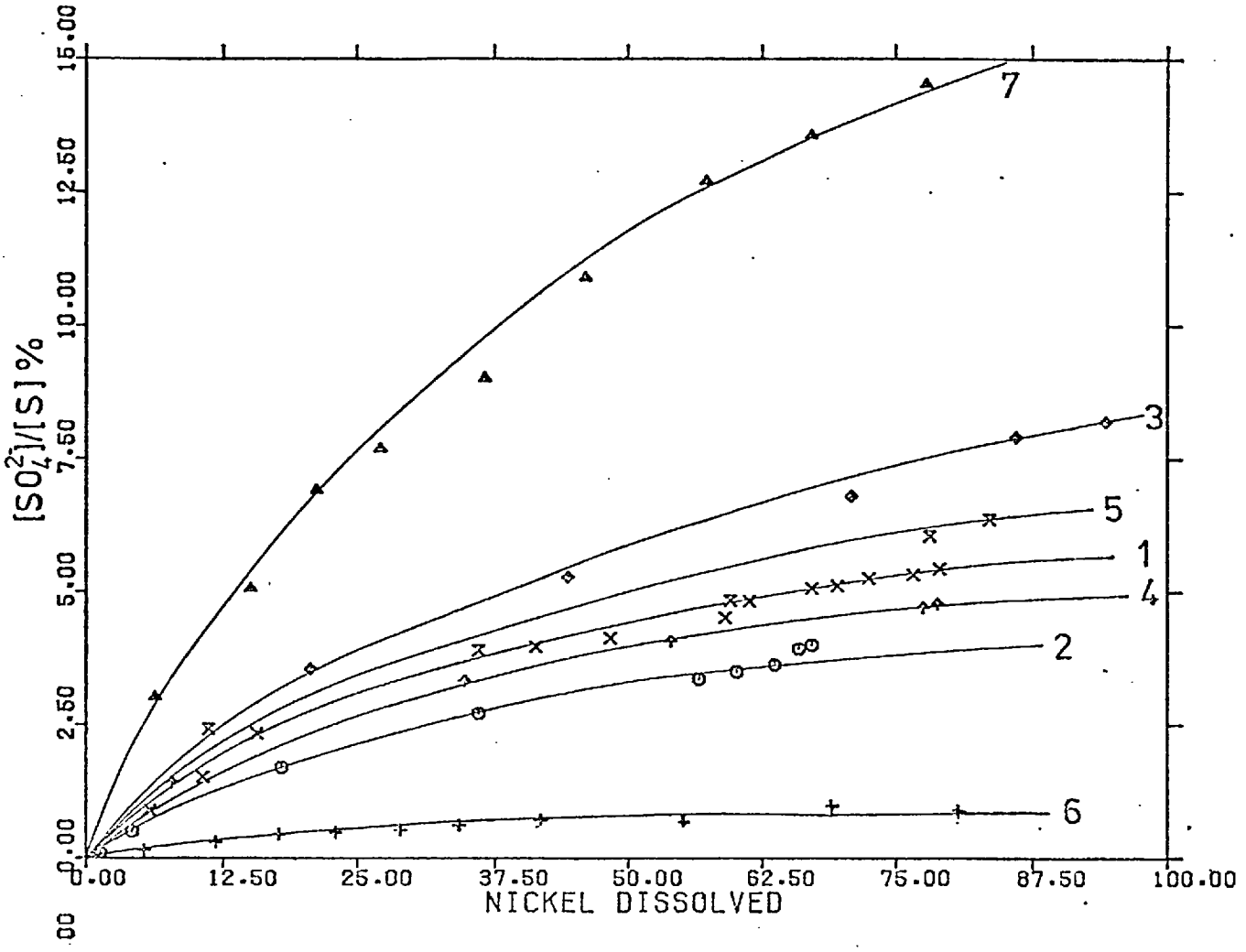

FIG. 60 Sulphate Analysis of the Leach Samples of Pentlandite

1: 80°C, 1000 rpm, 0.1M Fe^{3+}

2: 40°C, 1000 rpm, 0.1M Fe^{3+}

3: 90°C, 1000 rpm, 0.1M Fe^{3+}

4: 80°C, 700 rpm, 0.1M Fe^{3+}

5: 80°C, 1800 rpm, 0.1M Fe^{3+}

6: 80°C, 1000 rpm, 0.0M Fe^{3+}

7: Hydrogen peroxide leaching

in the residues, but a slightly higher sulphate production was observed at smaller particle sizes.

Absence of ferric ions in the initial solution led to the formation of a very small amount of sulphate in the solution and to the evolution of hydrogen sulphide.

4.4 MICROSCOPIC INVESTIGATION OF THE LEACH RESIDUES

Polished samples of the leach residues mounted in araldite, from which a different amount of nickel had dissolved were observed under the microscope. Some photomicrographs taken from these residues are presented in Appendix C, Fig C-3.1 to C-3.7

Figures C-3.1, C-3.2 and C-3.3 show unleached pentlandite. As can be noticed the original material is very porous.

Figure C-3.4 shows some grains of pentlandite from which about 20% of the nickel has been dissolved. There are more cracks and pores than in the unleached solid and attack seems to have started on the edges and along the cracks of the particles.

Another picture of particles from which 50% of the nickel has been dissolved is seen in figure C-3.5. The cracks have already increased markedly in size and the removal of further nickel has been accompanied by large-scale erosion of cracks internally in the particles suggesting preferential attack.

Figure C-3.6 shows a microphotograph of pentlandite particles taken after about 70% of the nickel had been dissolved. The attack around

the edges and along cracks which resulted in the breaking down of the particles into smaller ones, is very clear. The black areas around the particles are holes in the mounting material left due to the elemental sulphur being removed during the polishing of the samples.

The preferential dissolution of the material along the cracks resulting in the complete breakdown of the original large particles into very fine ones, when 80% of the nickel has been dissolved is shown in figure C-3.7.

A large piece of pentlandite was mounted in araldite and suspended in a stirred ferric chloride solution at 80°C. A macrophotograph of this piece is shown in figure C-3.8. The solid was leached for 10 hours and then it was removed from the solution, washed, polished and photographed. As can be seen from figure C-3.9, the attack had already began on the edges of the solid. Figure C-3.10 shows the same solid after 20 hours of leaching. The surface which in this case had not been polished before it was photographed shows a very low reflectivity due to an oxide layer formed during the leaching. However the surface shows a higher attack not only around the edges but also in the central part of the solid. The attack is distinguished from the 'black' areas inside the solid which are holes filled initially by sulphur which has been removed.

The further attack on the solid after 50 hours of leaching is shown in figure C-3.11. In this case the sample was polished before being photographed to remove the oxide layer. The sample was extremely brittle due to the presence of small particles badly eroded, often separate from each other.

Figure C-3.12 shows what remained from the initial sample after 100 hours of leaching.

In all the leach residues examined microscopically no new phase other than those previously noticed was detected. One thing observed was that the pyrrhotite areas in the leach residues were markedly reduced, an indication of preferential dissolution of pyrrhotite.

4.5 ELECTRON PROBE MICROANALYSIS

In order to investigate the homogeneity and the distribution of the elements in the leach residues of the dissolution of pentlandite, the residues were subjected to electron probe microanalysis. The operation of the electron probe microanalyser and the experimental procedure have already been discussed (section 2.4.3).

Electron probe scans across the polished particles of residues showed that the homogeneity and the composition of the particles remained virtually the same, agreeing well with the formula of pentlandite. No new phase other than those detected in the unleached material was found. It is therefore concluded that pentlandite dissolves readily in ferric chloride without the formation of any intermediate phase.

4.6 X-RAY DIFFRACTION ANALYSIS

X-ray powder photographs of pentlandite leach residues are shown in figure (C-1.2), appendix C. The x-ray diffraction data calculated from measurements of these photographs are presented in Table (B-3.2) and compared with the data of the original material and that given in the A.S.T.M. index for pentlandite and orthorhombic sulphur. It can be seen that the patterns of the synthesized material and the A.S.T.M. index are in good agreement. The extra lines in the synthetic material correspond to pyrrhotite, the A.S.T.M. values of which are given in Table (B-3.1).

As nickel was extracted from the solid new x-ray lines began to appear; these were identified as belonging to orthorhombic sulphur. The more nickel extracted the more the intensity of the lines belonging to sulphur increased and the intensity of the lines belonging to pentlandite decreased.

Pyrrhotite seems to dissolve preferentially from the fact that the intensities of its lines decrease proportionately more than the lines of pentlandite. In the leach residue from which 90% of the nickel had been dissolved, no pyrrhotite was detected.

In some of the leach residue lines corresponding to hematite appeared. The appearance of this phase is due to hydrolysis of ferric ions which takes place in the range of temperatures used in the leaching of pentlandite.

No other phase was detected in any of the leach residues analysed by x-ray diffraction. There was also no evidence of any line movement for any of the phases observed. Thus it was confirmed that both iron and nickel were extracted at the same speed from pentlandite without causing any distortion to the lattice or formation of any intermediate phase.

4.7 BEHAVIOUR OF THE PLATINUM AND PALLADIUM CONTENT OF PENTLANDITE DURING FERRIC CHLORIDE LEACHING

The original object was to study the behaviour or platinum and palladium in the ferric chloride leaching of pentlandite under different experimental conditions. Thus, the same leach samples which were analysed for nickel and iron were also analysed for platinum and palladium following the method described in section (2.3.3).

Unfortunately because of the small volume of the available lead solutions, the very low concentration of platinum and palladium and the high concentration of iron and nickel in the solutions no accurate results could be obtained.

The detection limit for 1 ml leach sample was 50 ppb for platinum and 25 ppb for palladium. As can be seen from tables B-2.23 - B-2.29, where the results of platinum and palladium analysis are given, in most of the samples the concentration of these metals is lower than the detection limits. For these samples no accurate analysis could be done. Where higher values of the detection limits than usual are reported in the tables, this is due to a smaller volume of sample being available for analysis. For earlier samples the detection limit, on a 1 ml sample, for palladium was 10 ppb. Deterioration of the palladium lamp later raised this to 25 ppb.

From the results obtained no conclusion can be drawn with respect to the effect of the different variables on the rate of leaching of platinum and palladium from pentlandite. What can be said is that no more than 4.5% of both platinum and palladium contained in pentlandite were dissolved under any experimental conditions and that the concentration of these metals in the leach solutions rose up to a maximum value before it started dropping again.

This tendency in the leaching of platinum and palladium was derived from the results of some analyses where the concentration of the metals was higher than the detection limits and therefore could be determined with higher accuracy (e.g. the results from table B-2.25 for platinum and from tables B-2.26, B-2.27 and B-2.29 for palladium show such a tendency).

Hougen and Zachariasen (166), who studied the recovery of precious metals from a nickel-copper concentrate by chloride leaching, found hat the platinum group metals do not pass into solution below a certain value of redox-potential, and this is much higher than that above which nickel and copper pass into solution. So when the redox-potential of the solution is kept between these two values copper and nickel dissolve while the precious metals are substantially kept out of solution, either because they are not dissolved, or because they are re-precipitated as sulphides.

In the present study the behaviour of platinum and palladium can be explained by considering that at the beginning of the dissolution the redox-potential of the solution is high enough to permit dissolution of precious metals, but as the ferric ions are reduced to ferrous and the redox-potential of the solution decreases, the conditions become unfavourable for precious metals, which start re-precipitating as sulphides.

4.8 PROPOSED MECHANISM FOR THE DISSOLUTION OF PENTLANDITE AND DISCUSSION

From the kinetic results obtained from the dissolution of pentlandite so far, a description of the mechanism controlling the dissolution can be given.

As was proved from the study of the effect of the variables on the rate of leaching and the value of the apparent activation energy derived from the study of the effect of temperature there was not, at any stage of the reaction, only a single rate determining mechanism occurring; the dissolution was controlled by a mixed regime of a chemical reaction and a transport controlled mechanism. The importance of each of these two factors on the rate of the dissolution changed during the experiments.

At the beginning of the dissolution a chemical reaction, probably the reaction of pentlandite with the ferric chloride was the main rate determinin mechanism. As pentlandite dissolves to produce soluble salts of the metals and elemental sulphur, the latter is not transported away from the particles, but forms a layer through which the nickel and iron salts diffuse outwards, while the ferric ions diffuse inwards to react with the unreacted pentlandite. So at any moment the particles consist of a sulphide core surrounded by a sulphur envelope.

In the first stages of dissolution when the sulphur layer is thin and therefore the resistance which it causes to the diffusion of the oxidant through it is small, the influence of the chemical reaction on the rate of reaction is greater; as dissolution proceeds the dimension of the sulphur layer surrounding the particles increase, the resistance to the diffusion of the ferric ions increases and so the dissolution becomes more transport-controlled.

The experimental results fit very well the proposed mechanism.

Temperature had a great effect on the rate of leaching because it affects both the mechanisms controlling the dissolution. The greater effect of the temperature on the rate of dissolution at the beginning of the experiments is due to the fact that temperature influences a chemical reaction more than it influences a diffusion controlled mechanism.

The opposite situation can be seen in the study of the effect of particle size. Although a reduction in the particle size favours both the mechanisms, the chemical reaction because it increases the total active surface of the particles and the diffusion process because it decreases the diffusion distances, the diffusion controlled mechanism is more affected and this is translated into a greater increase of the rate in the last stage of the reaction, with a decrease in the particle size, as can be seen in figure (52).

Changes in the concentration of the oxidant do not effect a chemically controlled mechanism, provided that there is sufficient initial concentration, while they have a substantial effect on a transport controlled mechanism. Thus, the ferric ion concentration did not have any effect on the rate of leaching until about 20% of nickel was dissolved, while as the dissolution proceeded and the diffusion controlled mechanism participated more in determining the rate of the reaction, the ferric ion concentration became an important factor.

The small effect of the stirring speed on the rate of leaching can be explained from the fact that it affects only the part of the dissolution reaction which is transport controlled. It also provides a proof that the transport controlled mechanism is the diffusion of the ferric chloride through the sulphur layer and not the diffusion of one of the soluble products outwards, because in this case the rate of the dissolution would not be affected by the stirring speed.

In all the leaching experiments both elemental sulphur and sulphate were formed; since ferric ion will generally oxidise the sulphide to sulphur, a second oxidizing agent, such as oxygen must have been reacting:

$$8S^{2-} + 16Fe^{3+} = 16\ Fe^{2+} + 8S^{o} \quad (4.1a)$$

$$8S^{2-} + 16\tfrac{1}{2}O_2 + 2H^{+} = 8SO_4^{2-} + H_2O \quad (4.1b)$$

$$FeS + 2Fe^{3+} = 3Fe^{2+} + S^{o} \quad (4.2a)$$

$$FeS + 2\tfrac{1}{2}O_2 + 2H^{+} = Fe^{2+} + SO_4^{2-} + H_2O \quad (4.2b)$$

Reactions (4.1a) and (4.2a) are much more important than reactions (4.1b) and (4.2b) and this is confirmed by the low concentration of the sulphate in the leaching solutions and the small increase of its pH. The reactions (4.1b) and (4.2b) would cause a significant increase.

Kelt (59) studying the ferric chloride leaching of pentlandite calculated the ferrous:nickel ratio by measuring the emf of the solutions. She found that this ratio was between 3 and 4 for most of the experiments. She suggested that if the dissolution of pentlandite occurred only according to reaction (4.1a), there would be a constant Fe^{2+}/Ni^{2+} ratio of 5.

If the ferric ions were to oxidise the sulphide to sulphate, the following reaction would occur:

$$8S^{2-} + 64Fe^{3+} + 32OH^{-} = 64Fe^{2+} + 8SO_4^{2-} + 32H^{+} \quad (4.3)$$

Such a reaction would cause a very large change in the pH of the solution and also in the ferric:ferrous ratio; however neither of these were observed.

In the experiments in which the ferric ions were exhausted but a large amount of sulphide had not been oxidised, the dissolution according

to reactions (4.1b) and (4.2b) continued slowly, independent of the ferric concentration. A re-oxidation of ferrous to ferric according to the reaction:

$$4Fe^{2+} + 4H^{+} + O_2 = 4F^{3+} + 2H_2O \qquad (4.4)$$

might also cause a low ferrous to nickel ratio in the solution.

From the x-ray diffraction analysis of the leach residues it was observed that pyrrhotite is preferentially dissolved compared to pentlandite. This trend is higher at low temperatures and it decreased as temperature increased and as the leaching proceeded.

In the case of the experiment run in the absence of ferric ions (section 4.1.3) the amount of sulphur detected in the forms of elemental sulphur and sulphate was less than the total amount of sulphur extracted from the sulphide. So it was concluded that the rest of sulphur was lost as hydrogen sulphide, while the existence of elemental sulphur and sulphate in small amount can be attributed to the oxidising effect of the oxygen dissolved in the solution.

An experiment was carried out in the absence of ferric chloride under nitrogen atmosphere. The nitrogen gas was provided above the solution through the condenser and the flow of the gas was fixed so that the nitrogen gas pressure was slightly higher than the atmospheric pressure. The experiment was run at 80°C with 1 gm sample of -125 + 90 microns particle size and a stirring speed of 1000 rpm. The results obtained are shown in fig (61) and table B-2.20. In this experiment evolution of hydrogen sulphide was noticed from the beginning of the reaction, while no elemental sulphur or sulphate was found in the residue. The following reaction corresponds to the direct dissolution of pentlandite in hydrochloric acid in the absence of oxygen:

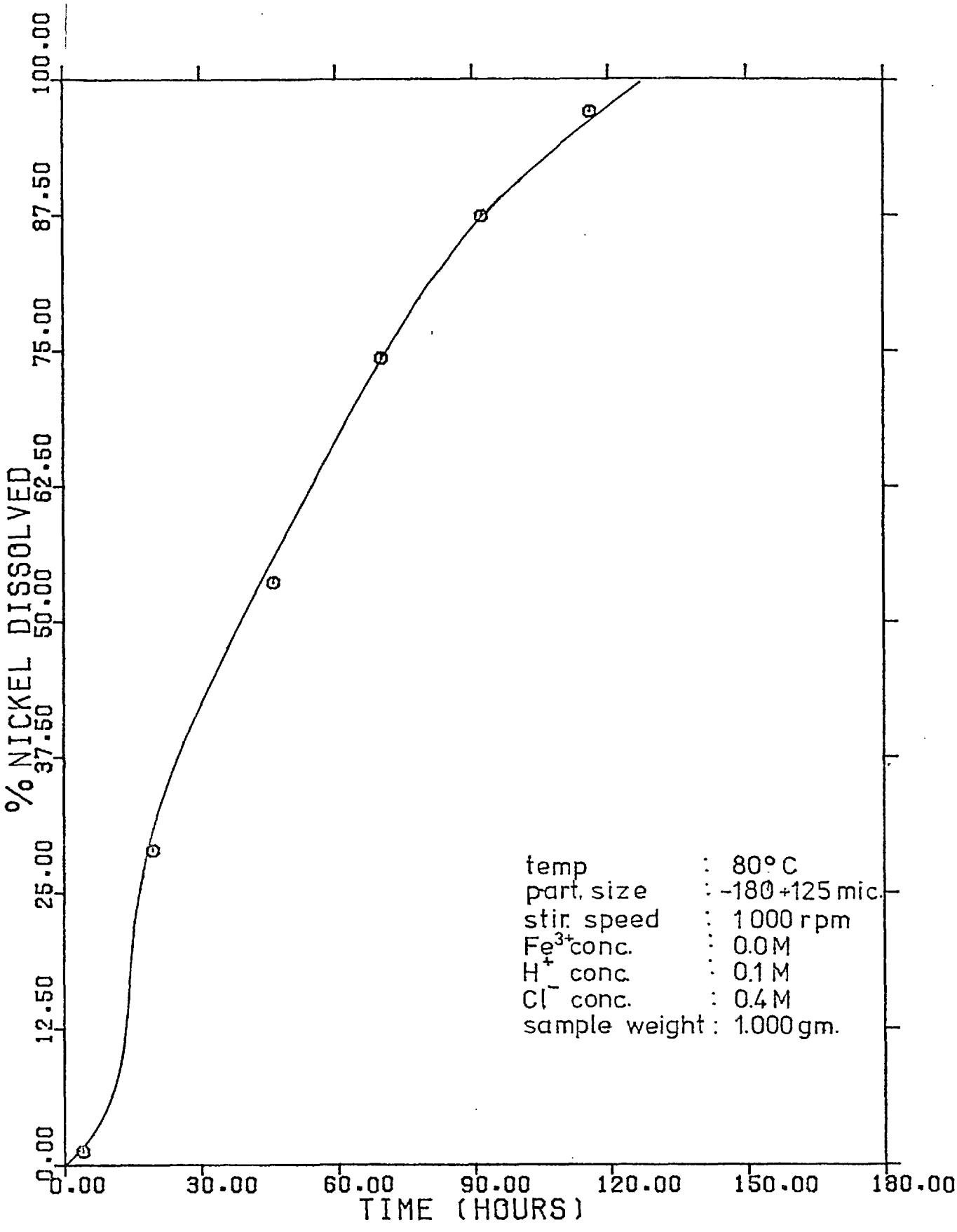

FIG. 61 Kinetic Curve for Leaching of Pentlandite under Nitrogen Atmosphere

$$(Fe,Ni)_9S_8 + 16H^+ + 18Cl^- = 4\tfrac{1}{2}FeCl_2 + 4\tfrac{1}{2}NiCl_2 + 8H_2S \qquad (4.5)$$

As can be seen, this reaction is accompanied by a high consumption of hydrogen ions resulting in the rising of the pH. Measurements of the pH during this experiment showed an increase of the pH from 1.16 in the original solution to 1.63 in the final.

The high rate of nickel dissolution observed during this experiment in the absence of any oxidising agent, is probably due to the non formation of a sulphur layer around the particles, which had an unfavourable effect on the rate of the ferric chloride leaching of pentlandite.

In order to investigate the sulphate formation under different experimental conditions, the following experiment was run. The experiment started with a 0.1M ferric chloride solution. The solution was heated under nitrogen atmosphere and when the temperature stabilized at 80°C, a 1 gram pentlandite sample of -125 + 90 microns particle size was added. The pentlandite was leached under a nitrogen atmosphere for 9 hours and then the stream of nitrogen was stopped and the experiment was continued under atmospheric air. After 22 hours of leaching 10 mls of H_2O_2 (20 vol.) were added and another 10 mls of H_2O_2 were added after 48 hours of leaching.

Figures (62) and (63) and table B-2.21 give the results of this experiment. As can be seen the presence of oxygen and the addition of hydrogen peroxide favoured both the rate of dissolution of nickel and the formation of sulphate.

The effect of chloride concentration was studied in an experiment where the chloride concentration of the solution was increased by the addition of sodium chloride, while the other conditions of the experiment were the

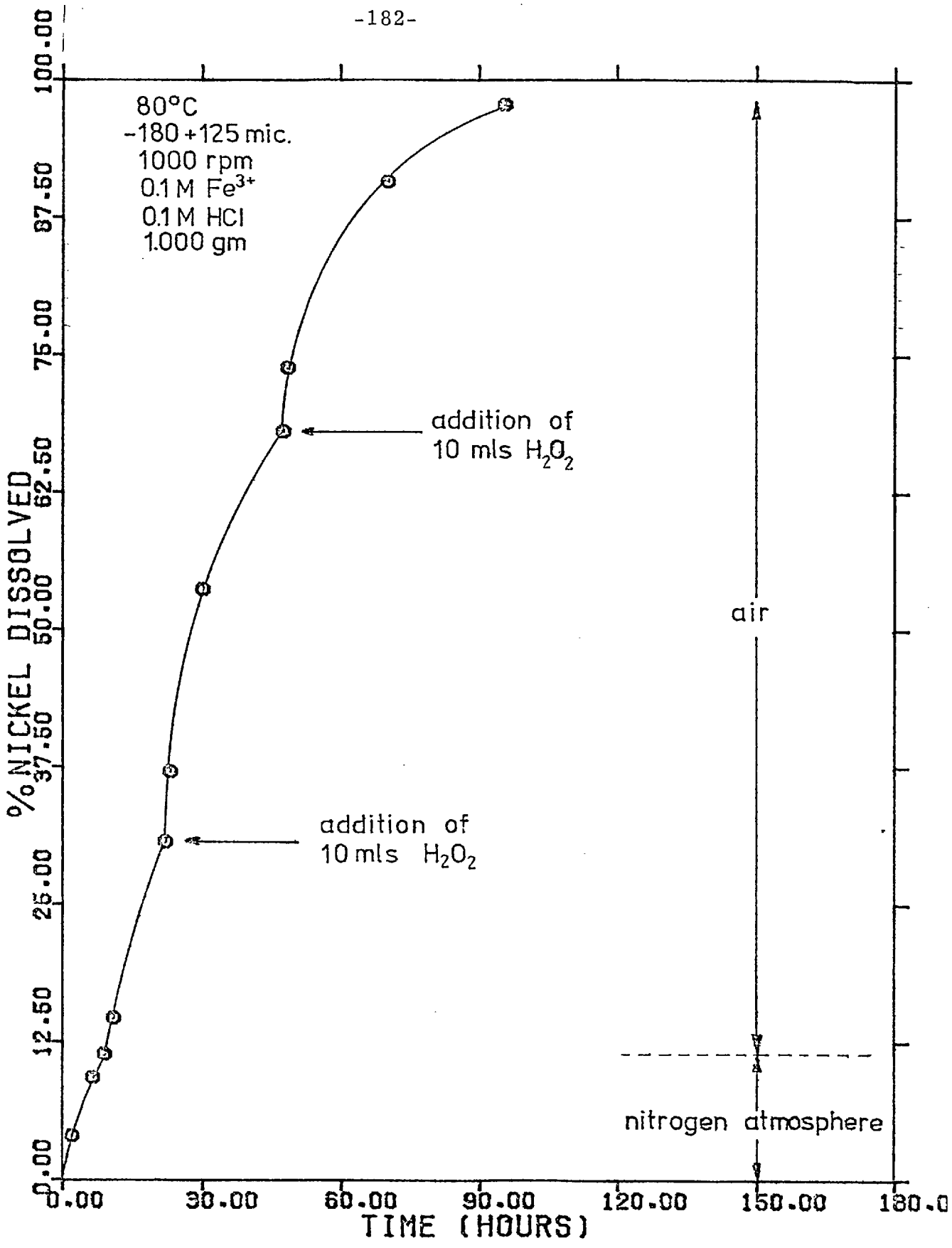

FIG. 62 Kinetic Curve Obtained from Leaching of Pentlandite with Different Oxidants (for Conditions see in the text)

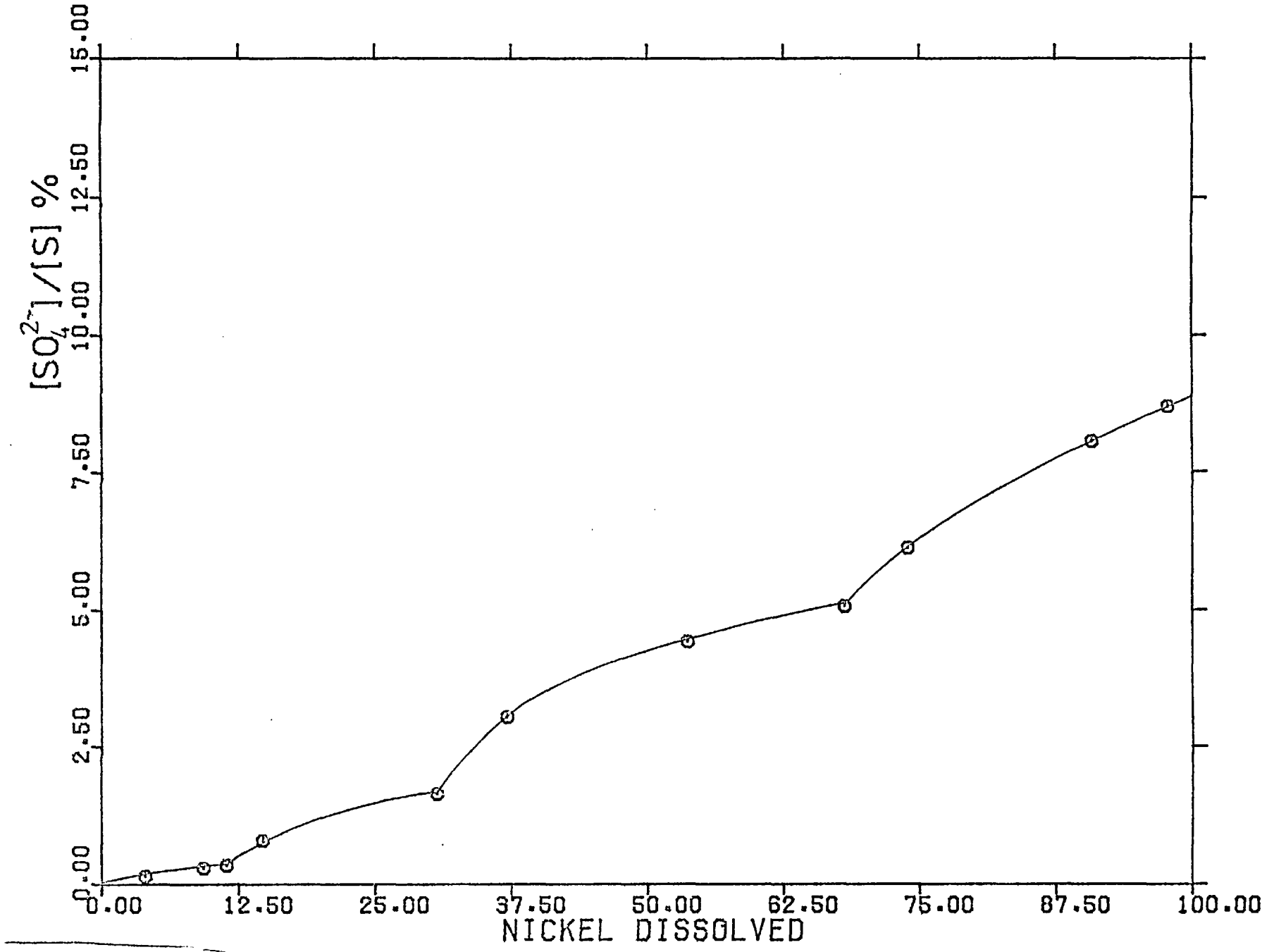

FIG. 63 Sulphate Analysis of Leach Samples of Pentlandite Dissolved with Different Oxidants (for conditions see in the text)

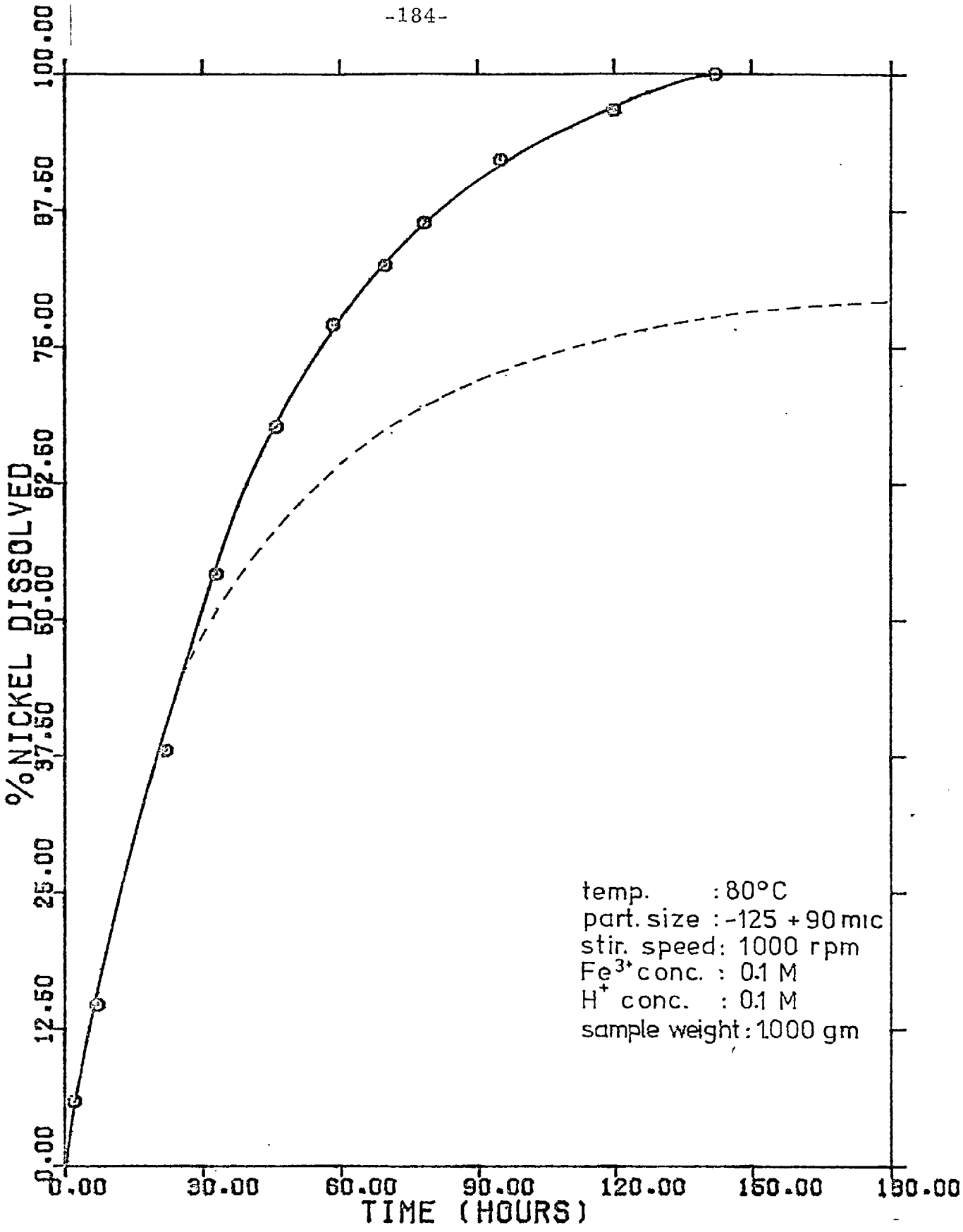

FIG. 64 Effect of Chloride Concentration on the Rate of Leaching of Pentlandite

Continuous line: 0.6M Cl^-

Dashed line: 0.4M Cl^-

most common ones. As can be seen from figure (64) and table B-2.22 the increase in the chloride concentration had a favourable effect on the rate of the reaction.

Hydrolysis of the ferric ions, especially in experiments run at high temperatures, led to the precipitation of hematite, which was detected in some of the residues by the x-ray diffraction analysis:

$$2Fe^{3+} + 4H_2O = Fe_2O_3H_2O + 6H^+ \qquad (4.6)$$

The complete leaching of metals from pentlandite containing platinum and palladium depends on the redox-potential of the solution. When a minimum value of redox-potential is not met in the solution for each of the metals, this metal will not dissolved or re-precipitate.

At the beginning of the experiment the redox-potential of the solution was high enough for all the metals to start dissolving. But as the experiment proceeded and the redox-potential of the solution decreased because of the reduction of the ferric ions, the minimum conditions of redox-potential for platinum and palladium to remain in solution were no longer met and thus these metals started precipitating as sulphides.

CHAPTER 5

COMPARISON WITH OTHER WORK

The present study confirmed that both monosulphide solid solution of iron and nickel and pentlandite dissolve in ferric chloride solutions, without the formation of any intermediate phase. Elemental sulphur and sulphate are formed in quantities depending upon the conditions of the experiment.

Choppin and Faulkenberry (2) studied the oxidation of aqueous sulphide solution by hypochlorites. They found that high sulphide concentration increase the formation of sulphur, while high hypochlorite concentrations and high temperatures increase the formation of sulphate. These results are in good agreement with the results of the present study.

Khudyakov and Yaroslavtsev (12) suggested that in the oxidative leaching of nickel mattes, the oxidation of the sulphur of the sulphides takes place step-waise. In the present work it was difficult to determine whether the formation of sulphate was due to the straight forward oxidation of the sulphide sulphur to sulphate by the oxygen dissolved in the solution, or to the step-wise oxidation of the elemental sulphur formed. This is because of the very low concentration of the intermediate oxidation products between sulphur and sulphate if indeed there were any.

Dobrokhotov (13) showed that nickel sulphides do not dissolve in sulphuric acid in the absence of air, while iron sulphides dissolve. In the presence of oxygen the ferrous sulphate is oxidised to ferric sulphate, which leads to the oxidative dissolution of nickel sulphides and the formation of sulphur and sulphate, according to the reactions (1.11), (1.12), (1.13) and (1.14), (Section 1.1.1). In the present study the ferric ions cause the

oxidation of the sulphide sulphur to elemental sulphur but the formation of the sulphate is due to the oxygen dissolved in the solution, and not to the effect of ferric ions.

Dobrokhotov suggested that, as also happened in the present work, high sulphide concentrations favour the formation of sulphur, while low sulphide concentration the formation of sulphate.

Dobrokhotov and Maiorova (19) studied the autoclave leaching of a cobalt-nickel matte. They found, in agreement with the results of the present work, that an increase in the acidity favours the formation of elemental sulphur. They also found that an increase in the acidity brought an increase in the rate of nickel and cobalt extraction. In the present work the increase of the acidity had an unfavourable effect in the rate of leaching of nickel from pentlandite in the beginning of the dissolution, but as the leaching proceeded the rate and the amount of nickel extracted increased.

The activation energy for the autoclave leaching of a cobalt-nickel matte calculated by Dobrokhotov and Mairova was indicative of a diffusion controlled mechanism, while in the present work the rate determining factor in the ferric chloride leaching of nickel sulphides was a mixed mechanism of a chemical reaction and a diffusion controlled process.

Jackson and Strickland (30) who studied the reaction between acid chlorine water and the most common sulphide minerals found that, with the exception of galena, the kinetics were transport-controlled. This is not in agreement with the results of the ferric chloride leaching of the iron-nickel sulphides of the present work where the dissolution was not entirely transport-controlled. They also found that the two iron minerals FeS and

FeS_2 gave only sulphate, while the Mss in the present work gave both elemental sulphur and sulphate as end-products.

Sericov and Orlova (31) leached nickel sulphide with cupric and ferric chloride. With cupric chloride 94% of the nickel was extracted after two hours at 130°C while with ferric chloride the same amount of nickel was extracted in the same time at 150°C; in the present work 100% of the nickel in the Mss extracted at 100°C after 75 hours and 95% of the nickel in pentlandite extracted after 164 hours at 90°C.

Tseft and Kryukova (34) found that by leaching nickel mattes with ferric chloride, the nickel was readily extracted in 0.5M ferric chloride at the boiling point of the solution with almost all the sulphur in the elemental form (less than 2% as sulphate). In the present study the amount of sulphate formed in the solution represented more than 2% of the total amount of sulphur, but this was due to the fact that the ferric concentrations used were always less than 0.5M.

Klets and Sericov (35) studied the autoclave and non autoclave leaching of sulphide complex ore with ferric chloride. They found that temperature was the main factor controlling the leaching rate, which is in agreement with the results of the present investigation, and that the amount of oxidant does not play an essential role in the rate of dissolution, which also fits the results obtained in the present work for the first stage of the dissolution of both Mss and pentlandite.

Tseft and Sericov (36) suggested that the dependence of the dissolution rate of sulphides of certain metals was more complex than purely diffusion or kinetic leaching and this is in agreement with the proposed mechanism occurring during the ferric chloride leaching of Mss and pentlandite.

Bjorling and Kolta (47) studied the wet oxidation of iron sulphide concentrates catalysed by nitric acid. They found that the oxidation of the sulphides is not dependent on high temperatures and this is not in agreement with respect to the effect of temperature on the rate of leaching in the present work. They calculated an activation energy of 20.90 Kcal/mole which is higher than that calculated for the ferric chloride leaching of the iron-nickel sulphides in the present study. An increase of the pH had an unfavourable effect on the formation of sulphate, which agrees with the results of the effect of the acidity on the sulphate formation in the leaching pentlandite.

Leaching of pentlandite in the present work with hydrochloric acid in the absence of ferric chloride resulted in the evolution of hydrogen sulphide. This is in agreement with the results obtained by Ingraham et al (41) and Van Weert et al (44). Ingraham et al,suggested that troïlite was leached in HCl in the absence of oxidant with formation only of hydrogen sulphide, while non-stoichiometric pyrrhotite dissolved with the formation of elemental sulphur and hydrogen sulphide. Van Weert et al,found that in hydrochloric acid pyrrhotite dissolves completely with only 10-50% excess of HCl, while pentlandite remains insoluble. In the present work, it was found that although pyrrhotite was dissolving faster than pentlandite, the latter was also soluble in hydrochloric acid.

There is a very little agreement among the results obtained for the leaching of pentlandite in nature, the ammoniacal leaching of pentlandite and the ferric chloride leaching of pentlandite of the present study.

Pentlandite when oxidised in nature is replaced by violarite. This replacement takes place with the loss of metal, the iron being lost more rapidly than the nickel. In HCl, the rate of dissolution of iron is more rapid

than that of nickel, but such a behaviour was not noticed in the ferric chloride leaching, where the rates of dissolution for both metals were similar. In the case of natural leaching of pentlandite the produced violarite has the same sulphur content aspentlandite; in the ferric leaching of pentlandite, the sulphide is converted to orthorhombic sulphur and sulphate. Finally, it is certain, that the oxidation of pentlandite by natural means takes place by electrochemical means, but the electrochemical corrosion is not important in the dissolution of pentlandite by ferric chloride.

In the ammoniacal leaching of pentlandite, nickel passes into the solution as a soluble ammine, while iron forms a ferric oxide envelope around the unreacted core of pentlandite. Sulphur finally is oxidised to $(NH_4)_2SO_4$. In the ferric chloride leaching of pentlandite both iron and nickel dissolve as chloride salts, the major part of the sulphide sulphur is oxidised to elemental sulphur forming a layer around the particles of pentlandite, while the rest of the sulphur is oxidised to sulphate.

Klets et al (67) studied the behaviour of pentlandite during the leaching of a pentlandite-pyrrhotite concentrate with ferric chloride. Although there is some agreement between their results and the results of the present study (e. g. formation of a sulphur layer around the particles) it is difficult to compare the leaching of pentlandite in this work with the leaching of pentlandite-pyrrhotite concentrates. Thus a precipitation of nickel by the iron sulphide has been reported in their results, while such a precipitation was not observed in this work. Probably this was due to the very small amount of pyrrhotite in the iron-nickel sulphide of this work, although pyrrhotite was preferentially dissolved compared to pentlandite.

Shneerson et al (68) reached the same results for the role of pyrrhotite in the oxidative leaching of sulphides. The higher the pyrrhotite

content the lower the leaching rate is due to the inhibitive action of pyrrhotite. They also suggested that the cause of the more rapid oxidation of pentlandite compared with millerite is the lattice structure of pentlandite, in which iron and nickel isomorphously replace each other. Owing to the more rapid oxidation of iron sulphides, the lattice becomes porous and the surface strongly increases and becomes activated, as a result of which nickel sulphide oxidises more rapidly. But there is no evidence that pentlandite is related to the monosulphide solid solution or iron and nickel and this theory is invalidated by the structure of pentlandite. In pentlandite, there is no observable ordering of the metal atoms, and some evidence has been put forward to confirm the theory that pentlandite is stabilized by a particular electron to atom ratio (151).

The results of this work are in good agreement with the results obtained by Dutrizac and MacDonald (76) for the percolation leaching of pentlandite with 0.1M $Fe_2(SO_4)_3$ solutions. They found that temperature had a favourable effect on the rate of leaching and that the rate decreased after a certain amount of nickel was dissolved due either to the unavailability of the nickel ore minerals or the formation of impermeable sulphur or jarosite coating on the minerals. They calculated the apparent activation energy for the dissolution of nickel to be 9 Kcal/mole and that this was constant throughout the whole of the dissolution. This is in very good agreement with the value of 7-11 Kcal/mole calculated from the results of the present work. In the leaching in the absence of bacteria only elemental sulphur was observed, while in the present study both elemental sulphur and sulphate were detected. This indicates that in the apparatus used for their leaching experiments (long columns of mixed ore) oxygen was inaccessible to the ore.

The results of the present work agree well with the experimental results obtained by Kelt (59) for the ferric chloride leaching of pentlandite.

The study of the effect of temperature on the rate of leaching by Kelt gave very similar results to those of the present work. The values of the activation energy varied between 16 and 11 Kcal/mole and they are in agreement with those calculated in this work. She suggested that pentlandite was dissolved according to the following reaction:

$$(Fe,Ni)_9S_8 + 18Fe^{3+} = 22.5Fe^{2+} + 4.5Ni^{2+} + S^o$$

where 18 ferric ions were needed to oxidise one molecule of pentlandite. In the present work, it is believed that 16 ferric ions are needed to oxidise one molecule of pentlandite, because as was proved from the study of the crystal structure of pentlandite (151), the metals in the lattice of pentlandite are in the ionic form and therefore the ferric ions are necessary to oxidise only S^{2-} to S^o.

CHAPTER 6

CONCLUSIONS

6.1 SUMMARY OF THE RESULTS

6.1.1 Leaching of Monosulphide Solid Solution of Iron and Nickel

Monosulphide solid solution of iron and nickel (Mss) was synthesized containing 25 wt % Ni and the x-ray powder pattern obtained was similar to that of Shewman and Clark (115). Mss was homogeneous with no apparent variation of composition under the electron probe.

The leaching of Mss with acidic ferric chloride solution proceeded in a single stage process indicating a uniform process taking place during the dissolution of Mss. The apparent activation energy was indicative of a reaction rate controlled by a mixed mechanism, where a chemical reaction was the most important factor. No new iron-nickel phases were formed. The rate of dissolution of nickel was higher than that of iron. A porous layer consisting of elemental sulphur and a small amount of iron sulphide was formed around a core of Mss. From the variables studied temperature and ferric concentration had the greatest effect on the rate of leaching.

Both elemental sulphur and sulphate were detected as end-products in all the leaching experiments and the amount of each formed depended on the conditions of the experiment.

Ferric ions generally caused the oxidation of the sulphide sulphur to elemental sulphur, while the formation of sulphate was due to the effect of oxygen dissolved in the solution.

6.1.2 Leaching of Pentlandite

Pentlandite was synthesized containing 0.25% platinum and 0.25% palladium. Platinum was found to be in the elemental form, forming

discrete crystals in the mass of pentlandite, while palladium formed a solid solution with pentlandite. The synthesized pentlandite contained also a small amount of pyrrhotite.

The dissolution of pentlandite in acid ferric chloride solutions occurred in two stages. The leaching rate of the first stage was faster than that of the second stage and this is connected with an increasing thickness of a sulphur layer formed around the particles of pentlandite during leaching. The apparent activation energy calculated for the two stages indicated a process controlled by a mixed mechanism, the oxidation of the sulphide sulphur to elemental sulphur and the diffusion of ferric ions through the sulphur layer.

The importance of these two factors is different in each of the two stages. The chemical reaction is the main rate determining factor in the first stage and the diffusion mechanism in the second stage.

Pentlandite was leached rapidly with dissolution of iron and nickel and the formation of sulphur and sulphate. No new phases, apart from the orthorhombic sulphur, were detected in the leach residues. The rate of dissolution of both iron and nickel from pentlandite were similar. Pyrrhotite dissolved faster than pentlandite, especially at low temperatures.

Sulphate was produced in all the leaching experiments except one run under nitrogen atmosphere in the absence of ferric ions, where all the sulphur in the sulphide formed hydrogen sulphide. High temperatures and high stirring speeds favoured the formation of sulphate, while high ferric concentrations, high sulphide concentrations and high acidities favoured the formation of sulphur.

Only a very small amount (about 4.5%) of platinum and palladium contained in pentlandite passed into solution, the rest remained in the solid residue. At the beginning of the experiment these two metals were dissolving slowly, but as the redox-potential of the solution decreased these metals started re-precipitating as sulphides.

APPENDIX A

POTENTIAL - pH DIAGRAMS FOR THE Fe-H_2O-Cl SYSTEM AT ELEVATED TEMPERATURES

A-1 INTRODUCTION

It is particularly appropriate to discuss solution-solid equilibria in terms of Eh-pH (Pourbaix) diagrams, because they provide, a very useful and easily understandable means of summarizing a large amount of thermodynamic data relating to hydrolysis and redox reactions. These diagrams have been used (167), (168) for describing hydrometallurgical systems, although the first extensive use of such diagrams was made by M. Pourbaix (169) for describing the thermodynamics of metallic corrosion. Garrels and Christ (170) found such diagrams useful in describing the thermodynamics of aqueous systems from which minerals form geologically. Burkin (163) has studied the thermodynamics of sulphide leaching using such diagrams.

The Eh-pH diagram primarily describes the solution composition or solid phase stability as a function of two variables - single electrode potential and pH. Such diagrams are drawn with all the other variables fixed by the choice of the investigator.

Most of the available diagrams have been calculated for $25^{o}C$, although some higher temperature diagrams have been presented recently (171)-(185) and (164).

In the present work the system $Fe-H_2O-Cl$ has been studied at different temperatures up to and including $150^{o}C$. The main interest of this study lies in the correlation of this system with the leaching of iron-nickel sulphide ores in acidified solutions of ferric chloride.

Several methods of extrapolation have been used in order to obtain the required thermodynamic data at elevated temperatures. These methods, all of which employ semi-empirical assumptions are described in the following sections.

Since some of the reactions which describe the solution composition of the system $Fe-H_2O-Cl$ do not involve either H^+ or OH^- or electron transfer, a new technique has been developed which combines the component parts $Fe-H_2O$ and $Fe-Cl$.

A-2 POTENTIAL -pH DIAGRAMS

A-2.1 Eh-pH Relationship at Elevated Temperatures

The lines on an Eh-pH diagram are computed from equilibria of the form:

$$aA + xH^{+} + ze^{-} = bB + cH_2O \qquad (A\text{-}1)$$

for which the half-cell single electrode potential at a temperature T is given by the Nerst equation:

$$Eh_T = Eh^{o}_T - \frac{RT}{ZF} \ln \frac{(a_B)^b \ (a_{H_2O})^c}{(a_A)^a \ (a_{H^+})^x} \qquad (A\text{-}2)$$

where Eh^{o}_T is the standard half-cell potential and (a_A), (a_B), (a_{H_2O}), (a_{H^+}), the activities of the respective species.

Assuming $(a_{H_2O}) = 1$, defining $pH_T = -\log (a_{H^+})$ and given that the Gibbs standard free energy change and the standard electrode potential are related by

$$Eh^{o}_T = \frac{\Delta G^{o}_T}{zF} \qquad (A\text{-}3)$$

equation (A-2) simplifies further, to the form:

$$Eh_T = -\frac{\Delta G^{o}_T}{zF} - 2.303 \frac{RTx}{zF} pH_T - 2.303 \frac{RT}{zF} \log \frac{(a_b)^b}{(a_A)^a} \qquad (A\text{-}4)$$

The above equation expresses the relationship between Eh and pH at a given temperature $T^{o}K$. In order to plot this equation on a Eh-pH diagram it is necessary to select fixed values for (a_B) and (a_A) so that

the final term is constant in value. Then a diagonal line is obtained with $-\frac{\Delta G^o}{zF}$ as the intersept (at pH = 0) and the slope is $2.303\frac{RTx}{zF}$.

When x = 0 the line is horizontal and when z = 0 the line is vertical. However, in the latter case, equation (A-4) is unsuitable for determining the position of the line and so the following equations are used instead:

$$\Delta G^o_T = -R.T.\ln \frac{(a_B)^b}{(a_A)^a (a_{H^+})^x} \qquad (A-5)$$

$$\Delta G = -2.303\, RTxpH_T - 2.303RT \log \frac{(a_B)^b}{(a_A)^a} \qquad (A-6)$$

Then the pH value at which the vertical line is placed is at:

$$pH_T = -\frac{1}{x}\left(\frac{\Delta G^o_T}{2.303RT} + \log \frac{(a_B)^b}{(a_A)^a}\right) \qquad (A-7)$$

The two half-cell reactions

$$2H^+ + 2e^- = H_2 \qquad (A-8)$$

$$O_2 + 4H^+ + 4e^- = 2H_2O \qquad (A-9)$$

are very important in the study of Eh-pH diagrams, because they express the stability of water under reducing and oxidizing conditions respectively.

The equation (A-4) written for the reactions (A-8) and (A-9) gives:

$$Eh_T(8) = Eh^o_T(8) - 2.303\frac{RT}{F}pH_T - 2.303\frac{RT}{2F}\log P_{H_2} \quad (A\text{-}10)$$

$$Eh_T(9) = Eh^o_T(9) - 2.303\frac{RT}{F}pH_T + 2.303\frac{RT}{4F}\log P_{O_2} \quad (A\text{-}11)$$

When the partial pressures $P_{H_2} = P_{O_2} = 1$ atm, equations (A-10) and (A-11) determine the limits of the thermodynamic stability of water under the standard-state conditions and are drawn as lines (a) and (b) respectively on Eh-pH diagrams.

A-2.2 Calculation of ΔG_T at Elevated Temperatures

For the calculations of ΔG^o_T the following reactions were used:

$$\Delta G^o_{T_I} = \Delta H^o_{T_1} - T_1\Delta S^o_{T_1} \quad (A\text{-}12)$$

$$\Delta H^o_{T_1} = \Delta H^o_{T_o} + \int_{T_o}^{T_1} \Delta C^o_p\, dT \quad (A\text{-}13)$$

$$\Delta S^o_{T_1} = \Delta S^o_{T_o} + \int_{T_o}^{T_1} \Delta C_p\, d(\ln T) \quad (A\text{-}14)$$

where T_o is the reference temperature.

The combination of these reactions gives:

$$(\Delta G) = \Delta G^o_{T_1} - \Delta G^o_{T_o} = -\Delta S^o_{T_o}(T_1 - T_o) + \int_{T_o}^{T_1} \Delta C_p^{\,o}\, dT - T_1\int_{T_o}^{T_1} \Delta C_p^{\,o}\, d(\ln T) \quad (A\text{-}15)$$

Thus, a knowledge of the variation in free energy with temperature is equivalent to knowing the $\Delta G^o_{T_o}$, $\Delta S^o_{T_o}$ and ΔC_p. Since $\Delta G^o_{T_o,f}$ and $\Delta S^o_{T_o,f}$ for individual species are normally known or can be reliably

calculated even for ions at 25°C, T_o is normally chosen as 298°K; consequently ΔG^o_T and ΔS^o_T may be easily calculated. So, from equation (A-15) knowing the temperature dependence of ΔC^o_p between T_o and T_1, $\Delta G^o_{T_1}$ is readily evaluated.

A-2.3 Assumptions used concerning the Temperature Dependence

If for a reaction it is assumed that the heat capacity

$$\Delta C^o_p = k$$

where k is a constant independent of temperature, equation (A-15) simplifies to the form.

$$\Delta(\Delta G) = \Delta G^o_{T_1} - \Delta G^o_{T_o} = -\Delta S^o_{T_o}(T_1 - T_o) + k(T_1 - T_o - T_1 \ln \frac{T_1}{T_o}) \qquad \text{(A-16)}$$

But this assumption is not very accurate, especially for non-ionic species. Having made this assumption there are two choices for k:

1(i) $\quad k = \Delta C^o_p, 298$

1(ii) $\quad k = \Delta C^o_p \Big]^{T_1}_{T_o}$

The first assumption which is less accurate than the second has been used and discussed by Helgeson (186).

In the second assumption k is taken as the average value of ΔC^o_p between the two temperatures. This may be derived from the equation:

$$dS = C_p d(\ln T)$$

By integration of this equation, assuming the definition above and converting to standard state function it follows that:

$$\int_{T_o}^{T} ds^o = C_p^o \Big]_{T_o}^{T_1} \int_{T_o}^{T_1} d(\ln T)$$

and therefore:

$$C_p^{\,o} \Big]_{T_o}^{T_1} = \frac{S^o_{T_1} - S^o_{T_o}}{\ln\ T_1/T_o} \qquad \text{(A-17)}$$

Thus, $C_p^{\,o} \Big]_{T_o}^{T_1}$ is defined in terms of entropy, without requiring any knowledge of Cp^o at 25°C.

Another empirical relationship proposed by Harned and Owen (187) is the following:

$$1(iii) \qquad \Delta C_p^o = -2cT$$

which means that ΔC_p^o is directly proportional to the absolute temperature. The coefficient has been chosen -2c only for convenience.

By replacement in equation (A-15) it follows:

$$\Delta(\Delta G) = -\Delta S^o_{T_o}(T_1 - T_o) + c(T_1 - T_o)^2 \qquad \text{(A-18)}$$

and also

$$\Delta H^o_T = a - cT \qquad \text{(A-19)}$$

$$\Delta S^o_T = d - 2cT \qquad \text{(A-20)}$$

$$\Delta G^o_T = a - dT + cT^2 \qquad \text{(A-21)}$$

Solving equations (A-19) (A-20) and (A-21) for a, c and d:

$$a = \frac{-2\Delta H^{o}_{T} - T\Delta C^{o}_{p,T}}{2} \qquad \text{(A-22)}$$

$$d = \Delta S^{o}_{T} - \Delta C^{o}_{p,T} \qquad \text{(A-23)}$$

$$c = \frac{\Delta C^{o}_{p,T}}{2T} \qquad \text{(A-24)}$$

where T is usually chosen to be $298^{o}K$. Thus, from equations (A-22), (A-23) and (A-24) a, b and c may be evaluated if $\Delta C^{o}_{p,298}$, ΔH^{o}_{298} and ΔS^{o}_{298} are known and therefore ΔG^{o}_{T} is given as a function of temperature from equation (A-21).

Several workers (187) - (189) have tested telationship (1(iii)) and in most cases agreement between predicted and experimental data was quite good.

A-2.4 Standard States

The values of the thermodynamic properties, tabulated for the individual ions in aqueous solution, are based on the usual convention that the values of ΔH^{o}_{f}, ΔG^{o}_{f}, $\bar{S}^{o}$ and C^{o}_{p} for H^{+} (aq, std. state, m = 1) are zero. It is also the normal convention to define ΔG^{o}_{298} and ΔH^{o}_{298} for the hydrogen half-cell reaction

$$2H^{+}(aq) + 2e^{-} = H_{2}(g) \qquad \text{(A-8)}$$

as zero, at all temperatures. By adopting the above convention the thermodynamic properties of electrons are ignored and it follows that the thermodynamic relation:

$$\Delta G_{T} = \Delta H_{T} - T\Delta S_{T} \qquad \text{(A-12)}$$

will not hold for any half-cell reaction.

In order to extrapolate Eh-pH diagrams to elevated temperatures, as it is not known how Eh^o for the hydrogen half-cell (A-8) varies with temperature, it is convenient to adopt an additional convention that Eh^o (and therefore ΔG^o) for reaction (A-8) is zero at all temperatures. Since equation (A-12) does not apply to half-cell reactions, it is possible to extrapolate ΔG^o_T for any such reaction by eliminating the electrons between the general half-cell reaction (A-1) and the hydrogen half-cell (A-8) to produce a full-cell reaction (A-25).

$$aA + (x-z)\,H^+ + \frac{z}{2}H_2 = bB + cH_2O \qquad \text{(A-25)}$$

ΔG^o_T for the full-cell reaction (A-25) may be extrapolated to any temperature using equation (A-15). Once ΔG^o_T for (A-8) has been defined to be zero at the elevated temperature Eh^o_T for (A-1) may be calculated.

We can obtain the same result, by extrapolating the free energies of the half-cell reactions themselves, although this method is less thermodynamically rigorous than that described above. Provided that the extrapolations are similarly carried out for reactions (A-1) and (A-8) to produce ΔG^o_T (A-1) (or Eh^o_T (A-1)) and ΔG^o_T (A-8) (or Eh^o_T (A-8)) respectively, the difference ΔG^o_T (A-1) - $\frac{z}{2}\Delta G^o_T$ (A-7) (or Eh^o_T (A-1) - Eh^o_T(A-8)) is then the free energy change for reaction (A-1) at temperature T with respect to the hydrogen-cell at the same temperature.

A-2.5 Thermodynamic Data

Most of the thermodynamic data for solids, liquids and gases were obtained from publications by the National Bureau of Standards (190) by JANAF (191) and by Barin and Knacke (192).

Many of the thermodynamic values of aqueous ions were obtained from tables by the National Bureau of Standards (190).

A-2.5.1 Estimation of Data at $25^{o}C$

Latimer (193), Lewis and Randall (194), JANAF(191), Barin and Knacke (192) describe several methods for estimating entropies of solid species. Methods for entropies of ionic species and for soluble neutral species are described by Latimer (193) and by Lewis and Randall (194).

A-2.5.2 Entropies at Elevated Temperatures

Criss and Cobble (195),(196) and Khodakovskiy (197) have established two empirical relationships between ionic entropies at $25^{o}C$ and entropies at elevated temperatures.

Criss and Cobble have introduced the correspondence principle. This principle shows that, if the standard state is chosen properly by fixing the entropy of $H^{+}(aq)$ at each temperature, then the ionic entropies at one temperature are linearly related to their corresponding entropies at $25^{o}C$. Their choice of standard state at $298^{o}K$ corresponded to an entropy for the hydrogen ion of -5.0 cal. $mole^{-1}$. $^{o}K^{-1}$ is in agreement with the values for the 'absolute' ionic entropy of $H^{+}(aq)$ suggested by other authors.

The Entropy Correspondence Principle can be described by the general realtionship:

$$\bar{S}^{o}_{T_1} = a_{T_1} + b_{T_1} \bar{S}^{o}_{298}\,(abs) \qquad (A\text{-}26)$$

where a_{T_1} and b_{T_1} are constants dependent on the class of ions (cations, anions, oxyanions, acidoxyanions) and on the temperature considered.

$\bar{S}^{o}_{298}$ (abs) is the partial molal entropy, at 298°k on an 'absolute' scale considering the above mentioned standard state at 298°k.

$$\bar{S}_{298}(\text{abs}) = \bar{S}_{298}\,(\text{conventional}) - 5.0z \qquad \text{(A-27)}$$

where z is the ionis charge.

Khodakovskiy (197) has found the following entropy correspondence relationship

$$\bar{S}^{o}_{T_1} = a_T - d_T|z| + c_T\bar{S}^{o}_{298} \qquad \text{(A-28)}$$

for both soluble ionic and neutral species, where a_T, c_T and d_T are constants dependent on temperature and the type of species (i.e. cations, oxygen free acids, their anions and dissolved gases, and oxygenated acids and their anions), z is the ionic charge, and $\bar{S}^{o}_{298}$ is the conventional partial molal entropy at 298°C i.e. choosing for ionic species, $\bar{S}^{o}_{H^+(aq)} = 0$ cal. deg^{-1}. $mole^{-1}$.

A-2.5.3 Heat Capacities at 25°C and Above

From equations (A-17) and (A-26) it may be seen that

$$\bar{C}^{o}_{p}\Big]^{T_1}_{298^o} = \frac{S^{o}_{T_1}(\text{abs}) - \bar{S}^{o}_{298}(\text{abs})}{\ln T_1/298^o} \qquad \text{(A-29)}$$

where $\bar{C}^{o}_{p}\Big]^{T_1}_{298}$ o is the average value of the partial molal heat capacity between 298^{o}k and T_1.

From equations (A-26) and (A-29) it follows that

$$\bar{C}_{p}{}^{o}\Big]^{T_1}_{298} = \frac{a_{T_1} - \bar{S}^{o}_{298}\,(1.000 - b_{T_1})}{\ln T_1/298^{o}} \qquad \text{(A-30)}$$

which can be written as

$$\bar{C}_{p}{}^{o}\Big]^{T_1}_{298} = a_{T_1} + \beta_{T_1}\,\bar{S}^{o}_{298}(\text{abs}) \qquad \text{(A-31)}$$

where $a_{T_1} = a_{T_1}/(\ln T_1/298)$ and $\beta_{T_1} = -(1.000 - b_{T_1})/(\ln T_1/298)$ are constants similar to a_T and b_T in equation (A-26).

Equation (A-31) suggests that, as the average heat capacity is taken over smaller and smaller temperature intervals, $\bar{C}_{p}{}^{o}\Big]^{T_1}_{T_o}$ will approach $\bar{C}^{o}_{p,298}$ at that mean temperature and

$$\bar{C}^{o}_{p,298}(\text{abs}) = A + B\,\bar{S}^{o}_{298}(\text{abs})$$

If the absolute entropy of H^{+}(aq) is plotted against temperature, the slope of the resulting curve at some temperature t is

$$\frac{d}{dt}\int_{t_1}^{t_2} d\bar{S}^{o}_{2} = \frac{d}{dt}\int_{t_1}^{t_2} \bar{C}^{o}_{p_2}\,\frac{dt}{T}$$

In the limit, as $t_1 \longrightarrow t_2$

$$\left(\frac{d\bar{S}^{o}_{2}}{dt}\right) T = \bar{C}^{o}_{p_2} \qquad \text{(A-32)}$$

$(\frac{dS}{dt})$ was evaluated from the previously assigned ionic entropies of $H^+(aq)$ as 0.0922 at 25°C, the 'absolute' ionic heat capacity of $H^+(aq)$ (from eq. (A-32) then becomes) 28 cal. $mole^{-1}$ deg^{-1}.

Thus

$$\bar{C}^o_p \text{ (abs)} = \bar{C}^o_p \text{ (conventional)} + 28z \qquad \text{(A-33)}$$

where z is the ionic charge.

Another similar equation has been given by Khodakovskiy (197)

$$\bar{C}^o_{p,298} = a - d|z| - \tfrac{2}{3}\bar{S}^o_{298} \qquad \text{(A-34)}$$

where a and d are constants dependent on the type of ion, $\bar{S}^o_{298}$ is the conventional entropy ($\bar{S}^o_{H^+(aq)} = O$) and $\bar{C}^o p$ is such that $\bar{C}^o p$ for $H^+(aq)$ is 21 cal. deg^{-1} $mole^{-1}$.

A-2-6 Construction of the Diagrams

The system $Fe-H_2O-Cl_2$ cannot be studied using an ordinary Eh-pH diagram, because some reactions, such as

$$Fe^{+++} + Cl^- = FeCl^{++} \qquad (A-35)$$

involve neither H^+ nor electron transfer and therefore cannot be represented by a line in the diagram.

This system could be very well studied with the help of a three dimensional diagram, where the third dimension would be - log Cl^- (or pCl in correspondence with pH).

In order to make this diagram handier and more easily understandable a knew technique has been developed.

The systems Fe-Cl and $Fe-H_2O$ have been dealt with separately. The system $Fe-H_2O$ has been drawn using Eh and pH as variables at different temperatures; while the system Fe-Cl has been drawn using Eh and pCl as variables, at the same temperatures as the system $Fe-H_2O$.

In order to combine the two systems all the possible reactions between the iron chloride and iron hydroxide species are considered. These reactions contain both pH and pCl as variables. If in these reactions pCl is given the limiting values of the stability area of the chloride species in the Fe-Cl diagram, the following reactions contain only pH as variable and therefore can be represented in an ordinary Eh-pH diagram.

For example in order to determine the stability area of $FeCl^{++}$ at 25^oC in the system $Fe-H_2O-Cl$ the following reactions were considered:

$$Fe(OH)^{++} + Cl^- + H^+ \quad FeCl^{++} \div H_2O \qquad \text{(A-36)}$$

$$Fe(OH)_2^+ \div Cl^- + 2H^+ = FeCl^{++} + 2H_2O \qquad \text{(A-37)}$$

$$FeCl^{++} + e^- = Fe^{++} + Cl^- \qquad \text{(A-38)}$$

$$FeO_4^{--} + Cl^- + 8H^+ 3e^- = FeCl^{++} + 4H_2O \qquad \text{(A-39)}$$

By substituting the thermodynamic values of the species of equations (A-36) and (A-37) at 25°C in equation (A-7) and of equations (A-38) and (A-39) in equation (A-2), it follows:

$$pH = 3.585 - pCl - \log \frac{(FeCl^{++})}{(Fe(OH)^{++})} \qquad \text{(A-36a)}$$

$$2pH = 8.589 - pCl - \log \frac{(FeCl^{++})}{(Fe(OH)_2^{+})} \qquad \text{(A-37a)}$$

$$E = 0.686 + 0.0591pCl - 0.0591 \log \frac{(Fe^{++})}{(FeO_4^{--})} \qquad \text{(A-38a)}$$

$$E = 1.727 - 0.1575pH - 0.0197pCl - 0.0197 \log \frac{(FeCl^{++})}{(FeO_4^{--})} \qquad \text{(A-39a)}$$

If in equation (A-36a) pCl is given the values 0.681 and 1.415 which are the limiting values of the stability area of $FeCl^{++}$ in the system Fe-Cl at 25°C (see fig. 1), the corresponding pH values are 2.92 and 2.17 respectively. These two values of pH represent in the $Fe\text{-}H_2O\text{-}Cl$ system the vertical limits of the stability area of $FeCl^{++}$ in equilibrium with $Fe(OH)^{++}$.

If the same values of pCl are given in equation (A-37a) the corresponding pH values will be 3.954 and 3.587. But $Fe(OH)_2^+$, as can be seen

from the $Fe-H_2O$ diagram is stable at pH values greater than 5.0. So no equilibrium between $FeCl^{++}$ and $Fe(OH)_2^+$ can be expected.

The other two equations (A-38a) and (A-39a) give the non vertical limits of the stability area of $FeCl^{++}$.

By substitution of the pCl values 0.681 and 1.415 in equ. (A-38a) and of the pCl value 1.415 in equation (A-39a) the other two lines of the stability area of $FeCl^{++}$ in equilibrium with $Fe(OH)^{++}$ are obtained.

By working out all the possible reactions between the iron chloride and the non chloride species the areas of equilibrium between these species are determined.

Two peculiarities in the system $Fe-H_2O-Cl$ at 25^oC should be explained. The lowest limit of the stability area of $FeCl_2^+$ in the diagram $Fe-H_2O-Cl$ is determined by the fact that $FeCl_2^+$ is not stable for Eh values below 0.669 as can be seen from the diagram Fe-Cl. The unusual form of the upper limit of the stability area of $FeCl_2$ in the system $Fe-H_2O-Cl$ is due to the fact that for pH values below 12.27 the following reaction is taking place.

$$Fe(OH)_2^+ + 2Cl^- + 2H^+ + e^- = FeCl_2 + 2H_2O \qquad (A-40)$$

while for pH value above 12.27 the following reaction occurs:

$$FeO_4^{--} + 2Cl^- + 8H^+ + 4e^- = FeCl_2 + 4H_2O \qquad (A-41)$$

Following exactly the same technique, the system $Fe-H_2O-Cl$ is studied at 100^o, 150^o and 200^oC.

A- 2.7 TABLE OF THE THERMODYNAMIC DATA

Species	$Cp^{\circ}, 298$ cal. deg.$^{-1}$ mole^{-1}	$\Delta H^{\circ}, 298$ cal. mole^{-1}	$S^{\circ}, 298$ cal. deg.$^{-1}$ mole^{-1}	$\Delta G^{\circ}, 298$ cal. mole^{-1}	$\int_{298}^{373} Cp$	$\int_{298}^{423} Cp$	$\int_{298}^{473} Cp$	$\Delta G^{\circ}375$	$\Delta G^{\circ}423$	$\Delta G^{\circ}475$
H^{+}	0	0	0	0						
H_2	6.89	0	31.21	0						
O_2	7.02	0	49.00	0						
H_2O	18.00	-68,315	16.71	-56,688				-53,864[m]	-52,015[m]	-50,216[m]
Fe	5.99	0	6.53	0						
Fe^{++}	8.00	-21,300	-32.9	-38,850	69.595[f]	71.311[f]	77.027[f]			
$Fe(OH)^{+}$	19.9	-77,600	-7.0	-66,300	52.60[f]	53.08	57.56[f]			
$HFeO_2^{-}$	-62[e]	-113,200	10[g]	-90,300	-75.45[f]	-83.75[f]	-88.40[f]			
Fe^{3+}	4.9[e]	- 11,600	-75.5	- 1,100	93[n]	96[n]	105[n]			
$Fe(OH)^{2+}$	8.6[e]	- 69,500	-34	-54,830	64[n]	66[n]	72[n]			
$Fe(OH)_2^{+}$	17.3[e]	-126,500[b]	-12.1[h]	-104,700	55.405[f]	56.089[f]	60.773[f]			
FeO_4^{2-}	-31.8[e]	-145,900[d]	16[a]	-110,240[c]	-124.56[f]	-119.38[f]	-129.82[f]			
$FeCl^{+}$			26.88[h]	- 50,713[i]	33.966[f]	33.091[f]	36.215[f]			
$FeCl_2$			5.25[j]	- 82,140[k]				-82,298[l]	-82,141[l]	-81,774[l]
$FeCl^{++}$			-27	- 34,400	66.35[f]	67.83[f]	73.31[f]			
$FeCl_2^{+}$			18.30[a]	- 66,700	38.688[f]	38.135[f]	41.602[f]			
$FeCl_3$			13.00[j]	- 96,700	-58[n]	-62[n]	-66[n]	-97,366[l]	-97,568[l]	-97,648[l]
Cl^{-}			13.50	- 31,372						

* Data for H_2, O_2H_2O, Cl^- and Fe from N. B. S.

a Estimated from values for similar and/or related ions.

b Calculated from $\Delta G = \Delta H - T\Delta S$ for the reaction:

$$Fe + 2H_2O = Fe(OH)_2^+ + 2H \text{ using above data.}$$

c Calculated assuming the standard potential, Eh° for $Fe^{3+}/FeO_4^{2-} = 1.7V$ (Pourbaix).

d Calculated from $\Delta G = \Delta H - T\Delta S$ for the reaction:

$$Fe + 4H_2O = FeO_4^{2-} + 8H^+ \text{ using the above data}$$

e Calculated from $\overline{Cp}^\circ(abs) = A + B\overline{S}^\circ(abs)$ and $\overline{Cp}^\circ(abs) = \overline{Cp}^\circ(conv) + 128z$. (195)

f Calculated from $\overline{Cp}^\circ\Big]_{298}^{t_2} = a(t_2) + \beta(t_2)\,\overline{S}^\circ_{25}(abs)$ (196)

g Given by H. E. Townsend (173).

h Calculated from $\overline{S}' = 49 - 99(z/r12)$ and $\overline{S}' = S^\circ - nS^\circ(H_2O)$

(J. W. Cobble: The Journal of chemical physics, 21, p. 1446).

i Calculated assuming the stability constant $k_1 = 0.36$.

(Stability Constants of metal-ion complexes, special publication No. 17, London, The Chemical Society, 1964, p. 280)

j Calculated from $\overline{S}' = 132 - 354/r12$

(J. W. Cobble: The Journal of chemical Physics, 21 p 1449)

k Calculated assuming the stability constant $K_2 = 0.04$

(Stability Constants of Metal-ion complexes, Special publication No. 17, London, The Chemical Society, 1964, p. 280).

l Calculated from $\Delta(\Delta G) = -\Delta S^\circ_{T_o}(T_1 - T_o) + c(T_1 - T_o)^2$ and $c = \frac{\Delta C^\circ_{p,T}}{2T}$ (187).

m Barin I, Knacke O. (192)

n Given by: C. M. Criss, J. W. Cobble (196).

A-2.8 REACTIONS IN THE $Fe-H_2O-Cl$ SYSTEM

A Reactions involving water stability

1. $2H^+ + 2e^- = H_2$

2. $O_2 + 4H^+ + 4e^- = 2H_2O$

B. Hydrogen-ion, chlorine-ion dissociation reactions.

3. $Fe^{+++} + H_2O = Fe(OH)^{++} + H^+$

4. $Fe(OH)^{++} + H_2O = Fe(OH)_2^+ + H^+$

5. $Fe^{++} + H_2O = Fe(OH)^+ + H^+$

6. $Fe(OH)^+ + H_2O = HFeO_2^- + 2H^+$

7. $Fe^{+++} + Cl^- = FeCl^{++}$

8. $FeCl^{++} + Cl^- = FeCl_2^+$

9. $FeCl_2^+ + Cl^- = FeCl_3$

10. $Fe^{++} + Cl^- = FeCl^+$

11. $FeCl^+ + Cl^- = FeCl_2$

12. $Fe(OH)^{++} + Cl^- + H^+ = FeCl^{++} + H_2O$

13. $Fe(OH)^{++} + 2Cl^- + H^+ = FeCl_2^+ + H_2O$

14. $Fe(OH)_2^+ + 2Cl^- + 2H^+ = FeCl_2^+ + 2H_2O$

15. $Fe(OH)_2^+ + 3Cl^- + 2H^+ = FeCl_3 + 2H_2O$

16. $Fe(OH)^+ + Cl^- + H^+ = FeCl^+ + H_2O$

17. $Fe(OH)^+ + 2Cl^- + H^+ = FeCl_2 + H_2O$

C. Reduction reactions

18. $Fe^{+++} + e^- = Fe^{++}$

19. $Fe(OH)^{++} + H^+ + e^- = Fe^{++} + H_2O$

20. $Fe(OH)_2^+ + 2H^+ + e^- = Fe^{++} + 2H_2O$

21. $Fe(OH)_2^+ + H^+ + e^- = Fe(OH)^+ + H_2O$

22. $Fe(OH)_2^+ + e^- = HFEO_2^- + H^+$

23. $FeO_4^{--} + 5H^+ + 4e^- = HFEO_2^- + 2H_2O$

24. $FeO_4^{--} + 8H^+ + 3e^- = Fe^{+++} + 4H_2O$

25. $FeO_4^{--} + 7H^+ + 3e^- = Fe(OH)^{++} + 3H_2O$

26. $FeO_4^{--} + 6H^+ + 3e^- = Fe(OH)_2^+ + 2H_2O$

27. $FeCl^{++} + e^- = Fe^{++} + Cl^-$

28. $FeCl^{++} + 3^- = FeCl^+$

29. $FeCl_2^+ + e^- = Fe^{++} + 2Cl^-$

30. $FeCl_2^+ + e^- = FeCl^+ + Cl^-$

31. $FeCl_2^+ + e^- = FeCl_2$

32. $FeCl_3 + e^- = FeCl_2 + Cl^-$

33. $Fe^{++} + 2e^- = Fe$

34. $Fe(OH)^+ + H^+ + 2e^- = Fe + H_2O$

35. $HFeO_2^- + 3H^+ + 2e^- = Fe + 2H_2O$

36. $FeCl^+ + 2e^- = Fe + Cl^-$

37. $FeCl_2 + 2e^- = Fe + 2Cl^-$

38. $Fe(OH)_2^+ + Cl^- + 2H^+ + e^- = FeCl^+ 2H_2O$

39. $Fe(OH)_2^+ 2Cl^- + 2H^+ + e^- = FeCl_2 + 2H_2O$

40. $FeCl_3 + H_2O + e^- = Fe(OH)^+ + H^+ + 3Cl^-$

41. $FeCl_2^+ + H_2O + e^- = Fe(OH)^+ + 2Cl^- + H^+$

42. $FeO_4^{--} + Cl^- + 8H^+ + 3e^- = FeCl^{++} + 4H_2O$

43. $FeO_4^{--} + 2Cl^- + 8H^+ + 3e^- = FeCl_2 + 4H_2O$

44. $FeO_4^{--} + 3Cl^- + 8H^+ + 3e^- = FeCl_3 + 4H_2O$

45 $FeO_4^{--} + 2Cl^- + 8H^+ + 4e^- = FeCl_2 + 4H_2O$

A-2.9 STANDARD FREE ENERGY ΔG^{o}_{T} AND EQUATIONS RELATING E_T, pH and ACTIVITY

Equation	Temp °C	G^{o}_{T} Cal/mole	E_T/pH Relationship, volts/pH/activity
1.	25	0	$E = 0 - 0.0591\ pH$
	100	-1859	$E = 0.040 - 0.0740\ pH$
	150	-2530	$E = 0.055 - 0.0838\ pH$
	200	-2712	$E = 0.059 - 0.0937\ pH$
2.	25	-113374	$E = 1.229 - 0.0591\ pH$
	100	-106644	$E = 1.156 - 0.0739\ pH$
	150	-100970	$E = 1.094 - 0.0838\ pH$
	200	-94340	$E = 1.022 - 0.0937\ pH$
3.	25	2957	$pH = 2.17 + \log \frac{(Fe(OH)^{++})}{(Fe^{+++})}$
	100	-2996	$pH = -1.757 +$ "
	150	-6972	$pH = -3.605 +$ "
	200	-10863	$pH = -5.024 +$ "
4.	25	6817	$pH = 5.000 + \log \frac{(Fe(OH)_2^{+})}{(Fe(OH)^{++})}$
	100	2156	$pH = 1.264 +$ "
	150	-1128	$pH = -0.583 +$ "
	200	-4521	$pH = -2.091 +$ "
5.	25	9237	$pH = 6.779 + \log \frac{(Fe(OH^{+}))}{(Fe^{++})}$
	100	4349	$pH = 2.550 +$ "
	150	985	$pH = 0.509 +$ "
	200	-2442	$pH = -1.129 +$ "
6.	25	32687	$2pH = 23.988 + \log \frac{(HFeO_2^{-})}{(Fe(OH)^{+})}$
	100	29165	$2pH = 17.102 +$ "
	150	27520	$2pH = 14.230 +$ "
	200	26548	$2pH = 12.277 +$ "

Equation	Temp °C	G^o_T Cal/mole	E_T/pH Relationship, volts/pH/activity
7.	25	-1928	$pCl = 1.415 - \log \frac{(FeCl^{++})}{(Fe^{+++})}$
	100	-4826	pCl = 2.830 - "
	150	-7086	pCl = 3.664 - "
	200	-9546	pCl = 4.415 - "
8.	25	-928	$pCl = 0.681 - \log \frac{(FeCl_2^{+})}{(FeCl^{++})}$
	100	-3580	pCl = 2.099 - "
	150	-5657	pCl = 2.925 - "
	200	-7991	pCl = 3.695 - "
9.	25	1372	$pCl = -1.007 - \log \frac{(FeCl_3)}{(FeCl_2^{+})}$
	100	2924	pCl = -1.715 - "
	150	3929	pCl = -2.032 - "
	200	4933	pCl = -2.281 - "
10.	25	-491	$pCl = 0.360 - \log \frac{(FeCl^{+})}{(Fe^{++})}$
	100	-4158	pCl = 2.438 - "
	150	-3372	pCl = 1.744 - "
	200	-4700	pCl = 2.174 - "
11.	25	-55	$pCl = 0.040 - \log \frac{(FeCl_2)}{(FeCl^{+})}$
	100	2675	pCl = -1.568 - "
	150	867	pCl = -0.448 - "
	200	1095	pCl = -0.506 - "
12.	25	-4885	$pH = 3.585 - pCl - \log \frac{(FeCl^{++})}{(Fe(OH)^{++})}$
	100	-1830	pH = 1.073-pCl - "
	150	-114	pH = 0.059 - pCl - "
	200	1317	pH = -0.609 - pCl - "
13.	25	-5813	$pH = 4.266 - 2pCl - \log \frac{(FeCl_2^{+})}{(Fe(OH)^{++})}$
	100	-5410	pH = 3.172 - 2pCl - "
	150	-5769	pH = 2.983 - 2pCl - "
	200	-6674	pH = 3.086 - 2pCl - "

14.	25	12630	$2pH = 9.269 - 2pCl - \log \frac{(FeCl_2^+)}{(Fe(OH)_2^+)}$
	100	-7566	2pH = 4.437 - 2pCl - "
	150	-4611	2pH = 2.400 - 2pCl - "
	200	-2153	2pH = 0.996 - 2pCl - "
15.	25	-11258	$2pH = 8.262 - 3pCl - \log \frac{(FeCl_3)}{(Fe(OH)_2^+)}$
	100	-4642	2pH = 2.722 - 3pCl - "
	150	-712	2pH = 0.368 - 3pCl - "
	200	2780	2pH = -1.286 - 3pCl "
16.	25	9728	$pH = 7.139 - pCl - \log \frac{(FeCl^+)}{(Fe(OH)^+)}$
	100	-8507	pH = 4.988 - pCl "
	150	-4358	pH = 2.253 - pCl "
	200	-2258	pH = 1.044 - pCl "
17.	25	-9783	$pH = 7.180 - 2pCl - \log \frac{(FeCl_2)}{(Fe(OH)^+)}$
	100	-6172	pH = 3.619 - 2pCl - "
	150	-4255	pH = 2.200 - 2pCl - "
	200	-2686	pH = 1.242 - 2pCl - "
18.	25	-17750	$E = 0.769 + 0.0591 \log \frac{(Fe^{+++})}{(Fe^{++})}$
	100	-20740	E = 0.899 + 0.0739 "
	150	-22503	E = 0.976 + 0.0838 "
	200	-23987	E = 1.040 + 0.0937 "
19.	25	-20707	$E = 0.895 - 0.0591pH - 0.0591 \log \frac{(Fe^{++})}{(Fe(OH)^+)}$
	100	-17744	E = 0.863 - 0.1479pH - 0.0739 "
	150	-15531	E = 0.624 - 0.1677pH - 0.0838 "
	200	-13124	E = 0.373 - 0.1875pH - 0.0937 "
20.	25	-27524	$E=1.193-0.1182pH-0.0591\log\frac{(Fe^{++})}{(Fe(OH)_2^+)}$
	100	-19900	E=0.863-0.1479pH-0.0739 "
	150	-14403	E=0.624-0.1677pH-0.0838 "
	200	-8597	E=0.373-0.1875pH-0.0937 "

21.	25	-18287	$E=0.793-0.0591pH-0.0591\log\frac{(Fe(OH^{+}))}{(Fe(OH)_2^{+})}$
	100	-15551	$E=0.674-0.0739pH-0.0739$ "
	150	-13418	$E=0.582-0.0838pH-0.0838$ "
	200	-11045	$E=0.479-0.0937pH-0.0937$ "
22.	25	14400	$E=-0.624+0.0591pH-0.0591\log\frac{(HFeO_2^{-})}{(Fe(OH)_2^{+})}$
	100	13610	$E=-0.590+0.0739pH-0.0739$ "
	150	14112	$E=-0.612+0.0838pH-0.0838$ "
	200	15503	$E=-0.672+0.0937pH-0.0937$ "
23.	25	-91989	$E=0.997-0.0738pH-0.0148\log\frac{(HFeO_2^{-})}{(FeO_4^{--})}$
	100	-86412	$E=0.937-0.0924pH-0.0185$ "
	150	-80341	$E=0.871-0.1048pH-0.0210$ "
	200	-73630	$E=0.798-0.1172pH-0.0234$ "
24.	25	-116163	$E=1.679-0.1575pH-0.0197\log\frac{(Fe^{+++})}{(FeO_4^{--})}$
	100	- 99186	$E=1.433-0.1971pH-0.0246$ "
	150	- 86353	$E=1.248-0.2236pH-0.0279$ "
	200	- 73749	$E=1.066-0.2500pH-0.0312$ "
25.	25	-113202	$E=1.636-0.1378pH-0.0197\log\frac{(Fe(OH)^{++})}{(FeO_4^{--})}$
	100	-102182	$E=1.477-0.1725pH-0.0246$ "
	150	-93325	$E=1.349-0.1956pH-0.0279$ "
	200	-84612	$E=1.223-0.2187pH-0.0312$ "
26.	25	-106389	$E=1.537-0.1182pH-0.0197\log\frac{(Fe(OH)_2^{+})}{(FeO_4^{--})}$
	100	-100026	$E=1.445-0.1472pH-0.0246\log$ "
	150	-94453	$E=1.365-0.1677pH-0.0279\log$ "
	200	-89133	$E=1.288-0.1875pH-0.0312\log$ "
27.	25	-15822	$E=0.686+0.0591pCl-0.0591\log\frac{(Fe^{++})}{(FeCl^{++})}$
	100	-15914	$E=0.690+0.0739pCl-0.0739$ "
	150	-15417	$E=0.668+0.0838pCl-0.0838$ "
	200	-14441	$E=0.626+0.0937pCl-0.0937$ "

28.	25	-16313	$E=0.707-0.0591 \log \frac{(FeCl^{+})}{(FeCl^{++})}$
	100	-20072	$E=0.870-0.0739$ "
	150	-18792	$E=0.815-0.0838$ "
	200	-19141	$E=0.830-0.0937$ "
29.	25	-14894	$E=0.646+0.1182pCl-0.0591 \log \frac{(Fe^{++})}{(FeCl_2^{+})}$
	100	-10672	$E=0.463+0.1472pCl-0.0739$ "
	150	-7046	$E=0.305+0.1677pCl-0.0838$ "
	200	-2957	$E=0.127+0.1875pCl-0.0937$ "
30.	25	-15385	$E=0.667+0.0591pCl-0.0591 \log \frac{(FeCl^{+})}{(FeCl_2^{+})}$
	100	-16492	$E=0.715+0.0739pCl-0.0739$ "
	150	-13134	$E=0.569+0.0838pCl-0.0838$ "
	200	-11150	$E=0.483+0.0937pCl-0.0937$ "
31.	25	-15440	$E=0.669-0.0591 \log \frac{(FeCl_2)}{(FeCl_2^{+})}$
	100	-13886	$E=0.602-0.0739$ "
	150	-12267	$E=0.532-0.0838$ "
	200	-10053	$E=0.436-0.0937$ "
32.	25	-16812	$E=0.729+0.0591pCl-0.0591 \log \frac{(FeCl_2)}{(FeCl_3)}$
	100	-16810	$E=0.729+0.0739pCl-0.0739$ "
	150	-16196	$E=0.702+0.0838pCl-0.0838$ "
	200	-14988	$E=0.650+0.0937pCl-0.0937$ "
33.	25	18850	$E=-0.409+0.0295 \log (Fe^{++})$
	100	16990	$E=-0.368+0.0370 \log$ "
	150	16390	$E=-0.355+0.0419 \log$ "
	200	16445	$E=-0.356+0.0469 \log$ "
34.	25	9613	$E=-0.208-0.0295pH+0.0295 \log (Fe(OH)^{+})$
	100	12641	$E=-0.274-0.0370pH+0.0370 \log$ "
	150	15405	$E=-0.334-0.0419pH+0.0419 \log$ "
	200	18887	$E=-0.409-0.0469pH+0.0469 \log$ "

35.	25	-23074	$E=0.500-0.0886pH+0.0295 \log (HFeO_2^-)$
	100	-16524	$E=0.358-0.1109pH+0.0370 \log$ "
	150	-12125	$E=0.263-0.1258pH+0.0419 \log$ "
	200	-7661	$E=0.166-0.1406pH+0.0469 \log$ "
36.	25	19341	$E=-0.419+0.0295pCl+0.0295 \log (FeCl^+)$
	100	21148	$E=-0.458+0.0370pCl+0.0370 \log$ "
	150	19763	$E=-0.428+0.0419pCl+0.0419 \log$ "
	200	21145	$E=-0.458+0.0469pCl+0.0469 \log$ "
37.	25	19396	$E=-0.420+0.0591pCl+0.0295 \log (FeCl_2)$
	100	18542	$E=-0.402+0.0739pCl+0.0370 \log$ "
	150	18895	$E=-0.410+0.0838pCl+0.0419 \log$ "
	200	20050	$E=-0.435+0.0937pCl+0.0469 \log$ "
38.	25	-28015	$E=1.215-0.1182pH0-0.0591pCl-0.0591 \log \frac{(FeCl^+)}{(Fe(OH)_2^+)}$
	100	-24058	$E=1.043-0.1479pH-0.0739pCl-0.0739$
	150	-17776	$E=0.771-0.1677pH-0.0837pCl-0.0838$
	200	-13303	$E=0.577-0.1875pH-0.0937pCl-0.0937$
39.	25	-28070	$E=1.217-0.1182pH-0.1182pCl-0.0591 \log \frac{(FeCl_2)}{(Fe(OH)_2^+)}$
	100	-21452	$E=0.930-0.1479pH-0.1479pCl-0.0739$
	150	-16988	$E=0.736-0.1677pH-0.1677pCl-0.0838$
	200	-12208	$E=0.529-0.1875pH-0.1875pCl-0.0937$
40.	25	- 7029	$E=0.305+0.059pH+0.1772pCl-0.0591 \log \frac{(Fe(OH)^+)}{(FeCl_3)}$
	100	- 10908	$E=0.473+0.0739pH+0.2218pCl-0.0739$
	150	- 12706	$E=0.551+0.0838pH+0.2515pCl-0.0838$
	200	- 13825	$E=0.599+0.0937pH+0.2812pCl-0.0937$

41.	25 100 150 200	-8892	$E=0.385+0.0937pH+0.1875pCl-0.0937 \log \frac{(Fe(OH)^{+})}{(FeCl_2^{+})}$
42.	25	-135849	$E=1.727-0.1575pH-0.0197pCl-0.0197 \log \frac{(FeCl^{++})}{(FeO_4^{--})}$
	100	-124084	$E=1.793-0.1971pH-0.0246pCl-0.0246$ "
	150	-112229	$E=1.622-0.2236pH-0.0279pCl-0.0279$ "
	200	-102436	$E=1.480-0.2500pH-0.0312pCl-0.0312$ "
43.	25	-120464	$E=1.741-0.1575pH-0.0394pCl-0.0197 \log \frac{(FeCl_2^{+})}{(FeO_4^{--})}$
	100	-107496	$E=1.553-0.1971pH-0.0492pCl-0.0246$ "
	150	-99094	$E=1.432-0.2236pH-0.0558pCl-0.0279$ "
	200	-91286	$E=1.319-0.2500pH-0.0624pCl-0.0312$ "
44.	25	-119092	$E=1.721-0.1575pH-0.0591pCl-0.0197 \log \frac{(FeCl_3)}{(FeO_4^{--})}$
	100	-104668	$E=1.512-0.1971pH-0.0739pCl-0.0246$ "
	150	-95166	$E=1.375-0.2236pH-0.0838pCl-0.0279$ "
	200	-86353	$E=1.248-0.2500pH-0.0937pCl-0.0312$ "
45.	25	-135904	$E=1.473-0.1182pH-0.0296pCl-0.0148 \log \frac{(FeCl_2)}{(FeO_4^{--})}$
	100	-121478	$E=1.317-0.1479pH-0.0370pCl-0.0185$ "
	150	-111361	$E=1.207-0.1677pH-0.0419pCl-0.0210$ "
	200	-101341	$E=1.098-0.1875pH-0.0469pCl-0.0234$ "

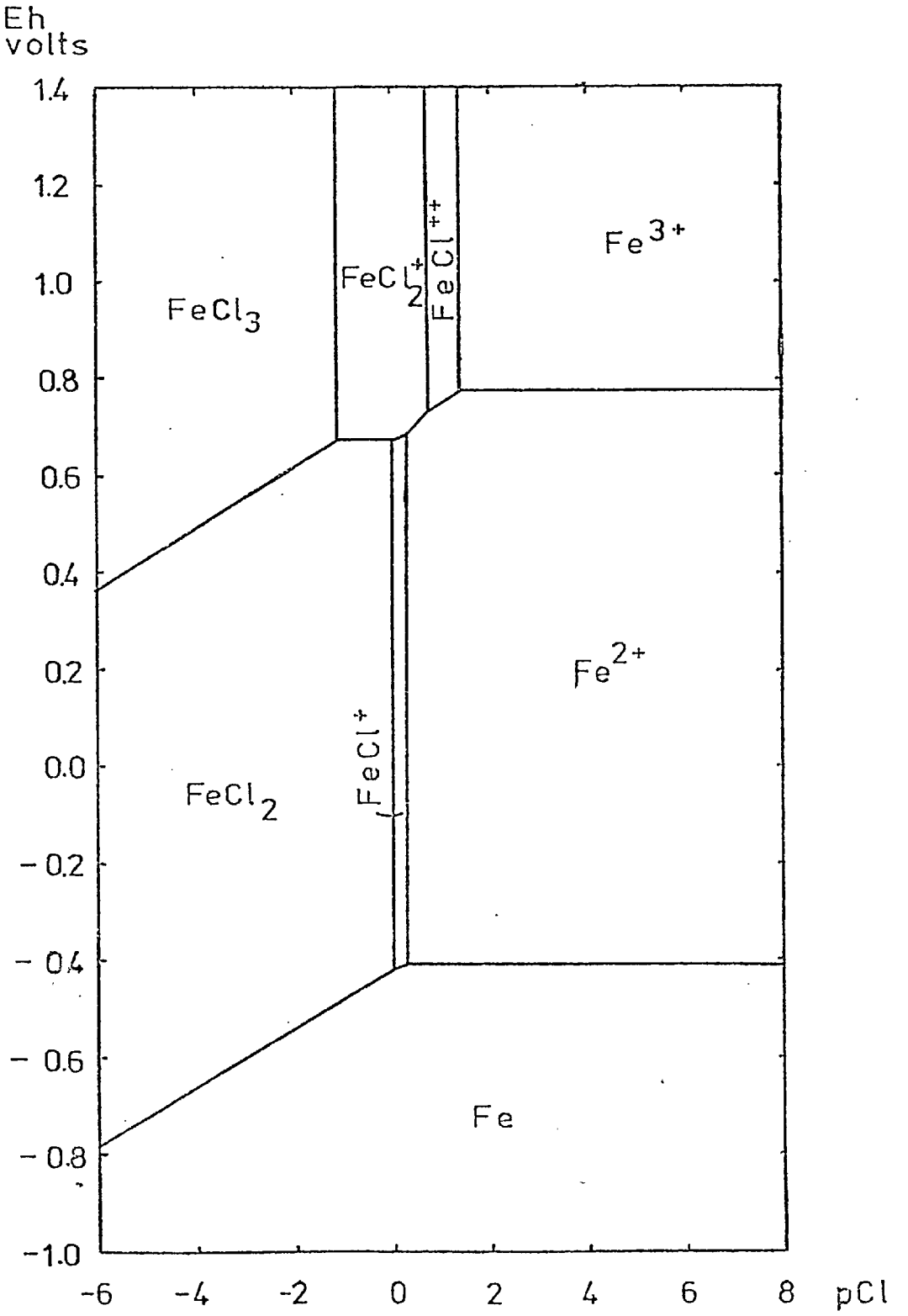

FIG.1 Eh-pCl DIAGRAM FOR THE Fe-Cl SYSTEM AT 25° C
All species at unit activity

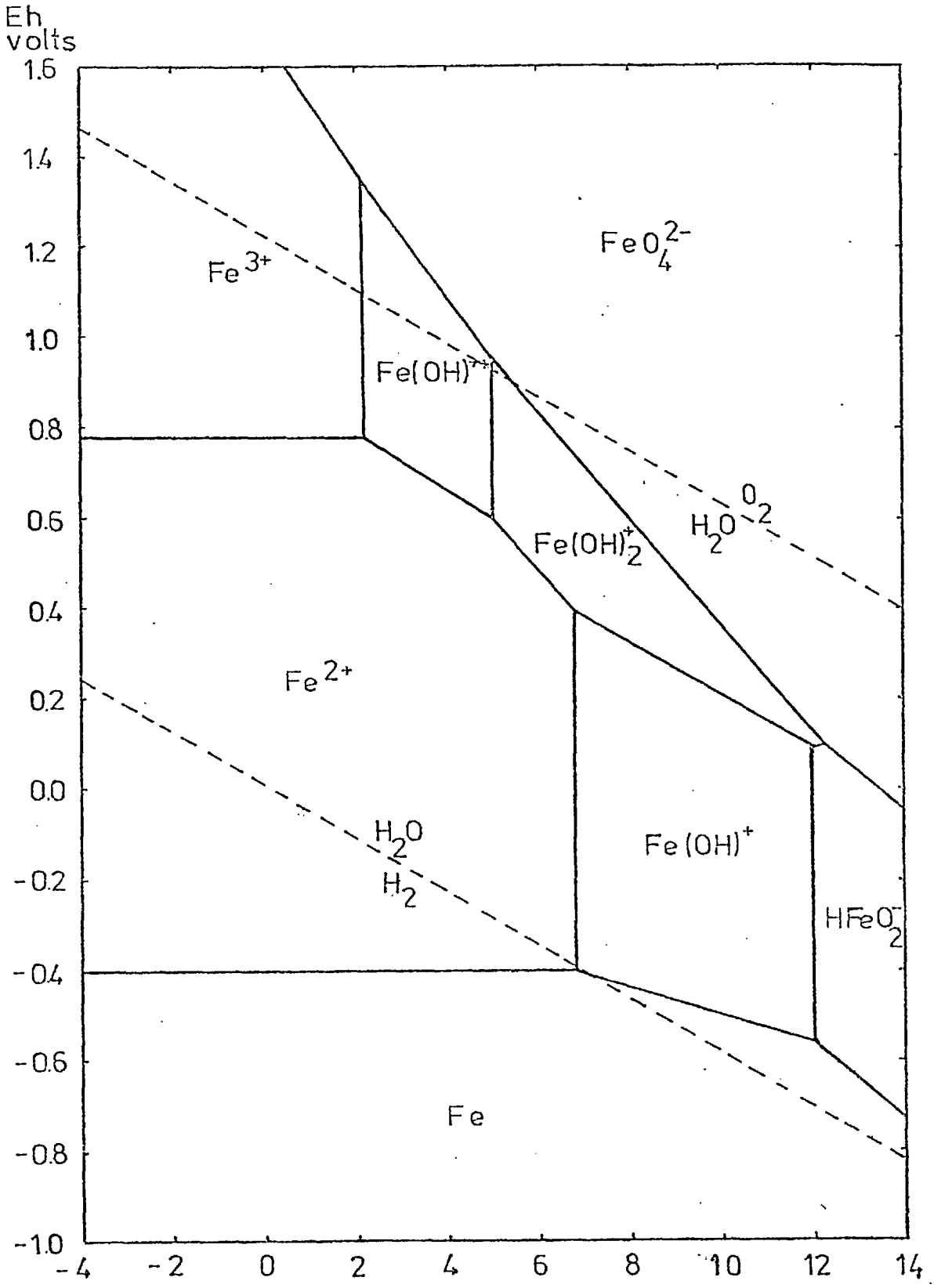

FIG.2 Eh-pH DIAGRAM FOR THE $Fe-H_2O$ SYSTEM AT 25° C

All species at unit activity

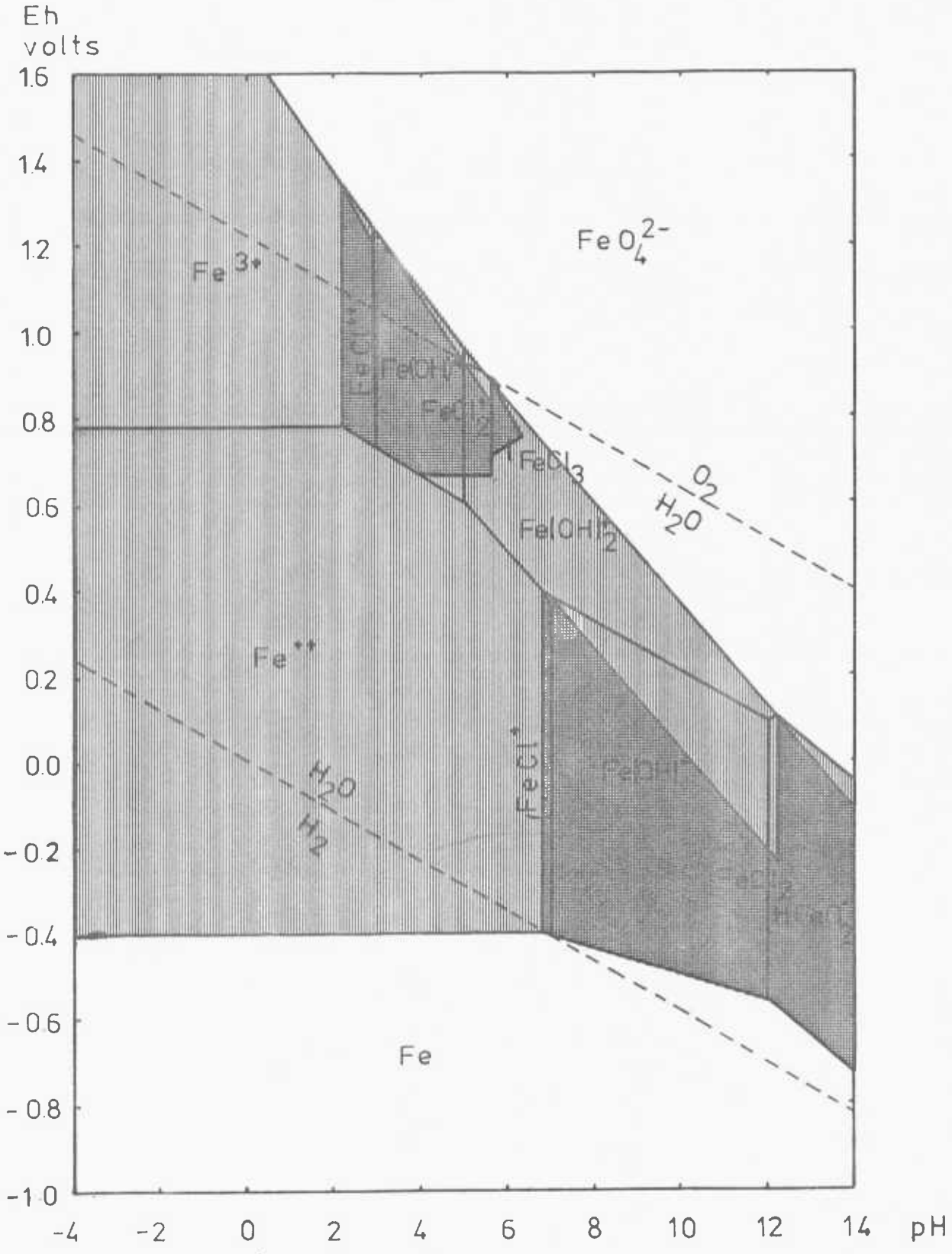

FIG.3 Eh-pH DIAGRAM FOR THE $Fe-H_2O-Cl$ SYSTEM AT 25° C

All species at unit activity

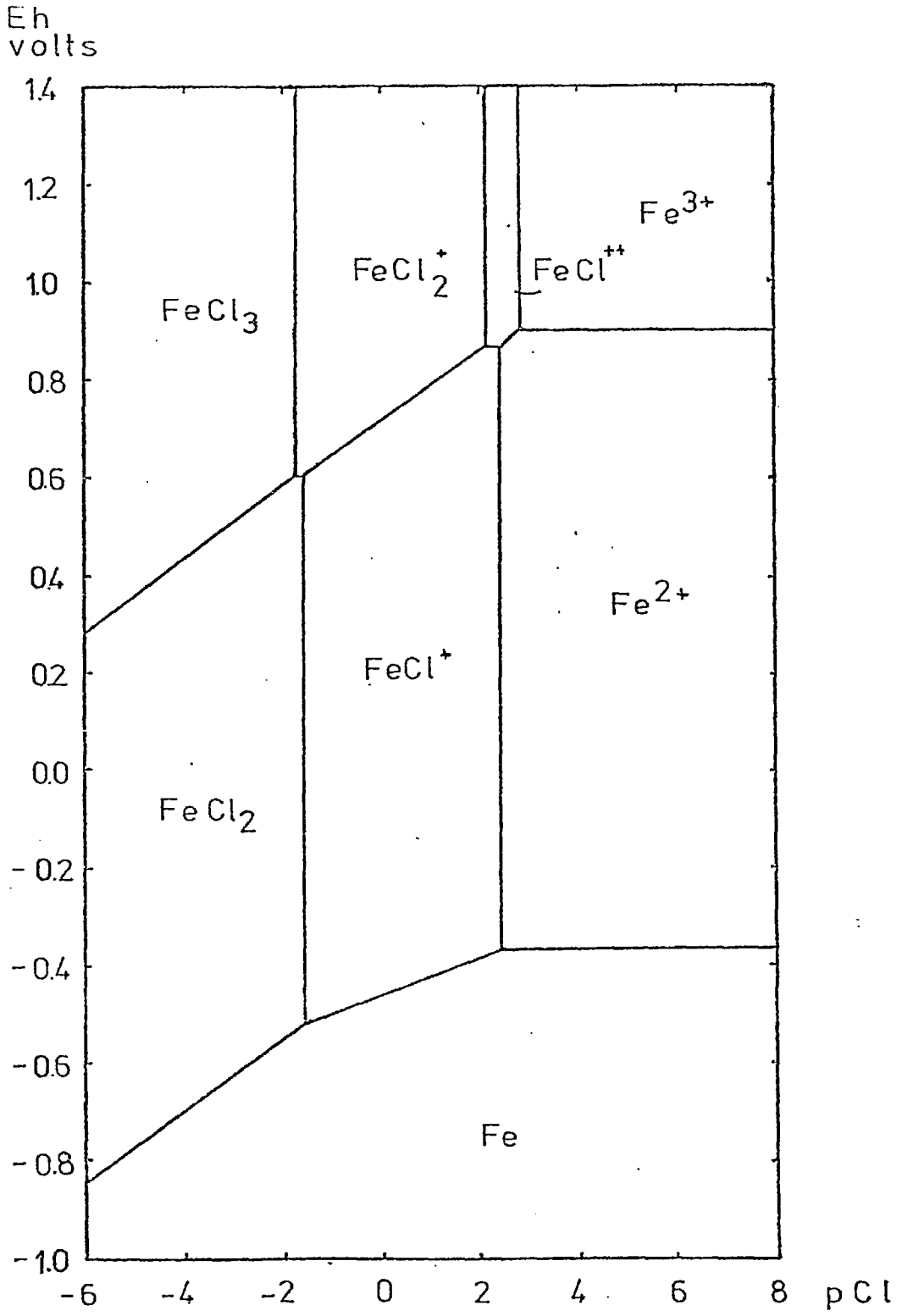

FIG. 4 Eh-pCl DIAGRAM FOR THE Fe-Cl SYSTEM AT 100°C

All species at unit activity

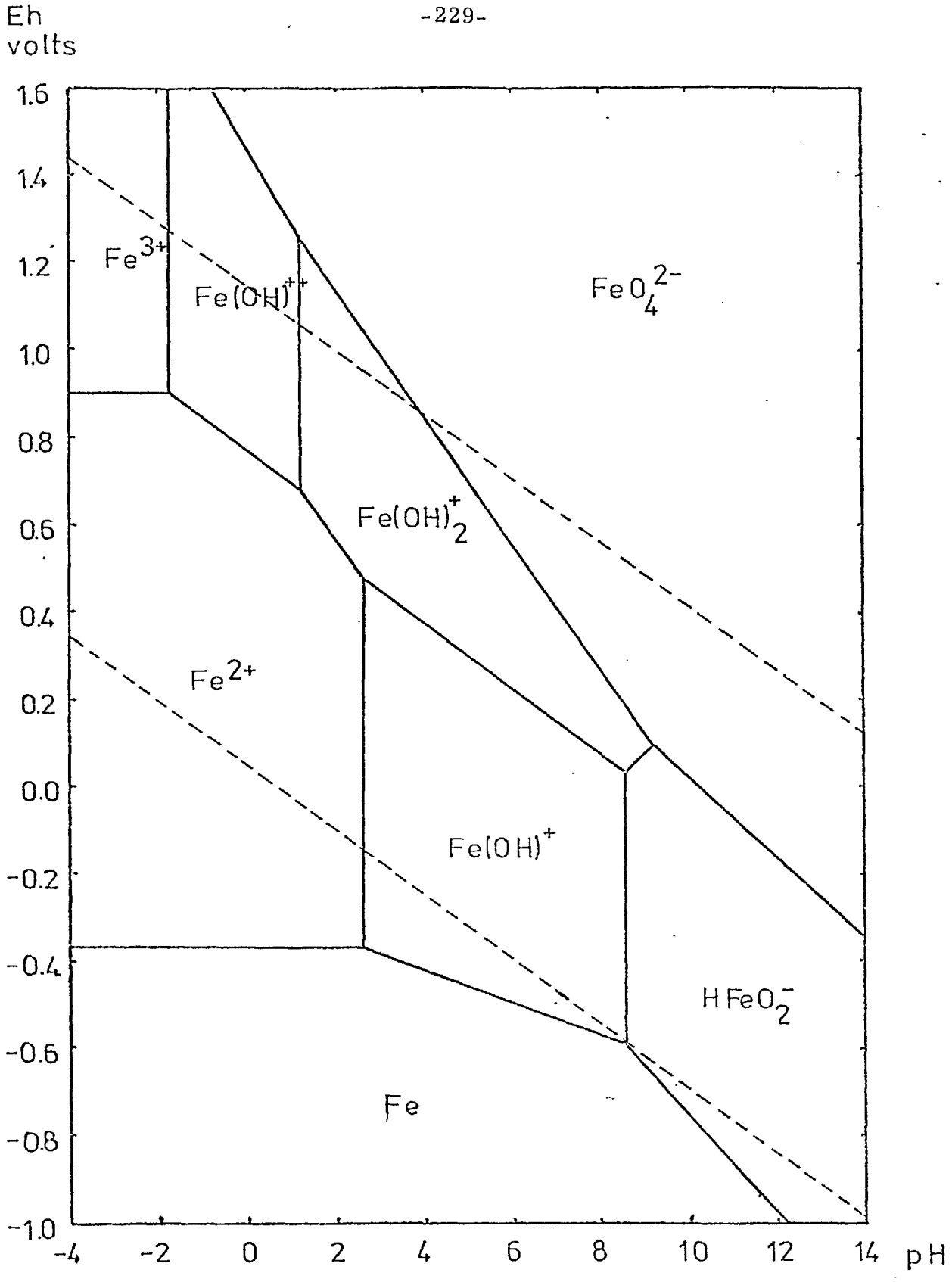

FIG.5 Eh-pH DIAGRAM FOR THE Fe-H_2O SYSTEM AT 100° C

All species at unit activity

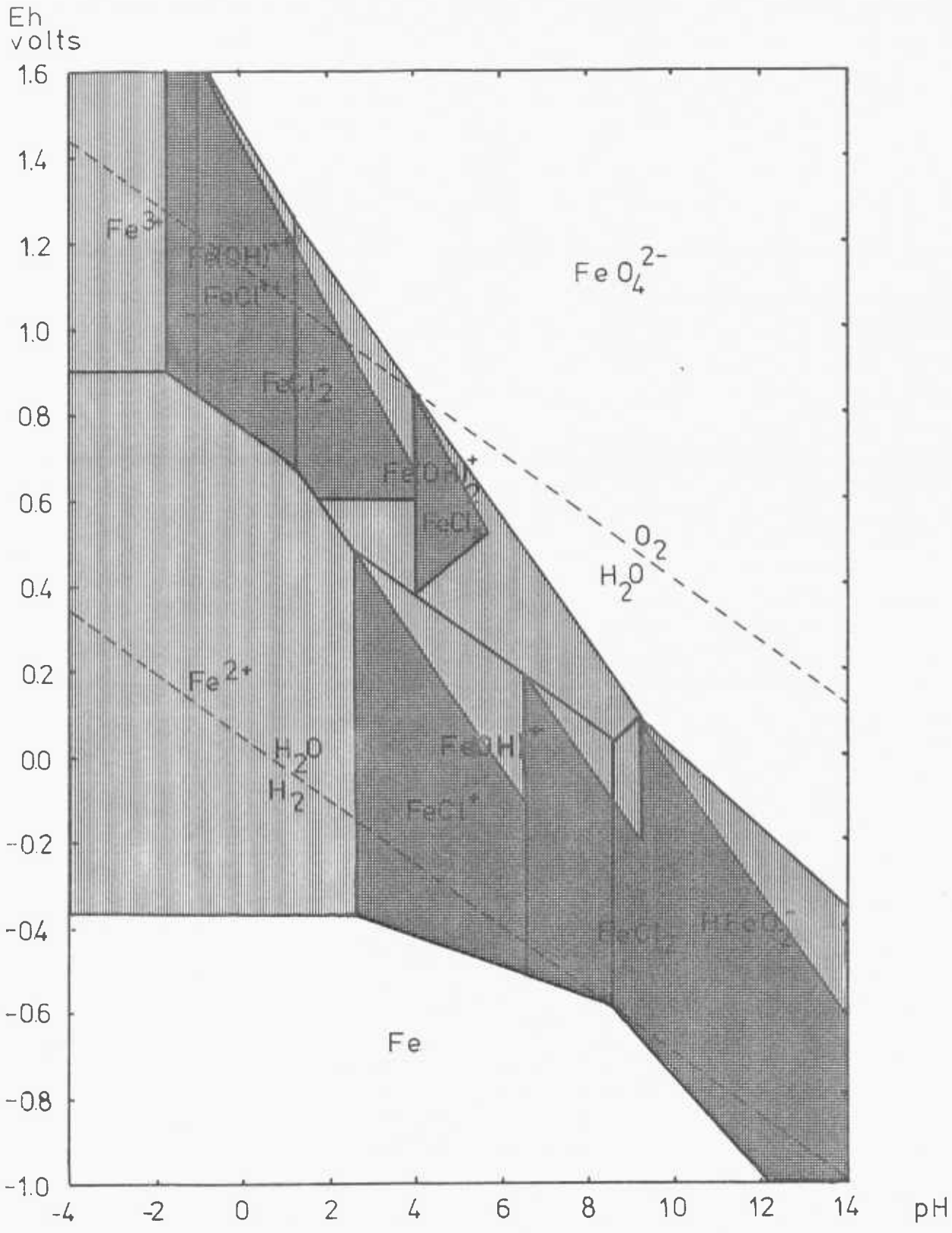

FIG. 6 Eh-pH DIAGRAM FOR THE $Fe-H_2O-Cl$ SYSTEM AT 100°C

All species at unit activity

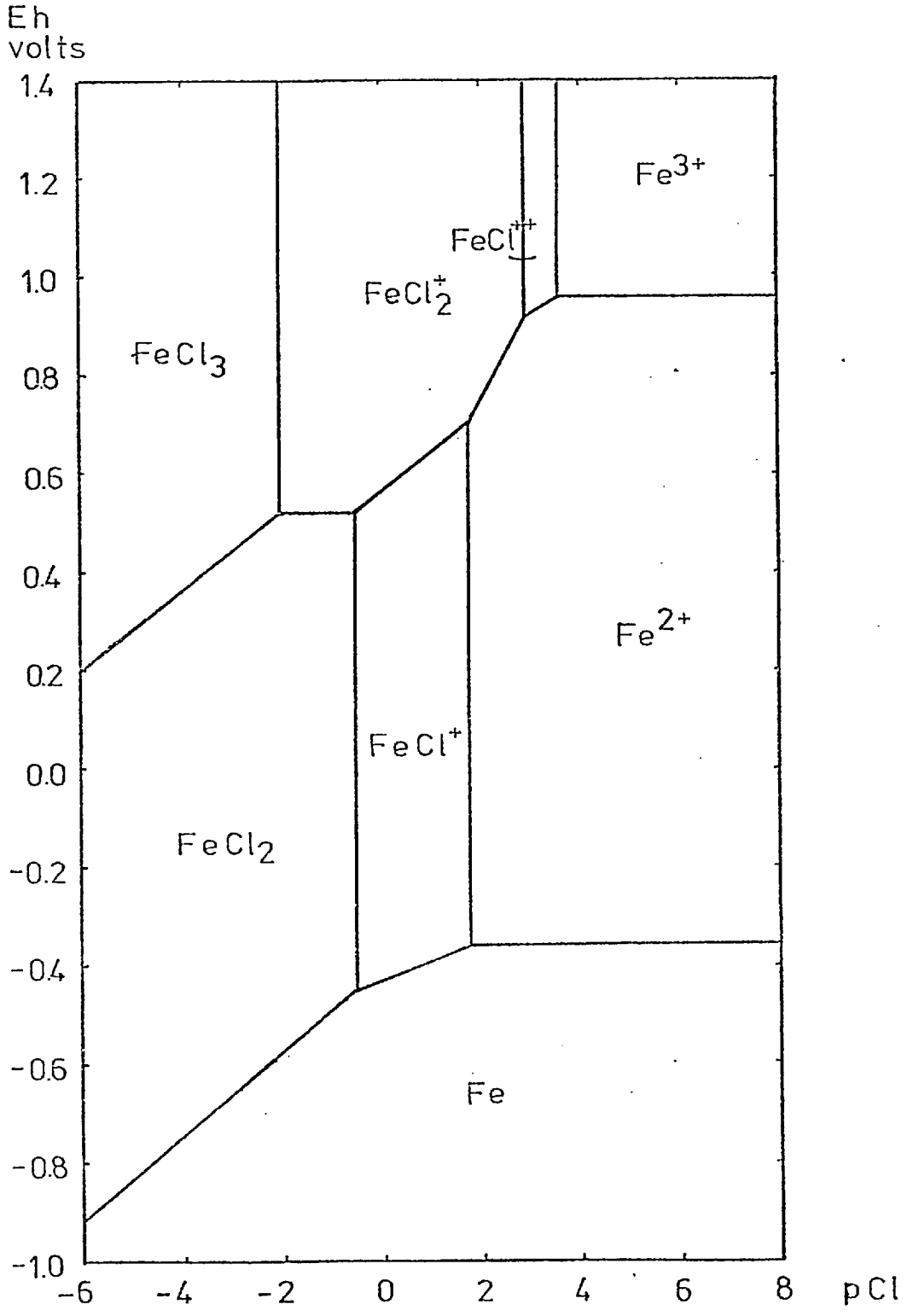

FIG.7 Eh-pCl DIAGRAM FOR THE Fe-Cl SYSTEM AT 150°C

All species at unit activity

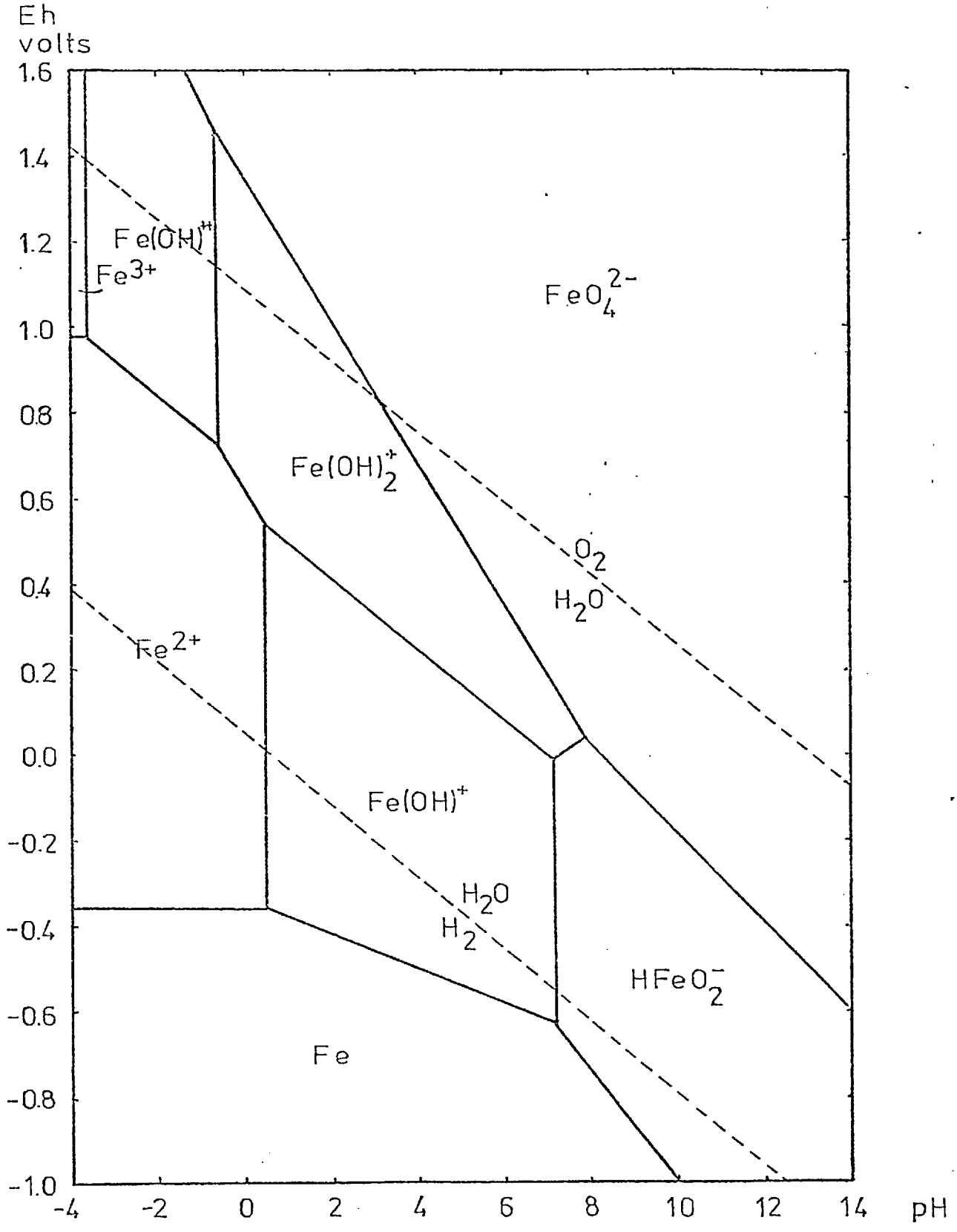

FIG.8 Eh - pH DIAGRAM FOR THE Fe - H_2O SYSTEM AT 150°C

All species at unit activity

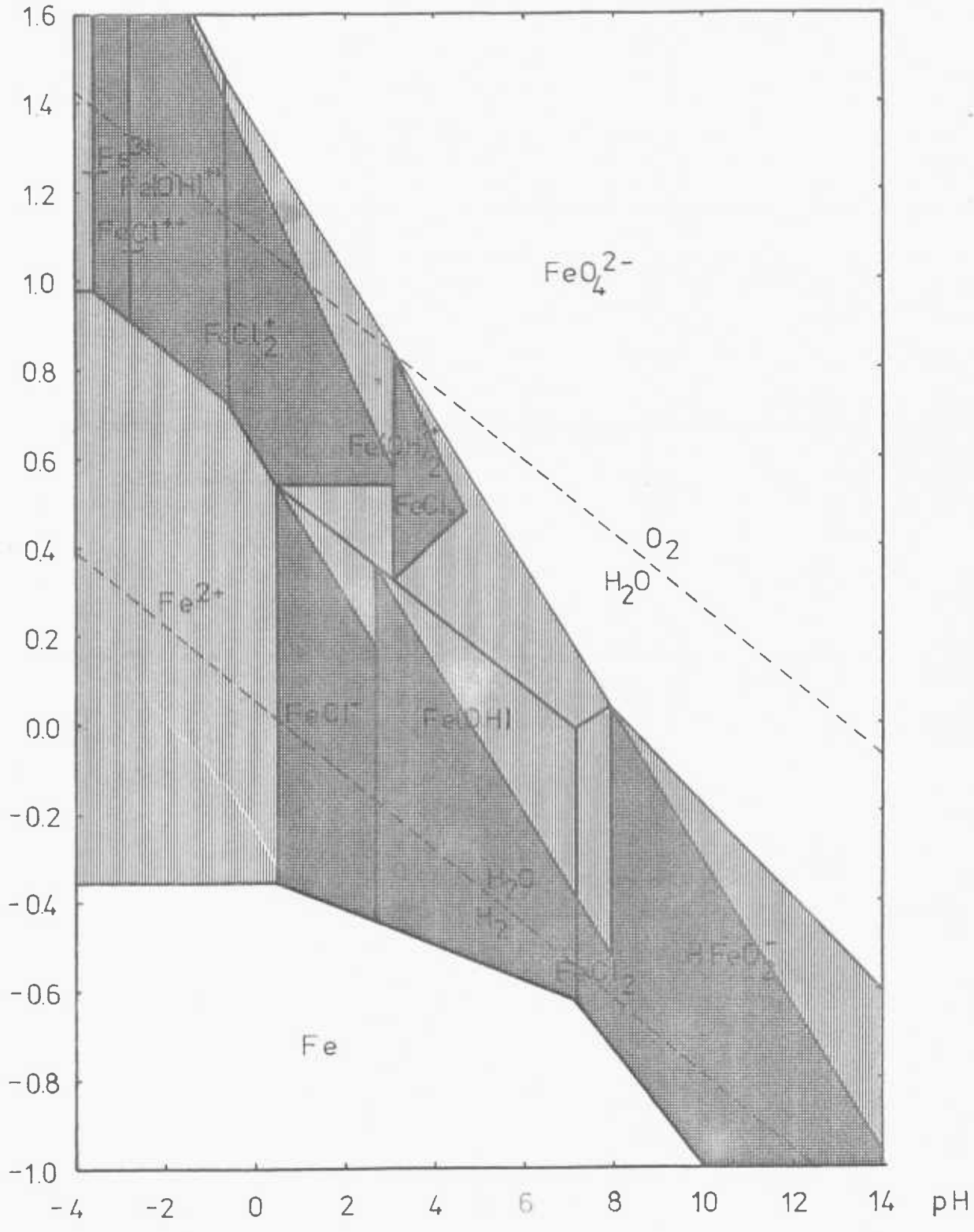

FIG.9 Eh-pH DIAGRAM FOR THE $Fe-H_2O-Cl$ SYSTEM AT 150°C

All species at unit activity

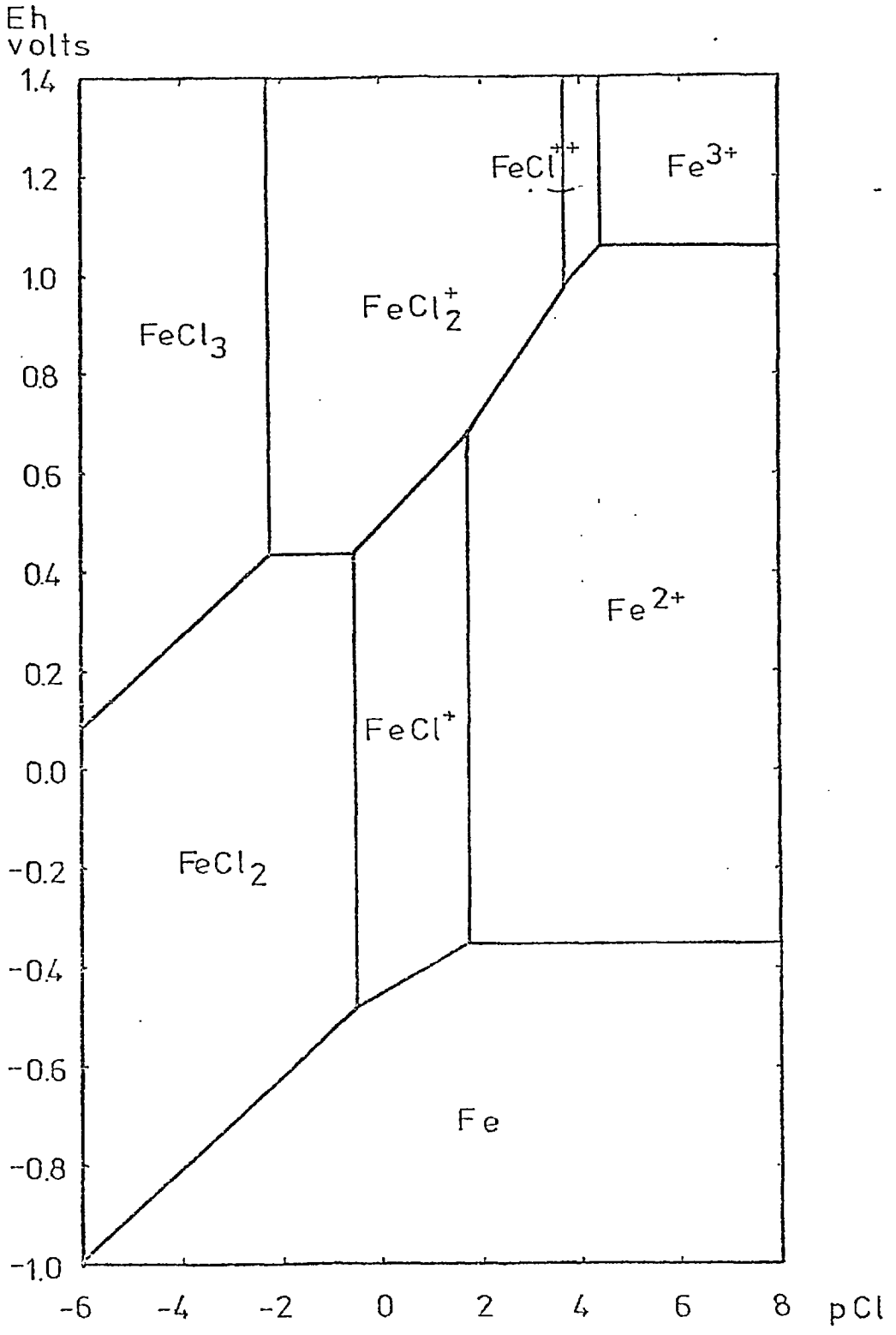

FIG.10 Eh-pH DIAGRAM FOR THE Fe-Cl SYSTEM AT 200°C

All species at unit activity

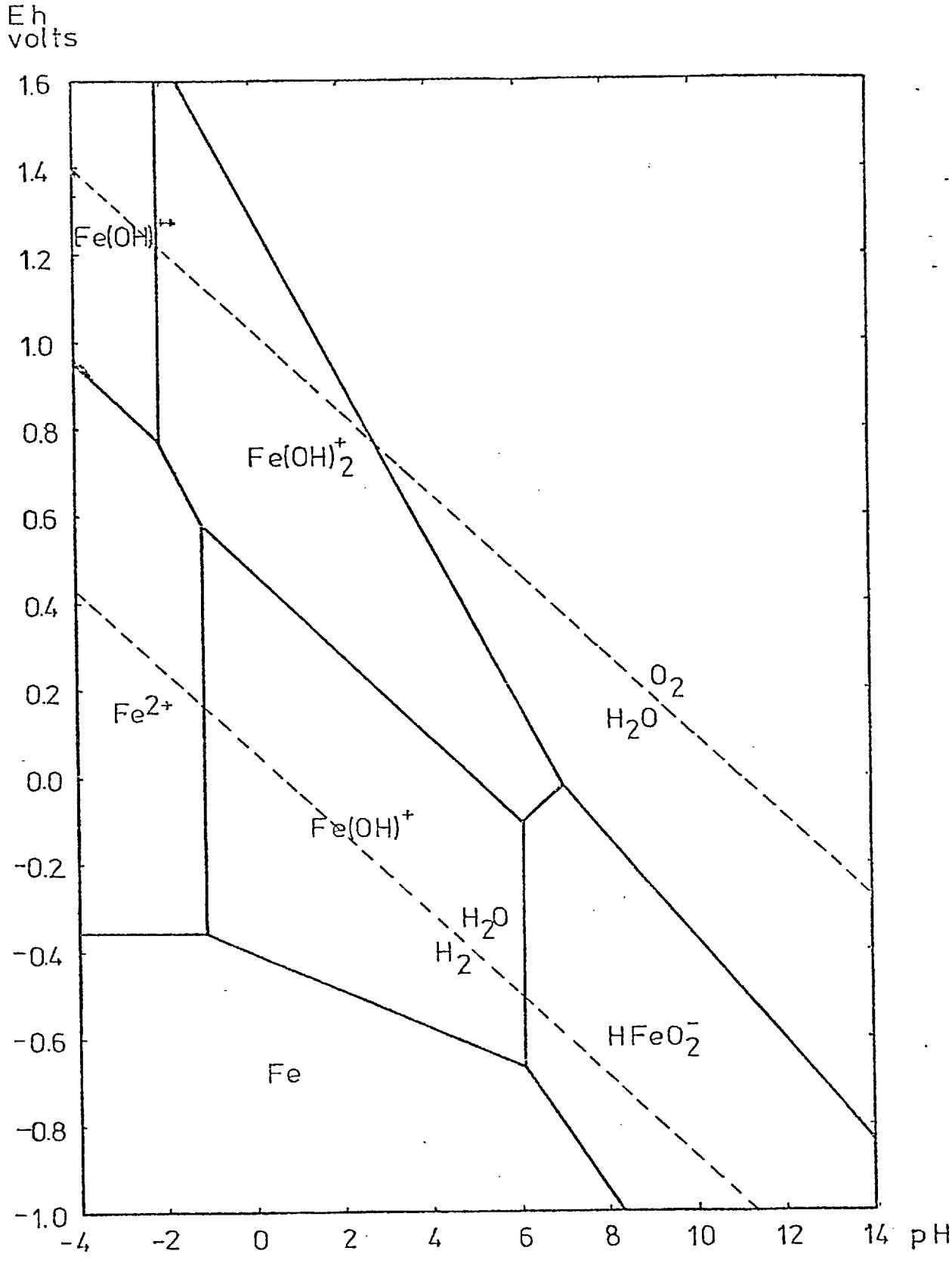

FIG. 11 Eh-pH DIAGRAM FOR THE Fe-H_2O SYSTEM AT 200° C

All species at unit activity

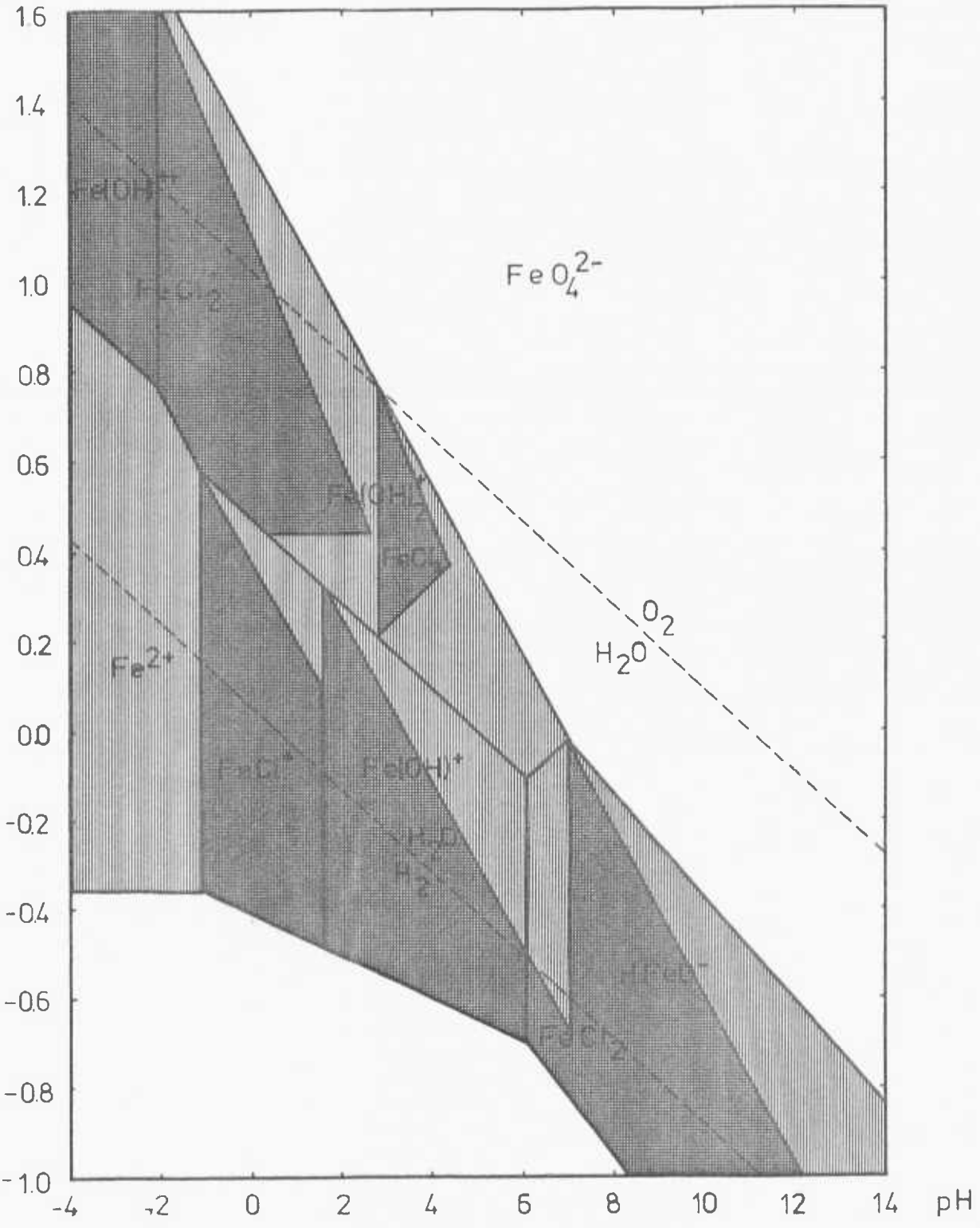

FIG.12 Eh-pH DIAGRAM FOR THE Fe-H_2O-Cl SYSTEM AT 200°C

All species at unit activity

APPENDIX B

EXPERIMENTAL RESULTS FROM THE LEACHING RUNS AND X-RAY DIFFRACTION DATA

TABLE B - 1.1

Leaching of Mss

Temperature:	60°C	Fe^{3+} conc:	0.1M
Particle Size:	-125 + 90 microns	HCl conc:	0.1M
Stirring speed:	1000 rpm	Sample weight:	1.000 gm

Leaching Time (hrs)	% Ni Dissolved
0.0	0.0
2.5	1.5
6.0	3.1
25.0	24.0
50.0	53.8
71.0	63.0
79.0	65.3
96.0	70.4
120.0	76.8
144.0	79.4
174.0	80.4

TABLE B - 1.2

Leaching of Mss

Temperature:	80°C	Fe^{3+} conc:	0.1M
Particle Size:	-125 + 90 microns	HCl conc:	0.1M
Stirring speed:	1000 rpm	Sample weight:	1.000 gm

Leaching Time (hrs)	% Ni Dissolved
0.00	0.0
1.00	1.8
5.50	5.7
18.00	14.0
25.50	19.0
42.00	25.1
49.50	27.9
65.25	31.6
74.00	32.3
90.50	34.8
98.50	35.5
116.00	36.1
136.00	38.3
143.50	38.6

TABLE B - 1.3

Leaching of Mss

Temperature:	95°C	Fe^{3+} conc:	0.1M
Particle Size:	-125 + 90 microns	HCl conc:	0.1M
Stirring Speed:	1000 rpm	Sample weight:	1.000 gm

Leaching Time (hrs)	% Ni Dissolved
0.00	0.0
1.00	5.5
5.00	13.2
19.50	26.7
28.00	33.6
43.50	44.0
52.00	48.3

Leaching Time (hrs)	% Ni Dissolved
72.00	57.7
78.25	60.2
95.25	68.4
103.50	71.5
117.00	76.5
121.00	79.1
139.75	84.1
147.75	86.0
163.75	91.6
170.75	93.0

TABLE B - 1.4

Leaching of Mss

Temperature:	100.5°C	Fe^{3+} conc:	0.1M
Particle Size:	-125 + 90°C	HCl conc:	0.1M
Stirring Speed:	1000 rpm	Sample weight:	1.000 gm

Leaching Time (Hrs)	% Ni Dissolved
0.00	0.0
1.00	10.6
5.00	25.1
23.00	49.3
31.75	59.7
47.50	75.3
56.25	83.6
68.75	92.0
75.50	100.0

TABLE B - 1.5

Leaching of Mss

Particle Size:	-63 + 53 microns	Fe^{3+} conc:	0.1M
Temperature:	95°C	HCl conc:	0.1M
Stirring Speed:	1000 rpm	Sample weight:	1.000 gm

Leaching Time (hrs)	% Ni Dissolved
0.00	0.0
1.00	13.6
4.00	27.3
8.00	38.4
24.50	61.4
33.00	67.4
48.00	73.4
56.50	75.5
72.00	80.0
83.25	82.0
101.00	86.1
126.00	90.3
144.00	92.5

TABLE B - 1.6

Leaching of Mss

Particle Size:	-90 + 63 microns	Fe^{3+} conc:	0.1M
Temperature	95°C	HCl conc:	0.1M
Stirring Speed:	1000 rpm	Sample weight:	1.000 gm

Leaching Time (Hrs)	% Ni Dissolved
0.0	0.0
1.0	9.0
3.0	18.2
19.0	54.6
27.0	61.4
42.5	67.5
51.0	70.4
67.0	77.7
76.0	78.5
94.0	81.9
117.5	87.2
139.0	94.7

TABLE B - 1.7

Leaching of Mss

Particle Size:	-180 + 125 microns	Fe^{3+} conc:	0.1M
Temperature:	95°C	HCl conc:	0.1M
Stirring Speed:	1000 rpm	Sample weight:	1.000 gm

Leaching Time (Hrs)	% Ni Dissolved
0.0	0.0
1.0	3.9
10.0	17.3
22.5	26.4
34.0	35.0
46.5	41.8
56.0	46.1
71.0	53.8
96.5	61.7

Leaching Time (Hrs)	% Ni Dissolved
124.0	70.0
142.5	73.4
167.0	76.8
193.0	79.4

TABLE B - 1.8

Leaching of Mss

Fe^{3+} conc:	0.05M	Stirring Speed:	1000 rpm
Temperature:	95°C	HCl conc:	0.1M
Particle Size:	-125 + 90 microns	Sample Weight:	1.000 gm

Leaching Time (Hrs)	% Ni Dissolved
0.0	0.0
1.0	2.3
3.0	5.5
9.5	12.8
22.5	23.7
47.0	35.5
54.0	38.4
78.0	42.2
119.5	46.1

TABLE B - 1.9

Leaching of Mss

Fe^{3+} conc:	0.15M	Stirring Speed:	1000 rpm
Temperature:	95°C	HCl conc:	0.1M
Particle Size:	-125 + 90 microns	Sample weight:	1.000 gm

Leaching Time (Hrs)	% Ni Dissolved
0.0	0.0
1.0	3.8
3.0	8.8
22.5	36.8
30.0	45.8
47.0	62.7
54.0	70.4
70.5	80.0
77.0	82.2
102.5	88.9
145.0	95.1
167.0	97.3

TABLE B - 1.10

Leaching of Mss

Stirring Speed:	700 rpm	Fe^{3+} conc:	0.1M
Temperature:	95°C	HCl conc:	0.1M
Particle Size:	-125 + 90 microns	Sample weight:	1.000 gm

Leaching Time (Hrs)	% Ni Dissolved
0.0	0.0
1.5	4.2
3.0	6.4
21.5	22.4
28.5	26.7
47.0	35.8
55.0	38.4
69.5	43.5
78.0	44.8
105.0	52.5
168.0	67.8

TABLE B - 1.11

Leaching of Mss

Stirring Speed:	1800 rpm	Fe^{3+} conc:	0.1M
Temperature:	95°C	HCl conc:	0.1M
Particle Size:	-125 + 90 microns	Sample Weight:	1.000 gm

Leaching Time (Hrs)	% Ni dissolved
0.0	0.0
2.0	9.6
5.5	19.0
23.5	37.2
29.5	41.8
50.5	54.6
79.0	68.3
94.0	74.2
118.0	84.3
143.0	92.2
167.0	98.5

TABLE B - 1.12

Leaching of Mss

Solution:	Fe^{3+} (0.1M) + HCl (0.1M) + H_2SO_4; pH = 0.7
Temperature:	95°C
Particle Size:	-90 + 63 microns
Stirring Speed:	1000 rpm
Sample Weight:	1.000 gm

Leaching Time (Hrs)	% Ni Dissolved
0.0	0.0
1.5	2.8
3.0	3.5
18.5	15.0
28.5	20.2
42.5	28.2
50.0	31.1
67.5	38.4
119.0	67.8
137.5	75.5

TABLE B - 1.13

Sample Weight: 0.250 gm
Temperature: 95°C
Particle Size: -125 + 90 microns
Stirring Speed: 1.000 rpm
Fe^{3+} conc: 0.1M
HCl conc: 0.1M

Leaching Time (Hrs)	% Ni Dissolved
0.0	0.0
2.0	7.7
5.5	24.6
22.5	60.8
29.0	69.6
47.5	81.5
53.5	83.6
79.5	88.0
118.0	92.0

TABLE B - 1.14

Leaching of Mss

Sample Weight:	2.000 gm	Stirring Speed:	1000 rpm
Temperature:	95°C	Fe^{3+} conc:	0.1M
Particle Size:	-125 + 90 microns	HCl conc:	0.1M

Leaching Time (Hrs)	% Ni Dissolved
0.0	0.0
2.0	5.5
5.0	9.2
24.5	24.3
31.0	28.2
48.0	36.1
54.5	39.0
73.0	42.3
79.0	43.6
105.0	45.0
143.5	48.0

TABLE B - 1.15

Leaching of Mss

Solution:	50 mls H_2O_2 (20 vol.) + 150 mls HCl (0.3M)
Temperature:	95°C
Particle Size:	-90 + 63 microns
Stirring Speed:	1000 rpm
Sample Weight:	1.000 gm
pH:	0.7

Leaching Time (Hrs)	% Ni Dissolved	% Fe Dissolved
0.0	0.0	0.0
1.0	4.8	4.5
3.0	5.4	5.5
5.0	6.2	6.4
19.0	8.6	8.7
27.0	11.8	11.5
44.0	17.1	16.1
51.5	18.9	16.7
69.5	22.8	22.4
93.5	29.4	29.6
143.0	35.5	35.9
187.5	42.2	41.6
216.0	52.0	51.0

TABLE B - 1.16

Leaching of Mss

Solution: 50 mls H_2O_2 (20 vol.) + 150 mls HCl (0.5M)
Temperature: 95°C
Particle Size: -93 + 63 microns
Stirring Speed: 1000 rpm
Sample Weight: 1.000 gm
pH: 0.5

Leaching Time (Hrs)	% Ni Dissolved	% Fe Dissolved
0.0	0.0	0.0
2.0	6.5	6.7
6.5	9.0	8.7
30.5	15.4	14.2
70.5	25.3	24.8

Leaching Time (Hrs)	% Ni Dissolved	% Fe Dissolved
97.0	34.6	33.5
119.0	41.9	40.2
143.0	50.3	49.5
168.0	63.0	61.8
193.0	66.6	64.5

TABLE B - 1.17

Leaching of Mss

Temperature:	95°C	Fe^{3+} conc:	0.1M
Particle Size:	-125 + 90 microns	HCl conc:	0.1M
Stirring Speed:	1000 rpm	Sample weight:	1.000 gm

% Ni Dissolved	Mgm SO_4^{--} in Solution	$\frac{(SO_4^{--})}{(S)}$ %
0.0	0.0	0.0
5.4	12.0	3.1
7.4	14.0	3.6
13.2	18.0	4.7
26.7	27.0	7.0
33.6	34.0	8.8
44.0	31.0	8.1
48.3	32.0	8.3
57.7	40.5	10.5
60.2	48.0	12.5
66.6	40.0	10.4
71.5	45.0	11.7
73.0	41.0	10.7
76.5	48.0	12.5
78.1	60.0	15.6
84.1	53.0	13.8
91.6	78.0	20.3
94.0	79.0	21.0

TABLE B - 1.18

Leaching of Mss

Hydrogen peroxide leaching

Temperature: 95°C Stirring Speed: 1000 rpm

Particle Size: -93 + 63 microns Sample Weight: 1.000 gm

% Ni Dissolved	mgm SO_4 in Solution	$\frac{(SO_4^{--})}{(S)}$ %
0.0	0.0	0.0
4.5	71.0	18.4
5.5	78.0	20.8
6.4	83.0	21.6
7.7	83.0	21.6
8.7	92.0	23.9
11.5	93.0	24.2
14.2	94.0	24.4
16.1	109.0	25.3
29.6	117.0	30.4
35.9	127.0	33.0
39.2	110.0	28.6
41.6	114.0	29.6
47.9	112.0	29.1
56.1	120.0	31.2
64.0	124.0	32.2

TABLE B - 2.1

Leaching of Pentlandite

Temperature:	80°C	Fe^{3+} conc:	0.1M
Particle size:	-125 + 90° microns	HCl conc:	0.1M
Stirring Speed:	1000 rpm	Sample weight:	1.000 gm

Leaching Time (Hrs)	% Ni Dissolved
0.0	0.0
2.0	5.8
5.0	10.6
8.0	15.6
23.0	41.3
30.0	48.3
46.5	59.0
53.5	61.3
71.5	67.2
77.5	69.6
96.0	72.5
146.0	76.6
168.0	79.0

TABLE B - 2.2

Leaching of Pentlandite

Temperature:	90°C	Fe^{3+} conc:	0.1M
Particle Size:	-125 + 90 microns	HCl conc:	0.1M
Stirring Speed:	1000 rpm	Sample Weight:	1.000 gm

Leaching Time (Hrs)	% Ni Dissolved
0.0	0.0
3.0	20.6
19.0	44.3
54.0	71.0
116.0	86.0
164.0	94.6

TABLE B - 2.3

Leaching of Pentlandite

Temperature:	60°C	Fe^{3+} conc:	0.1M
Particle Size:	-125 + 90 microns	HCl conc:	0.1M
Stirring Speed:	1000 rpm	Sample weight:	1.000 gm

Leaching Time (Hrs)	% Ni Dissolved
0.0	0.0
2.0	3.1
6.5	6.6
23.0	21.4
30.0	25.7
48.0	31.1
54.0	33.0
72.5	37.0
122.5	45.0
145.0	48.1
170.0	50.5

TABLE B - 2.4

Leaching of Pentlandite

Temperature:	40°C	Fe^{3+} conc:	0.1M
Particle Size:	-125 + 90 microns	HCl conc:	0.1M
Stirring speed:	1000 rpm	Sample weight:	1.000 gm

Leaching Time (Hrs)	% Ni Dissolved
0.0	0.0
4.0	0.9
20.5	4.4
28.0	5.8
45.0	9.1
72.0	14.2
96.5	18.9
165.0	27.1
190.5	30.7

TABLE B - 2.5

Leaching of Pentlandite

Particle Size:	-63 + 53 microns	Fe^{3+} conc:	0.1M
Temperature:	80°C	HCl conc:	0.1M
Stirring Speed:	1000 rpm	Sample Weight:	1.000 gm

Leaching Time (Hrs)	% Ni Dissolved
0.0	0.0
2.0	11.5
21.0	45.4
45.0	64.5
69.0	74.1

Leaching Time (Hrs)	% Ni Dissolved
95.0	83.2
116.5	90.0
141.0	95.3

TABLE B - 2.6

Leaching of Pentlandite

Particle Size:	-90 + 63 microns	Fe^{3+} conc:	0.1M
Temperature:	80°C	HCl conc:	0.1M
Stirring Speed:	1000 rpm	Sample Weight:	1.000 gm

Leaching Time (Hrs)	% Ni Dissolved
0.0	0.0
1.0	5.3
6.5	20.1
23.5	45.4
72.0	73.8
96.5	81.4
122.5	88.4
140.5	93.8

TABLE B - 2.7

Leaching of Pentlandite

Particle Size:	-180 + 125 microns	Fe^{3+} conc:	0.1M
Temperature:	80°C	HCl conc:	0.1M
Stirring Speed:	1000 rpm	Sample weight:	1.000 gm

Leaching Time (Hrs)	% Ni Dissolved
0.0	0.0
2.0	7.3
20.0	32.1
44.0	59.0
68.5	63.5
92.5	70.9
115.0	73.2
139.0	77.0

TABLE B - 2.8

Leaching of Pentlandite

Fe^{3+} conc:	0.15M	Stirring Speed:	1000 rpm
Temperature:	80°C	HCl conc:	0.1M
Particle Size:	-125 + 90 microns	Sample Weight:	1.000 gm

Leaching Time (Hrs)	% Ni Dissolved
0.0	0.0
3.0	14.2
20.0	35.6
68.5	73.2
93.0	82.7
119.0	88.7
167.5	93.6

TABLE B - 2.9

Leaching of Pentlandite

Fe^{3+} conc:	0.05M	Stirring Speed:	1000 rpm
Temperature:	80°C	HCl conc:	0.1M
Particle Size:	-125 + 90 microns	Sample Weight:	1.000 gm

Leaching Time (Hrs)	% Ni Dissolved
0.0	0.0
4.0	13.2
21.5	40.0
45.5	55.4
71.5	60.5
93.0	64.5
117.5	67.0
148.0	70.7

TABLE B - 2.10

Leaching of Pentlandite

Fe^{3+} conc:	0.0M	HCl conc:	0.1M
Temperature:	$80^{o}C$	Cl^{-} conc:	0.4M (addition 0.3M NaCl)
Particle Size:	-125 + 90 microns		
Stirring Speed:	1000 rpm	Sample Weight:	1.000 gm

Leaching Time (Hrs)	% Ni Dissolved
0.0	0.0
4.0	2.1
22.0	6.5
48.5	15.5
71.0	21.7
95.0	27.9
120.0	32.9
144.0	39.1

TABLE B - 2.11

Leaching of Pentlandite

Stirring Speed:	700 rpm	Fe^{3+} conc:	0.1M
Temperature:	80°C	HCl conc:	0.1M
Particle Size:	-125 + 90 microns	Sample Weight:	1.000 gm

Leaching Time (Hrs)	% Ni Dissolved
0.0	0.0
2.0	7.8
19.0	34.7
44.0	57.5
116.0	77.5
144.5	78.8

TABLE B - 2.12

Leaching of Pentlandite

Stirring Speed:	1400 rpm	Fe^{3+} conc:	0.1M
Temperature:	80°C	HCl conc:	0.1M
Particle Size:	-125 + 90 microns	Sample Weight:	1.000 gm

Leaching Time (Hrs)	% Ni Dissolved
0.0	0.0
2.5	11.1
18.5	36.0
42.5	59.5
114.5	78.1
140.0	83.6

TABLE B - 2.13

Leaching of Pentlandite

Stirring Speed:	1800 rpm	Fe^{3+} conc:	0.1M
Temperature:	80°C	HCl conc:	0.1M
Particle Size:	-125 + 90 microns	Sample Weight:	1.000 gm

Leaching Time (Hrs)	% Ni Dissolved
0.0	0.0
3.0	19.7
23.0	48.9
57.0	66.8
94.0	77.4
124.0	83.0
144.0	87.1

TABLE B - 2.14

Leaching of Pentlandite

HCl conc:	0.3M	Stirring Speed:	1000 rpm
Temperature:	80°C	Fe^{3+} conc:	0.1M
Particle Size:	-125 + 90 microns	Sample Weight:	1.000 gm

Leaching Time (Hrs)	% Ni Dissolved
0.0	0.0
3.0	2.7
19.5	27.2
45.0	70.0
67.5	83.5
92.5	95.8
164.5	100.0

TABLE B - 2.15

Leaching of Pentlandite

HCl conc:	0.5M	Stirring Speed:	1000 rpm
Temperature:	80°C	Fe^{3+} conc:	0.1M
Particle Size:	-125 + 90 microns	Sample Weight:	1000gm

Leaching Time (Hrs)	% Ni Dissolved
0.0	0.0
3.5	6.7
22.5	23.9
46.5	51.4
70.5	77.4
142.5	97.0

TABLE B - 2.16

Leaching of Pentlandite

Sample Weight:	0.500 gm	Stirring Speed:	1000 rpm
Temperature:	80°C	Fe^{3+} conc:	0.1M
Particle Size:	-125 + 90 microns	HCl conc:	0.1M

Leaching Time (Hrs)	% Ni Dissolved
0.0	0.0
2.0	8.8
20.0	54.6
45.0	75.2
71.5	84.1
139.0	100.0

TABLE B - 2.17

Leaching of Pentlandite

Sample Weight:	2.000 g	Stirring Speed:	1000 rpm
Temperature:	$80^{o}C$	Fe^{3+} conc:	0.1M
Particle Size:	-125 + 90 microns	HCl conc:	0.1M

Leaching Time (Hrs)	% Ni Dissolved
0.0	0.0
2.5	5.4
24.0	29.8
44.0	47.0
69.5	51.2
102.0	56.0
139.0	60.0

TABLE B - 2.18

Leaching of Pentlandite

Solution: 50 mls H_2O_2 (20 vol) + 150 mls HCl (0.3M)
Temperature: $80^{o}C$
Particle Size: -180 + 125 microns
Stirring Speed: 1000 rpm
Sample Weight: 1.000 gm

Leaching Time (Hrs)	% Ni Dissolved	% Fe Dissolved
0.0	0.0	0.0
1.0	6.3	7.1
7.0	10.0	10.7
22.0	15.0	16.7
31.5	21.2	22.3
46.0	27.1	26.0

Leaching Time (Hrs)	% Ni Dissolved	% Fe Dissolved
55.0	36.6	35.1
72.0	46.0	44.2
96.0	57.3	57.1
121.0	67.2	67.0
142.0	77.8	77.0

TABLE B - 2.19

Leaching of Pentlandite

Solution: 50 mls H_2O_2 (20 vol) + 150 mls HCl (0.5M)
Temperature: 80°C
Particle Size: -180 + 125 microns
Stirring speed: 1000 rpm
Sample Weight: 1.000 gm

Leaching Time (Hrs)	% Ni Dissolved	% Fe Dissolved
0.0	0.0	0.0
1.0	6.9	7.6
8.0	10.0	11.0
23.0	13.3	13.6
32.0	17.2	17.4
48.5	23.6	23.1
56.0	25.9	26.5
72.5	33.0	32.0
97.0	42.4	41.7
119.0	50.7	49.0
143.0	59.4	58.1

TABLE B - 2.20

Leaching of Pentlandite

Nitrogen atmosphere
Fe^{3+} conc: 0.00M
Temperature: 80°C
Particle Size: -125 + 90 microns
Stirring Speed: 1000 rpm
H^{+} conc: 0.1M
Sample weight: 1.000 gm
Cl^{-} conc: 0.4M (addition of 0.3M NaCl)

Leaching Time (Hrs)	% Ni Dissolved
0.0	0.0
4.0	1.2
19.5	28.9
46.0	53.6
70.0	74.3
92.0	87.4
116.0	97.0

TABLE B - 2.21

Leaching of Pentlandite

Temperature: 80°C
Particle Size: -125 + 90 microns
Stirring speed: 1000 rpm
Fe^{3+} conc: 0.1M
HCl conc: 0.1M
Sample weight: 1.000 gm

Leaching Time (Hrs)	% Ni Dissolved	$\frac{(SO_4)^{2-}}{(S)}$ %
Nitrogen atmosphere		
0.0	0.0	0.0
2.0	4.0	0.15
6.5	9.3	0.3
9.0	11.4	0.35
Atmospheric conditions		
11.0	14.7	0.80
22.0	30.7	1.65
1st addition of H_2O_2		
23.0	37.1	3.04
30.0	53.7	4.42
47.5	68.1	5.07
2nd addition of H_2O_2		
48.5	73.9	6.13
70.0	90.8	8.06
95.5	97.8	8.70

TABLE B - 2.22

Leaching of Pentlandite

Cl^- conc:	0.6M (addition of 0.2M NaCl)		
Temperature:	80°C	Fe^{3+} conc:	0.1M
Particle Size:	-125 + 90 microns	HCl conc:	0.1M
Stirring Speed:	1000 rpm	Sample Weight:	1.000 gm

Leaching Time (Hrs)	% Ni Dissolved
0.0	0.0
2.0	5.9
7.0	14.7
22.0	38.0
33.0	54.2
46.0	67.7
58.5	77.1
70.0	82.5
78.5	86.4
95.0	92.2
120.0	96.7
142.0	100.0

TABLE B-2.23

Leaching of Pentlandite

Temperature:	80°C	Fe^{3+} conc.:	0.1M
Particle size:	-125 + 90 microns	HCl conc.:	0.1M
Stirring Speed:	1000 rpm	Sample Weight:	1.000 gm

Leaching Time (hrs)	Pt(ppb)	Pt(%)	Pd(ppb)	Pd(%)
0.0	0	0.0	0	0.0
2.0	<100	<8.65	<50	<4.0
5.0	"	"	"	"
8.0	"	"	"	"
23.0	<50	<4.325	<25	<2.0
30.0	"	"	"	"
46.5	"	"	"	"
53.5	"	"	"	"
71.5	"	"	"	"
77.5	"	"	"	"
96.0	"	"	"	"
146.0	"	"	"	"
168.0	"	"	"	"

TABLE B-2.24

Leaching of Pentlandite

Temperature:	90°C	Fe^{3+} conc.:	0.1M
Particle Size:	-125 + 90 microns	HCl conc.:	0.1M
Stirring Speed:	1000 rpm	Sample Weight:	1.000 gm

Leaching Time (hrs)	Pt(ppb)	Pt(%)	Pd(ppb)	Pd(%)
0.0	0	0.0	0	0.0
3.0	<50	<4.325	<25	<2.0
19.0	"	"	"	"
54.0	"	"	"	"
116.0	"	"	"	"
164.0	"	"	"	"

TABLE B-2.25

Leaching of Pentlandite

Particle Size: -90 + 63 microns
Temperature: $80^{o}C$
Stirring Speed: 1000 rpm
Fe^{3+} conc.: 0.1M
HCl conc.: 0.1M
Sample Weight: 1.000 gm

Leaching Time (hrs)	Pt(ppb)	Pt(%)	Pd(ppb)	Pd(%)
0.0	0	0.0	0	0
1.0	<50	<4.325	<10	<0.8
6.5	"	"	"	"
23.5	"	"	"	"
72.0	50 ± 5	4.325 ± 0.432	"	"
96.5	<50	<4.325	"	"
122.5	"	"	"	"
166.5	"	"	"	"

TABLE B-2.26

Leaching of Pendlandite

Fe^{3+} conc.: 0.15M
Temperature: $80^{o}C$
Particle Size: -125 + 90 microns
Stirring Speed: 1000 rpm
HCl conc.: 0.1M
Sample Weight: 1.000 gm

Leaching Time (hrs)	Pt(ppb)	Pt(%)	Pd(ppb)	Pd(%)
0.0	0	0.0	0	0.0
3.0	<50	<4.325	<25	<2.0
20.0	"	"	"	"
68.5	"	"	$25^{+}_{-}3$	$2.0^{+}_{-}2.24$
93.0	<100	<8.65	<50	<4.0
119.0	<50	<4.325	<25	<2.0
167.5	"	"	"	"
192.0	<70	<6.055	<35	<2.8

TABLE B-2.27

Leaching of Pentlandite

Fe^{3+} conc.: 0.05M

Temperature: $80^{o}C$

Particle size: -125 + 90 microns

Stirring speed: 1000 rpm

HCl conc.: 0.1M

Sample weight: 1.000 gm

Leaching Time (hrs)	Pt(ppb)	Pt(%)	Pd(ppb)	Pd(%)
0.0	0	0.0	0	0.0
4.0	<50	<4.325	<25	<2.0
21.5	<70	<6.055	<35	<2.8
45.5	"	"	"	"
71.5	<50	<4.325	<25	<2.0
93.0	"	"	$35^{+}_{-}4$	$2.8^{+}_{-}0.32$
117.5	<70	<6.055	$50^{+}_{-}5$	$4.0^{+}_{-}0.4$
148.0	<50	<4.325	<25	<2.0

TABLE B-2.28

Leaching of Pentlandite

HCl conc.: 0.3M
Temperature: 80°C
Particle Size: -125 + 90 microns
Stirring speed: 1000 rpm
Fe^{3+} conc.: 0.1M
Sample Weight: 1.000gm

Leaching Time (hrs)	Pt(ppb)	Pt(%)	Pd(ppb)	Pd(%)
0.0	0	0.0	0	0.0
3.0	< 50	< 4.325	< 25	< 2.0
19.5	"	"	"	"
45.0	"	"	"	"
67.5	"	"	"	"
92.5	"	"	"	"
164.5	"	"	"	"

TABLE B-2.29

Leaching of Pentlandite

HCl conc.: 0.5M
Temperature: 80°C
Particle Size: -125 + 90 microns
Stirring Speed: 1000 rpm
Fe^{3+} conc.: 0.1M
Sample Weight: 1.000 gm

Leaching Time (hrs)	Pt(ppb)	Pt(%)	Pd(ppb)	Pd(%)
0.0	0	0.0	0	0.0
3.5	< 50	< 4.325	< 10	< 0.8
22.5	"	"	"	"
46.5	"	"	20 ± 2	1.6 ± 0.16
70.5	"	"	< 10	< 0.8
142.5	"	"	"	"

TABLE B-3.1

X-RAY DIFFRACTION DATA FOR THE MONOSULPHIDE SOLID SOLUTION LEACH RESIDUES

Sulphur A. S. T. M. Index		$Fe_{1-x}S$ A. S. T. M. Index		$Fe_{0.36}Ni_{0.57}S$ (29.5 at % Ni) Shewman and Clark (115)		Mss Original		L. R. 20% Nickel Dissolved		L. R. 35% Nickel Dissolved		L. R. 50% Nickel Dissolved		L. R. 75% Nickel Dissolved		L. R. 90% Nickel Dissolved		H_2O_2 Leaching	
d(Å)	I/I_1	d(Å)	I/I_1	d(Å)	I	d(Å)	I	d(Å)	I	d(Å)	I	d(Å)	I	d(Å)	I	d(Å)	I	d(Å)	I
7.69	6											7.70	vw	7.70	vw	7.70	vw	5.95	vvw
5.76	14							5.75	vw	5.75	vw	5.75	vw	5.75	vw	5.75	vw	5.75	w
		5.72	40																
5.68	6							5.65	vw	5.65	vw	5.65	vw						
		5.16	10																
4.80	2																		
		4.76	10																
		4.39	10																
4.19	2															4.19	vvw		
4.06	12									4.07	vw	4.07	w	4.07	w	4.07	w	4.07	w
3.91	12													3.92	vw	3.91	vw		
3.85	100									3.85	w	3.85	m	3.85	s	3.85	w	3.85	vw
3.57	8											3.57	w	3.57	w	3.57	w		
3.44	40											3.45	m	3.45	m	3.45	s	3.45	vvw
		3.40	10																
3.38	4																		
3.33	25							3.33	vw			3.33	m	3.33	m	3.33	m	3.33	vvw
3.21	60									3.22	w	e.22	m	3.22	m	3.22	s		
3.11	25									3.12	w	3.12	m	3.12	w	3.12	m		
3.08	18							3.09	vw	3.09	w	3.09	m	3.09	w	3.09	w		
3.06	2																		
		2.982	80	2.973	s	2.96	s	2.96	s	2.96	s	2.96	s	2.96	m	2.97	w	2.97	s

		2.017	10																
2.003	2																		
1.988	4											1.988	vw	1.988	vvw	1.988	vvw		
		1.981	10																
1.957	2											1.960	vw	1.960	vvw	1.960	vvw		
1.930	2																		
		1.927	10																
1.900	7											1.900	vw	1.900	vw	1.900	w		
		1.866	10																
1.856	1																		
1.838	1																		
1.823	4											1.817	vw	1.817	vw	1.817	vw		
		1.818	20																
1.781	11													1.780	w				
1.754	7											1.755	w	1.755	vw	1.755	w		
		1.746	10			1.74	vw												
1.725	8																		
		1.721	80	1.714	s	1.710	s	1.710	s	1.710	s	1.710	s	1.710	m	1.710	m	1.705	s
1.698	7											1.695	vw	1.695	vw	1.695	w		
1.665	2																		
1.658	2											1.655	vw			1.655	vw		
1.647	5													1.645	vvw				
1.622	6											1.622	vw	1.622	vw	1.622	vw		
		1.609	50	1.562	m	1.574	m	1.574	m	1.574	m	1.574	m	1.575	vvw	1.574	vw	1.575	m
1.607	6													1.605	vvw				
1.595	3																		
1.563	2													1.560	vvw	1.560	vvw		
1.542	1																		
1.531	1													1.530	vvw	1.530	vvw		
1.515	1																		
1.504	1																		

		2.861	30	2.765	w	2.78	vw	2.78	w	2.78	w	2.77	w						
2.842	18											2.84	w	2.84	w	2.84	w	2.84	vw
2.688	2																		
2.673	2																		
		2.647	80	2.617	s	2.63	s	2.63	s	2.63	s	2.63	s	2.63	s	2.630	m	2.63	s
2.621	14															2.620	m		
2.614	4																		
2.569	8													2.57	vvw	2.569	vw		
2.501	8													2.49	vvw				
		2.472	10																
2.424	14							2.425	vvw	2.425	vw	2.425	w	2.425	vw	2.425	w		
2.404	2																		
		2.394	20																
2.375	4													2.375	vw				
2.366	4											2.366	vw	2.366	vw	2.366	vw		
												2.350	vw			2.350	vvw		
2.288	6							2.288	vvw			2.288	vw	2.288	vw	2.288	vw		
		2.241	10																
2.215	2													2.215	vvw	2.215	vvw		
		2.165	20																
2.146	4													2.146	vvw	2.146	vvw		
2.112	10							2.112	vvw					2.112	vw	2.112	vw		
2.098	2							2.090	vvw			2.090	vw						
		2.067	100	2.019	vs	2.05	vs	2.05	vs	2.05	vs	2.05	vs	2.05	s	2.05	s	2.05	vs
2.057	2																		
2.041	2																		

		1.492	40	1.486	mw	1.480	m	1.480	m	1.480	m	1.480	m	1.480	vw	1.480	vw	1.480	w
1.490	1																		
		1.477	10	1.457	vvw														
1.475	2													1.473	vvw				
1.461	1							1.460	vw	1.460	vw	1.460	m			1.460	vw		
		1.444	50	1.434	m	1.430	vw	1.430	m	1.430	m	1.430	m	1.430	w	1.430	vvw	1.430	m
1.439	3																		
		1.434	50	1.371	m	1.390	vw	1.390	m	1.390	m	1.390	m	1.390	vvw	1.390	vvw	1.390	m
1.419	1																		

TABLE B-3.2

X-RAY DIFFRACTION DATA FOR THE PENTLANDITE LEACH RESIDUES

Sulphur A. S. T. M. Index		Pentlandite A. S. T. M. Index		Pentlandite Original		L. R. 20% Nickel Dissolved		L. R. 32% Nickel Dissolved		L. R. 45% Nickel Dissolved		L. R. 55% Nickel Dissolved		L. R. 67% Nickel Dissolved		L. R. 80% Nickel Dissolved		L. R. 90% Nickel Dissolved	
d(Å)	I/I_1	d(Å)	I/I_1	d(Å)	I	d(Å)	I	d(Å)	I	d(Å)	I	d(Å)	I	d(Å)	I	d(Å)	I	d(Å)	I
7.69	6							7.70	w	7.70	w	7.70	w	7.70	w	7.70	w	7.70	vw
		5.78	30	5.80	s	5.80	s	5.80	s	5.80	s	5.80	s	5.80	m	5.80	m	5.80	vw
5.76	14									5.75	m	5.75	m	5.75	m	5.75	w		
5.68	6									5.65	w	5.65	w	5.65	m	5.65	vw		
		5.01	5	5.01	w	5.01	w	5.01	w	5.01	w	5.01	w	5.01	w	5.01	w		
4.80	2																		
4.19	2									4.18	vw	4.18	vw	4.18	vw	4.18	vw		
4.06	12									4.06	w	4.06	w	4.06	w	4.06	w	4.06	w
3.91	12																	3.90	w
3.85	100					3.85	w			3.85	w	3.85	w	3.85	w	3.85	w	3.85	w
										3.66 (Fe_2O_3)	m	3.66	m	3.66	s	3.66	s		
		3.55	5	3.55	w	3.55	w	3.55	w	3.55	w	3.55	w	3.55	w	3.55	w	3.55	vw
3.44	40					3.45	vw			3.45	m	3.45	m	3.45	s	3.45	m	3.45	m
3.38	4																		
3.33	25					3.33	vw	3.33	m	3.33	m	3.33	m	3.33	s	3.33	m	3.33	w
3.21	60									3.20	m	3.20	m	3.20	s	3.20	m	3.20	m
3.11	25									3.10	m	3.10	m	3.10	m	3.10	w	3.10	w
3.08	18									3.08	w	3.08	w	3.08	m	3.08	w	3.08	vw
3.06	2									3.06	w	3.06	w	3.06	m	3.06	w	3.06	vw
		3.03	80	3.03	vs	3.03	vs	3.03	vs	3.03	vs	3.03	vs	3.03	m	3.03	vw	3.03	vw

				2.97 (FeS)	w														
		2.90	40	2.90	s	2.90	s	2.90	s	2.90	s	2.90	s	2.90	m	2.90	vw	2.90	vw
2.842	18									2.84	m	2.84	m	2.84	m	2.84	m	2.84	w
										2.69 (Fe_2O_3)	vw	2.69	vw	2.69	vw	2.69	vw		
2.688	2																		
2.673	2																		
				2.64 (FeS)	vw	2.64	vw	2.64	vw	2.64	vw	2.64	vw	2.64	w	2.64	vw	2.64	vw
2.621	14																		
2.614	4																		
2.569	8									2.56	vw	2.56	vw	2.56	vw	2.56	vw	2.56	vw
		2.51	5	2.51	w	2.51	w	2.51	w	2.51	vw	2.51	vw	2.51	vw	2.51	vw		
2.501	8																		
2.424	14									2.42	w	2.42	w	2.42	w	2.42	w	2.42	w
2.404	2																		
2.375	4									2.37	vw	2.37	vw	2.37	vw	2.37	vw		
2.366	4									2.365	vw	2.365	vw	2.365	vw	2.365	vw	2.365	vw
		2.30	30	2.30	s	2.30	s	2.30	s	2.30	m	2.30	m	2.30	w	2.30	vw	2.30	vw
2.288	6							2.28	w	2.28	w	2.28	w	2.28	w	2.28	w	2.28	vw
		2.25	5	2.25	w	2.25	w	2.25	w	2.25	w	2.25	w	2.25	w	2.25	vw		
2.215	2																		
								2.18 (Fe_2O_3)	vw	2.18 (Fe_2O_3)	vw	2.18	vw	2.18	vw	2.18	vw		
2.146	4									2.14	vw	2.14	vw	2.14	vw	2.14	vw	2.14	vw
2.112	10																		
2.098	2									2.10	w	2.10	w	2.10	w	2.10	w	2.10	w
										2.09	vw	2.09	vw	2.09	vw	2.09	vw		
2.057	2																		
				2.05 (FeS)	w	2.05	w	2.05	vw	2.05	vw	2.05	vw	2.05	vw	2.05	vw		
2.041	2									2.04	vw	2.04	vw	2.04	vw	2.04	vw		

2.003	2							2.02	vw	2.02	vw	2.02	vw	2.02	vw	2.02	vw
1.988	4							1.990	vw	1.990	vw	1.990	vw	1.990	vw	1.990	vw
1.957	2																
		1.931	50	1.937	s	1.937	s	1.937	s	1.937	s	1.937	s	1.937	s	1.937	s
1.930	2																
1.900	7					1.900	vw	1.900	w	1.900	w	1.900	w	1.900	w	1.900	vw
1.856	1																
1.838	1																
1.823	4							1.817	w	1.817	w	1.817	w	1.817	w	1.817	w
1.781	11																
		1.775	100	1.775	vs	1.775	vs	1.775	vs	1.775	vs	1.775	m	1.775	w	1.775	w
1.754	7					1.750	vvw	1.750	w	1.750	w	1.750	w	1.750	w	1.750	vw
1.725	8							1.718	w	1.718	w	1.718	w	1.718	w	1.718	w
1.698	7																
		1.697	5	1.700	w	1.700	w	1.700	vw	1.700	vw	1.700	vw				
								1.690 (Fe_2O_3)	vw	1.690	vw	1.690	vw	1.690	vw	1.690	vw
				1.670 (FeS)	vw	1.670	vw	1.670	vw	1.670	vw	1.670	vw	1.670	vw		
1.665	2																
1.658	2							1.655	vw	1.655	vw	1.655	vw	1.655	vw		
1.647	5																
1.622	6					1.628	vw	1.628	vw	1.628	vw	1.628	vw	1.628	vw	1.628	vw
1.607	6							1.615	vw	1.615	vw	1.615	vw	1.615	vw	1.615	vw
						1.595 (Fe_2O_3)	vw	1.595	vw	1.595	vw	1.595	vw	1.595	vw		
1.563	2							1.555	vw	1.555	vw	1.555	vw	1.555	vw		
1.542	1																
1.531	1																
		1.530	10	1.530	m	1.530	m	1.530	m	1.530	m	1.530	w	1.530	vw	1.530	vvw
1.515	1																
		1.514	10	1.515	m	1.515	m	1.515	m	1.517	m	1.517	w	1.517	vw	1.517	vvw

1.504	1						1.497	vw	1.497	vw	1.497	vw	1.497	vw	1.497	vw			
1.490	1																		
									1.484 (Fe_2O_3)	vw	1.484	vw	1.484	vw	1.484	vw			
1.475	2						1.473	vw	1.473	vw	1.473	vw	1.473	vw	1.473	vw	1.473	vw	
1.461	1																		
			1.455	vw	1.455	vvw	1.455	vw	1.455	vw	1.455	vw	1.455	vw	1.455	vw	1.455	vvw	
1.439	3								1.430	vw	1.430	vw	1.430	vw	1.430	vw	1.430	vvw	
1.419	1																		
			1.410	vw	1.410	vw	1.410	vw	1.410	vw	1.410	vw	1.410	vw	1.410	vw	1.410	vvw	

APPENDIX C

X-RAY POWDER PHOTOGRAPHS AND PHOTOMICROGRAPHS OF RESIDUES

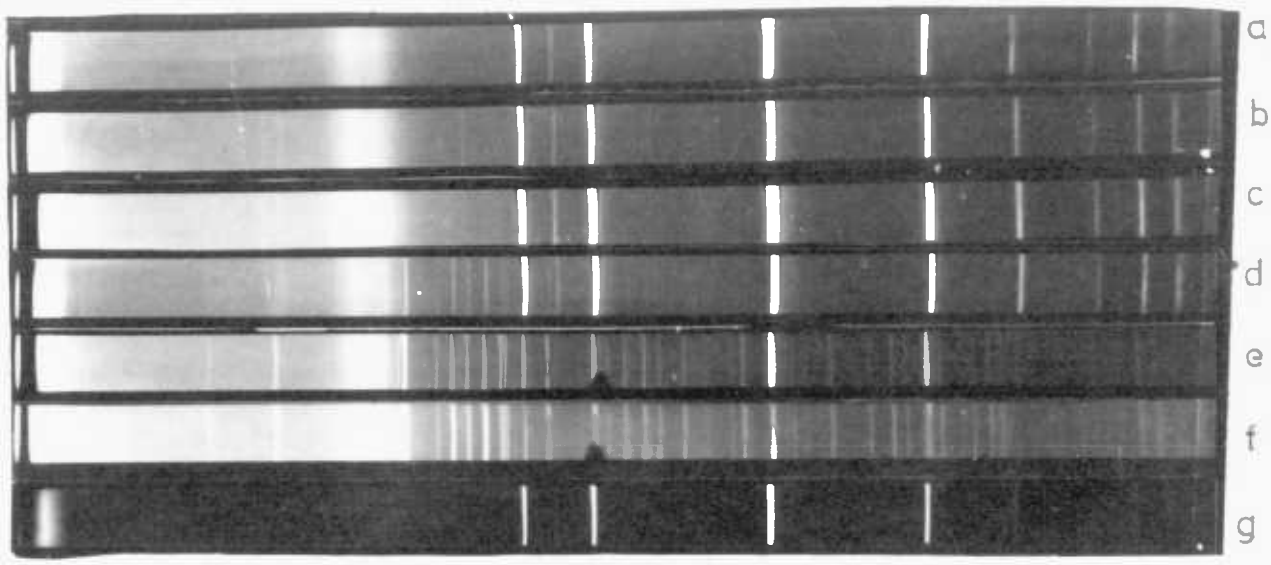

FIG. C-1.1 X-ray Patterns of the Residues from the Leaching of the Monosulphide Solid Solution of Iron and Nickel (Co radiation)

a. Unleached Mss

b. 20% nickel dissolved

c. 35% nickel dissolved

d. 50% nickel Dissolved

e. 75% nickel dissolved

f. 90% nickel dissolved

g. hydrogen peroxide leaching

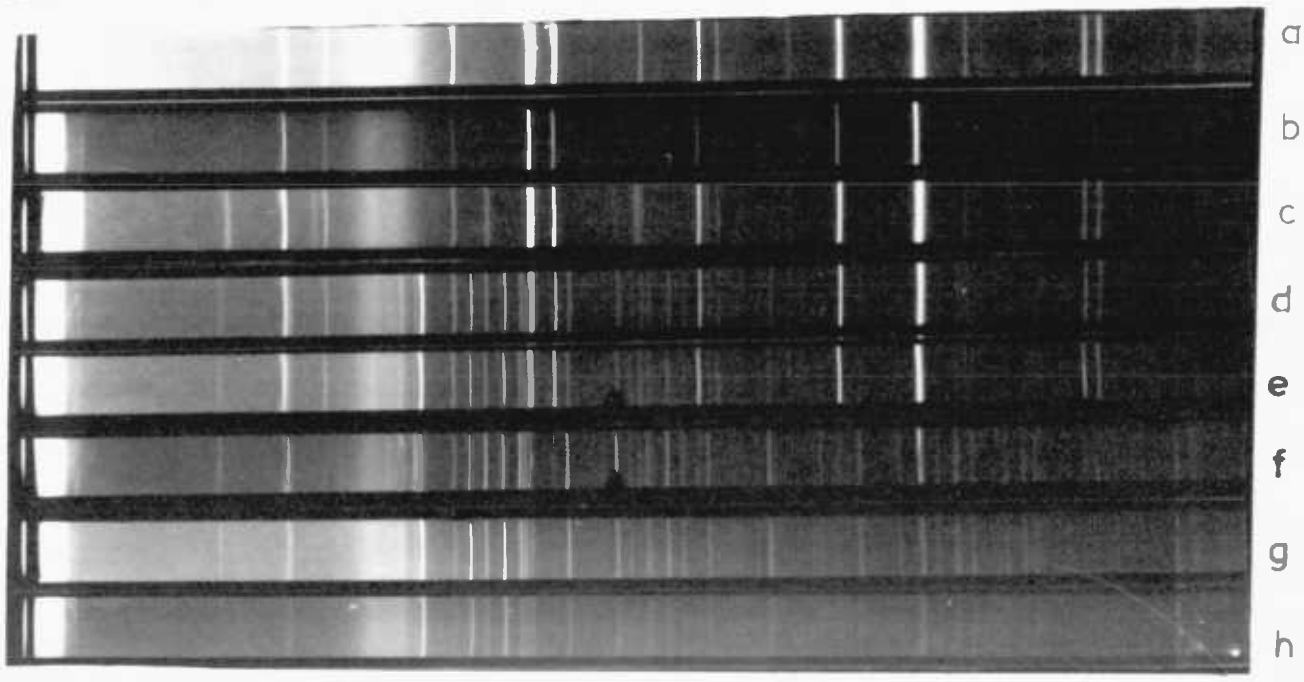

FIG. C-1.2 X-ray Patterns of the Residues from the Leaching of Pentlandite (Co - radiation)

a. Unleached Pentlandite
b. 20% nickel dissolved
c. 32% nickel dissolved
d. 45% nickel dissolved
e. 55% nickel dissolved
f. 67% nickel dissolved
g. 80% nickel dissolved
h. 90% nickel dissolved

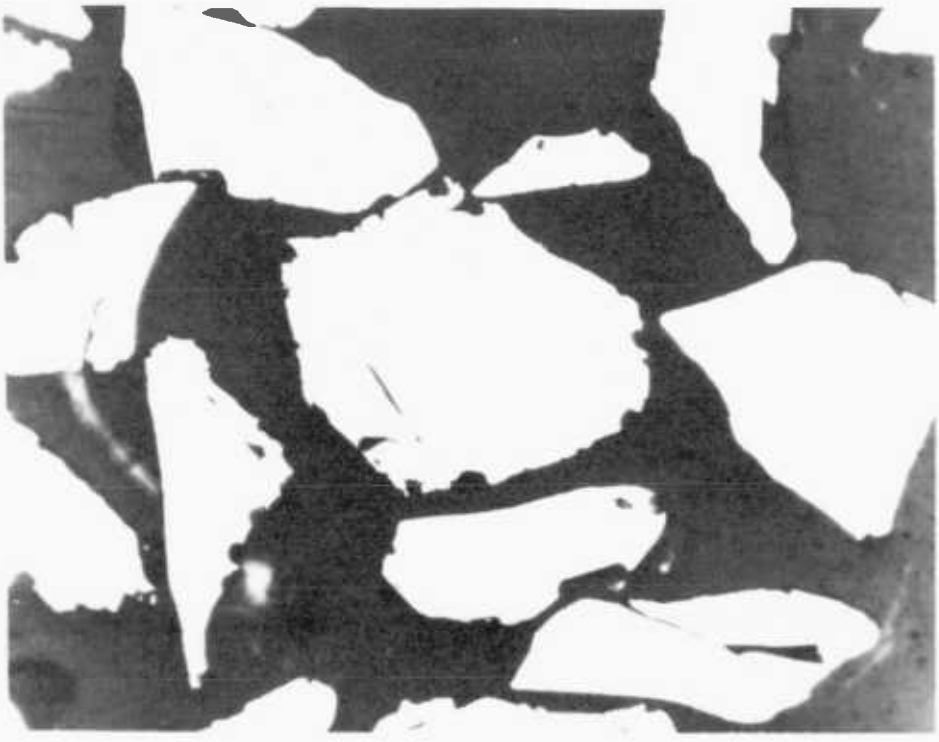

FIG. C-2.1 Unleached Sample of the Monosulphide Solid Solution of Nickel and Iron (Mss)

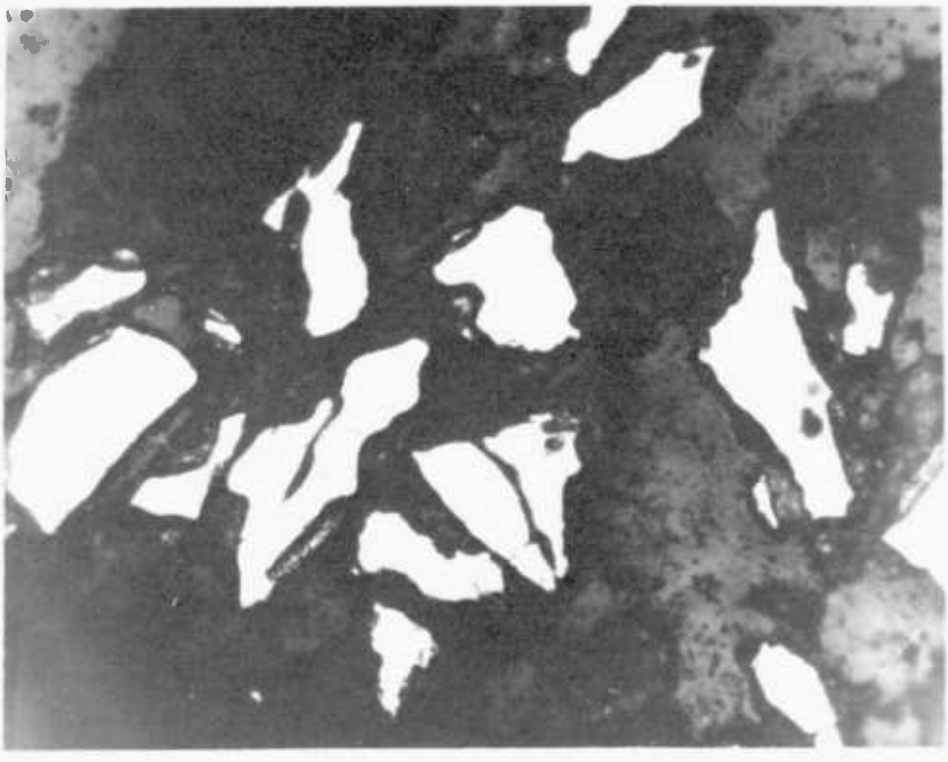

FIG. C-2.2 Mss Leach Residue With about 40% of the Nickel Dissolved

FIG. C-2.3 Mss Leach Residue with about 60% of the Nickel Dissolved

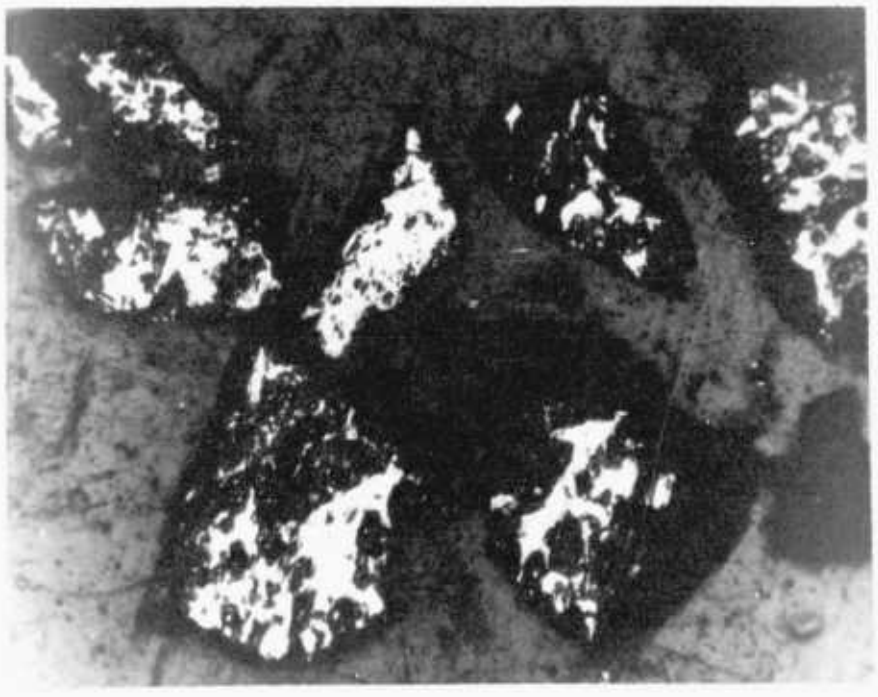

FIG. C-2.4 Mss Leach Residue with about 80% of the Nickel Dissolved

FIG. C - 3.1 Appearance of Pentlandite in Ordinary Light

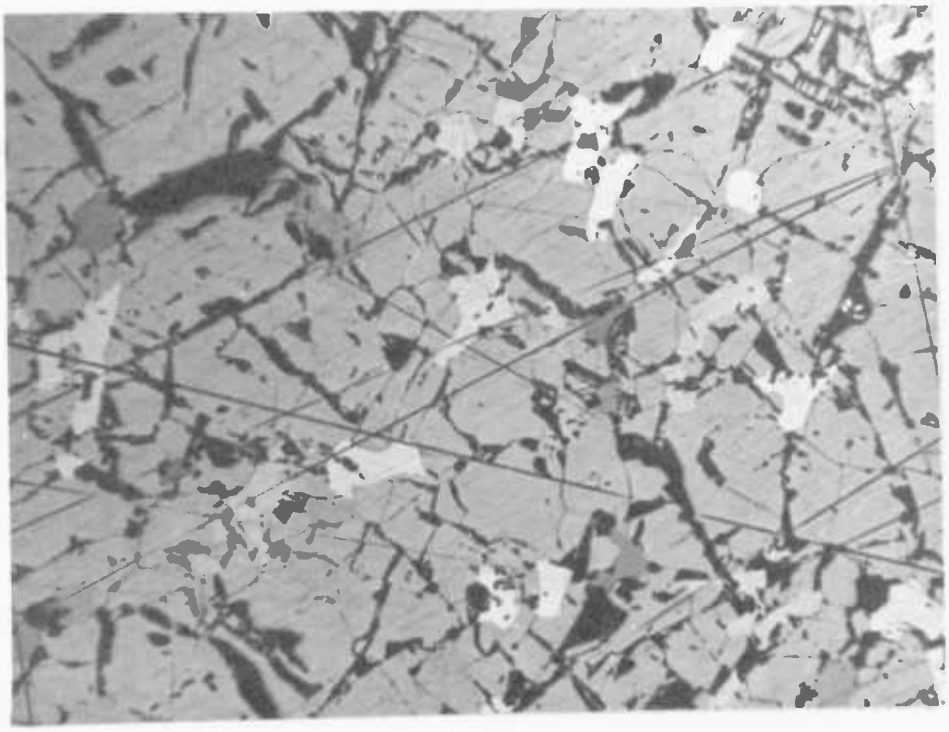

FIG. C - 3.2 Appearance of Pyrrhotite under Polarised Light Distinguished by its Anisotropic Behaviour (light areas)

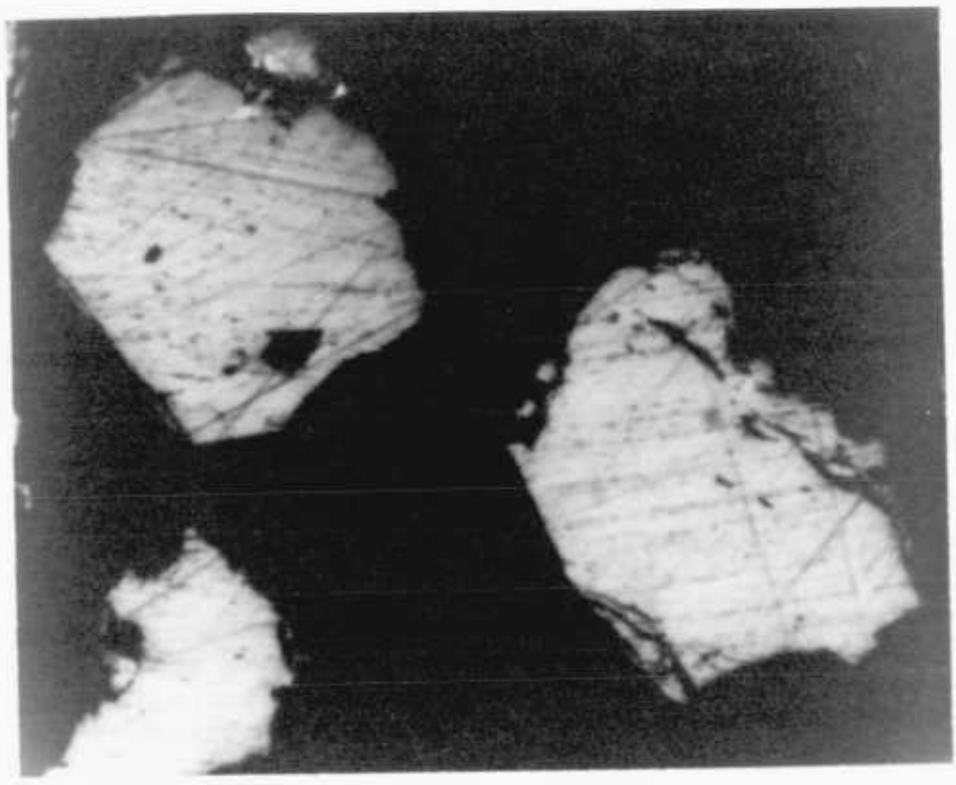

FIG. C - 3.3 Particles of Pentlandite before Leaching

FIG. C - 3.4 Pentlandite Leach Residue from which about 20% Nickel was Dissolved

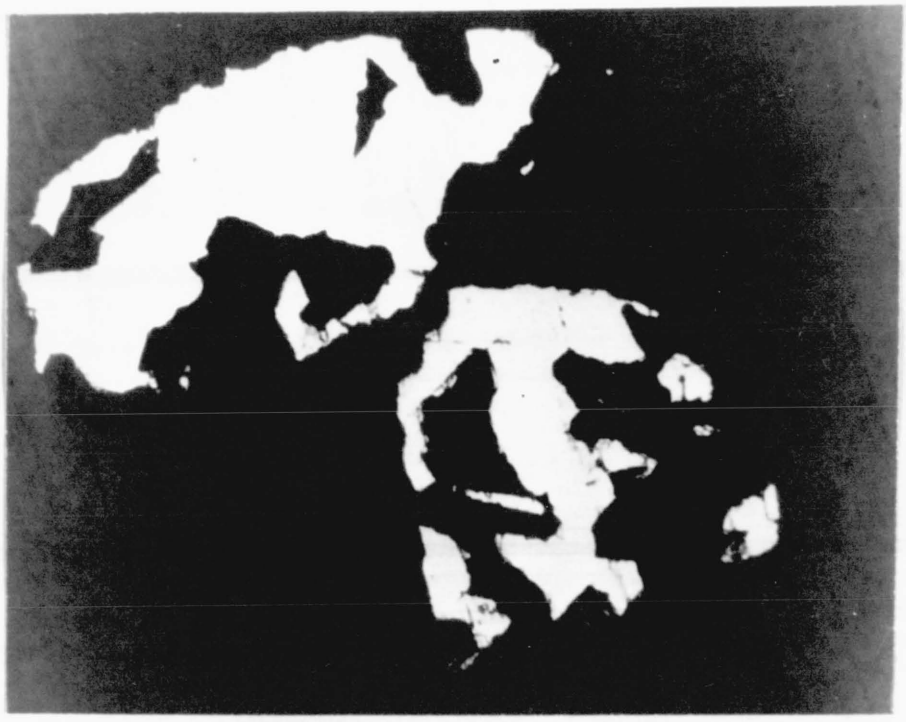

FIG. C - 3.5 Pentlandite Leach Residue from which about 50% Nickel was Dissolved

FIG. C - 3.6 Pentlandite Leach Residue from which about 70% Nickel was Dissolved

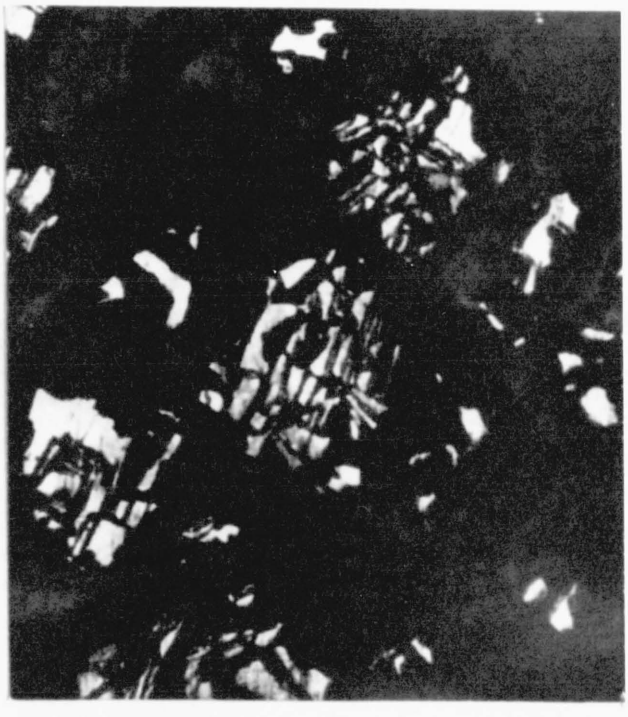

FIG. C - 3.7 Pentlandite Leach Residue from which about 80% Nickel was Dissolved

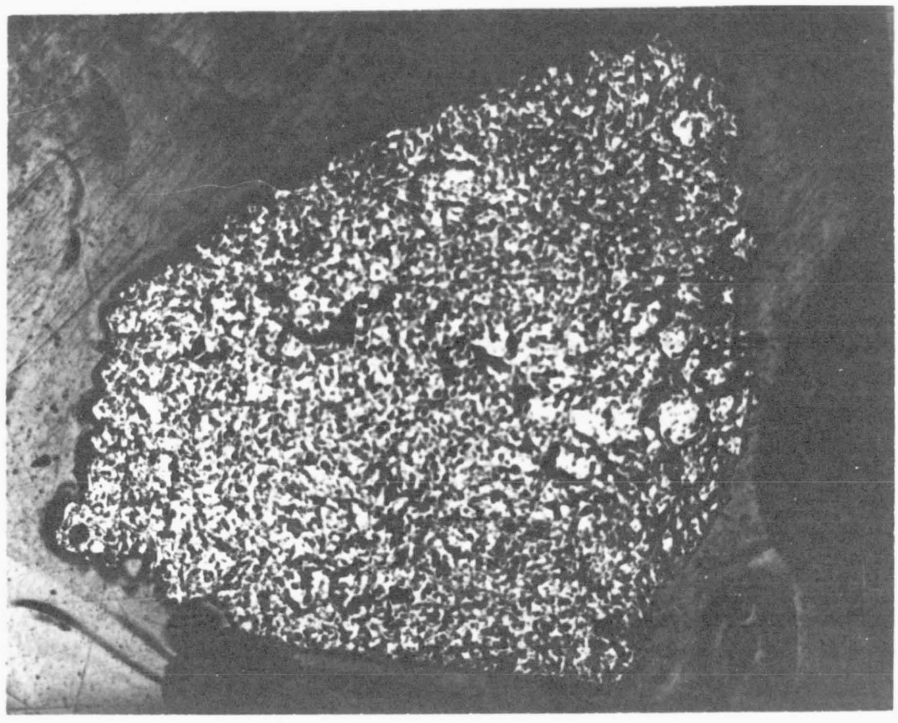

FIG. C - 3.8 Macrophotograph of a Pentlandite Piece Mounted in Araldite before Leaching

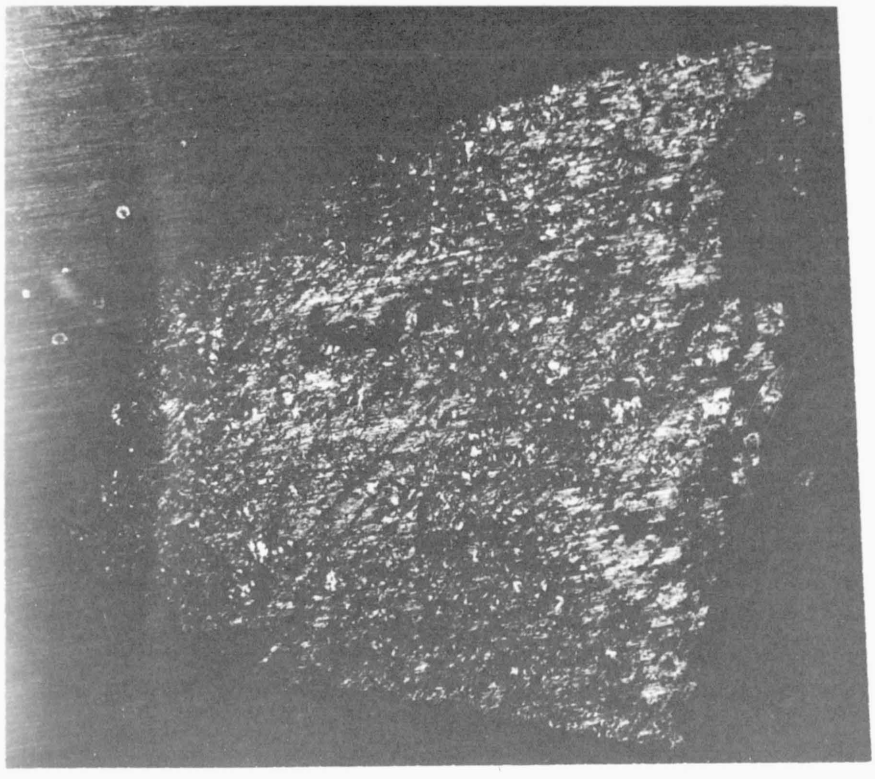

FIG. C - 3.9 Macrophotograph of the Pentlandite Piece (Fig. C - 3.8) after 10 hours of Leaching

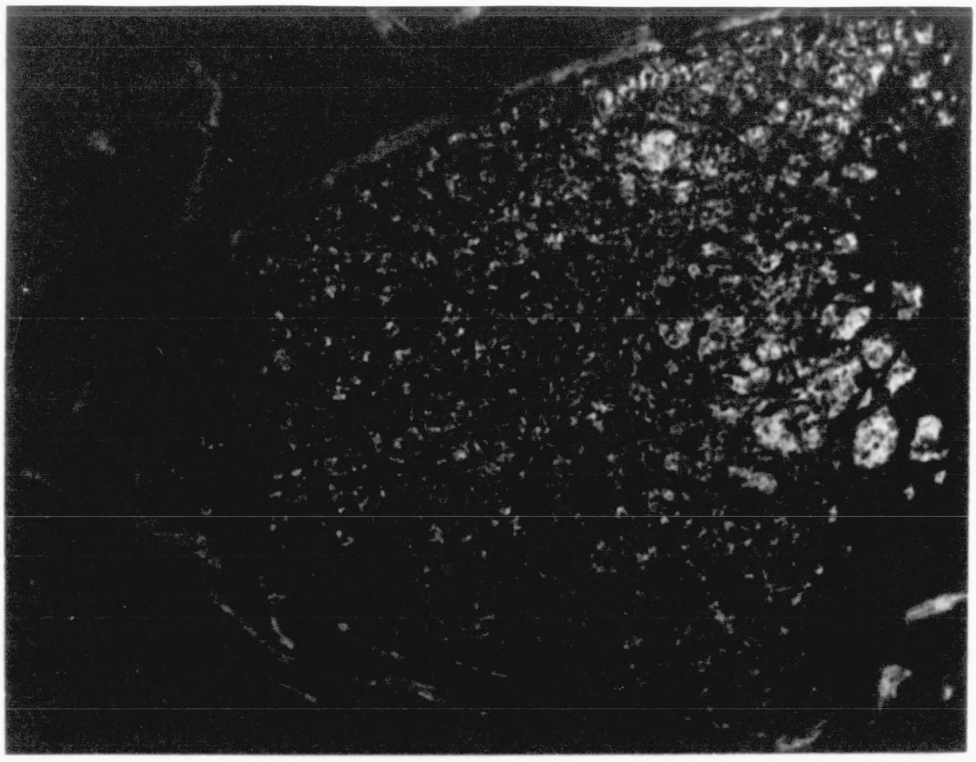

FIG. C - 3.10 Macrophotograph of the Pentlandite Piece (Fig. C - 3.8) after 20 hours of Leaching

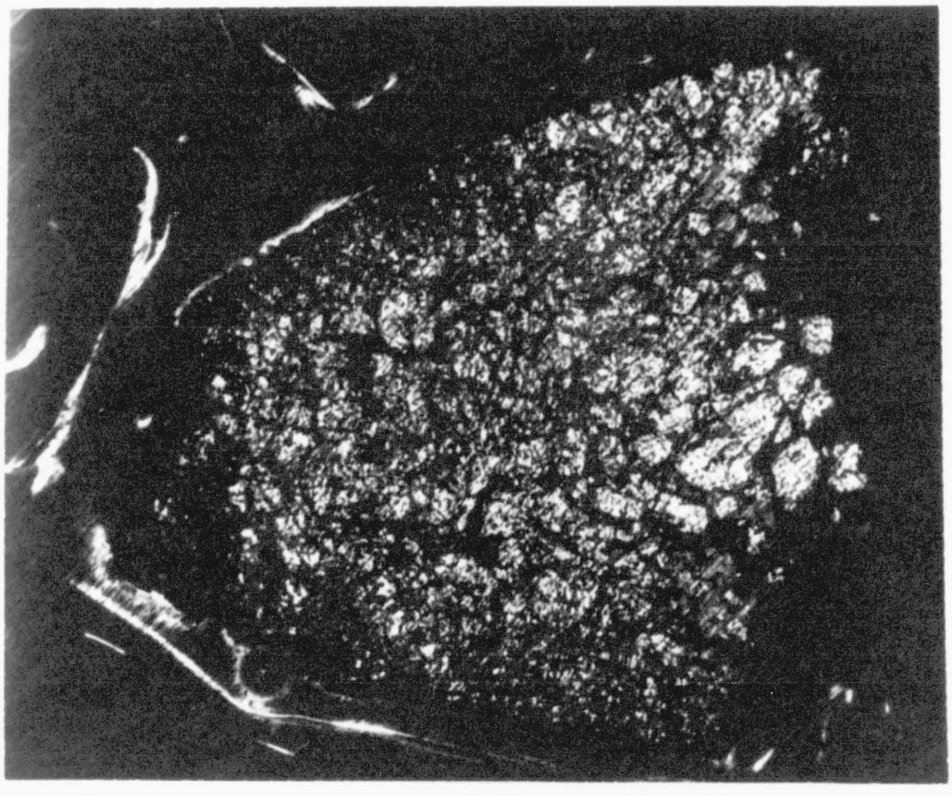

FIG. C - 3.11 Macrophotograph of the Pentlandite Piece (Fig. C-3.8) after 50 hours of Leaching

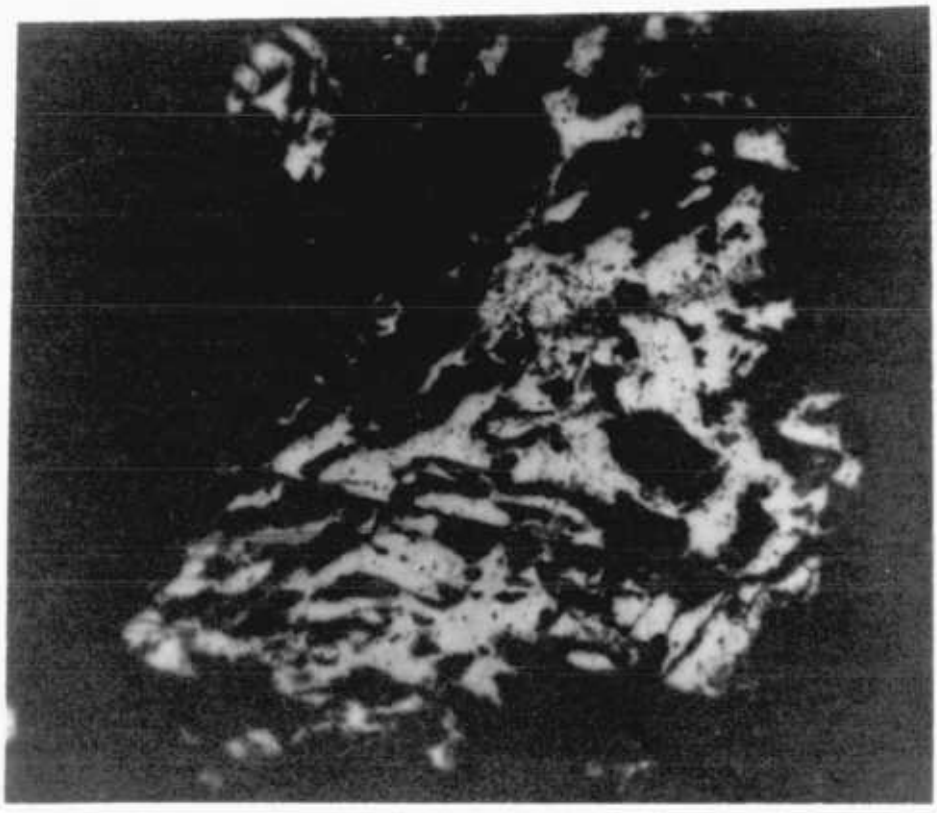

FIG. C - 3.12 Macrophotograph of the Pentlandite Piece (Fig. C-3.8) after 100 hours of Leaching

ACKNOWLEDGMENTS

The author wishes to express his sincere thanks to his supervisor, Dr. A.R. Burkin, Reader in Hydrometallurgy, for his invaluable help, advice and encouragement during this work and also for his consideration and personal kindness.

The author also wishes to express his gratitude to the other members of the Hydrometallurgy Group for their advice, encouragement and the warm atmosphere they created during the period of this work and especially to Mr. J. Burgess for his practical advice, and Mr. J. Phillis for drawing on the computer many of the pictures of the present work.

Thanks are also due to the Analytical Services Laboratory for the electron probe microanalyses and to Mr. M.H. Folder for his perseverance while analysing the leach samples for platinum and palladium and to the photographic section for the reproduction of the photographs. Special thanks to Mrs. M. Smit for her excellent and fast typing.

Acknowledgment is also due to Bodossakis Foundation, Greece, for their financial assistance over the last three years.

The author is indebted to all his friends inside and outside the University for their interest and companionship during the period of this work.

REFERENCES

1. E. GUNTHER and R. FRANKE: U.S. patent 879,633, 1908.
2. A.R. CHOPPIN and L.C. FAULKENBERRY: Journal and Proceeding of the Am. Chem. Soc., 59, 1937, 2203-7.
3. I.G. FALBENINDUSTRIE: British patent 512,079, 1938.
4. I.G. FALBENINDUSTRIE: U.S. patent 2,180,520, 1939.
5. J.A. O'CONNER: Chem. Eng., 59, 1952, 164.
6. F.A. FORWARD and J. HALPERN: J. Metals, N. Y. 7, 1955, 463-6.
7. P.M.J. GRAY: Trans. Instn. Min. Metal. Lond., 65, 1955-56, 55
8. K.W. DOWNES and R.W. BRUCE: Trans. Canad. Inst. Min. Metal., 58, 1955, 77.
9. J. HALPERN and F.A FORWARD: Trans. I.M.M., 66, 1957, 181-9.
10. J. HALPERN: J. Metals, 9, 1957, 280-9.
11. D.R. McKAY and J. HALPERN: Trans. AIME., 212, 1958, 301-9.
12. I.F. KHUDYAKOV and A.S. YAROSLAVTSEV: Tr. Ural. Politekn. Inst., 155, 1967, 30-38.
13. G.N. DOBROKHOTOV: J. Appl. Chem. USSR, 32, 1959, 2524-30.
14. P.J. McGAULEY: U.S. patent 2,647,827, 1953.
15. P.J. McGAULEY, S. NASHNER and V. KUDRYK: U S patent 2,746,859, 1956.
16. J.W. DONALDSON and H.F. DAVIS Jr.,: U.S. patent 2,934,428, 1960

17. V.P. GOVOROV: Tsvet. Met. 32(2), 1959, 41-46.

18. G.N. DOBROKHOTOV and N.I. ONUCHKINA: Tsvet. Met., 30(3) 1957, 35-40.

19. G.N. DOBROKHOTOV and E.V. MAIROVA: Tsvet. Met., 36(8), 1963, 31-37.

20. I.N. MASLENITSKII and N V. ZVEREVICH: Tsvet. Met., 38(1) 1965, 46-47.

21. I.N. MASLENITSKII and L.V. CHUGAEV: Tsvet. Met., 38(4), 1965, 35-39.

22. V.N. MACKIW, D.J.I. EVANS and W. KUNDA: U.S. patent 3,293,027, 1966.

23. A.B. KLYUEVA. Tr. Vral. Politekn. Inst., 155, 1967, 39-44.

24. T. KENTARO: Nippon Kogyo Kaishi, 83(1), 1967, 32-35 (C.A.: 69-45374).

25. A. BLACK and J.B. GOODSON: J. Amer. Water Works Assoc., 44, 1952, 309.

26. V.N. GRINEVICK: Zhurnal Prikladnoi Khimii, 14, 1941, 63.

27. M.I. SHERMAN and J.D.H. STRICKLAND: Trans. AIME, 209, 1957, 1386-88.

28. H.B. SLATER: U.S. patent 1,066,855, 1913.

29. E. BRUNNER: Australian patent 171,405, 1952.

30. K.J. JACKSON and J.D.H. STRICKLAND: Trans. AIME, 212, 1958, 301-9.

31. A.R. SERIKOV and I.B. ORLOVA: Sbornik Nauch. Trudov, Irkutsk. Nauch. - Issledovatel. Inst. Redkikh Metal. 7, 1958, 227-38.

32. A. L. TSEFT and V. N. KRYUKOVA: Tr. Vostochno - Sibir. Filia Akad. Nauk. SSSR., 25, 1960, 69-75.

33. V. N. KRYUKOVA: Materialy K Konf. Molodykh Nauch. Sodrudnikov, Vostoch. Sibir. Filiala Sibir. Otdel Akad. Nauk. SSSR, Blagoveshchensk 3, 1960, 39-46, (C.A. 56-213).

34. V. N. KRYUKOVA and A. L. TSEFT: Tr. Irkut. Polit. Inst., 18, 1963, 40-47 (C A. 61-5317).

35. V. E. KLETS and A. P. SERIKOV: Tr. Irkut. Polit. Inst., 18, 1963, 31-39.

36. A. L. TSEFT and A. P. SERIKOV: Tr. Irkut. Polit. Inst., 18, 1963, 14-25.

37. V. N. KRYUKOVA and A. L. TSEFT: Tr. Inst. Metal i Obogashch, Akad. Nauk. Kaz. SSR, 11, 1964, 3-9.

38. G. I. GORBATENKO and I. I. GOGOLINSKAYA: Tr. Kaz. Politekn. Inst., 27, 1967, 12-25.

39. B. TOUGARINOFF, M. WILLEKENS and A. VAN PETEGHEM: Ind. Chim. Belge, 32 (Spec. No.) (Pt. 2), 1967, 169-73, (C.A. 72-5340).

40. Y. P. P. MAYOR and P. F. TORD: U.S. patent 3,637,372, 1972.

41. T. R. INGRAHAM, H. W. PARSONS and L. J. CABRI: Can. Met. Quart., 11(2), 1972, 407-11.

42. K. N. SUBRAMANIAN, E. S. STRATIGAKOS and P. H. JENNINGS: Can. Met. Quart., 11(2), 1972, 425-34.

43. P. G. THORNHILL, E. WIGSTAL and G. VAN WEERT: J. Metals, 23, 1971, 13-18.

44. VAN WEERT, K. MAH and N. L. PIRET: CIM Bulletin, 67 (741), 1974, 97-103.

45. T. B. JOSEPH: Canadian patent 173,452, 1916.

46. P.A. PAZDNIKOV and R.A. PAVLYUK: Tsvet. Met., 36(5), 1963, 41-45.

47. G. BJORLING and G.A. KOLTA: J. Chem. U.A.R., 9(2), 1966, 187-203.

48. LE NICKEL: Fr. 1,597,569, 1970.

49. K. KMETOVA: Sb. Ved. Pr. Vys. Sk. Banske Ostrave, Rada Hutn., 16 (1), 1970, 137-50 (C.A. 76-27288).

50 F.A. PETRACHKOV et al: Ukr. Khim. Zh., 38(5), 1972, 425-9. (C.A. 77-156989).

51. L. GARDON and C. BOZEK: Fr. Demande 2,129,917, 1972.

52. L.V. CHUGAEV: Russian J. Inorg. Chem., 10(8), 1965, 969-71.

53. I.F. KHUDYAKOV and V.I. SMIRNOV: Tsvet. Met., 38(1), 1965, 36-41.

54. L.V. CHUGAEV: Izv. Vyssh. Ucheb. Zaved., Tsvet. Met., 2, 1968, 24-28.

55. L.V. CHUGAEV: Izv. Vyssh. Ucheb. Zaved., Tsvet. Met., 4, 1968, 22-26.

56. J. GERLACH, F. PAWLEK and H. RIETESEL: Erzmetall., 23(10), 1970, 486-92.

57. M. TOTLANI and J. BALACHANDRA: Trans. Ind. Inst. Metals, 26(1), 1973, 48-54.

58. Z.R. LLANOS, P.B. QUENEAU and R.S. RICKARD: C.I.M. Bulletin, 67(742), 1974, 74-82.

59. S.M.M. KELT: Ph.D. Thesis, R.S.M., University of London, 1975.

60. V.H. GOTTSCHALK and H.A. BUEHLER: Econ. Geol., 7, 1912, 15-34.

61. B.T. SANDEFUR: Econ. Geol., 37, 1942, 173-87.

62. W.H. DENNEN: Econ. Geol., 38, 1943, 28-55.

63. C.E. MICHENER and A.B. YATES: Econ. Geol., 39, 1944, 506-14.

64. J. SIERRA LOPEZ and A. de VERGARA SCHULZE: Bol. Geol. y Min., 80(4), 1969, 352-59.

65. E.H. NICKEL, J.R. ROSS and M.R. THORNBER: Econ. Geol., 69, 1974, 93-107.

66. E.N. ELISEEV and S.I. SMIRNOVA: Materialy po Mineralogii Kol'sk Poluostrova, Kirovsk, 1, 1959, 176-9.

67. V.E. KLETS, A.L. TSEFT and V.A. LIOPO: Tr. Irkut. Polit. Inst., 27, 1966, 115-22.

68. Y.M. SHNEERSON, I.Y. LESHCH and L.M. FRUMINA: Tr. Proekt. Nauch. - Issled. Inst. Gipronikel., 29, 1966, 24-38.

69. H. SAARINEN: Metall., 25(7), 1971, 778-83.

70. J.A. VEZINA: Can., Mines Br., Tech. Bull., TB129, 1970.

71. J.A. VEZINA: C.I.M. Bulletin, 66(733), 1973, 57-60.

72. W.E. RAZZELL and P.C. TRUSSELL: Appl. Microbiol. 11, 1963, 105-10.

73. D.W. DUNCAN and P.C. TRUSSELL: Can. Met. Quart., 3(1), 1964, 43-55.

74. D.W. DUNCAN, C.C. WALDEN and P.C. TRUSSELL: U.S. patent 3,305,353, 1967.

75. A.E. TORMA: T.S.M. Paper A72-7.

76. J.E. DUTRIZAC and R.J.C. MACDONALD: C.I.M. Bulletin, 67(742), 1974, 169-75.

77. N.F. DYSON and T.R. SCOTT: Hydrometallurgy, 1, 1976, 361-72.

78. J. HANES: J. Can. Min. Inst., 8, 1905, 358-62.

79. F.A. FORWARD: Trans. Can. Inst. Min. Metall., 56, 1953, 363-80.

80. F.A. FORWARD: Min. Congr. J., Wash., 40, 1954, 49.

81. F.A. FORWARD and J. HALPERN: J. Metals, N.Y., 6, 1954, 140-8.

82. F.A. FORWARD and V.N. MACKIW: J. Metals, N.Y., 7, 1955, 457-63.

83. C.F. BRENTHEL: Z. Enzbergb. Metallhüttenw., 8, 1955, 422.

84. S. NASHNER: Trans. Can. Inst. Min. Metall., 58, 1955, 212.

85. F.A. FORWARD and J. HALPERN: Trans. Inst. Min. Metall., 66, 1957, 191-218.

86. S. NABOICHENKO and V. SMIRNOV: Tr. Ural. Polit. Inst., 155, 1967, 45-52.

87. S. NABOICHENKO and V. SMIRNOV: Tr. Ural. Polit. Inst., 155, 1967, 14-22.

88. K. BORNEMANN: Metallurgie, 5, 1908, 61-68.

89. W.H. NEWHOUSE: Econ. Geol., 22, 1927, 288-99.

90. R. VOGEL and W. TONN: Archiv Eisenhuttenwessen, 12, 1930, 769.

91. H.F. ZURBRIGG: M.A. Thesis, Queen's University, Canada, 1933.

92. G.G. URAZOV and N.A. FILIN: Metallurgie, 13, 1938, 3-17.

93. G.L. COLGROVE: M.A. Thesis, Queen's University, Canada, 1940.

94. G.A. HARCOURT: Am. Mineral., 27, 1942, 63.

95. G.L. COLGROVE: Ph.D. Thesis, Wisconsin University, U.S.A., 1942.

96. D. LUNDQVIST: Ark. för Kemi, Mineralogi och Geologi, 24A, No. 21 1947, 1-12.

97. D. LUNDQVIST: Ibid., 24A., 22, 1947, 1.

98. Y. ITAYA, H. SHIMADA and J. ANDO: J. Min. Met. Inst. Japan, 74, 1958, 927.

99. G. KULLERUD: Carnegie Inst. Washington, Year Book 55, 1956, 175-80.

100. G. KULLERUD: Carnegie Inst., Washington, Year Book 61, 1962, 144-50.

101. G. KULLERUD: Can. Mineral., 7, 1963, 353-66.

102. G. KULLERUD: Carnegie Inst., Washington, Year Book 62, 1963, 175-89.

103. G. KULLERUD, R.A. YUND and G.H. MOH: Econ. Geol., Mon. 4, 1969, 323-343.

104. L.A. CLARK and G. KULLERUD: Econ. Geol., 58, 1963, 853-85.

105. A.J. NALDRETT and G. KULLERUD: Carnegie Inst., Washington, Year Book 65, 1966, 320-26.

106. A.J. NALDRETT, J.R. CRAIG and G. KULLERUD: Econ. Geol., 62, 1967, 827-47.

107. J.R. CRAIG: Carnegie Inst., Washington Year Book 66, 1967, 434-6.

108. J.R. CRAIG: Am. Mineral, 56, 1971, 1303-11.

109. J.R. CRAIG and A.J. NALDRETT: Abstracts of Papers, Geological Association of Canada - Mineralogical Association of Canada, Ann. Mtg., Sudbury, Ontario, May 13-15, 1971, 16-17.

110. J.R. CRAIG, A.J. NALDRETT and G. KULLERUD: Carnegie Inst. Washington, Year Book 66, 1967, 440-1.

111. E. JENSEN: Am. J. Sci., 240, 1942, 695-709.

112. L.A. CLARK and G. KULLERUD: Carnegie Inst., Washington, Year Book 58, 1959, 142-5.

113. G. KULLERUD and R.A. YUND: J. Petrol., 3, 1962, 126-75.

114. J.E. HAWLEY, G.L. COLGROVE and H.F. ZURBRIGG: Econ. Geol., 38, 1943, 335-88.

115. R.W. SHEWMAN and L.A. CLARK: Can. J. Earth Sci., 7, 1970, 67-85.

116. K.C. MISRA and M.E. FLEET: Econ. Geol., 68, 1973, 518-39.

117. H. HARALDSEN: Zeit. anorg. u. allg. chem., 231, 1937, 78-96.

118. H. HARALDSEN: Zeit. anorg. u. allg. Chem., 246, 1941, 169-94.

119. H. HARALDSEN: Zeit. anorg. u. allg. chem., 246, 1941, 194-226.

120. M. CORLETT: Zeit Krist, 126, 1968, 124-34.

121. G.A. DESBOROUGH and R.H. CARPENTER: Econ. Geol., 60, 1965, 1431-50.

122. A. BYSTROM: Arkiv for Kemi, Mineral. och Geol., 19B, No. 8, 1945, 1-8.

123. A.H. CLARK: Trans. Inst. Min. Met., 75, 1966, B232-B235.

124. H.T. HALL and R.A. YUND: Geol. Soc. America, Program, San Francisco, 1966.

125. M. LINDQVIST, D. LUNDQVIST and A. WESTGREN: Svensk. Kemisk Tidskrift, 48, 1936, 156-60.

126. E.N. ELISEEV: Zapiski Všesojuz. Mineral. Obščestva, 84, 1955, 54.

127. M.A. IBRAHIM: Unpublished M. Sc. Thesis, Nova Scotia Technical University, 1959.

128. O. KNOP and M.A. IBRAHIM: Can. J. Chem., 39, 1961, 297-317.

129. O. KUOVO, M. HUHMA and Y. VUORELAINEN: Am. Mineral., 44, 1959, 897-900.

130. O. KNOP, M.A. IBRAHIM and SATURNO: Can. Mineral., 8, 1965, 291-316.

131. M. GRATEROL and A.J. NALDRETT: Econ. Geol., 66, 1971, 886-900.

132. D.C. HARRIS and E.H. NICKEL: Can. Mineral., 11, 1972, 861-878.

133. G.P. POPOVA, V.V. YERSOV and V.A. KAZNETSOV: Dokl. Akad. Nauk SSSR, 156, 1964, 114-18.

134. N. ALSEN: Geol. Fören. Förhandl. Stockholm, 47, 1925, 19-72.

135. G. HAGG and I. SUCKSDORFF: Zeit. physik. chem., B22, 1933, 444-52.

136. M.J. BUERGER: Am. Mineral., 32, 1947, 411-14.

137. E.F. BERTAUT: Acta Cryst., 6, 1947, 557-61.

138. F. GRØNVOLD and H. HARALDSEN: Acta Chem. Scand., 6, 1952, 1452-69.

139. B. WUENSCH: Mineral. Soc. Am. Spec. Paper 1, 1963, 157-62.

140. R.H. CARPENTER and G.A. DESBOROUGH: Am. Mineral., 49, 1964, 1350-65.

141. M.E. FLEET: Am. Mineral., 53, 1968, 1846-55.

142. M.E. FLEET: Can. J. Earth Sci., 5, 1968, 1183-85.

143. N. MORIMOTO and H. NAKAZAWA: Science, 161, 1968, 577-79.

144. M.E. FLEET and N. MACRAE: Can. Mineral., 9, 1969, 699-705.

145. H.T. Jr. EVANS: Proc. Apollo 11 Lunar Sci. Conf., 1, 1970, 399-408.

146. A.D. PEARSON and M.J. BUERGER: Am. Mineral., 41, 1956, 804-5.

147. S. GELLER: Acta Cryst., 15, 1962, 1195-98.

148. O. KNOP, HUANG CHUNG-HSI and F.W. WOODHAMS: Am. Mineral., 55, 1970, 1115-30.

149. D.J. VAUGHAN and M.S. RIDOUT: J. Inorg. Nucl. Chem., 33, 1971, 741-46.

150. D.J. VAUGHAN and R.G. BURNS: G.S.A Ann. Mtg., Washington, 3, p.737 (Abs). G S.A. Abstracts with programs, 3, 1971.

151. V. RAJAMANI and C.T. PREWITT: Can. Mineral., 12, 1973, 178-87.

152. F. HULLIGER: Structure and Bonding, 4, 1968, 83-229.

153. J.A. KING: Ph.D. Thesis, R.S.M. University of London, 1966.

154. J.R. WEST: Ind. Engng. Chem., 42, 1950, 713-8.

155. E.H. BAKER: Trans. Inst., Min. Met., 80, 1971, C93.

156. A.I. VOGEL: A Textbook of Quantitative Inorganic Analysis, Third Edition, Longmans.

157. A.I. VOGEL: Macro and Semimicro Qualitative Inorganic Analysis, Fourth Edition, Longmans.

158. Perkin Elmer Analytical Methods for Atomic Absorption Spectrophotometry. (Perkin Elmer Corp.), 1971.

159. D.A. PANTONY: A laboratory Manual of Elementary Metallurgical Analysis, Part 2, Imperial College, London, 1956.

160. P. MASON, M. FROST and S. REED: B.M. - I.G. - N.P.L. Computer programs for calculating corrections in quantitative x-ray microanalysis, Nat. Physical Lab., IMS Report 2 (April, 1969).

161. P.M. De WOLFF: Acta Crystall., 1, 1468, 207.

162. H.P. KLUG and L.E. ALEXANDER: X-ray Diffraction Procedures for Polycrystalline and Amorphus Materials, Wiley, 1974.

163. A.R. BURKIN: The Chemistry of Hydrometallurgical Processes, Spon. London, 1966.

164. G.D. MANNING and J. MELLING: " Potential Eh-pH Diagrams at Elevated Temperatures - A Survey", Warren Spring Laboratory, 1971.

165. R.C.H. FERREIRA: PhD Thesis, R.S.M. University of London 1972.

166. L.R. HOUGEN and H. ZACHARIASEN: JOM, 1975, 6-9.

167. J. HALPERN: Trans. Met. Soc. AIME, 209, 1957, 280-9.

168. E. PETERS and H. MAJIMA: "The Physical Chemistry of Hydrometallurgy" unpublished manuscript (TMS paper selection A68-32) AIME Annual Meeting, 1968.

169. M. POURBAIX: "Atlas of Electrochemical Equilibria in Aqueous Solutions", Pergamon Press, London and Cebelcor, Brussels, translated from French by J.A. Franklin, 1966.

170. R.M. GARRELS and C.L. CHRIST: "Solution, Mineral and Equilibria" N. York and London, Harper and Row, Tokyo, John Weatherhill Inc., 1965, p172.

171. R.G. ROBINS; "The Application of Potential-pH Diagrams to the Prediction of Reactions in Pressure Hydrometallurgical Process" Stevenage, Warren Spring Laboratory, 1968, LR 80 (MST).

172. R.J. BIERNAT and R.G. ROBINS: Electrochim. Acta, 14, 1969, 809-20.

173. H.E. Jr. TOWNSEND: Corrosion Sci., 10(5), 1970, 343-58.

174. V. ASHWORTH and P.J. BODEN: Corrosion Sci., 10 (10), 1970, 709-18.

175. E. BARDAL: Corrosion Sci., 11(6), 1971, 371-82.

176. P.A. BROOK: Corrosion Sci., 11(6), 1971, 389-96.

177. H. MAJIMA and E. PETERS: Trans. Met. Soc. AIME,236, 1966, 1409-13.

178. H.L. BARNES and G. KULLERUD: Econ. Geol., 56, 1961, 648-88.

179 R.J. BIERNAT and R.G. ROBINS: Electrochim. Acta, 14, 1969, 809-20.

180. I.B. D'YACHKOVA and I.L. KHODAKOVSKIY: Geochem. Interl., 5(6), 1968, 1108-25.

181. A.J. ELLIS and W. GIGGENBACH: Geochim. Cosmochim. Acta., 35, 1971, 247-60.

182. E.I. SERGEYEVA and I.L. KHODAKOVSKIY: Geochem. Interl., 6(4), 1969, 681-94.

183. R.G. RODINS: "The production of VO_2 by hydrothermal reduction", Paper given to conference on 'Recent Progress in Research in Chemical and Extractive Metallurgy' Australian Inst. Min. and Metall., Sydney Branch and University, N.S.W., Feb. 1965.

184. R.G. RODINS: J. Appl. Chem., 16, 1966, 187-90.

185. B.W. EDENBOROUGH and R.G. ROBINS: Electrochim. Acta, 14, 1969, 1285-95.

186. H.C. HELGENSON: J. Phys. Chem., 71(10), 1967, 3121-36.

187. H.S. HARNED and B.B. OWEN: "The Physical Chemistry of Electrolytic Solutions", 3rd Edition, N. York, Reinhold Publishing Corp., 1958, 644p.

188. J.V. DOBSON and H.R. THIRSK: Electrochim. Acta, 16(3), 1971, 315-38.

189. I.L. KHODAKOVSKIY, V.N. RYZHENKO and G.B. NAUMOV: Geochem. Interl., 5(6), 1968, 1200-19.

190. D.D. WAGMAN et al., "Selected Values of Chemical Thermodynamic Properties", Washington, National Bureau of Standards, 1969, Technical note 270, parts 1-4.

191. D.R. STULL et al, "JANAF Thermochemical Tables", Midland, Michigan, Dow Chemical Company, 1965, PB 168 370 and Addenda PB 168 370 1-3.

192. I. BARIN and O. KNACKE: "Thermochemical properties of Inorganic Substances", 1973, Springer-Verlag, Berlin, Heidelberg, N. York, Verlag Stahleisen, m.b.H Dusseldorf.

193. W.M. LATIMER: "The oxidation States of the Elements and their Potentials in Aqueous Solutions", 2nd Edition, New Jersey, Prentice-Hall Inc., 1952, 359p.

194. G.N. LEWIS and M. RANDALL: "Thermodynamics" 2nd edition, by K.S. Pitzer and L. Brewer, N. York, Toronto and London, McGraw-Hill Book Co., 1961, 723p.

195. C.M. CRISS and J.W. COBBLE: J. Amer. Chem. Soc., 86 (24), 1964, 5385-90.

196. C.M. CRISS and J.W. COBBLE: J. Amer. Chem. Soc., 86(24), 1964, 5390-93.

197. I.L. KHODAKOVSKIY: Geochem. Interl., 6(1), 1969, 24-34.